Modelling Water Table Depth Effects on Net Ecosystem CO2 Exchange of Two Contrasting Forested Peatlands – A Tropical Bog and a Boreal Fen

by

Mohammad Mezbahuddin

A thesis submitted in partial fulfillment of the requirements for the degree of

Doctor of Philosophy
in
Soil Science

Department of Renewable Resources
University of Alberta

ABSTRACT

Peatlands have been accumulating carbon (C) in wet soils under shallow water table (WT) over millennia. Increased frequency and intensity of droughts and artificial drainage for promoting agriculture have recently been causing peatland WT depth (WTD) drawdown. This could alter peatland C balance and shift peatlands from net sinks to sources of C. To conserve the resilience of these C stocks, improved predictive capacity is required to forecast how these C stocks would be affected by potentially deeper WT under future drier and warmer climates. Process-based peatland eco-hydrology modelling could provide such capacity. However, such modelling is thus far limited due to lack of prognostic WTD dynamics and poor representation of WTD feedbacks to peatland biogeochemistry. We aimed at using basic processes for water and O_2 transport and their effects on ecosystem water, C and nutrient (nitrogen, phosphorus) cycling to model the effects of seasonal and interannual variations of WTD on surface energy exchange, water stress and net ecosystem CO_2 exchange across contrasting peatlands under variable weather conditions. For this purpose we tested a process based ecosystem model *ecosys* under contrasting precipitation in a tropical drained Indonesian bog from a drier El-Niño year 2002 to a wetter year 2005 and in a boreal pristine Western Canadian fen from a wetter year 2004 to a drier year 2009.

WTD was modelled from hydraulically-driven water transfers controlled vertically by precipitation (*P*) vs. evapotranspiration (*ET*), and laterally by discharge vs. recharge to or from an external reference WTD (WTD_x). These transfers caused WTD drawdown and soil drying to be modelled during drier vs. wetter seasons and years in the tropical peatland, which reduced *ET* and caused plant water stress. WTD drawdown initially increased net ecosystem productivity (NEP) in the tropical peatland by increasing gross primary productivity (GPP) facilitated by improved plant nutrient (phosphorus) availability and uptake due to rapid mineralization in better aerated peats. This better aeration also enhanced microbial O_2 availability and energy yields that increased ecosystem respiration (R_e). When WT fell below a threshold of ~1.0 m below the hollow surface, increased R_e along with

reduced GPP from plant water stress reduced NEP. Negative NEP modelled and measured in this drained tropical peatland indicated that it was a large C source. Our undrained model projection showed that this peatland would have been a much smaller source of C had it not been drained.

Gradually declining *P* to *ET* ratio in the boreal fen peatland caused WTD drawdown and peat drying from 2004 to 2009. Reduction in lateral recharge and increase in lateral discharge from the wettest to the driest year modelled from increasing WTD_x also contributed to this WTD drawdown simulating watershed-scale drying effects on fen hydrology. When WT fell below a threshold of ~0.35 m below the hollow surface, intense drying of mosses caused reduction in late growing season ecosystem *ET*. However, rapid mineralization in better aerated peat improved plant nutrient (nitrogen) availability and uptake that increased vascular and hence ecosystem GPP. Improved microbial O_2 availability and energy yields also increased R_e in better aerated peats. Similar increases in GPP and R_e with WTD drawdown, therefore, caused no net WTD drawdown effects on NEP. Our drainage projection showed that this peatland NEP would decline should WT fell below a threshold of ~0.45 m below the hollow surface due to reduced GPP from both vascular plant water stress and moss drying along with continued increase in R_e.

This study showed that non-linear interactions between peatland hydrology and ecology across contrasting peatlands can be modelled by adequately simulating dynamic WTD and its effects on peatland biogeochemistry and physiological ecology. The insights gained from this study would aid peatland C monitoring, assessing and restoration initiatives predicting how these C stocks would behave under future drier and warmer climates. This modelling can also provide a platform for scaling up peatland C modelling to regional, continental and/or global scale which is the major challenge current peatland C modelling community is facing.

PREFACE

Chapter 2 of this thesis has been submitted with revisions to *Journal of Geophysical Research-Biogeosciences* as M. Mezbahuddin, R.F. Grant, and T. Hirano, "How hydrology determines seasonal and interannual variations in water table depth, surface energy exchange and water stress in a tropical peatland: modelling vs. measurements".

Chapter 3 of this thesis has been published as M. Mezbahuddin, R.F. Grant, and T. Hirano, "Modelling effects of seasonal variation in water table depth on net ecosystem CO2 exchange of a tropical peatland", *Biogeosciences*, vol. 11, issue 3, 577-599.

In both of the publications, I was responsible for the research concept formation; modelling experiment layout, model input collections and model runs; and analyses and evaluation of modelled outputs against measurements as well as the manuscript composition. R.F. Grant was the supervisory author and was involved with research concept formation, model development, modelling supervision and manuscript composition. T. Hirano was the principal investigator of the field project in which measurements of eddy covariance fluxes, soil water contents and WTD used for model evaluation were taken.

ACKNOWLEDGEMENTS

I would like to express my gratitude to my supervisor Dr. Robert Grant, Professor of Department of Renewable Resources, University of Alberta for his excellent guidance and support throughout my PhD research. I would like to thank Dr. Takashi Hirano, Professor, Hokkaido University; and Dr. Lawrence B. Flanagan, Professor, University of Lethbridge for providing the field data used for model evaluation in this thesis. I also thank my supervisory committee members Dr. Victor Lieffers, Professor and Chair, Dr. David Chanasyk, Professor, and Dr. Uwe Hacke, Associate Professor and Canada Research Chair, Department of Renewable Resources, University of Alberta; Dr. Suzanne Bayley, Professor, Department of Biological Sciences, University of Alberta; and Dr. Gary Kachanoski, President and Vice-Chancellor, Memorial University of New Foundland and Labrador for providing their invaluable inputs along my PhD research. I am also thankful to Dr. Nigel Roulet, Professor and Chair, Department of Geography, McGill University and Dr. Vincent St. Louis, Professor, Department of Biological Sciences, University of Alberta for their time and efforts in examining this thesis. I would like to thank NSERC Discovery Grant and FGSR of University of Alberta for funding this research. I would also thank University of Alberta and Compute Canada for providing computing resources for this research. Thanks to AsiaFlux and Fluxnet Canada Research Networks for providing platforms for data sharing which got this research going. I also thank academic and support staffs of Renewable Resources family for their supports throughout my graduate study.

Personally I am grateful to my lovely wife Manjila Shahidi who has been outstanding in supporting me throughout and sharing all the pains while I used to be exhausted of working. I am also thankful to my sweet daughter ‘Saafteeha’ who made my life ever charming. Special thanks and gratitudes to Taibul Azam Maznu and Dr. Fardausi Akhter Shathi, without who it would not be possible for me to come this far. I would be ever grateful to my parents and all other family members who supported me throughout my academic and personal life so far. Heartfelt thanks to all of my friends and well-wishers for always being there for me.

TABLE OF CONTENTS

LIST OF TABLES

LIST OF FIGURES

Chapter 1 : Introduction

1-1. Modelling water table depth effects on peatland CO_2 exchange

Globally, peatlands store approximately 400-600 Pg of carbon (C) which is about 20-33% of global soil C (Lappalainen 1996, Tarnocai 2006, Yu et al. 2010, Page et al. 2011, Rydin and Jeglum 2013). Northern boreal peatlands comprise 75-80% of this C storage while tropical peatlands comprise 10-15% (Andriesse 1988, Lappalainen 1996). Canada has one of the largest boreal peat C storages with about 143 Pg (Tarnocai et al. 2006). On the other hand, 65% of total tropical peat C is stored in Indonesia (Tarnocai et al. 2006, Page et al. 2011). Northern boreal peatlands are broadly classified into bogs and fens based on hydrology whereas tropical peatlands are mostly bog peat swamps (Tarnocai et al. 2006). Bogs are the peatlands that are mainly precipitation-fed whereas fens can be affected by water from surrounding mineral soils. Boreal peatlands are dominated or co-dominated by mosses, sedges, shrubs and trees as opposed to their tropical counterparts that are dominated by trees and devoid of mosses (Page et al. 2006).

Northern boreal peatlands have been accumulating C at a rate of 19-24 g m^{-2} yr^{-1} (Flanagan and Syed 2011) over more than 6,000 years (Zoltai and Vitt 1990). This accumulation has been facilitated by slower decomposition under saturated soil conditions resulting from above ground or shallow WT. However, these peatlands are projected to shift from sinks to sources of atmospheric CO_2 as a result of water table depth (WTD) drawdown and consequent improved peat aeration and more rapid decomposition due to increased frequency and intensity of droughts during the upcoming millennium (Frolking et al. 2011). Although tropical peat C storage is much smaller than the northern boreal storage, it is much older (>26,000 years) than that in boreal peatlands (Page et al. 2004). Moreover, tropical peatlands have been accumulating C at a faster rate of ~56 g C m^{-2} yr^{-1} (Page et al. 2004) due to higher productivity enhanced by

warmer weather and year round growing season. However, WTD drawdowns due to higher frequencies of climate extremes like El-Niño and large-scale artificial drainage to promote agriculture have been causing shifts in C balance of these peatlands during recent decades. Drier weather-driven WTD drawdowns have already switched these peatlands from C sink (e.g. ~56 g C m^{-2} yr^{-1}) to large C sources (~174 g C m^{-2} yr^{-1}) (Hirano et al. 2012). Artificial drainage in these peatlands has added CO_2 emissions of ~250 g C m^{-2} yr^{-1} per 0.1 m of WTD drawdown (Couwenberg et al. 2010). Projections of future drying and further WTD drawdown in these peatlands by the end of this century (Li et al. 2007) make the situation even more alarming. Consequently reducing CO_2 emissions from these peatlands and restoring their C sink potential have been the key foci of international C monitoring and assessment initiatives like REDD+ (Reducing Emissions from Deforestation and forest Degradation).

However, conservation of peat C storage under future drier and warmer climates requires improved understanding and predictive capacity of hydrological controls on peatland ecology and hence C balance. Experience from short-term peatland restoration projects has also indicated the need for long-term projection on how hydrology affects peat C processes before undertaking long-term projects for restoring peatland C functioning (Page et al. 2009).

1-2. Present status and challenges of modelling WTD effects on peatland CO_2 exchange

Despite the need for improved predictive capacity of WTD effects on peatland C balance, peatland C processes are poorly represented in current global C models (Limpens et al. 2008). The major reason behind this is the peatland-specific nature of hydrological feedbacks to peatland C processes that makes it difficult to generalize these feedbacks across peatlands. Poor understanding and consequent inadequate representation of these feedbacks in C models further aggravates this poor representation (Waddington et al. 2015).

Hydrological effects on peatland net ecosystem productivity (NEP) are mediated by WTD variation that affects peatland respiration (R_e) and gross primary productivity (GPP) through its effects on peat moisture content, aeration, and consequent root/rhizoid and microbial oxidation-reduction reactions, energy yields, nutrient availability, water and nutrient uptake and growth (Grant et al. 2012b). WTD effects on peatland R_e and hence NEP, however, vary across peatlands depending upon climate, peat moisture retention and peat type. A given WTD drawdown can cause greater peat CO_2 emissions and hence greater R_e in warmer tropical peats than in cooler boreal peats (Page et al. 2009). Moreover, peats with low moisture retention capacity facilitate more rapid aeration than those with high moisture retention capacity, thus causing more increase in R_e for similar WTD drawdowns (Parmentier et al. 2009, Sulman et al. 2009, Cai et al. 2010, Sulman et al. 2010). Besides, peats formed by *Sphagnum* mosses degrade at rates slower than those formed from remains of vascular plants (Moore and Basiliko 2006) and hence would experience less increase in microbial decomposition (Updegraff et al. 1995) and hence R_e with WTD drawdown than would sedge, reed or woody peats.

WTD can also affect peatland NEP by affecting GPP. WTD effects on peatland GPP again vary across peatlands depending upon interactions among peat and vegetation water and nutrient cycles. WTD drawdown can cause increased root O_2 and nutrient availability and hence improved root growth and uptake that in turn raises vascular GPP (Macdonald and Lieffers 1990, Choi et al. 2007, Murphy et al. 2009, Sulman et al. 2009, Flanagan and Syed 2011, Ballantyne et al. 2014, Peichl et al. 2014). However, mosses can experience drying and hence reduced GPP due to low water uptake by shallow rhizoids which mainly colonize near surface peat layers that can drain and dry quickly due to WTD drawdown (Lafleur et al. 2005, Riutta et al. 2007, Dimitrov et al. 2011).

These WTD effects on R_e and GPP for a given peatland ecosystem can also be self-compensating and non-linear. When WT falls to a threshold level, capillary rise from deeper WT can no longer adequately recharge the near surface peat layers that cause desiccation of those layers. During periods when WT is at this level, increase in heterotrophic respiration (R_h) in newly aerated deeper peat layers can be partially or fully offset by reduction in R_h in near surface desiccated peat layers (Dimitrov et al. 2010a, Hirano et al. 2014, Peichl et al. 2014). This near surface peat desiccation due to WT falling below threshold can also suppress root water uptake from these desiccated layers and hence can cause water stress in deep-rooted vascular plants. This water stress can either partially or fully offset increases in vascular GPP due to improved root growth and nutrient availability stimulated by enhanced aeration with WTD drawdown (Sonnentag et al. 2010, Peichl et al. 2014). This threshold WTD, however, varies across peatlands depending upon peat moisture retention and rooting depth of the peat-specific vegetation. Peat with low moisture retention capacity and shallow rooted vegetation can have a shallower WTD threshold than peat with high moisture retention capacity and deep rooted vegetation (Lafleur et al. 2005, Sonnentag et al. 2010, Peichl et al. 2014).

Process-based ecosystem models can provide us with means of coupling and testing basic mechanisms behind the WTD effects on net ecosystem CO_2 exchange across peatlands described above. To accomplish this, a model should explicitly represent aerobic and anaerobic oxidation-reduction reactions, coupled with aqueous and gaseous transfers of their reactants and products, within robust and comprehensive schemes for water, C and nutrient cycling among soil-plant-atmosphere systems. These schemes require modelling WTD dynamics, soil moisture retention characteristics, gas transport through soil, differential substrate quality for microbial degradation and hydrolysis (e.g. labile vs. recalcitrant), nutrient transformations driven by these reactions,

and microbial and plant nutrient uptake (Grant et al. 2012b). In line with these requirements, significant efforts have been made so far to test process-based models such as DLEM (Tian et al. 2010), Wetland-DNDC (Zhang et al. 2002), ORCHIDEE (Krinner et al. 2005), MWM (St-Hilaire et al. 2010), LPJ (Sitch et al. 2003, Gerten et al. 2004), PCARS (Frolking et al. 2002), Biome-BGC (Bond-Lamberty et al. 2007), SiBCASA (Schaefer et al. 2008), BEPS (Sonnentag et al. 2008), Forest-DNDC (Kurbatova et al. 2009), TECO (Weng and Luo 2008), PEATLAND (Van Huissteden et al. 2006) and SiB (Baker et al. 2008) in simulating hydrological feedbacks to peatland C processes across northern boreal peatlands.

However, most of these models (1) either do not have prognostic WTD dynamics that prevent these models from simulating a continuous anaerobic zone below WT (Baker et al. 2008, Schaefer et al. 2008, Tian et al. 2010), or (2) do not simulate peat saturation since any water in excess of field capacity is drained in these models (Gerten et al. 2004, Krinner et al. 2005, Weng and Luo 2008). Moreover, instead of explicitly simulating the above-described hydrological and biological interactions between peat aeration and biogeochemistry, most of these models use scalar functions of soil moisture contents to inhibit R_e and GPP in low or high moisture conditions (Frolking et al. 2002, Zhang et al. 2002, Bond-Lamberty et al. 2007, St-Hilaire et al. 2010, Sulman et al. 2012). Consequently, these peatland C models failed to simulate decreases in GPP and R_e due to shallow WTD periods while modelling WTD effects on peatland C processes across Northern US and Canadian peatlands (Sulman et al. 2012). Furthermore, the approach of using scalar functions to simulate moisture limitations to GPP and R_e requires site-specific parameterization of these functions thereby making this approach less suitable when scaling up across different peatlands in different climates. In contrast, a general purpose terrestrial ecosystem model *ecosys* included site-independent algorithms representing all the processes

representing hydrological feedbacks to peatland CO_2 exchange described above that enabled the model to successfully simulate WTD effects on R_e and GPP of a northern boreal Canadian bog (Dimitrov et al. 2011) and a boreal US fen (Grant et al. 2012b).

To date, all of these models have been tested in northern boreal/temperate peatlands. Process-based modelling to understand the fate of vulnerable tropical peatland C storage due to WTD drawdown under drier climates is thus far limited if not non-existent. Since tropical peatlands are very different than boreal peatlands in climate, peat forming materials, and vegetation, the interactions between WTD and tropical peatland C processes would be very different. So, testing a process-based peatland C models that is built upon our understandings of northern boreal and temperate peatland eco-hydrology in tropical peatlands would provide us with a robust test of adequacy of our understanding and modelling hydrological feedbacks to peatland C processes.

1-3. Objective and rationale

Given the research need, we therefore deploy the process-based ecosystem model *ecosys* to simulate the effects of WTD variations on seasonal and interannual variations in net ecosystem CO_2 exchange of two contrasting forested peatlands – an Indonesian drained tropical bog (Hirano et al. 2007) and a pristine Western Canadian boreal fen (Syed et al. 2006, Flanagan and Syed 2011). These two peatlands are situated in two of the hotspots of tropical and boreal peatlands and are very different in climate (mean annual temperature: 26.3 vs. 2.1°C; total annual precipitation: 2600 vs. 504 mm), peat type (bog vs. fen), peat forming materials (woody vs. moss peat), vegetation (tree dominated vs. tree, shrub and moss co-dominated) and disturbance (drained vs. pristine) (Syed et al. 2006, Hirano et al. 2007). Testing the same model *ecosys* against site measurements at these two contrasting peatlands would thus be an important

test of the versatility of its algorithms representing the basic processes affecting peatland eco-hydrology. Such a test will allow us to determine whether our current understanding of peatland water, nutrient and C interactions is sufficiently robust to capture complex WTD effects on peatland R_e and GPP over a wide range of climates and peat types. Since the same algorithms in *ecosys* successfully simulated two other boreal peatlands (Dimitrov et al. 2011, Grant et al. 2012b) that are different than these peatlands in peat type, climate and vegetation, the present study would thus also be a continuation of finer spatial and temporal scale testing of this model across peatlands that would lead to a platform for larger spatial and temporal scale peatland C modelling.

1-4. Overview of the studies

To fulfill the objective we deployed *ecosys* to simulate seasonal and interannual variations in WTD, peat water contents, surface energy exchange and net CO_2 exchange over the two contrasting peatlands under study. These simulations were based on peat specific inputs of vertical and lateral model boundary conditions; peat physical, chemical, biological and hydrological properties; and plant functional types from available measurements at the sites and/or at similar sites. The modelled outputs for ecosystem net CO_2 and energy exchange, soil water contents and WTD were then tested against measurements from eddy covariance (EC) towers and automated surface chambers; water level logger and potentiometer; time domain reflectometry (TDR); and other biometric techniques collected at flux and micrometeorological stations of AsiaFlux and Fluxnet Canada Research Networks installed at the tropical (Hirano et al. 2007) and the boreal peatland (Syed et al. 2006, Flanagan and Syed 2011) sites respectively. After successful corroboration, the modelled outputs along with available measurements were used to analyze possible mechanisms behind WTD effects on surface energy exchange and net

CO_2 exchange of these two peatlands. Any disagreements between modelled outputs and measured parameters were also examined for plausible reasons.

Chapter 2 of this thesis aims at using basic processes for water and O_2 transport and their effects on ecosystem water, carbon and nitrogen cycling to model seasonal and interannual variations of WTD and surface energy exchange. We tested these processes in the process-based model *ecosys* in the drained tropical Indonesian peatland from an El-Niño year 2002 to a wetter year 2005. WTD was modelled from hydraulically-driven water transfers controlled vertically by precipitation (*P*) vs. evapotranspiration (*ET*), and laterally by discharge vs. recharge to or from an external reference WTD. These transfers caused WTD drawdown and soil drying to be modelled during dry seasons, which reduced *ET* and increased Bowen ratio (β) by lowering stomatal conductance. More pronounced dry seasons in drier years 2002-2004 vs. wetter year 2005 caused deeper WTD, more intense peat drying, and greater plant water stress. These modelled trends of effects of seasonal and interannual variations in WTD on those of *ET* and β were well corroborated by the site measurements.

Chapter 3 aims at modelling effects of seasonal variation in WTD on NEP of the tropical peatland. Both the modelled and the EC-gap filled NEP suggested that the peatland was a C source during rainy seasons with shallow WTD, C neutral or a small sink during early dry seasons with intermediate WTD and a substantial C source during late dry seasons with deep WTD from 2002 to 2005. There was also a gradual increase in modelled and EC-gap filled NEP from the driest year of 2002 with deepest WTD to the wettest year of 2005 with shallowest WTD. These effects of seasonal and interannual variations in WTD on those of NEP in this tropical peatland were modelled by adequately simulating (1) poor aeration in wet soils during shallow WTD which caused slow nutrient (predominantly phosphorus) mineralization and

consequent slow plant nutrient uptake that supressed GPP and hence NEP (2) better soil aeration during intermediate WTD which enhanced nutrient mineralization and hence plant nutrient uptake, GPP and NEP and (3) deep WTD which supressed NEP through a combination of reduced GPP due to plant water stress and increased ecosystem respiration (R_e) from enhanced deeper peat aeration.

Chapter 4 describes modelling peat water content, WTD and surface energy exchange in boreal Western Canadian peatland. Our modelling showed that incorporating a van Genuchten type (VGM) (Van Genuchten 1980) soil moisture retention equation into *ecosys* enabled a better simulation of peat water retention in this boreal peatland than did the existing version of *ecosys* which used a modified version of a Campbell model (MCM) (Campbell 1974) . With this improved peat moisture simulation, *ecosys* simulated a gradual drawdown of growing season (May-August) WTD that was measured over the site from 2004-2009. This simulation was achieved by adequately modelling gradually lower P to ET ratio and gradually slower net lateral water gain from a reference external WTD representing catchment hydrological effects characteristic of a fen peatland. This gradual WTD increase from 2004-2009 caused ecosystem drying thereby reducing ET and increasing β in late growing seasons (mid-July to mid-August) of 2008 and 2009 which was modelled mainly through moss drying. However, reduction in ET and increase in β over May-June period as evident in EC-gap filled site measurements could not be modelled and explained by our eco-hydrology modelling.

Chapter 5 includes modelling WTD drawdown effects on NEP of the northern boreal peatland. WTD drawdown from 2004 to 2009 increased modelled and EC-derived R_e at seasonal and annual time scales. This increase was modelled by adequately simulating improved peat aeration which increased microbial O_2 availability and energy yields. Warmer weather and

consequent warmer peat also caused increases in both modelled and EC-gap filled R_e. However, this warming effect on R_e was more severe with deeper than shallower WTD further indicating significance of WTD drawdown on increasing R_e at this boreal fen. Beside R_e, WTD drawdown also caused increases in modelled and EC-derived growing season and annual GPP from 2004-2009. This increase was modelled by simulating increased nutrient (mainly nitrogen) availability due to enhanced mineralization in better aerated peat, and consequently improved root nutrient uptake, foliar nutrient status and hence CO_2 fixation. Although modelled non-vascular GPP decreased with this WTD drawdown, increased in vascular GPP more than fully offset this decrease. Confounding effects of WTD drawdown and temperature on R_e and GPP as well as similar increases in R_e and GPP with WTD drawdown left no net effects of WTD drawdown on modelled and EC-gap filled NEP at this boreal peatland. A modelled projection of drainage effects on C exchange, however, indicated that further WTD drawdown would cause reduction in NEP by increasing R_e and limiting GPP.

Chapter 6 describes synthesis of the findings of the study. It also presents the test of suitability of VGM model for simulating the tropical peatland water content. VGM similarly well simulated peat water contents at the tropical peatland as the MCM indicating its ability to simulate wide range of peat moisture retention.

Chapter 2 : How Hydrology Determines Seasonal and Interannual Variations in Water Table Depth, Surface Energy Exchange and Water Stress in a Tropical Peatland: Modelling vs. Measurements

2-1. Introduction

Tropical peatlands in Southeast Asia have been accumulating and storing thick deposits of soil carbon (C) as peat blankets (e.g. 9 m) over a large area (2.48×10^5 km^2) for thousands of years (e.g. > 26,000 years) (Page et al. 2004, 2011). However these large C stores have recently been reported to be large sources of atmospheric CO_2. For instance pristine Indonesian peatlands, which have been accumulating C at a rate of about 56 g m^{-2} yr^{-1} over more than last 26,000 years, were reported to be a net C source of about 174 g C m^{-2} yr^{-1} over a period of 5 years (2004-05 to 2008-09) (Hirano et al. 2012). The dramatic shift of these tropical peatlands from being net sinks to large sources of C was caused by rapid oxidative peat decomposition stimulated by water table depth (WTD) drawdown as a result of recent increases in intensity and frequency of weather extremes like El-Niño (Dommain et al. 2011). WTD in Southeast Asian peatlands has been further deepened by large-scale artificial drainage for facilitating agriculture (Hirano et al. 2012) that emitted additional CO_2 at a rate of ~250 g C m^{-2} yr^{-1} per 0.1 m of drainage-induced WTD drawdown (Couwenberg et al. 2010). Apart from triggering peat decomposition, deep water table (WT) towards the end of prolonged and intense dry seasons also caused reductions in canopy stomatal conductance (g_c) of tropical peatland vegetation (Hirano et al. 2015). Since these tropical peatlands are tree-dominated reductions in g_c contributed to the reductions in evapotranspiration (*ET*) and hence gross primary productivity (GPP) (Hirano et al. 2007, 2012, 2015). So, WTD drawdown resulting from dry weather conditions and artificial drainage not only hastened peat decomposition but also hindered peat accumulation through

reduced GPP and hence net primary productivity (NPP) in these tropical peatlands. Therefore, to avoid further loss of these huge C stores and possibly to restore peat accumulation, it is imperative to have an improved understanding and a consequent better predictive capacity of seasonal and interannual variations in WTD and their effects on eco-hydrology and hence C balance of tropical peatlands.

Tropical peatlands are ombrotrophic bogs and so the seasonal WTD variation in those peatlands is predominantly determined by the balance between precipitation (P) and ET, and the lateral discharge (Q_w). During the rainy seasons P frequently exceeds ET that results in very shallow or sometimes above-ground WT in most of the pristine tropical peatlands (Takahashi et al. 1999). However, the surplus water generates a large Q_w in the forms of surface run-off and sub-surface discharge. Surface run-off in these peatlands is mainly governed by peat surface gradient at a watershed scale and by hummock-hollow micro-topography at micro- and/or meso-scale (Page et al. 2009). Sub-surface lateral discharge mainly occurs through near surface layers with high drainable porosity (Page et al. 2009, Dommain et al. 2010). A shallower WTD in rainy seasons can create a large hydraulic gradient between the peatland WT and that of an adjacent landscape which can drive lateral discharge through both peat matrices and macropores. During subsequent dry seasons, however, ET in access of P causes the WT to fall about 0.5 m below the surface and ceases such surficial and lateral subsurface discharge in pristine tropical peatlands (Page et al. 2009). The seasonality of WTD also shows interannual variation with relatively deeper WTD during prolonged dry seasons compared to that during shorter dry seasons in pristine Southeast Asian peatlands (Takahashi et al. 1999, Hirano et al. 2015). In addition, artificial drainage causes consistently deeper WT throughout the year than that in pristine tropical peatlands (Hirano et al. 2015). Therefore, prognostically simulating WTD variation in

tropical peatlands requires adequate representation of i) seasonality of balance between *P* and *ET*, ii) seasonality of lateral drainage as affected by both peat matrix and rapid macropore flow, and iii) artificial drainage for drainage-affected tropical peatlands.

Seasonality in tropical peatland *ET* does not only affect but is also affected by the seasonality in WTD. When WT in a tropical peatland falls below a certain threshold level during late dry seasons low water retention capacity of macroporous near-surface peat layers causes inadequate vertical recharge through capillary rise from the WT. This in turn causes near surface peat desiccation and a consequent reduction in g_c and *ET*, and hence a concurrent increase in Bowen ratio (β = sensible heat (*H*)/latent heat (*LE*)) (Hirano et al. 2005, 2015). An increase in β indicates stomatal limitation to transpiration and hence ecosystem drying due to vegetation water stress. However, the intensity of this vegetation water stress demonstrates interannual variation depending upon the intensity and duration of dry seasons. The reduction in g_c and a concurrent increase in β are generally more pronounced in drier dry seasons of El-Niño years when the WT falls well below a certain level at which tropical peatland trees start to experience water stress (Hirano et al. 2015). This WTD threshold, however, varies with different rooting depth of vegetation resulting from either adaptation to wet soils or a disturbance e.g. drainage. For instance, shallow-rooted trees in pristine Indonesian peatlands experienced water stress when WTD fell below 0.4 m from the hollow surface (Hirano et al. 2015). On the contrary, tree roots could grow into newly aerated deeper layers in a surrounding drained Indonesian peatlands and hence those trees did not experience water stress until WT fell below 0.9 m from the hollow surface (Hirano et al. 2015).

Given the importance of interactions between *ET* and WTD in controlling tropical peatland productivity and hence C balance, a tropical peatland model requires a prognostic water

transfer scheme that determines WTD coupled with algorithms for root growth and water uptake as affected by WTD that determine transpiration and hence GPP. Root growth and water uptake are governed by soil and root O_2 and water status, so that these algorithms in the model should be coupled with those representing O_2 and water transport through soils and roots as affected by WTD (Grant et al. 2012b). Such coupling of hydrological processes with ecological processes enabled a general purpose process-based terrestrial ecosystem model *ecosys* to successfully simulate seasonal and interannual variations in WTD and surface energy exchange of a boreal fen peatland (Grant et al. 2012b), a boreal bog peatland (Dimitrov et al. 2010b), and a boreal peat-mineral soil transitional ecotone (Dimitrov et al. 2014). Building upon the success of those studies, the present study aims to test whether the same algorithms in *ecosys* could simulate seasonal and interannual variations in WTD and surface energy exchange under very different climatic, edaphic and ecological conditions in the Palangkaraya Drained Peat Swamp Forest (PDPSF) of Central Kalimantan, Indonesia (Hirano et al. 2005, 2015).

2-1.1. Rationale of modelling seasonal and interannual variations in tropical peatland WTD and surface energy exchange

Given the effects of WTD drawdown from dry weather and artificial drainage on C storage, predictions of further drier weather by 3 global circulation models (GCMs) over tropical Southeast Asian peatlands by the end of this century (Li et al. 2007) make it even more important to have improved predictive capacity for how these peatlands will behave in the future. Despite the immense importance, research into modelling the interaction between hydrological and ecological processes in tropical peatlands is still very limited. Our modelling of seasonal and interannual variation in WTD and its effects on surface energy exchange of tropical peatland is intended to fill this research gap. Moreover, such modelling will provide us with an excellent

opportunity to rigorously examine whether our current understanding of peatland eco-hydrological interaction, that are currently based solely on studies from northern temperate/boreal peatlands, are adequate to explain the interaction among hydrology, WTD and surface energy balance in tropical peatlands. Therefore, the understanding from our modelling will improve our predictive capacity of hydrological controls on ecosystem productivity over a wide range of peatlands (e.g. boreal to tropical). This in turn will largely improve the precision of our projections of peatland eco-hydrology when done at a regional or global spatial scale and a much longer temporal scale e.g. from century to millennium.

2-1.2. Hypotheses

Hypothesis 1: Hydrological controls on seasonal and interannual variations in tropical peatland WTD

A gradual wetting trend from an El-Niño year 2002 to a wetter year 2005 was evident in gradually higher annual and dry season (May-October) *P* measurements from 2002-2005 by Hirano et al. (2007) at PDPSF that caused gradually shallower dry season WTD and consequent less soil drying from 2002-2005 (Hirano et al. 2007, 2012, 2015). We hypothesize that this interannual variation in seasonality of WTD could be explained by changes in influxes vs. effluxes of water in vertical and lateral directions through surface and subsurface boundaries respectively that could be modelled from basic hydrological processes. These processes included vertical water fluxes between modelled grid cells and the atmosphere from *P* inputs and *ET* calculated by coupling atmospheric moisture demand driven by surface energy balances with hydraulically-driven water uptake driven by water potential gradients (e.g. soil, root and canopy water potentials) through a series of resistances (e.g. soil, root and stomatal resistances). These processes were coupled with ones for lateral water fluxes between modelled grid cells in *ecosys*

and the adjacent watershed governed by hydraulic gradients between modelled WTD and an external reference WTD (WTD_x) over a specified distance (L_t) in a Darcy's equation.

Hypothesis 2: WTD effects on seasonal and interannual variations in surface energy exchange and water stress

We also hypothesize that these coupled hydrological processes could explain greater plant water stress with deeper WT and consequent greater peat drying during prolonged and intense late dry seasons (August-October) in 2002-2004 than during a less pronounced late dry season in 2005. Explanation of plant water stress requires that root water uptake modelled in *ecosys* be fully coupled with a shoot-root C transfer scheme in which vertical and lateral root growth is affected by root O_2, water and nutrient status through the soil profile. Soil O_2 concentrations, modelled in *ecosys* from convective-dispersive transport, transition sharply between aerobic and anaerobic values with changes in soil water content caused by changes in WTD (Grant et al. 2012b). This transition controls root access to O_2 and hence vertical root distribution in *ecosys* (Grant et al. 2009b). WTD drawdown from rainy to dry seasons thus causes modelled roots to follow the receding WT and grow into deeper aerobic layers with improved O_2 status. This in turn increases root growth and hence root water uptake from deeper, wetter peat layers. However, when WTD falls below certain threshold level towards the end of prolonged and intense dry seasons, vertical recharge of near surface layers through capillary rise from the deeper WT becomes inadequate. This causes near surface peat desiccation and suppresses root water uptake from these desiccated layers. Since most roots are in those desiccated near surface layers which remain unsaturated and consequently better oxygenated during most of the year, suppression of root water uptake from these layers more than fully

offsets the increase in deeper root uptake, thereby causing plant water stress reducing g_c and ET and raising β.

2-2. Methods

2-2.1. Model development

2-2.1.1. General

Ecosys is a general purpose terrestrial ecosystem model that successfully simulated 3D soil-plant-microbes-atmosphere water, energy, carbon and nutrient (nitrogen, phosphorus) schemes across peatlands (Dimitrov et al. 2010a, b, 2011, Grant et al. 2012b). Algorithms governing seasonal and interannual variations in WTD and surface energy exchange that are related to our hypotheses are described in the following sections. Necessary equations are listed and described in appendices A to H at the end of the chapter and are cited in the text within round brackets by a letter representing a particular appendix followed by the equation number.

2-2.1.2. Water table depth (WTD)

The WTD in the process-based ecosystem model *ecosys* is the position where lateral water flux is in equilibrium with the difference between vertical influxes and effluxes. The lateral sub-surface boundary condition governs the lateral flow in *ecosys* that is defined by a specified external water table depth (WTD_x) and a specified lateral distance (L_t) over which lateral sub-surface water flow occurs (Fig. 2-1). This WTD_x represents average WTD of the surrounding watershed with which modelled boundary grid cells exchange water. The rates of the lateral water fluxes are governed by the hydraulic gradient between the WTD within the modelled grid cell and WTD_x over L_t in a Darcy's equation, and by macropore and matrix hydraulic conductivity of the soil layer in which these water transfers occur (Fig. 2-1). Thus when WTD within modelled grid cells is shallower than WTD_x, discharge through the model

lateral boundary occurs and when WTD falls below WTD_x recharge into the modelled grid cells occurs (Fig. 2-1). This modelled WTD in *ecosys* is calculated from the uppermost position in a soil profile to the top of the saturated zone below which air-filled porosity is zero (C1). A negative WTD output from *ecosys* represents depth below the surface of a modelled soil profile. The WTD within the modelled grid cells in *ecosys* is not therefore prescribed, but rather controls, and is controlled by, vertical surface boundary fluxes, and by lateral surface and subsurface boundary fluxes (A1-B12).

2-2.1.3. Vertical water fluxes

Vertical surface boundary influxes from *P* are provided as inputs to the model, as are solar radiation, air temperature, humidity and wind speed used to drive energy balance calculations. These calculations drive vertical surface boundary effluxes of *ET* from canopy surfaces (E2-E3), and of evaporation (*E*) from residue (A6) and soil surfaces (A7). These effluxes are coupled with subsurface water transfers through root (F1-F7) and soil (B1-10) profiles within the modelled grid cells. Vertical and lateral subsurface water flows through soil matrices within the modelled grid cells (B2) are calculated from the Richard's equation using total soil water potentials (ψ_s) (matric + osmotic + gravimetric) of adjacent cells if both source and destination cells are either saturated or unsaturated (B3), or from the Green-Ampt equation using ψ_s beyond the wetting front of the unsaturated cell if either cell is saturated (B4-B5) (Grant et al. 2004). Vertical and lateral subsurface water flows can also occur within the soil profiles through macropores using Hagen-Poiseuille's theory for laminar flow in tubes (B6-B9), depending on inputs for macropore volume fraction (B10) (Dimitrov et al. 2010b).

2-2.1.4. Lateral water fluxes

Lateral surface runoff within the modelled grid cells and across lower surface boundaries is modelled using Manning's equation (A2) with surface water velocity (A3) calculated from surface geometry (A4) and slope (A5), and with surface water depth (A2) calculated from surface water balance (A1) using kinematic wave theory. Lateral subsurface flows from saturated boundary grid cells are calculated from their lateral hydraulic conductivities, hydraulic gradients from elevation differences between these grid cells and the WTD_x, and L_t (B11-B12).

2-2.1.5. Surface energy exchange

Vertical surface boundary effluxes from transpiration (T) (E3) are governed by canopy stomatal conductance ($g_c=1/r_c$, where r_c = canopy stomatal resistance) determined by equilibrating plant water uptake (U_w), calculated from gradients of ψ_s, ψ_r (root water potential) and ψ_c regulated by soil and root hydraulic resistances (Ω_s and Ω_r) in each rooted soil layer, with T calculated from canopy energy exchange within a soil-plant-atmosphere continuum (F7). Root growth used to calculate Ω_s and Ω_r in each plant population is calculated from its assimilation of the non-structural C product of CO_2 fixation (σ_C) (G8). Assimilation is driven by growth respiration (R_g) (G7) remaining after subtracting maintenance respiration (R_m) (G6) from autotrophic respiration (R_a) (G1) driven by oxidation of σ_C (G2-G5). This oxidation in roots may be limited by root O_2 reduction (G3), required to sustain C oxidation and nutrient uptake (G5). Reduction is driven by root O_2 demand, and constrained by root O_2 uptake controlled by concentrations of aqueous O_2 in the soil ($[O_{2s}]$) and roots ($[O_{2r}]$) (G4). Values of $[O_{2s}]$ are maintained by convective-dispersive transport of O_2 through soil gaseous and aqueous phases (H3, H5) and by dissolution of O_2 from soil gaseous to aqueous phases (H1). Values of $[O_{2r}]$ are maintained by convective-dispersive transport of O_2 through the root gaseous phase (H4) and by

dissolution of O_2 from root gaseous to aqueous phases (H2). This transport depends on species-specific values used for root air-filled porosity (aerenchyma) (θ_{pr}) (H5).

Reduced O_2 transport in saturated soils below the WT results in low [O_{2s}] (H5) and forces [O_{2r}] to rely mostly on the gaseous O_2 transfer through aerenchyma (H6). If this transport is inadequate, decline in [O_{2r}] slows root O_2 uptake (G4), R_a (G3) and R_g (G7) and hence root growth (G8). Low root growth decreases root density (G9-G10) and hence increases Ω_s and Ω_r (F4-F6) in those saturated layers below the WT. Consequently U_w (F2) from the soil layers below the WT is minimal in spite of high (e.g. near zero) ψ_s (F7) and low Ω_s (F3) if the value for aerenchyma is low. Thus modelled U_w is predominantly governed by the uptake from unsaturated layers above the WT where adequate ([O_{2s}]) favours root O_2 uptake (G4), R_a (G3), R_g (G7), growth (G8) and hence higher root density (G9-G10) and consequently lower Ω_r (F4-F6).

WTD drawdown hastens soil O_2 transport (H5), raising [O_{2s}] and hence root respiration (G3, G7), growth (G8) thereby increasing root density (G9-G10), decreasing Ω_r (B9-B13) and hence increasing U_w from newly aerated deeper soil layers. However, when WTD deepens past a certain point, inadequate capillary rise causes near-surface peat desiccation (B2-B5), reducing ψ_s and increasing Ω_s (F3), and hence decreasing U_w (F1-F2) from those layers. If the increase in U_w from newly aerated deeper layers cannot offset the decrease in U_w from desiccated near surface layers, a decrease in net U_w forces lower ψ_r, ψ_c (F7) and hence ψ_t (canopy turgor potential) (E7), g_c (E6) and ET (E3) to be calculated when equilibrating uptake with T (F7).

2-2.2. Modelling experiment

2-2.2.1. Site conditions

The *ecosys* algorithms for simulating hydrological effects on seasonal and interannual variations in WTD and surface energy exchange were tested against WTD, soil water contents (θ) and surface energy exchange measured by Hirano et al. (2005), Hirano et al. (2007) and Hirano et al. (2012) from 2002 to 2005 at an eddy covariance (EC) flux station over PDPSF (2°20′42″ S and 114°2′11″ E). The site is a tropical ombrotrophic bog peatland where the only source of water and nutrient input is through precipitation. These tropical bogs are mainly formed by tree roots, dominated by trees and generally devoid of bryophytes (Page et al. 2009). These peatlands were drained by excavating drainage canals during 1996-97 as a part of land development for agriculture in a former Mega Rice Project, Central Kalimantan, Indonesia [*Page et al.*, 2009]. Peat depth around the flux station site was around 4 m. More detailed description of the peat characteristics, vegetation and management history of the site can be found in Hirano et al. (2007), Jauhiainen et al. (2008) and Page et al. (2009).

2-2.2.2. Field datasets

Hourly *LE*, *H* and CO_2 fluxes were measured by Hirano et al. (2005) and Hirano et al. (2007) from a combination of EC and storage fluxes using a micro-meteorological approach at the flux tower established over PDPSF in November 2001. Flux data during rain and stable air conditions at night (determined by a friction velocity (u*) of below 0.17 m s^{-1}) were screened out by Hirano et al. (2005) and Hirano et al. (2007) to maintain the data quality. The resultant gaps in flux data were filled by using look up tables as described in Hirano et al. (2005) and Hirano et al. (2007).

Hourly weather variables (e.g. solar radiation, wind speed, relative humidity, air temperature, precipitation etc.) were also measured at the flux station. Hourly net radiation (R_n) was calculated from measured incoming and outgoing long wave and shortwave radiation (Hirano et al. 2005). θ was measured hourly at a depth from 0-0.2 m at 3 points in a hummock (Hirano et al. 2007). Hourly WTD measurement at the site was started in April 2004 as reported in Sundari et al. (2012) and Hirano et al. (2012). However, monthly WTD measurement at the site was reported by Hirano et al. (2012) from June 2002. All WTD measurements were performed at a water level logger installed at 10 m from the flux tower by setting the zero position of the WT at the level of a hollow surface.

2-2.2.3. Model run

The micro-topography modelled in *ecosys* included one hummock and one hollow grid cell of same dimension (1 m×1 m) between which gas, water, solute and heat were transferred.. The surface of the hollow grid cell was 0.15 m lower than that of the hummock grid cell to represent the average site micro-topography described by Jauhiainen et al. (2008) (Fig. 2-1). To best represent the vertical peat profile in the actual site as described by Jauhiainen et al. (2008), the 0-0.25 m depth of the modelled hummock profile had dry bulk density for less decomposed fibric layers measured by Takakai et al. (2006) at drained peat swamp forests surrounding our study site (Fig. 2-1). Dry bulk densities for the modelled transitional hemic peat layer of 0.25-0.4 m and well decomposed sapric peat layers > 0.4 m depth were obtained from Jauhiainen et al. (2012b) measured for drained peatlands surrounding our study site (Fig. 2-1).

A soil moisture retention curve was constructed by using site measured θ and assuming measurement depths above WTD as soil water matric potentials to derive θ at field capacity and permanent wilting point ($\theta_{v,fc}$ and $\theta_{v,wp}$ used as inputs for the fibric layers of 0-0.25 m (Fig. 2-1).

$\theta_{v,fc}$ and $\theta_{v,wp}$ values for the hemic (0.25-0.4 m) and sapric (> 0.4 m) layers were derived from moisture retention measurements by Kurnain et al. (2001) at surrounding peatlands.

Due to the lack of pore-size distribution measurements over the tropical peatlands, we could not use measured values for macropore volume fractions (θ_{mac}) as our model inputs. Instead we applied the analogy used by Wösten et al. (2008) for a tropical Indonesian peatland where they estimated a 0.50 macroporosity for the fibric peat layers since their measurements showed some 50% drainage of total pore spaces with a drop of WTD by only 0.40 m below the surface. We therefore assumed the fraction of total porosity drained at a water potential of -0.002 MPa as θ_{mac} for a particular layer and used those values as model inputs (Fig. 2-1). Our inputs for θ_{mac} (Fig. 2-1) corresponded to those used by Wösten et al. (2008) in their hydrological modelling.

Macropore saturated hydraulic conductivities in the model were calculated from the θ_{mac} inputs by using Hagen-Poiseuille's equation (B6-B10) (Dimitrov et al. 2010b). However, saturated hydraulic conductivities for the remaining soil matrices ($K_{s,mat}$) were given as model inputs (Fig. 2-1). Since the soil matrix in our modelling represented the fraction of bulk soil excluding macropores, we used $K_{s,mat}$ values measured by Ong and Yogeswaran (1992) for well decomposed peat layers in similar tropical peatlands. Lateral saturated hydraulic conductivity of the macropore and the soil matrix fraction of each layer were assumed to be equal to its macropore and soil matrix vertical saturated conductivity.

WTD_x was set at 0.6 m below the hummock surface (0.45 m below the hollow surface) representing long term (2002-2009) average WTD measured over our drained peatland site (Hirano et al. 2012) (Fig. 2-1). L_t was set to 400 m in all directions which was the nearest distance to the drainage canal (Hirano et al. 2012) (Fig. 2-1). The lower boundary condition in

our model run was defined as such there was no exchange of water to represent the presence of nearly impervious mineral sub-stratum underlying the peat deposition (Page et al. 2004) (Fig. 2-1).

Both hummock and hollow grid cells were seeded with evergreen tropical over- and under-storey vascular plants using the same plant functional types (PFTs) used in an earlier study on Amazonian rainforest (Grant et al. 2009b). However, atmosphere to rhizosphere O_2 transport through adventitious roots and enlarged aerenchyma in the dominant tree species growing in our wetland site (Pangala et al. 2013) was absent in PFTs modelled for Amazonian upland forests by Grant et al. (2009b). To include this wetland adaptation, we selected a value of 0.2 as the model input for root porosity (θ_{pr}) used in calculating root O_2 transport through aerenchyma (H6) for PFTs modelled in this study. Due to the scarcity of root porosity measurements in tropical peat swamp tree species, we adopted this value (θ_{pr}=0.2) from Visser et al. (2000) measured for wetland adapted sedges. This value for θ_{pr} used as our model input also falls within the range of root porosity (0.01-0.34) measured for various plants taken from northern temperate and boreal bogs, fens and reed swamps (Cronk and Fennessy 2001). θ_{pr} in wetland adapted species can also vary with intensity of waterlogging (Cronk and Fennessy 2001). However, the current version of *ecosys* used the set input for θ_{pr} to simulate O_2 transport from the atmosphere to rhizosphere through roots with θ_{pr} that did not vary with intensity in waterlogging.

The model was run for 44 years (40 years of spin up run and 4 years of simulation run) under repeating 4-year sequences of hourly weather data (solar radiation, air temperature, wind speed, humidity and precipitation) recorded at the site from 2002 to 2005. The spin up period allowed energy and CO_2 exchanges in the model to achieve stable values through successive

weather sequences. Model results for the 4 years of simulation run were compared with measurements at PDPSF from 2002-2005.

2-2.2.4. Model validation

Hourly R_n, LE and H fluxes modelled over hummocks and hollows were averaged to represent a 50:50 hummock hollow ratio as mentioned by Jauhiainen et al. (2008) and then regressed on hourly measured EC fluxes. Hourly near surface (0-0.2 m) θ of the modelled hummock was regressed against hourly measured θ for the same depth in a field hummock. Daily modelled WTDs were spatially averaged for hummock and hollow grid cells (50:50) and regressed against observed daily WTDs. Since the site WTD measurements were with respect to the average hollow surface (Hirano et al. 2007), modelled WTDs are also referenced with respect to the hollow surface to facilitate comparisons of modelled vs. measured WTD. Model performance was evaluated from regression intercepts ($a \rightarrow 0$), slopes ($b \rightarrow 1$), coefficients of determination ($R^2 \rightarrow 1$) and root mean squares for errors ($RMSE \rightarrow 0$).

2-2.2.5. Sensitivity of modelled WTD to artificial drainage

Artificial drainage is a key disturbance reported to alter WTD of Southeast Asian peatlands (Hirano et al. 2012, 2015). Changes in seasonality of WTD due to drainage can exert a considerable control on seasonality of peatland water, carbon, energy and nutrient cycling. To test the sensitivity of the modelled WTD to artificial drainage we performed a parallel simulation with WTD_x raised from 0.45 m below the hollow surface to 0.15 m above the hollow surface (i.e. level with the hummock surface) with everything else unchanged to represent the undrained condition. The difference between the two WTD_xs was based on the maximum observed difference between mean annual WTDs over our drained site and a similar undrained site nearby as reported by Hirano et al. (2012).

2-2.2.6. Analyses of model results

Seasonal variation in Bowen ratio (β) was used as an indicator for examining WTD effects on seasonal variation in surface energy exchange. For this purpose, we examined hourly measured and modelled β during two periods of 15 days each from the late rainy/early dry season (May-July) and the late dry season (August-October) for each year of the study. To control for effects of radiation on β, we first screened the mid-day (10:00-14:00 local time) β values that were measured and modelled under incoming solar radiation > 700 W m^{-2} representing cloudless sky (Hirano et al. 2007). We then performed single factor analyses of variance (ANOVA) for the sorted mid-day measured and modelled β values to test whether the means of hourly mid-day β significantly differed between the two 15-day periods in each year of study. A significant difference in mean mid-day β between those two periods in a particular year meant the inter-seasonal variation in mean β values in that year was larger than the short-term intra-seasonal variation in β values. This test would signify the consistency of seasonal variations in β as a result of WTD fluctuations.

2-3. Results

2-3.1. Modelled vs. measured θ and WTD

A gradual wetting trend from 2002 to 2005 over PDPSF was apparent from annual precipitation measurements with 2002 being the driest (El-Niño) and 2005 being the wettest (La-Niña) year (Table 2-1). Hydrological processes for vertical and lateral water fluxes enabled *ecosys* to simulate hourly near surface (0-0.2 m depth of a hummock) θ at PDPSF during this wetting period with co-efficients of determination (R^2) > 0.80 ($P < 0.0001$) and very little model discrepancies (root mean squares for errors (RMSE) from regressions of measured on modelled θ ≤ 0.02 m^3 m^{-3}) (Fig. 2-2b) (Table 2-1).

These processes also enabled simulated daily WTDs to correlate well with measured values ($R^2 > 0.80$, $P < 0.0001$) (Fig. 2-2c) (Table 2-1). Low RMSEs *ca.* ~ 0.1 m (Table 2-1) further indicated a minimal model discrepancy in simulating seasonal and interannual fluctuations in WTDs at PDPSF. This test provided additional confidence in model explanations of seasonal weather effects on tropical peatland hydrology.

2-3.2. Modelled vs. measured ecosystem energy fluxes

Ecosys reasonably well simulated diurnal and seasonal variations in ecosystem surface energy exchange. Regressions of hourly modelled vs. measured R_n, *LE* and *H* gave intercepts within 20 W m^{-2} of zero, and slopes within 0.1 of one, indicating minimal bias in modelled values for all years of the study except 2003 when variation in *LE* was overestimated (Table 2-2). Values for R^2 were ~ 0.8 ($P < 0.0001$) for modelled vs. measured regressions of *LE* whereas those for *H* were relatively lower (~ 0.7) (Table 2-2). These lower R^2 for *H* fluxes were caused by smaller diurnal and seasonal variations in *H* vs. *LE* datasets. However, some of the unexplained variance in EC *LE* and *H* could also be attributed to a random error of *ca.* 20% in EC methodology (Wesely and Hart 1985). This attribution was corroborated by root mean squares for random error (RMSRE) in EC measurements over forests calculated from Richardson et al. (2006) that were similar to RMSE, indicating that further constraint in model testing could not be achieved without further precision in EC measurements. Modelled vs. measured *LE* and *H* flux divergence may also have been affected by incomplete energy balance closure of about 80% in the EC measurements (Wilson et al. 2002) as opposed to complete energy balance closure in the model.

2-3.3. Seasonal and interannual variations WTD and θ

During the rainy season in 2002 when P exceeded ET, the modelled WTD came close to the hollow surface until lateral discharge through both the macropores and the soil matrix offset excess P (Figs. 2-2a, c and 2-3a). The modelled lateral discharge (Q_{sim}) was equal to the residual between P and modelled ET (P-ET_{sim}), which was corroborated by the difference between P and EC gap-filled ET (P-$ET_{EC\ gap\text{-}filled}$) (Fig. 2-3a). We did not have any WTD measurements *in situ* to corroborate the modelled WTDs for the rainy season in 2002, although the high near surface θ measured and modelled during this period (Fig. 2-2b) corroborated the shallow modelled WTDs.

At the onset of the dry season in mid-April, P declined below ET so that the modelled WTD increased (Fig. 2-2c). This increase in WTD slowed and eventually ceased lateral discharge and caused modelled and measured near surface peat to dry (Figs. 2-2b and 2-3a). As the dry season progressed, $P < ET$ caused the WTD to fall further and eventually stabilize at a deeper position where recharge offset $P - ET$ (Figs. 2-2c and 2-3a). This deepening was also apparent in monthly WTD measurements by Hirano et al. (2012) and corroborated by very dry near-surface soil both modelled and measured from June to October (Figs. 2-2b and 2-2c).

At the onset of the rainy season in November when P again exceeded ET, the modelled WT rose until increasing discharge again offset excess P (Figs. 2-2c and 2-3a), rewetting the near surface peat as was also apparent in the θ measurements (Fig. 2-2b).

P in 2003 was greater than in 2002 (Table 2-1) so that both modelled and measured WT remained closer to the hollow surface and θ remained high until mid-May, almost two months later than in 2002 (Figs. 2-2b, c and 2-3). This interannual trend between 2002 and 2003 was also apparent in higher cumulative modelled discharge sustained for a longer period in 2003 than in 2002. This trend was consistent with that in the differences between P and modelled ET and

between *P* and EC gap-filled *ET* (Fig. 2-3a). At the onset of the dry season in mid-May 2003, the deepening of both modelled and measured WTDs and the drying of the near-surface peat was more gradual than in 2002 (Figs. 2-2b, c). Sporadic precipitation events throughout the dry season in 2003 caused simulated as well as observed WTD to deepen less than in 2002 (Fig. 2-2c).

P in 2004 was greater than in 2003 (Table 2-1), so that both observed and modelled WT remained close to the hollow surface and kept near-surface peat wet until mid-June (Figs. 2-2b, c). Shallower WTD drove more rapid cumulative modelled lateral discharge in 2004 for a longer period than in 2003 as corroborated by the differences between *P* and modelled *ET* and between *P* and EC gap-filled *ET* (Fig. 2-3). The late dry season in 2004 did, however, receive less precipitation than in 2003 and hence modelled and measured WTDs were slightly deeper than in the same period of 2003 (Fig. 2-2c).

The year 2005 was the wettest in our study with no prolonged dry period, and hence modelled and measured WTDs seldom dropped below 1.0 m from the hollow surface even in the late dry season (Fig. 2-2c). Consequently the near surface soil dried less in 2005 than in the previous three years of study because there was enough precipitation to rewet the near surface peat layers even in the dry season (Fig. 2-2b). *ET* barely exceeded *P* even in the late dry season of 2005, causing the shallowest WTD in that year (Fig. 2-3a).

Interannual variation in WTD due to differences in the intensity and duration of dry seasons from 2002-2005 was also apparent in average modelled and observed dry season (May-October) WTD. Gradually wetter dry seasons from 2002 to 2005 caused gradually shallower dry season WTD in PDPSF (Figs. 2-3b, c). This trend of gradually shallower dry season WTD from 2002 to 2005 was reasonably well simulated by our model from basic processes for vertical and

lateral water transfer described earlier (Fig. 2-3c). However, the rate of decrease in dry season WTD with an increase in dry season *P* from 2002 to 2003 was less rapid in the model than in the measurements (Fig. 2-3c). Gradually shallower WTD and higher *P* compared to *ET* from the driest year of 2002 to the wettest year of 2005 also caused a gradual increase in cumulative discharge from 2002 to 2005 (Fig. 2-3a).

2-3.4. Sensitivity of simulated WTD to artificial drainage

Both the modelled and the measured WTD in our study site (Fig. 2-2c) would be unusually deep for a pristine tropical peatland. Since our study site was a drained peatland, this deeper than normal WT might be artifacts of drainage. To examine the effect of artificial drainage on WTD at PDPSF we performed drained vs. undrained simulations as described in Sect. 2-2.2.5. During the rainy seasons (November-April) from 2002-2005, simulated undrained WTD was always above the hollow surface as opposed to the simulated drained WTD where WT never rose above the hollow surface (Fig. 2-4). Though the undrained WTD always remained ~0.5 m shallower than the drained WTD, presence of distinct dry seasons in 2002-2004 caused the undrained WTD to reach ~1.0 m below the hollow surface (Fig. 2-4). The seasonal variation in simulated undrained WTD followed that in a nearby undrained tropical peat swamp forest measured by Hirano et al. (2009) during 2002-2003 and Sundari et al. (2012) during 2004-2005 (Fig. 2-4). This simulated change in WTD with drainage indicated that the basic hydrological processes used to model vertical and lateral water fluxes are robust if they are used with accurately determined changes in external boundary conditions.

2-3.5. WTD effects on seasonal and interannual variations in surface energy exchange

Seasonal variation in WTD, predominantly governed by seasonality in *P*, may have a profound effect on seasonal changes in surface energy exchange. Daily EC gap-filled *ET* showed

a decline from ~4 mm d^{-1} during late rainy/early dry season (May-July) with a shallower WTD to ~2 mm d^{-1} during the late dry season (August-October) with a deeper WTD in 2002 (Figs. 2-5a, c). EC gap-filled *ET* showed the same trend of decrease with WTD drawdown during late dry seasons in 2003 and 2004 (Fig. 2-5a). Unlike 2002-2004, the decrease in EC gap-filled *ET* was less prominent in the wettest dry season of 2005 when WT was shallower than in 2002-2004 (Figs. 2-5a, c). Coupled processes for transpiration and root water uptake enabled *ecosys* to reasonably well capture the decrease in *ET* towards the ends of prolonged dry seasons in 2002-2004 with deeper WTD as well as the lack of a prominent decline in *ET* during the less pronounced late dry season in 2005 (Fig. 2-5a).

Seasonal variation in *ET* might be driven by the available energy for *ET* from R_n and atmospheric vapour demand from vapour pressure deficit (*D*). A large decline in dry season R_n due to smoke haze shading from a surrounding forest and peat fire in 2002 (Hirano et al. 2007) contributed to the large decline in modelled and EC gap-filled *ET* during that period (Figs. 2-5a, b). Absence of large declines in R_n during late dry seasons in smoke-free years of 2003 and 2004 caused smaller decreases in modelled and EC gap-filled *ET* than in 2002 (Figs. 2-5a, b). However, the late dry season decline in both modelled and EC gap-filled *ET* was less prominent in 2005 than in 2003 and 2004 despite having a nearly similar seasonal pattern in R_n (Figs. 2-5a, b). Observed vapour pressure deficit (*D*) in PDPSF showed a distinct seasonality with consistently higher *D* in late dry seasons compared to the rainy/early dry seasons throughout the study period (Fig. 2-5c). This seasonality meant the drier weather caused higher potential *ET* during late dry seasons of 2002-2005. Despite this, we found reduced modelled and EC gap-filled actual *ET* during late dry seasons of 2002-2004 (Fig. 2-5a). This reduction suggested that the late dry season decrease in *ET* and the interannual variation in the intensity of this decrease

were not solely controlled by weather variables (R_n and D) that drive ET. Rather this seasonality and interannual variation of ET might have been driven by changes in plant water status and consequent stomatal regulation as affected by peat moisture conditions. EC gap-filled mid-day β rose from ~0.3 to ~0.6 from late rainy/early dry to late dry season of 2002 indicating an increase in stomatal constraint to ET and this trend was reasonably captured by *ecosys* (Fig. 2-5d). As in 2002, EC gap-filled β also rose with a WTD drawdown from late rainy/early dry seasons to late dry seasons in 2003 and 2004 (Fig. 2-5d). This trend of rises in β during the late dry seasons in 2003 and 2004 were also well captured in the model (Fig. 2-5d). Unlike the other three years (2002-2004), both EC gap-filled and modelled mid-day β during the wettest year of 2005 did not rise from late rainy/early dry season to late dry season (Fig. 2-5d). This indicated the lack of stomatal constraint to both EC gap-filled and modelled ET during the wettest dry season of 2005 when the WT seldom fell below 1 m.

Our results, therefore, indicated a consistent decline in ET and a concurrent rise in mid-day β caused by deeper WTD during late dry seasons of 2002-2004 EC gap-filled (Figs. 2-5a, d). This trend is further supported by regressions of daily EC gap-filled ET and β vs. observed WTD and of daily simulated ET and β vs. simulated WTD during 2004-2005 (Fig. 2-6). These regressions showed an overall decrease in both EC gap-filled and modelled ET and a concurrent increase in β with deepening WT further illustrating stomatal constraint on tropical peatland energy balance during late dry seasons (Fig. 2-6). However, there was also a tendency of a slight decrease in both EC gap-filled and modelled ET and a concurrent small increase in β as WT came up to the hollow surface indicating a very weak flooding stress to ET (Fig. 2-6). Unfortunately we could not include data from 2002 and 2003 in these regressions due to the lack of daily WTD measurements over that period.

Closer comparisons of energy exchange between selected 15-day periods of late rainy/early dry seasons and late dry seasons can provide us with better insights about how variations in WTD affect seasonality in β in this tropical peatland. Both the EC gap-filled and modelled β were significantly higher (P<0.01) during the late dry seasons with deeper WTD in 2002, 2003 and 2004 than during late rainy/early dry seasons with shallower WTD (Fig. 2-7). This was caused mainly by late rainy/early dry to late dry season reduction of LE fluxes with respect to H fluxes (Fig. 2-8). This reduction in LE and a concurrent increase in β were modelled by a reduction in ψ_c and a consequent decline in mid-day g_c during late dry seasons with deeper WTD in 2002-2004 (Fig. 2-9). This clearly indicated that deeper WTD caused stomatal limitations to tropical peatland LE and β. However, no increase in β and no concurrent decrease in LE was modelled and measured during the late dry season of 2005 (Figs. 2-7 and 2-8). This indicated the absence of stomatal limitation during the 'wet' late dry season of 2005 when the WT seldom fell below 1 m. This absence was also evident in fewer declines of ψ_c and mid-day g_c modelled during the late dry season in 2005, in contrast to those in the other years of the study (2002-2004) (Fig. 2-9).

2-4. Discussion

2-4.1. Hypothesis 1: Hydrological controls on seasonal and interannual variations in tropical peatland WTD

Distinct seasonality in P to ET ratio controlled seasonal variation in WTD during 2002-2005 at PDPSF with shallower WTD in the rainy seasons (November-April) when P exceeded ET and deeper WTD in the dry seasons (May-October) when ET exceeded P (Figs. 2-2 and 2-3). However, gradually less pronounced dry seasons (May-October) and hence less deficit between ET and P caused progressively shallower dry season WT and hence less peat drying from the

driest year 2002 to the wettest year 2005 at the PDPSF (Figs. 2-2 and 2-3). Modelled deficits between dry season *ET* and *P*, however, were larger than deficits between dry season EC gap-filled *ET* and *P* (Fig. 2-3a). These divergences were caused by larger modelled vs. EC gap-filled *ET* due to complete energy balance closure in the model (D, E1) vs. ~80% closure in the EC data (Wilson et al. 2002) (Figs. 2-3a and 2-5a) (Table 2-2) (Sect. 2-3.2). Increasingly wetter and longer rainy seasons caused more surplus water from *P* in excess of *ET* and generated gradually larger simulated lateral discharge from 2002 to 2005 (Fig. 2-3a).

During the rainy seasons when modelled WTD rose above the referenced external WTD (WTD_x), the resultant hydraulic gradient drove lateral discharge through soil matrix and macropores (Figs. 2-1, 2-2c and 2-3a) (B11-12). The modelled WTD in rainy seasons (C1) hence were at positions very close to the hollow surface where lateral discharge equilibrated with the surplus water from *P* in excess of *ET* (Figs. 2-2c and 2-3a). When modelled WTD fell below WTD_x during the dry seasons, lateral discharge ceased and the modelled WTD were stabilized at deeper positions where lateral recharge equilibrated with the deficit between *ET* and *P* (Figs. 2-1, 2-2c and 2-3a) (B11-12, C1). However, we modelled very negligible rates of (~0.1 mm d^{-1}) lateral recharge during all dry seasons due to low lateral hydraulic conductivities in well decomposed deeper peat layers in which the WT was located (Fig. 2-1) (B11). This indicates simulation of an important hydrological characteristic of tropical bogs those are not fed by recharge from surrounding WT (Rieley and Page 2005). We also simulated negligible (~0 mm h^{-1}) surface run-off (A1-A5) due to the lack of standing surface water resulting from rapid infiltration through preferential flow which matched site observations in Hirano et al. (2009). Lack of saturation of near surface peat layers (0-0.2 m of the hummock) even in the peak rainfall periods i.e. P > 60 mm h^{-1} was also well modelled by simulating rapid vertical and lateral

preferential flow through macropores (Figs. 2-1 and 2-2a, b) (B6-10, B12) as described in Dimitrov et al. (2010b). These changes in WTD and θ were modelled from basic hydrological processes that required inputs for measureable peat hydrological characteristics and an external WT (Fig. 2-1), but did not require adaptation through site-specific parameterization and should therefore be generally applicable to diverse ecosystems including peatlands.

2-4.2. Hypothesis 2: WTD effects on seasonal and interannual variations in surface energy exchange and water stress

Seasonal and interannual variations in WTD and resultant variations in peat θ also affected variations in surface energy exchange in PDPSF. WTD drawdown and resultant peat drying caused vegetation water stress during late dry seasons as indicated by increases in both modelled and EC-gap filled β caused by declines in *LE* with respect to *H* (Figs. 2-2, 2-5a, d, 2-7 and 2-8). This late dry season water stress was, however, more prominent in drier years of 2002-2004 when WT was persistently deeper than a threshold level of ~1.0 m, and less prominent in the wetter year of 2005 when WT seldom fell below this threshold (Figs. 2-2c, 2-5a, d, 2-7 and 2-8). These WTD effects on seasonal and interannual variations in surface energy exchange and vegetation water stress in this tropical peatland was modelled in *ecosys* by adequately simulating the coupling between root water uptake and transpiration in a soil-plant-atmosphere water scheme as affected by vertical distributions of θ, $[O_{2s}]$ and root density controlled by WTD dynamics. These algorithms are robust since they were also applicable to a wide range of peatlands [e.g. a boreal bog (Dimitrov et al. 2010b) and a boreal fen peatland (Grant et al. 2012b)] without any site-specific parameterization.

Modelled root densities for the tropical peatland vegetation sharply declined with depth (Fig. 2-10). Most of the modelled roots were within the near surface layers farther above the WT (Fig. 2-10). Root densities in deeper layers closer to the WT remained lower than those in near surface layers by 2-3 orders of magnitude (Fig. 2-10). This vertical rooting pattern was simulated from better vs. poorer soil O_2 status ($[O_{2s}]$) in near surface vs. deeper layers (Fig. 2-11). Near surface peat layers remained unsaturated throughout the year (Fig. 2-2b) which facilitated adequate $[O_{2s}]$ from rapid diffusive-dispersive transfers of O_2 from atmosphere (H3, H5) (Fig. 2-11). $[O_{2s}]$ values in these layers were well above the Michaelis-Menten constant (K_{O2} = 0.064 gm^{-3}) used to calculate root and mycorrhizal O_2 uptake (Fig. 2-11) that enhanced root O_2 uptake, growth respiration (R_g) (G7) and growth (G8) and hence higher root densities (G9) in these near surface layers (Fig. 2-10). During dry seasons, when WTD receded, vertical extension of aerobic zones and consequent improved $[O_{2s}]$ in the newly aerated deeper layers enabled modelled root systems to grow into these layers (Figs. 2-10 and 2-11). However, since these deeper layers remained saturated during most of the rainy (November-April) and early dry (May-August) seasons with shallower WTD, consequent low $[O_{2s}]$ in these layers slowed R_g (G3-G5, G7), root growth (G8) and hence reduced modelled root densities from those in the near surface layers which remained unsaturated and hence had improved $[O_{2s}]$ almost all the year round (G9) (Figs. 2-2b, 2-10 and 2-11). Due to the lack of $[O_{2s}]$, roots in these deeper layers depended heavily on transfer of O_2 from atmosphere to root through aerenchyma ($[O_{2r}]$) (G4, H2, H6) (Fig. 2-11). Our input of root porosity (θ_{pr} = 0.2) to represent this wetland adaptation (H6) was not enough to maintain adequate $[O_{2r}]$ to simulate large root densities in those deeper layers. This simulated vertical root distribution is consistent with vertical root biomass profile measurements by Sulistiyanto (2004) who found 83% of total live root biomass in a surrounding undrained

peatlands were within the top 0.25 m and the remaining 17% within 0.25-0.5 m from the ground surface. This shallow root distribution indicated much lower root growth in deeper, wetter peat than in near surface, drier peat. Shimamura and Momose (2005) found significantly higher root biomass in elevated mounds of a tropical peat swamp forest that remained above the WT compared to low-lying non-mounds that remained closer to the WT indicating preference of those tropical peatland species for shallow lateral rooting to avoid waterlogging in deeper layers. While studying root growth pattern of the seedlings of the dominant tree species of tropical peat swamp forests, Nishimura and Suzuki (2001) found the tendency of roots to grow predominantly in the top 0.25 m that remained unsaturated most of the year. Rachmanadi et al. (2014) also found similar shallow rooting preferences in seedlings of 15 dominant tropical peat swamp species.

During the late rainy/early dry seasons shallower WTD resulted in higher near surface peat θ and consequently higher ψ_s and lower Ω_s (F3) (Figs. 2-2b, c). Higher root densities in these layers also meant lower Ω_r (F4). Hence, higher ψ_s, and lower Ω_s and Ω_r facilitated greater root water uptake (U_w) (F2) from these near surface peat layers that reduced stomatal limitation, i.e. higher g_c (Fig. 2-9b), higher ψ_c (Fig. 2-9a) and thus higher transpiration and lower β during late rainy/early dry seasons (Figs. 2-5a, d, 2-7 and 2-8).During the late dry seasons of drier years 2002-2004, WTD fell frequently well below the threshold of ~1.0 m (Fig. 2-2c). During this period, the absence of adequate vertical recharge through frequent P meant θ in near surface peat layers had to entirely depend upon vertical recharge of those layers through capillary rise from the WT. But low water holding capacity of the macropores and low hydraulic conductivity of the remaining soil matrices originating from highly decomposed woody materials (Fig. 2-1) slowed vertical recharge of near surface modelled peat layers through capillary rise from WT (B1-B5).

Consequently, modelled near surface (0-0.2 m of a hummock) θ approached the wilting point during the late dry seasons of these years (Fig. 2-2b) as corroborated by site measurements (Hirano et al. 2007). This desiccation caused sharp declines in ψ_s in near surface peat layers and consequent rises in near surface Ω_s (F2), contributing to slower root water uptake (U_w) (F1-F2) from these layers.

Despite the desiccation of the near surface peat layers during the deeper WTD period during late dry seasons of 2002-2004, the well decomposed peat layers in the model below 0.3 m had soil moisture contents well above the field capacity (Fig. 2-1). This differential vertical soil moisture profile distribution was analogous to the field observations by Hirano et al. (2009) over PDPSF and Jaya et al. (2010) over a similar tropical peatland. Therefore, U_w in those deeper peat layers was not constrained by reductions in ψ_s and consequent increases in Ω_s. Moreover, improved aeration of deeper peat layers in deep WTD periods during the late dry seasons caused improved [O_{2s}] (Fig. 2-11) that facilitated root growth and hence increased root densities in these layers (Fig. 2-10) that resulted in lower Ω_r than in late rainy/early dry seasons with shallow WTD. Higher ψ_s and lower Ω_s and Ω_r caused increased U_w (F2) from these deeper peat layers during late dry seasons with deeper WTD. However, these increases in U_w from deeper wetter layers could not offset the suppression in near surface U_w that comprised most of the root volumes for uptake. So, the resultant net decrease in U_w during late dry seasons of 2002-2004 caused modelled ψ_c to decrease (Fig. 2-9a) (E7, F2) and to cause a consequent decline in g_c (Fig. 2-9b) (E5-E6). This explained declines in LE vs. H and rises in β apparent in the EC measurements during these drier periods. Late dry season declines in g_c over PDPSF were also shown by Hirano et al. (2015) in an EC measurement study.

During the wettest dry season of 2005, however, modelled near surface θ remained well above wilting point (Fig. 2-2b) and hence enabled higher U_w to be sustained from the near surface layers. Consequently the stomatal limitation to *ET* was not simulated during that hydroperiod. This was apparent in the absence of a prominent decrease in modelled ψ_c (Fig. 2-9a) and g_c (Fig. 2-9b), and explained the absent of declines in EC gap-filled *ET* (Fig. 2-5a) and of concurrent rises in EC gap-filled β (Fig. 2-5d) during the late dry season of 2005 in contrast to the declines measured in other years (e.g. 2002-2004).

2-5. Conclusions

Seasonal and interannual variations in WTD of the tropical peatland at PDPSF were governed by variations in *P* to *ET* ratio during a gradually wetting period from an El-Niño year 2002 to a wetter year 2005. However, these variations in WTD again affected variations in peat water contents, surface energy exchange and vegetation water stress. *P* less than *ET* during dry seasons caused deeper WT and hence peat drying (Figs. 2-2 and 2-3). Gradually smaller deficits between *ET* and *P* caused progressively shallower dry season WTD and less peat drying from the driest year 2002 to the wettest year 2005 (Figs. 2-2 and 2-3). Increasingly higher *P* than *ET* during rainy seasons generated gradually larger lateral discharge from 2002-2005 (Fig. 2-3a). WTD frequently deeper than a threshold of ~1.0 m below the hollow surface caused near surface peat desiccation that eventually triggered plant water stress during the late dry seasons of drier years 2002-2004 (Figs. 2-5a, d and 2-6 to 2-8). This late dry season water stress, however, was not prominent in the 'wettest' late dry seasons of 2005 (Figs. 2-5a, d and 2-6 to 2-8) thus indicating interannual variation in seasonality of surface energy exchange in this tropical peatland.

Successful simulation of WTD variation in *ecosys* was achieved by calculating seasonal variations in the balance between *P*, *ET* and lateral discharge governed by hydraulic gradients between modelled and an external reference WTD (WTD_x) over a distance (L_t) as described in our first hypothesis. WTD effects on surface energy exchange and vegetation water stress was modelled in *ecosys* by simulating suppression of near surface root water uptake due to desiccation and suppression of deeper layer root water uptake due to low root densities and high root hydraulic resistances as described in our second hypothesis. This simulation is of a great importance since lack of these processes in models can result in a completely misleading prediction of WTD effects on peatland *ET* and hence productivity. For instance, Li et al. (2007) predicted a drying trend over Southeast Asian peatlands by the end of this century by using 3 GCMs that shows a decrease in dry season precipitation and hence an increase in WTD together with an increase in atmospheric dryness, R_n and hence potential *ET*. However, if we tried to simulate the effects of these drier weather projections on *ET* and hence productivity using a model where root depths are prescribed rather than arising from root-WTD interactions as in this study, we could come up with two completely contrasting outcomes. A prescribed shallow root depth would result in strong plant water stress and hence reduced productivity caused by this future drier weather scenario regardless of interannual variations. Conversely, a prescribed deep root depth, which might reasonably be assumed for those tall tropical peatland trees with a canopy height of 26-35 m (Page et al. 1999, Hirano et al. 2007), would result in an increase in *ET* and hence productivity with future drying.

The present study thus opens a new window in the use of process-based ecosystem modelling to study WTD effects on eco-hydrological processes in tropical peatlands. Such modelling of WTD effects on vegetation water stress is also essential in modelling seasonal and

interannual variations in GPP in tropical peatlands as shown in Chapter 3. This type of modelling can also be scaled up to simulate regional-level WTD effects on tropical peatland *ET* and productivity when provided with regional-level inputs for soil physical and hydrological characteristics (Fig. 2-1), land use (forested vs. agriculture), PFTs, and disturbance (e.g. drainage, fire, logging). Hence such up scaling of our modelling has a high potential in guiding WTD management and peatland rehabilitation projects that are undergoing across tropical peatlands that are severely affected by seasonality of precipitation together with human interventions like drainage. This predictive capacity building would also contribute to the current tropical peatland carbon monitoring and assessment initiatives.

Table 2-1. Summary statistics of regressions between modelled and measured hourly soil water contents (θ) and daily water table depths (WTD) for a drainage affected tropical peat swamp forest at Palangkaraya, Indonesia

Year	2002	2003	2004	2005
Precipitation (mm)	1852	2291	2560	2620
Modelled vs. observed soil water content (θ) from 0-20 cm depth below the hummock surface				
n	8760	8760	8784	8760
R^2	0.85	0.83	0.80	0.78
RMSE (m^3 m^{-3})	0.02	0.02	0.02	0.01
Modelled vs. observed water table depth (WTD) from the hollow surface				
n			263	228
R^2			0.92	0.81
RMSE (m)			0.13	0.1

R^2 and RMSE = coefficient of determination and root mean square for errors from simple linear regressions of measured on simulated

Table 2-2. Summary statistics of regressions between modelled and measured ecosystem surface energy fluxes for a drainage affected tropical peat swamp forest at Palangkaraya, Indonesia

Year	2002	2003	2004	2005
Modelled vs. measured ecosystem net radiation (R_n)				
n	8760	8760	8784	8760
a	11	14	17	15
b	0.98	0.97	0.97	0.97
R^2	0.99	0.99	0.99	0.99
RMSE (W m^{-2})	8	8	8	8
Modelled vs. eddy covariance (EC) measured ($u^* > 0.17$ m s^{-1}) ecosystem latent heat fluxes (*LE*)				
n	5375	3866	5065	4993
a	-17	-18	-20	-26
b	1.04	1.19	1.09	1.03
R^2	0.83	0.83	0.82	0.74
RMSE (W m^{-2})	63	57	60	75
RMSRE (W m^{-2})	56	53	55	57
Modelled vs. EC measured ($u^* > 0.17$ m s^{-1}) ecosystem sensible heat fluxes (*H*)				
n	5659	4042	5153	5087
a	-6	-11	-13	-19
b	1.03	0.97	1.05	0.9
R^2	0.71	0.72	0.7	0.6
RMSE (W m^{-2})	33	34	35	45
RMSRE (W m^{-2})	25	27	27	28

(*a, b*) from simple linear regressions of modelled on measured; R^2 = coefficient of determination and RMSE = root mean square for errors from simple linear regressions of measured on simulated; RMSRE= root mean square for random errors in eddy covariance (EC) measurements calculated by inputting EC *LE* and *H* fluxes recorded at u^* (friction velocity) > 0.17 m s^{-1} into algorithms for estimation of random errors in EC *LE* and *H* measurements developed for forests by Richardson et al. (2006)

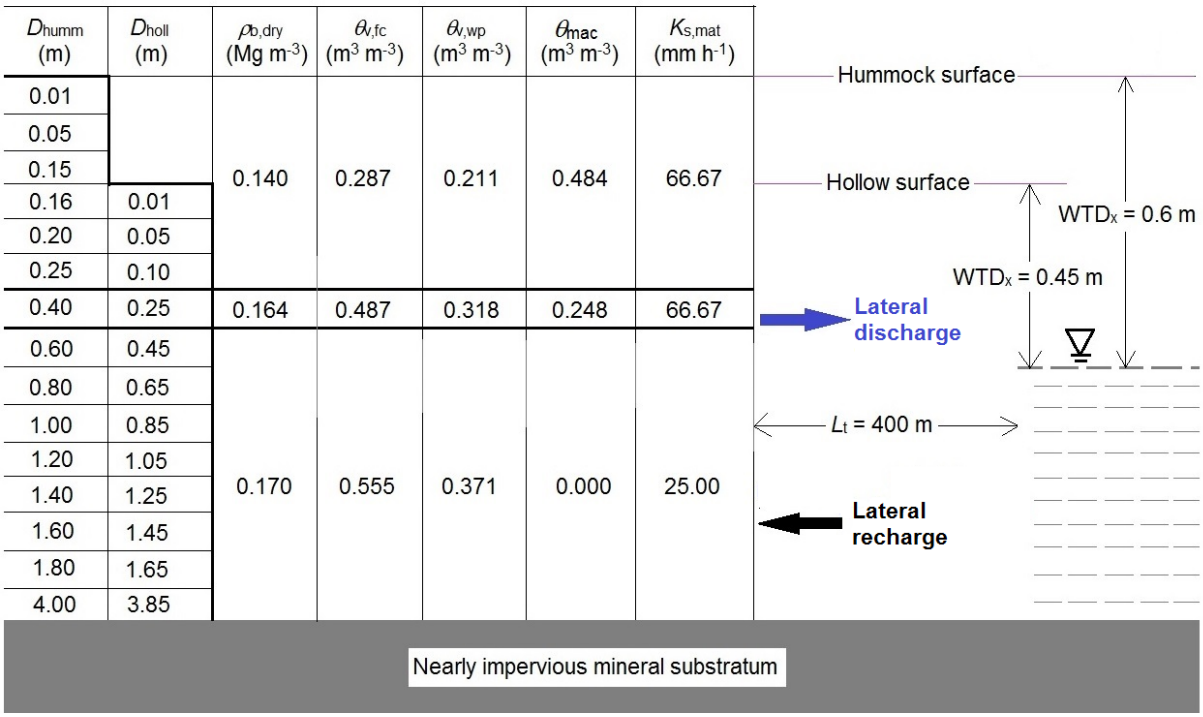

Fig. 2-1. Experimental modelling layout in *ecosys* and key inputs for soil physical and hydrological properties representative of a drainage affected tropical peat swamp forest at Palangkaraya, Indonesia. Figure was not drawn to scale. D_{humm} = depth to the bottom of a layer from the hummock surface; D_{holl} = depth to the bottom of a layer from the hollow surface; $\rho_{b,dry}$ = dry bulk density (Takakai et al. 2006, Jauhiainen et al. 2012b); $\theta_{v,fc}$ = volumetric soil water content at field capacity (-0.01 MPa) and $\theta_{v,wp}$ = volumetric soil water content at wilting point (-1.5 MPa) (Kurnain et al. 2001); $K_{s,mat}$ = saturated hydraulic conductivity of soil matrix (Ong and Yogeswaran 1992); θ_{mac} = volumetric macropore fractions; WTD_x = external reference water table depth representing average water table depth of the adjacent ecosystem; L_t = distance from modelled grid cells to the adjacent watershed over which lateral discharge/recharge occurs

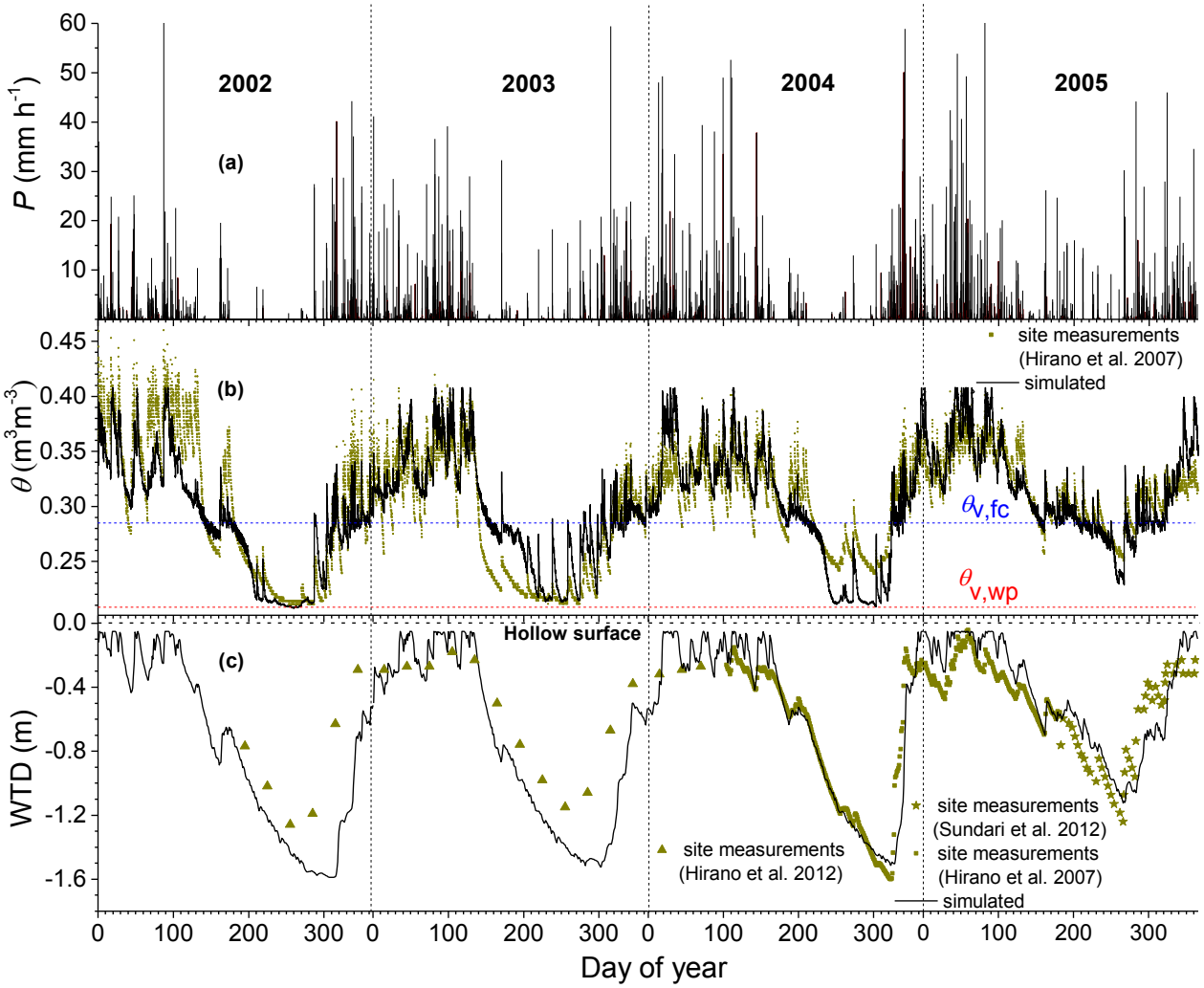

Fig. 2-2. (a) Hourly measured precipitation (*P*) (Hirano et al. 2007) (b) hourly measured (Hirano et al. 2007) and modelled soil water contents (θ) from 0-0.2 m of the hummock and (c) water table depths (WTD) measured monthly (Hirano et al. 2012) and daily (Hirano et al. 2007, Sundari et al. 2012), and modelled during 2002-2005 over a drainage affected tropical peat swamp forest at Palangkaraya, Indonesia. Negative values of WTD mean depths below the hollow surface

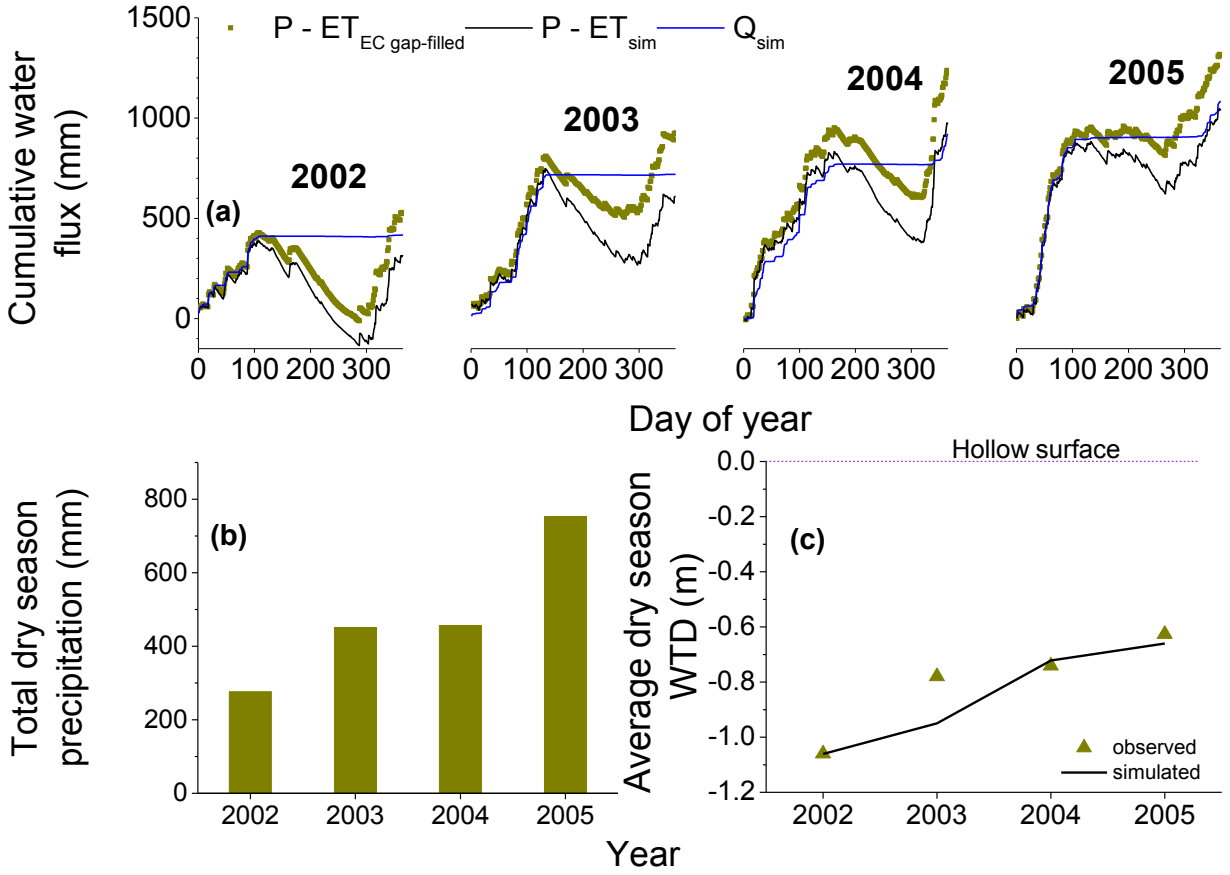

Fig. 2-3. (a) Cumulative difference between observed precipitation (*P*) and eddy covariance (EC) gap-filled (Hirano et al. 2005, 2015) evapotranspiration ($ET_{\text{EC gap-filled}}$) ($P$-$ET_{\text{EC gap-filled}}$), cumulative difference between observed *P* and simulated evapotranspiration (ET_{sim}) (P-ET_{sim}), and modelled lateral discharge (Q_{sim}) (b) total dry season (May-October) observed *P* (Hirano et al. 2007), and (c) average dry season (May-October) observed (Hirano et al. 2012) and modelled water table depths (WTD) from hollow surface during 2002-2005 over a drainage affected tropical peat swamp forest at Palangkaraya, Indonesia. Negative values of WTD mean depths below the hollow surface

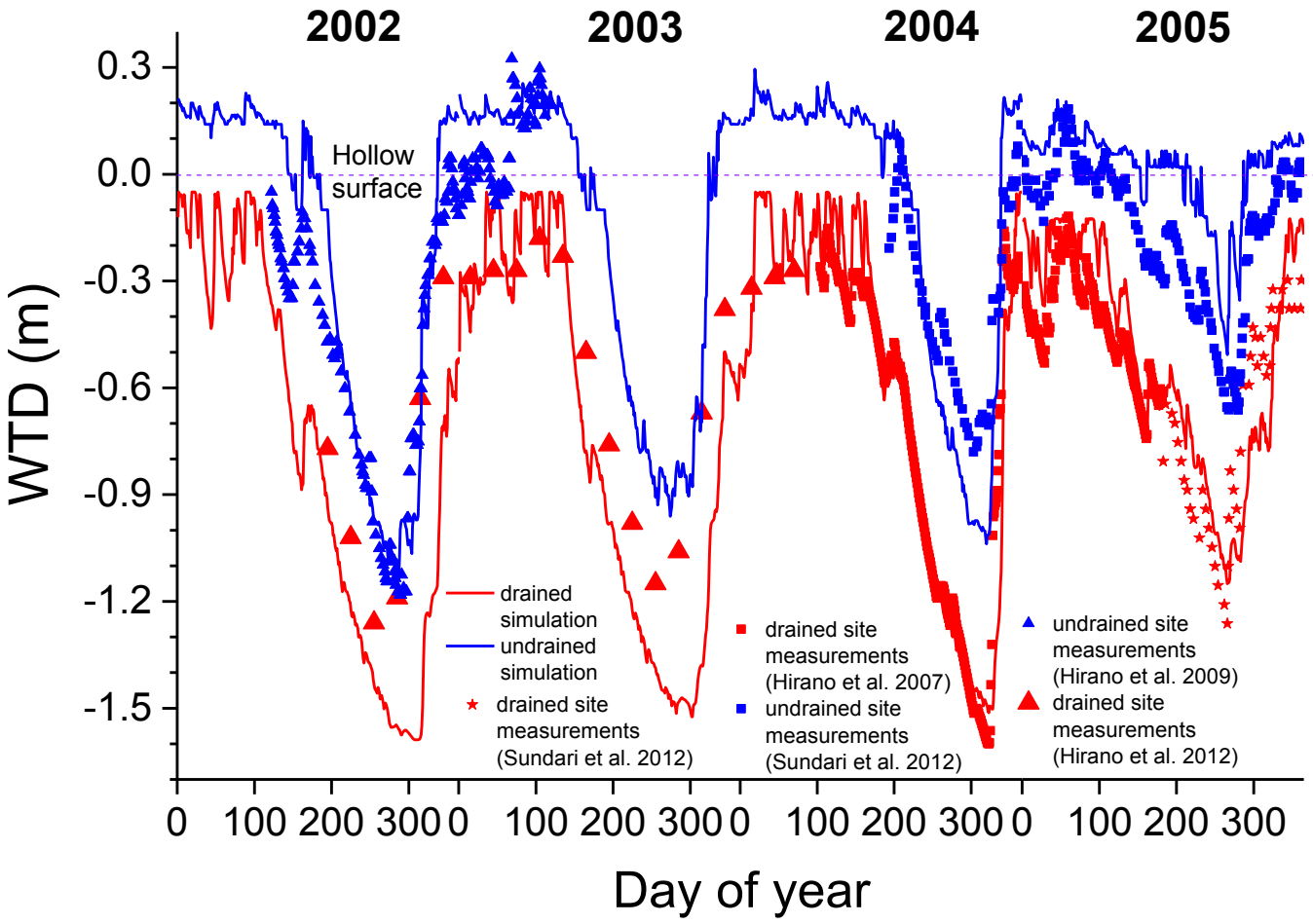

Fig. 2-4. Simulated daily drained vs. undrained water table depths (WTD) (Sect. 2-2.2.5) during 2002-2005 over a drainage affected tropical peat swamp forest at Palangkaraya, Indonesia. Drained WTDs are the same as those in Fig. 2-2c. Negative values of WTD mean depths below the hollow surface and positive values mean depths above the hollow surface

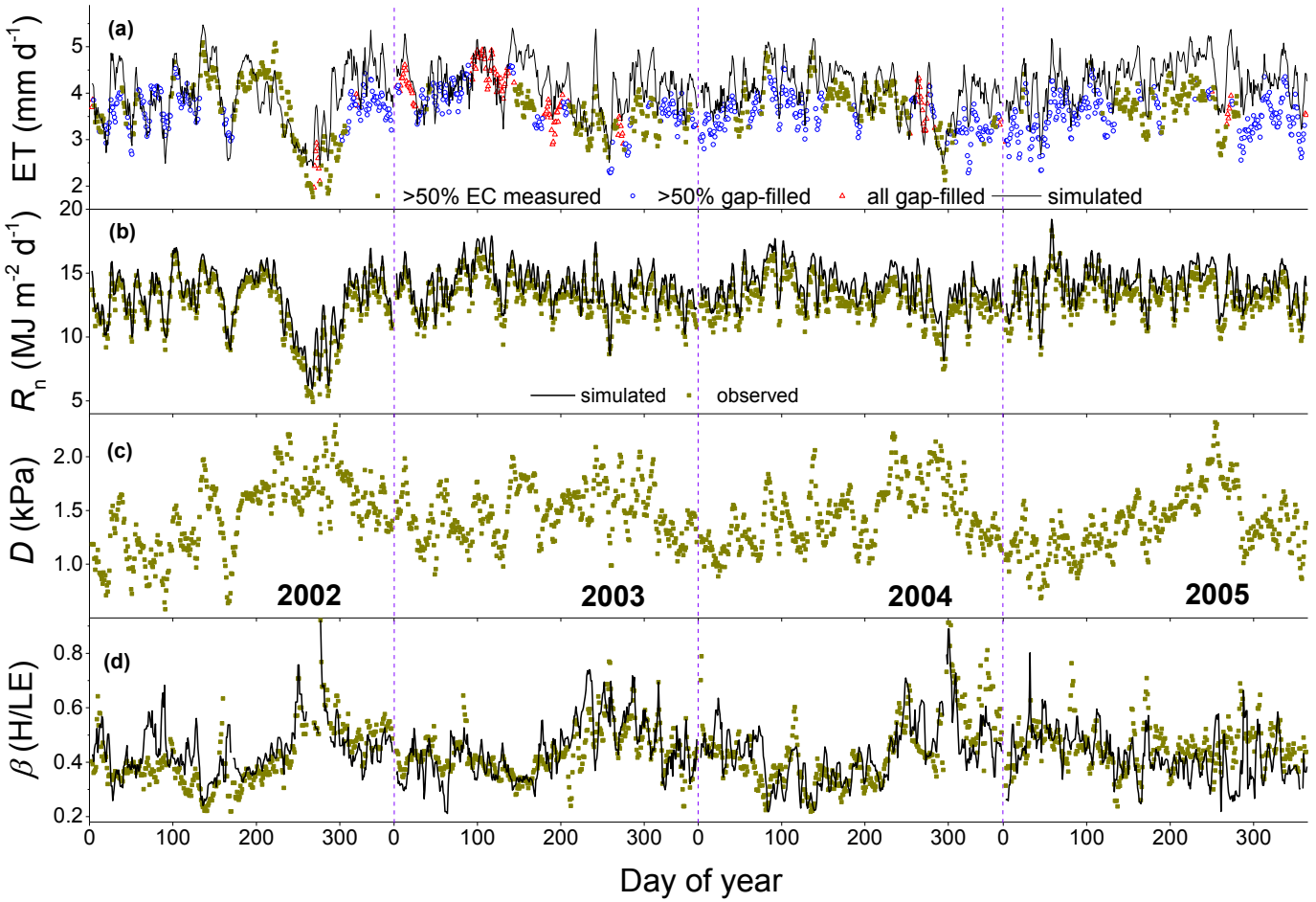

Fig. 2-5. Five-day moving averages of (a) eddy covariance (EC)-gap filled (Hirano et al. 2005, 2015) and modelled evapotranspiration (*ET*); (b) observed and modelled net radiation (R_n) (c) observed mid-day (10:00-14:00 local time) vapour pressure deficit (*D*) (Hirano et al. 2005, 2015), and (d) EC gap-filled (Hirano et al. 2005, 2015) and modelled mid-day (10:00-14:00 local time) Bowen ratios (β) under downward shortwave radiation > 700 Wm^{-2} during 2002-2005 over a drainage affected tropical peat swamp forest at Palangkaraya, Indonesia

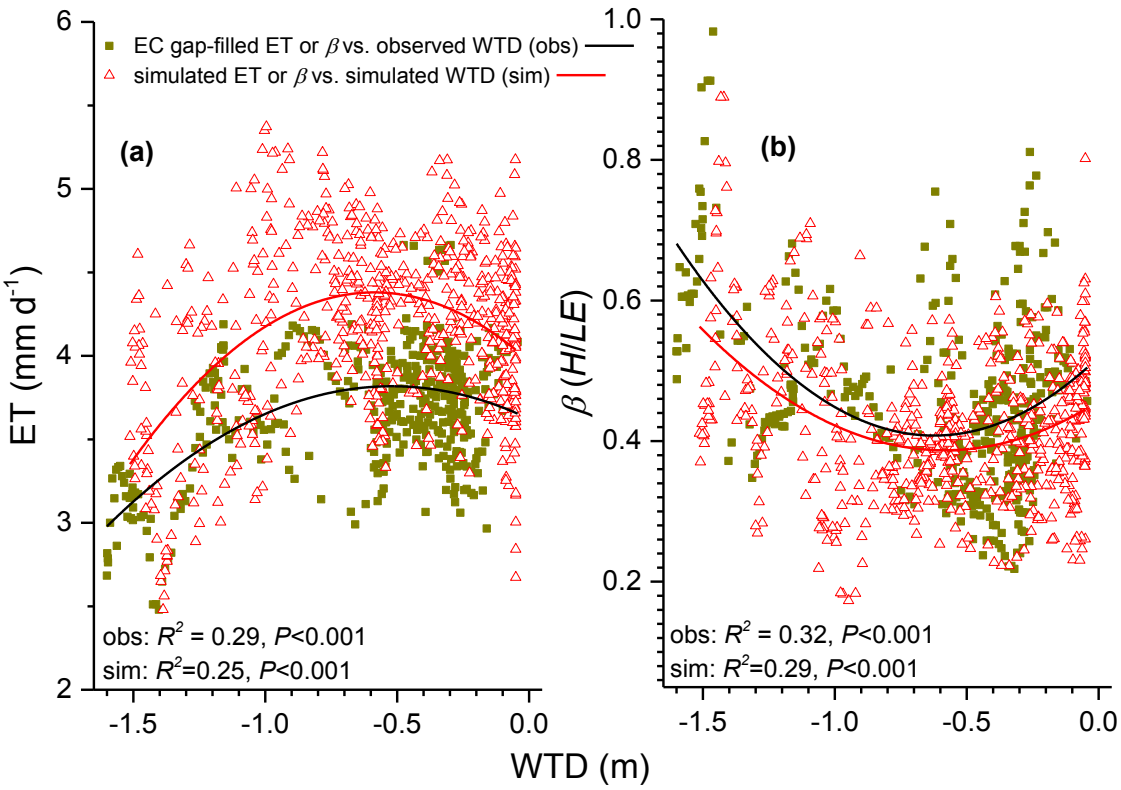

Fig. 2-6. (a) Regressions between modelled daily evapotranspiration (*ET*) and modelled daily water table depth (WTD), and between eddy covariance (EC)-gap filled daily *ET* and observed daily WTD, and (b) regressions between average daily modelled mid-day (10:00-14:00 local time) Bowen ratios (β) under downward shortwave radiation > 700 Wm^{-2} and daily modelled WTD, and average daily EC gap-filled mid-day β under similar radiation conditions and observed daily WTD during 2004-2005 over a drainage affected tropical peat swamp forest at Palangkaraya, Indonesia. Negative values of WTD mean depths below the hollow surface

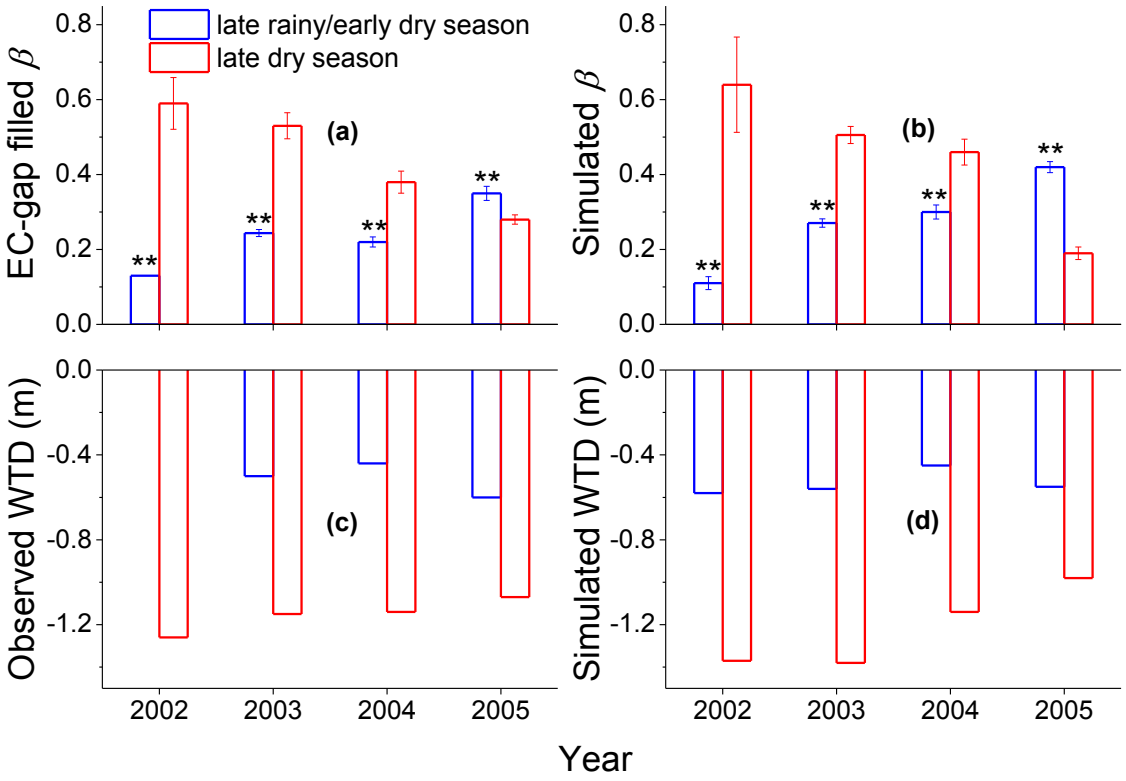

Fig. 2-7. Mean hourly (a) eddy covariance (EC) measured (u^* (friction velocity) > 0.17 m s^{-1}) and (b) modelled mid-day (10:00-14:00 local time) Bowen ratio (β) sorted by using criteria described in Sect. 2-2.2.6; (c) mean daily observed and (d) modelled water table depths (WTD) for 15-day periods in late rainy/early dry seasons (DOY 135-150, 145-160, 170-185 and 145-160 during 2002, 2003, 2004 and 2005 respectively) and 15-day periods in late dry seasons (DOY 240-255 during 2002 and DOY 245-260 during 2003, 2004 and 2005) over a drainage affected tropical peat swamp forest at Palangkaraya, Indonesia. Asterisks (**) on the top of a column represent significant ($P < 0.01$) difference with the adjacent column(s). Bars represent standard errors of means. Negative values of WTD mean depths below the hollow surface

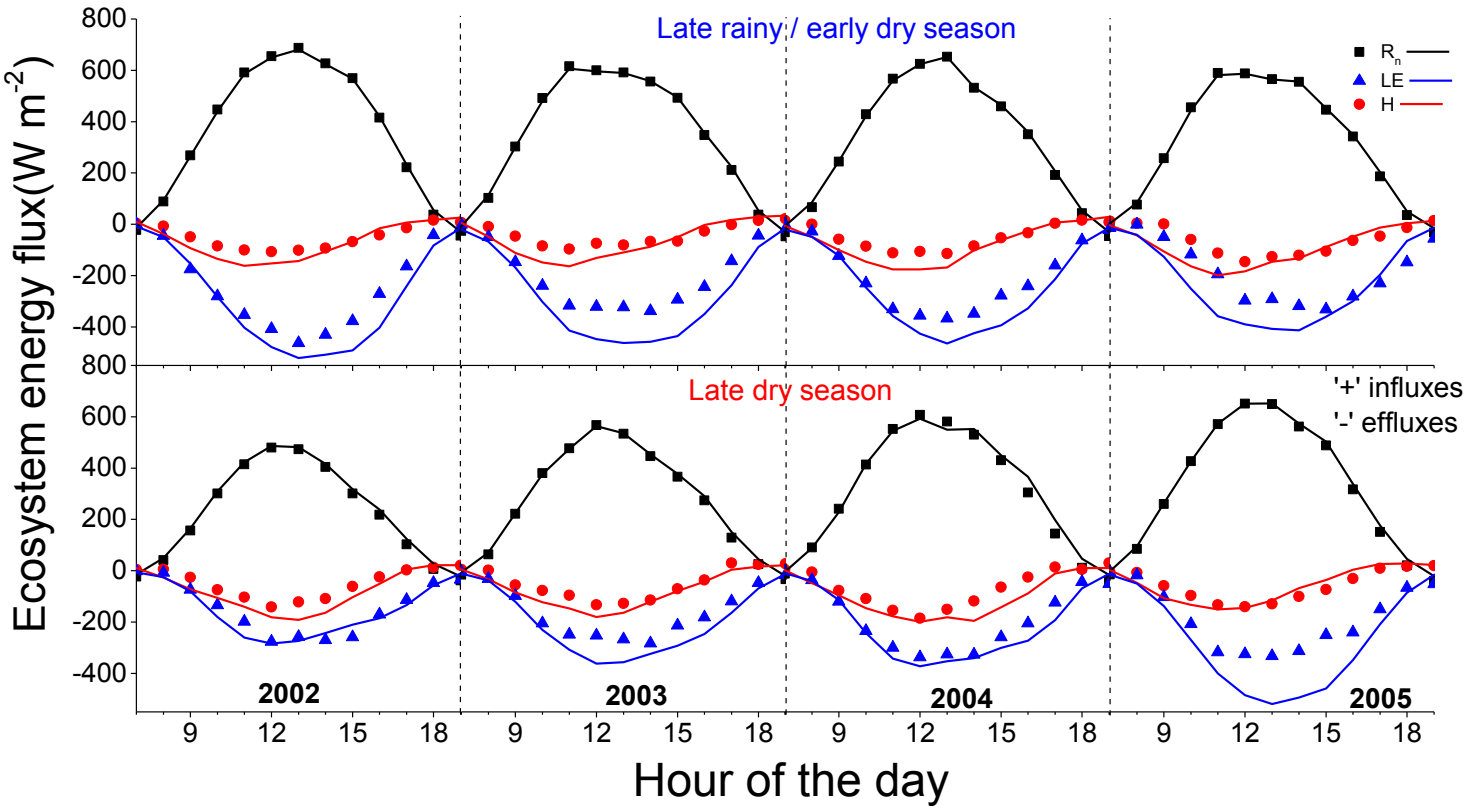

Fig. 2-8. Hourly binned eddy covariance (EC) measured (u^* (friction velocity) > 0.17 m s^{-1}) (symbols) and modelled (lines) ecosystem net radiation (R_n), latent heat (LE) and sensible heat (H) fluxes for 15-day periods in late rainy/early dry seasons (DOY 135-150, 145-160, 170-185 and 145-160 during 2002, 2003, 2004 and 2005 respectively) and 15-day periods in late dry seasons (DOY 240-255 during 2002 and DOY 245-260 during 2003, 2004 and 2005) over a drainage affected tropical peat swamp forest at Palangkaraya, Indonesia

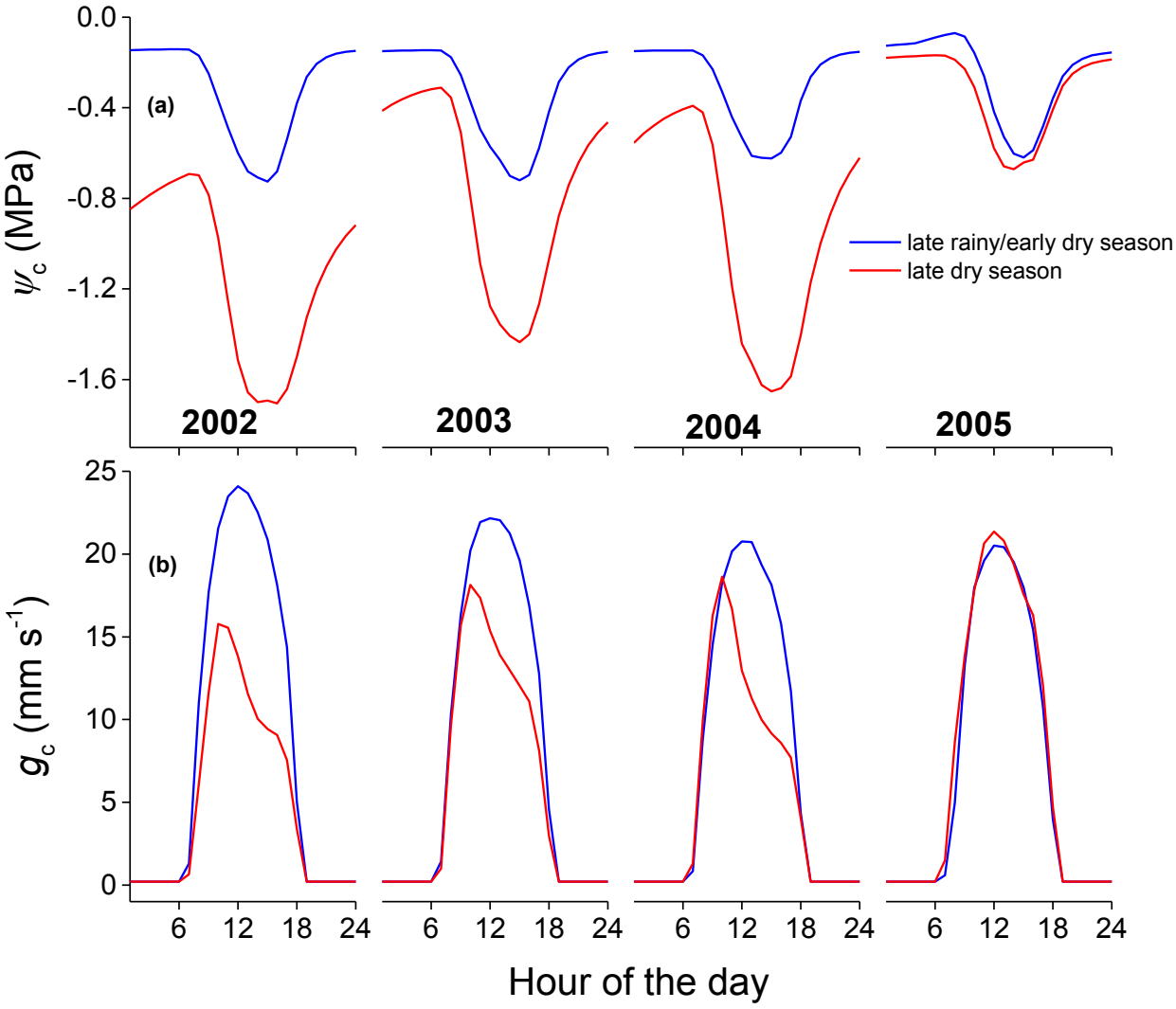

Fig. 2-9. Hourly binned simulated (a) canopy water potentials (ψ_c) and (b) canopy stomatal conductance (g_c) during 15-day periods in late rainy/early dry seasons (DOY 135-150, 145-160, 170-185 and 145-160 during 2002, 2003, 2004 and 2005 respectively) and 15-day periods in late dry seasons (DOY 240-255 during 2002 and DOY 245-260 during 2003, 2004 and 2005) over a drainage affected tropical peat swamp forest at Palangkaraya, Indonesia

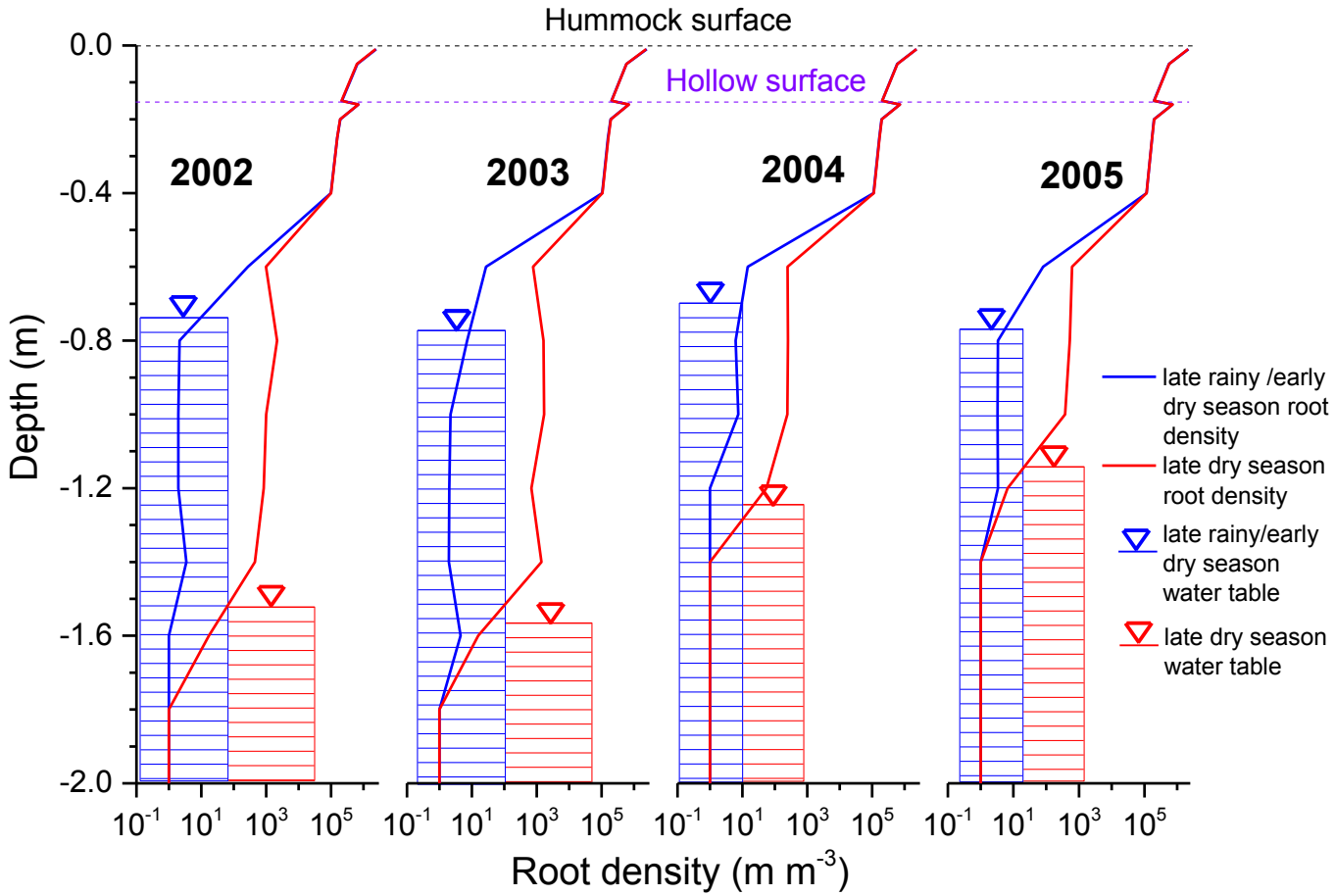

Fig. 2-10. Vertical profile distributions of modelled root density at different depths and position of modelled water table depth (WTD) in late rainy/early dry seasons (DOY 143, 153, 178 and 153 during 2002, 2003, 2004 and 2005 respectively), and late dry seasons (DOY 248, 253, 253 and 253 during 2002, 2003, 2004 and 2005 respectively) over a drainage affected tropical peat swamp forest at Palangkaraya, Indonesia. Negative numbers represented depths below the hummock surface

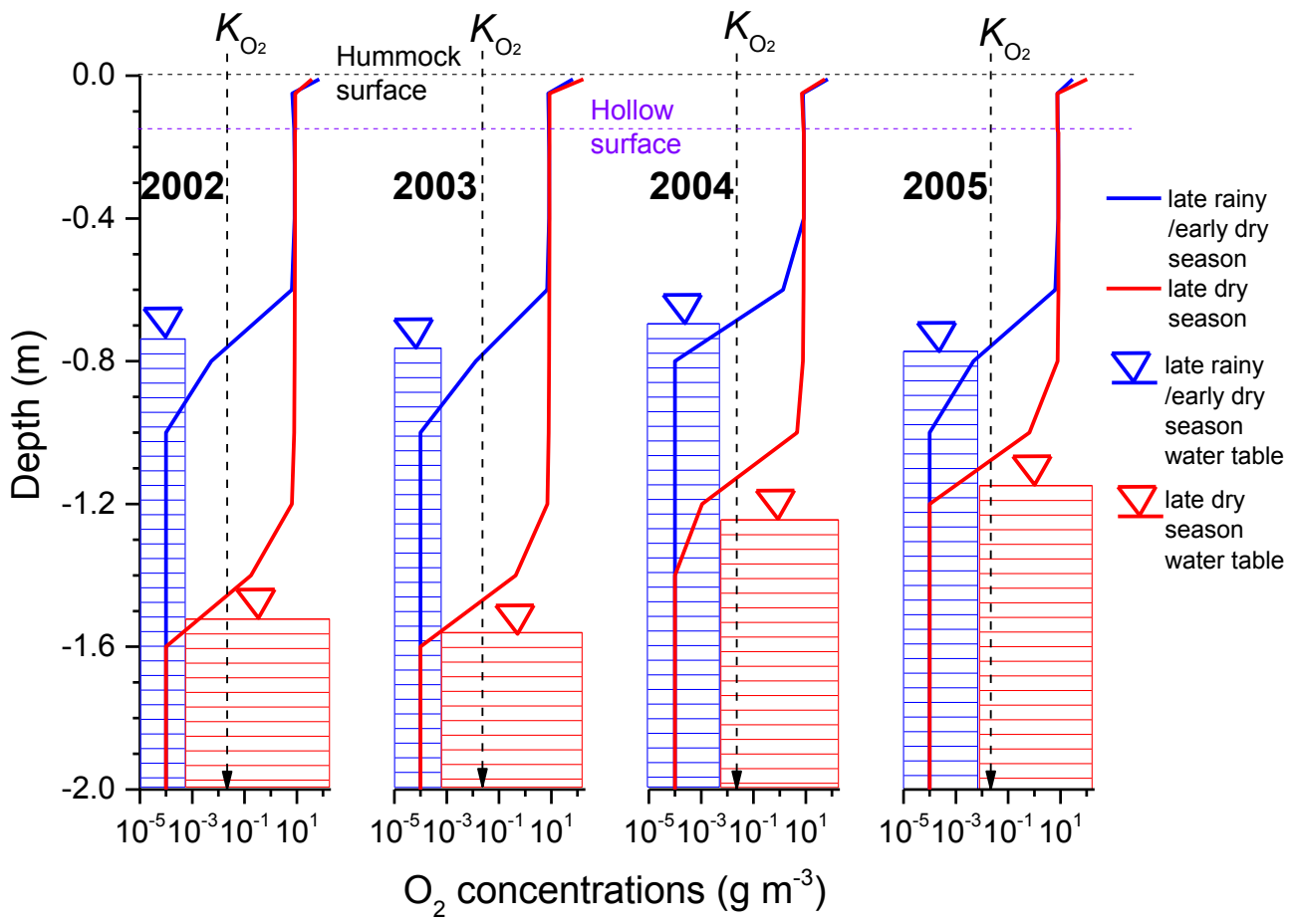

Fig. 2-11. Vertical profile distributions of modelled aqueous O_2 concentrations ($[O_{2s}]$) at different depths and position of modelled water table depth (WTD) in late rainy/early dry seasons (DOY 143, 153, 178 and 153 during 2002, 2003, 2004 and 2005 respectively), and late dry seasons (DOY 248, 253, 253 and 253 during 2002, 2003, 2004 and 2005 respectively) over a drainage affected tropical peat swamp forest at Palangkaraya, Indonesia. K_{O_2} = Michaelis-Menten constant (0.064 g m^{-3}) for root and mycorrhizal O_2 uptake (G4) (Griffin 1972) in *ecosys*. Negative numbers represented depths below the hummock surface

Appendices

Appendix A: Surface water flux

$$\frac{\Delta(d_w A)}{\Delta t} = \sum_i Q_{w,in_i} + \sum_i Q_{w,out_i} + P - E_{res} - E_{surf} \text{ ; kinematic wave theory of overland flow} \quad \text{(A1)}$$

$$Q_{w_i} = v_i \left(d_w - d_{sw}\right) L_i \quad \text{(A2)}$$

$$v_i = \frac{R^{0.67} S_i^{0.5}}{z_r} \quad \text{(A3)}$$

$$R = \frac{s_r d_{mw}}{s_r^2 + 1} \quad \text{(A4)}$$

$$S_i = \frac{2abs[\left(Z + d_{sw} + d_{mw}\right)_{s_i} - \left(Z + d_{sw} + d_{mw}\right)_{d_i}]}{L_{s_i} + L_{d_i}} \quad \text{(A5)}$$

$$E_{res} = \frac{e_{air} - e_{res}(\psi_{res} T_{res})}{r_{a_{res}} + r_{s_{res}}} \quad \text{(A6)}$$

$$E_{surf} = \frac{e_{air} - e_{surf}(\psi_{surf} T_{surf})}{r_{a_{surf}} + r_{s_{surf}}} \quad \text{(A7)}$$

Where, subscripts i=dimensions (i=x, y), s=source cell, d=destination cell, in=flow into the grid cells, and out=flow out of the grid cells; d_w=depth of surface water (m); A=area of landscape position (m^2); t=time (h); Q_w=surface water flux (m^3 m^{-2} h^{-1}); P=precipitation flux (m^3 m^{-2} h^{-1}); E_{res}=evaporation flux from surface residue (m^3 m^{-2} h^{-1}); E_{surf}=evaporation flux from soil surface (m^3 m^{-2} h^{-1}); v=velocity of surface water flow (m h^{-1}); d_{sw}= maximum depth of surface water storage (m); L=length of grid cells (m); R=ratio of cross-sectional area to perimeter of surface flow (m); S=slope (m m^{-1}); z_r=Manning's roughness coefficient (=0.01 m$^{-1/3}$ h); s_r=slope of channel sides during surface flow (m m^{-1}); Z=surface elevation (m); d_{sw}= maximum depth of surface water storage (m); d_{mw}=depth of mobile surface water (m); e_{air}=atmospheric vapour density (g m^{-3}); e_{res}=vapour density at surface residue (g m^{-3}) at current residue water potential (ψ_{res}) and temperature (T_{res}); $r_{a_{res}}$ =boundary layer resistance to evaporation from surface residue (h m^{-1}); $r_{s_{res}}$ =surface resistance to evaporation from surface residue (h m^{-1}); e_{surf}=vapour density at soil surface (g m^{-3}) at current soil surface water potential (ψ_{surf}) and temperature (T_{surf}); $r_{a_{surf}}$ =boundary layer resistance to evaporation from soil surface (h m^{-1}); and $r_{s_{surf}}$ =surface resistance to evaporation from soil surface (h m^{-1}).

Appendix B: Sub-surface water flux

$$\frac{\Delta\theta_w}{\Delta t} = \sum_i (Q_{w_{mat,in_i}} + Q_{w_{mac,in_i}} - Q_{w_{mat,out_i}} - Q_{w_{mac,out_i}}) + \sum_j \left(Q_{w_{b,mat,in_j}} + Q_{w_{b,mac,in_j}} - Q_{w_{b,mat,out_j}} - Q_{w_{b,mac,out_j}} \right) - U_w$$ in (F1) ; 3D continuity equation for water balance of each soil layer (B1)

$Q_{w_{mat_i}} = K'_{mat_i}(\psi_{s_s} - \psi_{s_d})$; soil matrix water flow (B2)

$K'_{mat_i} = \frac{2K_{mat_{s_i}} K_{mat_{d_i}}}{K_{mat_{s_i}} L_{d_i} + K_{mat_{d_i}} L_{s_i}}$; when both the source and destination grid cells are either saturated or unsaturated (Richard's equation) (B3)

$K'_{mat_i} = \frac{2K_{mat_{s_i}}}{L_{s_i} + L_{d_i}}$; when the source cell is saturated and the destination cell is unsaturated (Green-Ampt equation) (B4)

$K'_{mat_i} = \frac{2K_{mat_{d_i}}}{L_{s_i} + L_{d_i}}$; when the source cell is unsaturated and the destination cell is saturated (Green-Ampt equation) (B5)

$Q_{w_{mac_i}} = K'_{mac_i}(\psi_{g_s} - \psi_{g_d})$; soil macropore water flow (B6)

$K'_{mac} = \frac{2K_{mac_s} K_{mac_d}}{K_{mac_s} L_{d_i} + K_{mac_d} L_{s_i}}$ (B7)

$K_{mac} = N_{mac} K^*_{mac}$ (B8)

$K^*_{mac} = \frac{\pi R^4}{8\eta}$; Hagen-Poiseuille's theory of laminar flow in tubes (B9)

$N_{mac} = \theta_{mac} \pi R^2$ (B10)

$Q_{w_{b,mat_j}} = \frac{K_{b,mat_j}\left[\psi'_b - \psi_{s_b} + 0.01\left(d_{z_b} - WTD_x\right)\right]}{L_{t_j}}$; lateral discharge occurs when $d_{z_b} < WTD_x$ and $\psi_{s_b} > \psi'_b + 0.01\left(d_{z_b} - WTD_x\right)$ and lateral recharge occurs when

$d_{z_b} > WTD_x$ (B11)

$$Q_{w_{b,mac_j}} = \frac{K_{b,mac_j} 0.01\left[d_{z_b} - L_{z_b}\left(\theta_{w,mac} - 0.5\right) - WTD_x\right]}{L_{t_j}}$$; lateral discharge occurs when $d_{z_b} < WTD_x$ and lateral recharge occurs when $d_{z_b} > WTD_x$ (B12)

Where, subscripts *i*=dimensions (*i*=*x*, *y, z*), *j*=dimensions (*j*=*x*, *y*), *s*=source cell, *d*=destination cell, *in*=flow into the grid cells, and *out*=flow out of the grid cells; *b*=boundary grid cell; *mat*=soil matrix/micropore; *mac*=soil macropore; θ_w=soil water content (m^3 m^{-3}); Q_w=sub-surface water flux (m^3 m^{-2} h^{-1}); U_w=total root water uptake flux (m^3 m^{-2} h^{-1}); K=hydraulic conductance (m MPa^{-1} h^{-1}); ψ_s=total soil water potential (MPa); K=hydraulic conductivity (m^2 MPa^{-1} h^{-1}); L=length of the grid cells (m); ψ_g=gravitational soil water potential (MPa); N_{mac}=number of macropore channels (m^{-2}); K^*_{mac}=individual macropore hydraulic conductivity (m^4 MPa^{-1} h^{-1} macropore $channel^{-1}$); η=dynamic viscosity of water (MPa h); θ_{mac}=volumetric macropore fraction (m^3 m^{-3}); R=radius of a macropore channel (m); ψ'=soil water potential at saturation (MPa); d_z=depth of the mid-point of a grid cell from the surface (m); L_z=vertical thickness of a grid cell (m); WTD_x=depth of the water table depth at the adjacent watershed with which modelled grid cells exchange water laterally (m); and L_t=lateral distance over which lateral discharge/recharge occurs (m).

Appendix C: Water table depth

$$WTD = -[d_{z,sat} - L_{z,sat}(1 - \frac{\theta_g}{\theta_g^*})]$$; negative sign represents depth below the surface of the a particular grid cell (C1)

Where, WTD=water table depth (m); $d_{z,sat}$=depth to the bottom of the layer immediately above the uppermost saturated layer (m); $L_{z,sat}$=vertical thickness of the layer immediately above the uppermost saturated layer (m); θ_g=current air-filled porosity of the layer immediately above the uppermost saturated layer (m^3 m^{-3}); and θ_g^*=air-filled porosity at air-entry potential of the layer immediately above the uppermost saturated layer (m^3 m^{-3}).

Appendix D: Surface energy balance

$R_n + LE + H + G = 0$; energy balance for each of the canopy, residue and soil surface (D1)

Where, R_n=net radiation (Wm^{-2}); LE=latent heat flux (Wm^{-2}); H=sensible heat flux (Wm^{-2}); and G=ground heat flux (Wm^{-2}).

Appendix E: Canopy transpiration

$R_{nc_i} + LE_{c_i} + H_{c_i} + G_{c_i} = 0$; canopy energy balance (E1)

$$LE_{c_i} = \frac{L\left[e_a - e_{c_i}\left(T_{c_i}, \psi_{c_i}\right)\right]}{r_{a_i}}$$; LE from canopy evaporation (E2)

$$LE_{c_i} = \frac{L\left[e_a - e_{c_i}\left(T_{c_i}, \psi_{c_i}\right)\right]}{r_{c_i} + r_{a_i}} - LE_{c_i} \text{ from } (\text{E2}); \; LE \text{ from canopy transpiration} \tag{E3}$$

$$H_{c_i} = \frac{\rho C_p (T_a - T_{c_i})}{r_{a_i}} \tag{E4}$$

$$r_{cmin_i} = \frac{0.64(C_b - C_{i_i}')}{V_{c_i}'}; \; r_c \text{ driven by rates of carboxylation vs. diffusion} \tag{E5}$$

$$r_{cmin_i} = r_{cmin_i} + \left(r_{cmax_i} - r_{cmin_i}\right) e^{\left(-\beta \psi_{t_i}\right)}; \; r_c \text{ constrained by water stress} \tag{E6}$$

$$\psi_{t_i} = \psi_{c_i} - \psi_{\pi_i} \tag{E7}$$

Where, subscript i=species or plant functional type (PFT); R_{nc}=net radiation at canopy surface (Wm^{-2}); LE=latent heat flux at canopy surface (Wm^{-2}); H=sensible heat flux at canopy surface (Wm^{-2}); G=canopy storage heat flux (Wm^{-2}); L=latent heat of evaporation (=2460 Jg^{-1}); e_a= atmospheric vapour density (g m^{-3}) at ambient T_a and relative humidity; e_c= canopy vapour density (g m^{-3}) at T_c and ψ_c; r_a=boundary layer resistance to evaporation and transpiration from canopy (s m^{-1}); r_c=canopy stomatal resistance (s m^{-1}) to transpiration (=1/g_c; g_c=canopy stomatal conductance in m s^{-1}); ρC_p=volumetric heat capacity of air (=1250 J m^{-3} °C^{-1}); T_a=air temperature (°C); T_c=canopy temperature (°C); r_{cmin}=minimum r_c at ψ_c=0 MPa (s m^{-1}); C_b=[CO_2] in canopy air (μmol mol^{-1}); C_i'=[CO_2] in canopy leaves at ψ_c=0 MPa (μmol mol^{-1}); V_c'=potential canopy CO_2 fixation rate at ψ_c=0 MPa (μmol m^{-2} s^{-1}); r_{cmax}=canopy cuticular resistance to vapour flux (=5.0×10^3 s m^{-1}) (Larcher 2003); β=stomatal resistance shape parameter (=-5 MPa^{-1}) (Grant and Flanagan 2007); ψ_t=canopy turgor potential (MPa); ψ_c=canopy water potential (MPa); and ψ_π=canopy osmotic potential (MPa).

Appendix F: Root and mycorrhizal water uptake

$$U_{w_i} = \sum_l \sum_r U_{w_{i,r,l}} \tag{F1}$$

$$U_{w_{i,r,l}} = \sum_l \sum_r \frac{\psi_{\varsigma_l}' - \psi_{s_l}'}{\Omega_{s_{i,r,l}} + \Omega_{r_{i,r,l}} + \sum_x \Omega_{a_{i,r,l,x}}} \tag{F2}$$

$$\Omega_{s_{i,r,l}} = \ln \left[\frac{\left(\frac{d_{i,r,l}}{r_{i,r,l}}\right)}{\left(\frac{2\pi L_{i,r,l}}{\kappa_{r_{i,r,l}}}\right)} \right] \frac{\theta_{P_l}}{\theta_{w_l}} \tag{F3}$$

$$\Omega_{r_{i,r,l}} = \frac{\Omega'_{r_{i,r}}}{L_{i,r,l}} \quad \text{(F4)}$$

$$\Omega_{a_{i,r,l,x=1}} = \frac{\Omega_{a_{i,r}} Z_l}{\left[n_{i,r,l,1} (\frac{r_{i,r,l,1}}{r'_{i,r}})^4 \right]} + \gamma \Omega'_{a_{i,r}} \left[\frac{Z_{b_i}}{n_{i,r,l,1} (\frac{r_{b_i}}{r'_{b_i}})^4} \right] \left[\frac{\sum_{i,r,l} M_{i,r,l}}{M_{i,r,l}} \right] \quad \text{(F5)}$$

$$\Omega_{a_{i,r,l,x=2}} = \Omega_{a_{i,r}} \frac{\left[\frac{L_{i,r,l,2}}{n_{i,r,l,2}} \right]}{\left[n_{i,r,l,2} (\frac{r_{i,r,l,2}}{r'_{i,r}})^4 \right]} \quad \text{(F6)}$$

$$\frac{\left[e_a - e_{c_i}\left(T_{c_i}, \psi_{c_i}\right) \right]}{r_{c_i} + r_{a_i}} = \sum_l \sum_r \frac{\psi'_{c_i} - \psi'_{s_i}}{\Omega_{s_{i,r,l}} + \Omega_{r_{i,r,l}} + \sum_x \Omega_{a_{i,r,l,x}}} + X_{c_i} \frac{\Delta \psi_{c_i}}{\Delta t} \quad \text{(F7)}$$

Where, subscripts i=species or plant functional type (PFT), r=root/mycorrhizae, l=soil/canopy layer, x=1, 2 (1=primary root/ mycorrhizae, 2=secondary root/ mycorrhizae); U_w=water uptake by root and mycorrhizal surfaces (m^3 m^{-2} h^{-1}); ψ_c=canopy water potential (MPa); $\psi'_c = \psi_c$ + canopy gravitational potential (MPa); ψ'_s=soil water potential (ψ_s)+ soil gravitational potential (MPa); Ω_s = radial resistance to water transport from soil to surface of roots or mycorrhizae (MPa h m^{-1}); Ω_r = radial resistance to water transport from surface to axis of roots or mycorrhizae (MPa h m^{-1}); Ω_a = axial resistance to water transport along axes roots or mycorrhizae (MPa h m^{-1}); d= half distance between adjacent roots (m); r=radius of roots or mycorrhizae at ambient root/mycorrhizal water potential (ψ_r); L=length of roots or mycorrhizae (m); κ_r = hydraulic conductivity between soil and root surface (m^2 MPa^{-1} h^{-1}); θ_P=total soil porosity (m^3 m^{-3}); θ_w=soil water content (m^3 m^{-3}); Ω'_r = radial resistivity to water transport from surface to axes of roots or mycorrhizae (MPa h m^{-2}) (1.0×10^4) (Doussan et al. 1998); Z_l=depth of soil layer l from soil surface (m); n= number of root/mycorrhizal axes; r' = radius roots or mycorrhizae at ψ_r=0 MPa; Ω'_a = axial resistivity to water transport along root or mycorrhizal axes (MPa h m^{-4}) (4.0×10^9 for deciduous) (Larcher 2003); Z_b= length of bole from soil surface to top of canopy (m); r_b=radius of bole at ambient ψ_c; r'_b=radius of bole at ψ_c=0 MPa; M= mass of roots or mycorrhizae (g m^{-2}); e_a= atmospheric vapour density (g m^{-3}) at ambient T_a and relative humidity; e_c= canopy vapour density (g m^{-3}) at T_c and ψ_c; r_a=boundary layer resistance to evaporation and transpiration from canopy (s m^{-1}); r_c=canopy stomatal resistance (s m^{-1}) to transpiration; T_a=air temperature (°C); T_c=canopy temperature (°C); ψ_c=canopy water potential (MPa); X_c= canopy capacitance (m^3 m^{-2} MPa^{-1}) ; and t=time (h).

Appendix G: Root and mycorrhizal respiration and growth

$$R_a = \sum_i \sum_j \left(R_{c_{i,j}} + R_{s_{i,j}} \right) + \sum_i \sum_l \sum_z (R_{c_{i,r,l}} + R_{s_{i,r,l}}) + E_{N,P}(U_{NH_4\,i,r,l} + U_{NO_3\,i,r,l} + U_{PO_4\,i,r,l}) \quad \text{(G1)}$$

$$R_{c_{i,j}} = R_c' \sigma_{C_{i,j}} f_{Ta_i} \quad \text{(G2)}$$

$R_{c_{i,r,l}} = R_c' \sigma_{C_{i,r,l}} f_{T_{a_i}} \frac{U_{O_2\,i,r,l}}{U_{O_2}{}'_{i,r,l}}$; O_2 constraint on root respiration from active uptake (G3)

$U_{O_2\,i,r,l} = U_{O_2}{}'_{i,r,l} \frac{\left[O_{2r_{i,r,l}}\right]}{\left[O_{2r_{i,r,l}}\right] + K_{O_2}} = U_{w_{i,r,l}} \left[O_{2s_l}\right] + 2\pi L_{i,r,l} D_{s_{O_2}} \left(\left[O_{2s_l}\right] - \left[O_{2r_{i,r,l}}\right] \right)$
$ln\left[\frac{r_{s_l} + r_{r_{i,r,l}}}{r_{r_{i,r,l}}}\right] + 2\pi L_{i,r,l} D_{r_{O_2}} \left(\left[O_{2q_{i,r,l}}\right] - \left[O_{2r_{i,r,l}}\right] \right) ln\left[\frac{r_{q_{i,r,l}}}{r_{r_{i,r,l}}}\right]$
; active O_2 uptake by roots coupled with diffusion of O_2 through root aerenchyma (G4)

$$U_{O_2}{}'_{i,r,l} = 2.67 R_a{}'_{i,r,l} \quad \text{(G5)}$$

$$R_{m_{i,j}} = \sum_z N_{i,j,z} R_m{}' f_{Tm_i} \quad \text{(G6)}$$

$$R_{g_{i,j}} = \left(R_{c_{i,j}} - R_{m_{i,j}} \right) \left(\psi_{t_i} - \psi_t' \right); \text{growth when } R_m < R_c \text{and } \psi_{t_i} > \psi_t' \quad \text{(G7)}$$

$\frac{\Delta M_{R_{i,r,l}}}{\Delta t} = \left[R_{g_{i,r,l}} \frac{1 - Y_{g_{i,r}}}{Y_{g_{i,r}}} \right] - R_{s_{i,r,l}} - l_{C_{i,r,l}}$; root growth driven by R_g (G8)

$\frac{\Delta L_{i,r,l,1}}{\Delta t} = \frac{\frac{\Delta M_{R_{i,r,l,1}}}{\Delta t}}{y_i} \frac{\nu_r}{\rho_r \pi r_{r\,i,r,l,1}^2 \left(1 - \theta_{pr_{i,r}}\right)}$; extension of primary root axis driven by root mass growth (G9)

$\frac{\Delta L_{i,r,l,2}}{\Delta t} = \frac{\Delta M_{R_{i,r,l,2}}}{\Delta t} \frac{\nu_r}{\rho_r \pi r_{r\,i,r,l,2}^2 (1 - \theta_{pr_{i,r}})}$; extension of secondary root axis driven by root mass growth (G10)

Where, subscripts *i*=species or plant functional type (PFT), *j*=branch/tiller, *l*=soil or canopy layer, *z*=organ (root (*r*), canopy, stem, mycorrhizae); R_a= total autotrophic respiration (g C m^{-2} h^{-1}); R_c= autotrophic respiration of σ_C (g C m^{-2} h^{-1}), *1*=primary root axis, *2*=secondary root axis; R_s=respiration from remobilization of leaf carbon (g C m^{-2} h^{-1}); $E_{N,P}$=energy cost of nutrient uptake (=2.15 g C g N^{-1} or P^{-1}) (Veen 1981); U_{NH_4} =NH_4^+ uptake by roots or mycorrhizae (g N m^{-2} h^{-1}); U_{NO_3} = NO_3^- uptake by roots or mycorrhizae (g N m^{-2} h^{-1}); U_{PO_4} = $H_2PO_4^-$ uptake by

roots or mycorrhizae (g P m^{-2} h^{-1}); R_c' =specific autotrophic respiration of σ_C at 25°C (=0.015 g C g C^{-1} h^{-1}); σ_C= non-structural C product of CO_2 fixation (g C g C^{-1}); f_{Ta}=temperature effect on R_a; U_{O_2} = O_2 uptake by roots and mycorrhizae under ambient O_2 (g O m^{-2} h^{-1}); U'_{O_2} = O_2 uptake by roots and mycorrhizae under non-limiting O_2 (g O m^{-2} h^{-1}); [O_{2r}]= aqueous O_2 concentration at root or mycorrhizal surfaces (g m^{-3}); K_{O_2} = Michaelis-Menten constant for root or mycorrhizal O_2 uptake (=0.064 g m^{-3}) (Griffin 1972); U_w=root or mycorrhizal water uptake flux (m^3 m^{-2} h^{-1}); [O_{2s}]= aqueous O_2 concentration is soil (g m^{-3}); L=root length (m m^{-2}); $D_{s_{O_2}}$ =aqueous diffusivity of O_2 from soil to root or mycorrhizal surfaces (m^2 h^{-1}); r_s= thickness of soil water films (m); r_r= root or mycorrhizal radius (=1.0 × 10^{-4} m); $D_{s_{O_2}}$ =aqueous diffusivity of O_2 from root aerenchyma to root or mycorrhizal surfaces (m^2 h^{-1}); [O_{2q}]=aqueous O_2 concentration in root or mycorrhizal aerenchyma (g m^{-3}); r_q= radius of root aerenchyma (m); R_a' = R_a under non-limiting O_2 (g C m^{-2} h^{-1}); R_m= above-ground maintenance respiration (g C m^{-2} h^{-1}); N=number of species, or branch/tiller or organs; R_m' = specific maintenance respiration of σ_C at 25°C (=0.0115 g C g N^{-1} h^{-1}) (Barnes et al. 1997); f_{Tm}= temperature effect on R_m (Q_{10}=2.25); R_g=growth respiration (g C m^{-2} h^{-1}); ψ_t= canopy turgor potential (MPa); ψ_t'=canopy turgor potential (MPa) at ψ_c=0 MPa; M_R=; t=time (h); Y_g= fraction of σ_C used for growth expended as R_g by organ z (g C g C^{-1}) [0.28 (z = leaf), 0.24 (z = root and other non-foliar), 0.20 (z = wood)] (Waring and Running 1998); l_C=carbon litter fall from leaf or root (g C m^{-2} h^{-1}) ; y=plant population (m^{-2}); v_r= specific volume of root biomass (m^3 g^{-1}); and θ_{pr}= root or mycorrhizal porosity representing aerenchyma fraction (m^3 m^{-3}).

Appendix H: Gas flux

$$Q_{ds\gamma_s} = \alpha_{gs_s} D_{d\gamma} \left(S'_\gamma f_{T_{d\gamma_s}} \left[\gamma_{gs}\right]_s - \left[\gamma_{ss}\right]_s \right)$$; volatilization-dissolution between aqueous and gaseous phases in soil (H1)

$$Q_{dr\gamma_s} = \alpha_{gr_s} D_{d\gamma} \left(S'_\gamma f_{T_{d\gamma_s}} \left[\gamma_{gr}\right]_s - \left[\gamma_{sr}\right]_s \right)$$; volatilization-dissolution between aqueous and gaseous phases in roots (H2)

$$Q_{gs\gamma_i} = -Q_{w_i} \left[\gamma_{gs}\right]_s + \frac{2D_{gs\gamma_i} \left(\left[\gamma_{gs}\right]_s - \left[\gamma_{gs}\right]_d \right)}{L_{s_i} + L_{d_i}}$$; 3D convective-conductive gas flux between two adjacent grid cells (H3)

$$Q_{gr\gamma_{i=z}} = \frac{D_{gr\gamma_{i=z}} \left(\left[\gamma_{gr}\right]_d - \left[\gamma_a\right] \right)}{\sum_{1,i=z} L_{d_{i=z}}}$$; convective-conductive gas flux between roots and the atmosphere (H4)

$D_{gs\gamma_i} = \frac{D'_{g\gamma} f_{T_{g_s}} \left[0.5\left(\theta_{g_s} + \theta_{g_d}\right)\right]^2}{\theta_{P_s}^{0.67}}$; 3D gaseous diffusivity between two adjacent grid cells as functions of air-filled porosities in those cells (H5)

$D_{gr\gamma_{i=z}} = \frac{D'_{g\gamma} f_{T_{g_s}} \theta_{pr_s}^{1.33} A_{r_s}}{A_{i=x,y}}$; gaseous diffusivity as a function of air-filled porosity in the roots (H6)

Where, subscripts i=dimensions (i=*x, y, z*), s=source cell, d=destination cell; $Q_{ds\gamma}$=volatilization – dissolution of gas γ between aqueous and gaseous phases in soil (g m^{-2} h^{-1}); α_{gs}=air-water interfacial area in soil (m^2 m^{-2}); $D_{d\gamma}$= volatilization - dissolution transfer coefficient for gas γ (m^2 h^{-1}); S'_γ=Ostwald solubility coefficient of gas γ at 30°C (0.0293 for $\gamma = O_2$) (Wilhelm et al. 1977); $f_{T_{d\gamma}}$ =temperature dependence of S'_γ (Wilhelm et al. 1977); [γ_{gs}]=gaseous concentration of gas γ in soil (g m^{-3}); [γ_{ss}]= aqueous concentration of gas γ in soil (g m^{-3}); $Q_{dr\gamma}$= volatilization – dissolution of gas γ between aqueous and gaseous phases in root (g m^{-2} h^{-1}); α_{gr}= air-water interfacial area in roots (m^2 m^{-2}) (Skopp 1985); [γ_{gr}]= gaseous concentration of gas γ in root (g m^{-3}); [γ_{sr}]= aqueous concentration of gas γ in root (g m^{-3}); $Q_{gs\gamma}$= gaseous flux of gas γ in soil (g m^{-2} h^{-1}); Q_w=sub-surface water flux (m^3 m^{-2} h^{-1}); $D_{gs\gamma}$=gaseous diffusivity of gas γ in soil (m^2 h^{-1}) (Millington and Quirk 1960); L=length of grid cells (m); $Q_{gr\gamma}$=gaseous flux of gas γ between roots and the atmosphere (m^2 h^{-1}); $D_{gr\gamma}$=gaseous diffusivity of gas γ in root (m^2 h^{-1}) (Luxmoore et al. 1970a, b); [γ_a]=atmospheric concentration of gas γ (g m^{-3}); $D'_{g\gamma}$ =diffusivity of gas γ in air at 0°C (m^2 h^{-1}) (6.43×10^{-2} m^2 h^{-1} for γ=O_2) (Campbell 1985); f_{T_g} =temperature dependence of $D'_{g\gamma}$ (Campbell 1985); θ_g=air-filled porosity (m^3 m^{-3}); θ_P=total porosity of soil (m^3 m^{-3}); θ_{pr}=root or mycorrhizal porosity representing aerenchyma fraction (m^3 m^{-3}); A_r=root cross-sectional area (m^2); and A=area of landscape position (m^2).

Chapter 3 : Modelling Effects of Seasonal Variation in Water Table Depth on Net Ecosystem CO_2 Exchange of a Tropical Peatland

3-1. Introduction

Seasonal and interannual fluctuations in water table depth (WTD) can affect peatland net CO_2 exchange through complex effects on soil oxidation-reduction reactions and hence on nutrient transformations. Shallow WTD during rainy seasons slows convective-dispersive transport of O_2 through wet soils. Consequent reduction in soil O_2 concentrations slows O_2 uptake used to drive aerobic oxidation-reduction reactions by soil microbes and roots and hence reduces heterotrophic and root respiration. Microbial energy yield from oxidation of reduced C coupled to reduction of O_2 under aerobic conditions exceeds that from oxidation coupled to reduction of alternative electron acceptors (Thomas et al. 1991) under anaerobic conditions. Lower anaerobic energy yields slow microbial growth and therefore reduce heterotrophic respiration. Root oxidation-reduction reactions driving root growth and nutrient uptake also require O_2 which is scarce when WTD is shallow. Reduced heterotrophic and root respiration thus result in reduced ecosystem respiration (R_e) with shallow WTD during rainy seasons, as reported in many field studies (Limpens et al. 2008, Couwenberg et al. 2010, Sulman et al. 2010, Flanagan and Syed 2011). Slower microbial growth also reduces decomposition and nutrient mineralization, as well as root growth and nutrient uptake and hence gross primary productivity (GPP) (Cai et al. 2010, Murphy and Moore 2010, Flanagan and Syed 2011, Sulman et al. 2012).

More rapid O_2 transport with WTD drawdown during early dry seasons may increase root and heterotrophic respiration and hence R_e (Cai et al. 2010, Sulman et al. 2010). Consequent increases in mineralization and root growth, and thereby nutrient availability and uptake can also raise GPP during this hydroperiod (Cai et al. 2010, Sulman et al. 2010, Flanagan and Syed 2011,

Jauhiainen et al. 2012b, Sulman et al. 2012). Increased GPP in this hydroperiod may further hasten R_e through increased production of fresh labile C in the forms of litter fall and root exudates (Limpens et al. 2008).

These increases, however, may not sustain with further WTD drawdown in the later part of a prolonged dry season when WTD falls below a critical depth. This critical WTD is highly site-specific depending upon peat forming vegetation and artificial drainage. For instance, this critical WTD may vary from as shallow as 0.4 m (Sonnentag et al. 2010) for pristine peatlands dominated by moss with shallow rhizoids to as deep as 0.9 m (Schwärzel et al. 2006) for drained peatlands dominated by vascular plants with deep root system. When WTD falls below the critical depth for a particular peatland, near surface peat desiccation occurs. This desiccation can reduce near surface peat decomposition by reducing microbial access to substrate e.g. dissolved organic C (DOC) in desiccated near-surface soil (Dimitrov et al. 2010a), thereby slowing oxidation-reduction reactions and hence microbial growth. The reduction in decomposition of desiccated near surface peat can be partially or fully offset by increases in decomposition of better aerated deeper peat, thereby causing no net changes in R_e during this hydroperiod (Lafleur et al. 2005, Strack and Waddington 2007, Dimitrov et al. 2010a). However, plant water stress from near surface peat desiccation might also cause a decline in GPP during deep WTD hydroperiods (Sulman et al. 2010, Dimitrov et al. 2011), thereby lowering net ecosystem productivity (NEP). Therefore, responses of peatland ecosystem net CO_2 exchange to WTD fluctuations are governed by basic soil hydrological and biological processes and their interactions with plant physiology.

Process-based ecosystem models can provide us with means of understanding basic mechanisms behind WTD effects on peatland net ecosystem CO_2 exchange. To accomplish this,

a model should explicitly represent oxidation-reduction reactions, coupled with aqueous and gaseous transfers of their reactants and products. These processes require modelling WTD dynamics, soil moisture retention characteristics, gas transport through soil, differential substrate quality for microbial degradation and hydrolysis (e.g. labile vs. recalcitrant), nutrient transformations driven by these reactions, and microbial and plant nutrient uptake. However, in a review of 7 widely used ecosystem models, Sulman et al. (2012) found only *ecosys* (Grant 2001) included processes to limit both CO_2 fixation and respiration under shallow WTD. The predictive capacity of the other models were limited by (1) not explicitly simulating WTD dynamics and consequently not modelling aerobic vs. anaerobic zones from water influxes (e.g. precipitation, lateral recharge) vs. effluxes (e.g. evapotranspiration, lateral discharge) (Van Huissteden et al. 2006, St-Hilaire et al. 2008, Kurbatova et al. 2009), (2) parameterizing models with empirical rate constants and/or scalar functions for aerobic vs. anaerobic decomposition (Frolking et al. 2002, Bond-Lamberty et al. 2007, St-Hilaire et al. 2008) instead of simulating biogeochemical oxidation-reduction reactions affected by soil aerobicity, and (3) using scalar functions that reduce productivity in wet soils through a driver variable such as stomatal conductance (g_s) (Frolking et al. 2002, Bond-Lamberty et al. 2007) instead of simulating nutrient limitations to CO_2 fixation imposed by reduced nutrient availability and root nutrient uptake caused by slower oxidation-reduction reactions resultant of slower O_2 transport processes through soils and roots. The general purpose terrestrial ecosystem model *ecosys* includes site-independent algorithms representing all the processes affected by aerobicity mentioned above, thereby excluding the need for arbitrary model parameterization. The model could therefore successfully simulate WTD effects on R_e and GPP of different peatlands without site-specific parameterization (Dimitrov et al. 2010a, 2011, Grant et al. 2012b).

All of the previous peatland modelling studies mentioned above have been tested only against measurements from northern temperate and boreal peatlands. Modelling the fate of vulnerable C storage in tropical peatlands under WTD fluctuations is still largely under-investigated. For instance, modelling WTD effects on tropical peat soil respiration has to date predominantly included regressions of soil CO_2 fluxes against WTD (Melling et al. 2005, Jauhiainen et al. 2008, Hirano et al. 2009, Couwenberg et al. 2010, Hooijer et al. 2010, Jauhiainen et al. 2012a) without taking other confounding factors like land use, nutrient availability, nature of the peat, ecosystem productivity etc. into consideration (Murdiyarso et al. 2010). Modelling eco-physiological response to hydrology in tropical peatlands is particularly important since climates in tropical peatlands are very different from those in northern temperate and boreal peatlands. Tropical peatlands are formed under high temperature and precipitation, an important consequence of which is that a small WTD drawdown might cause a large increase in peat decomposition (Page et al. 2009). Distinct dry seasons almost every year together with human intervention such as drainage have been reported to deepen WTD, thereby causing rapid decomposition of very old and thick (up to > 26,000 years old and 9 m thick (Page et al. 2004)) tropical peat deposits (Jauhiainen et al. 2008, Hirano et al. 2009, Couwenberg et al. 2010, Hirano et al. 2012). Moreover, tropical peatlands are generally formed by roots and remains of trees and devoid of bryophytes (e.g. mosses) as opposed to the northern peatlands that are mainly formed by mosses or co-dominated by mosses and vascular plants. Trees have well developed root systems and stomatal regulations that are lacking in bryophytes. These differences can alter plant water and nutrient uptake processes in tree dominated peatlands from those in bryophyte dominated peatlands. Consequently WTD effects on productivity of tropical peatlands may be very different than of those in northern boreal and temperate peatlands. Besides, tropical peat

deposits formed by tree remains can have very different substrate quality for microbial decomposition than boreal and temperate moss peatlands and hence may have a different WTD – peat respiration interaction. This difference in peat forming materials can also cause different hydrological characteristics thereby producing very different water retention and transport phenomena between tropical and temperate / boreal peatlands. Variations in climate and peat forming vegetation thus necessitate rigorous testing of process models against measurements across peatlands developed under very different climate (e.g. boreal vs. tropical) and vegetation (e.g. moss vs. tree) to improve predictive capacity for eco-hydrological controls on peatland C balance.

The process-based hourly time step ecosystem model *ecosys* previously simulated the effects of WTD fluctuations on net CO_2 exchange of northern boreal peatlands (Dimitrov et al. 2011, Grant et al. 2012b). Testing the same model against site measurements of a tropical peatland would thus be an important test of the versatility of its algorithms representing the processes described above. Such a test will allow us to determine whether our current understanding of peatland water, nutrient and C interactions is sufficiently robust to capture complex WTD effects on peatland R_e and GPP over a wide range of climates (boreal to tropical). Our study hereby uses *ecosys* to simulate WTD effects on net CO_2 exchange of a tropical peat swamp forest at Palangkaraya, Central Kalimantan, Indonesia (Hirano et al. 2007). These effects are summarized in modelling hypotheses during three seasonal hydroperiods as follows:

(1) Shallow WTD in the rainy season (November-April) causes lower net ecosystem productivity (NEP) mainly through slower CO_2 fixation due to reduced nutrient availability and uptake caused by slower nutrient transformation and root growth and uptake resulting from slower O_2 diffusion through wet soils.

(2) When WTD increases during the early dry season (May-July), more rapid O_2 transport into larger unsaturated soil zones enables faster root growth and microbial nutrient transformations that in turns results in more rapid root nutrient uptake and CO_2 fixation which contributes to a higher NEP. Increased O_2 availability in this hydroperiod may, however, result in more rapid aerobic decomposition in deeper peat layers. Drying of surface residues and near surface peat layers at the same time can reduce surface and near surface soil respiration thereby offsetting the increase in deeper peat respiration, resulting in no net increase of R_e.

(3) Deeper WTD during the late dry season (August-October), causes greater desiccation of near surface peat which forces declines in root and canopy water potentials, and consequently in canopy conductance and CO_2 fixation, thereby reducing NEP. Further deepening of the aerobic peat zone during this hydroperiod may lead to an increase in deeper peat respiration which exceeds reduction in near surface peat respiration through desiccation, raising R_e and further lowering NEP.

3-2. Methods

3-2.1. Model development

3-2.1.1. General

Ecosys is a general purpose terrestrial ecosystem model that simulates 3D soil-microbes - plant -atmosphere water, energy, C and nutrient (nitrogen, phosphorus) transfer schemes (Grant 2001). Algorithms governing WTD effects on net ecosystem CO_2 exchange that are related to our modelling hypotheses are described in the following sections. Related equations are described in Appendices A to E in the Supplementary Material at the end of the thesis. Necessary

equations are cited within the text within round brackets with the letter representing a particular appendix in the supplementary materials.

3-2.1.2. Heterotrophic respiration

Organic transformations in *ecosys* occur in five organic matter-microbe complexes (coarse woody litter, fine non-woody litter, animal manure, particulate organic C (POC), and humus), each of which consists of five organic states (three decomposition substrates: solid organic C, sorbed organic C and microbial residue C, as well as the decomposition product: DOC, and the decomposition agent: microbial biomass) in a surface residue layer and in each soil layer. The decomposition rates of each of the three substrates and resulting production of DOC in each complex is a first-order function of the active biomasses (M) of diverse heterotrophic microbial functional types, including obligate aerobes (bacteria and fungi), facultative anaerobes (denitrifiers), obligate anaerobes (fermenters), heterotrophic (acetotrophic) and autotrophic (hydrogenotrophic) methanogens, and aerobic and anaerobic heterotrophic diazotrophs (non-symbiotic N_2 fixers) (A1, A2). Decomposition rates are calculated from the fraction of substrate mass colonized by M (A4). Growth of M by each microbial functional type (A25) is calculated from its uptake of DOC (A21), driven by energy yields from growth respiration (R_g) (A20) remaining after subtracting maintenance respiration (R_m) (A18) from heterotrophic respiration (R_h) (A11) driven by DOC oxidation (A13). This oxidation may be limited by microbial O_2 reduction (A14) driven from microbial O_2 demand (A16) and constrained by O_2 diffusion calculated from aqueous O_2 concentrations in soil ($[O_{2s}]$) (A17). Values of $[O_{2s}]$ are maintained by convective-dispersive transport of O_2 from the atmosphere to gaseous and aqueous phases of the soil surface layer (D15), by convective-dispersive transport of

O_2 through gaseous and aqueous phases in adjacent soil layers (D16, D19), and by dissolution of O_2 from gaseous to aqueous phases within each soil layer (D14a).

With shallower WTD during the rainy season, air-filled porosity (θ_g) above the water table may decline to values at which low O_2 diffusivity in the gaseous phase (D_g) (D17) may reduce gaseous O_2 transport (D16), while θ_g below the water table is zero and so prevents gaseous O_2 transport. During this hydroperiod, [O_{2s}] relies more on O_2 transport through the slower aqueous phase (D19). A consequent decline in [O_{2s}] slows O_2 uptake (A17) and hence R_h (A14), R_g (A20) and growth of M (A25). Lower M in turn slows decomposition of organic C (A1, A2) and production of DOC which further slows R_h (A13), R_g and growth of M. Although some microbial functional types can sustain DOC oxidation by reducing alternative electron acceptors (e.g. methanogens reducing acetate or CO_2 to CH_4, and denitrifiers reducing NO_x to N_2O or N_2), lower energy yields from these reactions reduce R_g (A21), and hence M growth, organic C decomposition and subsequent DOC production. Slower decomposition of organic C under low [O_{2s}] also causes slower decomposition of organic nitrogen and phosphorus (A7) and production of dissolved organic nitrogen (DON) and phosphorus (DOP), which causes slower uptake of microbial nitrogen and phosphorus (A22) and hence growth of M (A29). This slower growth causes slower mineralization of N and P and hence greater aqueous concentrations of NH_4^+, NO_3^- and $H_2PO_4^-$ (A26).

Increase in θ_g with WTD drawdown during the dry season results in greater D_g (D17) and hence more rapid gaseous O_2 transport. A consequent rise in [O_{2s}] increases O_2 uptake (A17) and hence R_h (A14), R_g (A20) and growth of M (A25). Larger M in turn hastens decomposition of organic C (A1, A2) and production of DOC which further hastens R_h (A13), R_g and growth of M. More rapid decomposition of organic C under adequate [O_{2s}] in this hydroperiod also causes

more rapid decomposition of organic nitrogen and phosphorus (A7) and production of DON and DOP, which increases uptake of microbial nitrogen and phosphorus (A22) and hence growth of *M* (A29). This rapid growth causes rapid mineralization of N and P and hence greater aqueous concentrations of NH_4^+, NO_3^- and $H_2PO_4^-$ (A26).

However, desiccation of surface litter and near surface soil resulting from deepening WTD decreases litter and soil water contents and potentials (ψ_s) which cause an increase in aqueous microbial concentrations [*M*] (A15). This reduces microbial access to the substrate for decomposition through an algorithm for competitive inhibition of microbial exo-enzymes (A4) from Lizama and Suzuki (1991), thereby reducing R_h (A13).

3-2.1.3. Autotrophic respiration and growth

Growth of root and shoot phytomass in each plant population is calculated from its assimilation of the non-structural C product of CO_2 fixation (σ_C) (C20). Assimilation is driven by R_g (C17) remaining after subtracting R_m (C16) from autotrophic respiration (R_a) (C13) driven by oxidation of σ_C (C14). This oxidation in roots may be limited by root O_2 reduction (C14b) which is driven by root O_2 demand to sustain C oxidation and nutrient uptake (C14e), and constrained by O_2 uptake controlled by concentrations of aqueous O_2 in the soil ($[O_{2s}]$) and roots ($[O_{2r}]$) (C14d). Values of $[O_{2s}]$ are maintained by convective-dispersive transport of O_2 through soil gaseous and aqueous phases and by dissolution of O_2 from soil gaseous to aqueous phases. Values of $[O_{2r}]$ are maintained by convective-dispersive transport of O_2 through the root gaseous phase (D16d) and by dissolution of O_2 from root gaseous to aqueous phases (D14b) through processes analogous to those described under Sect. 3-2.1.2. This transport depends on species-specific values used for root air-filled porosity (θ_{pr}) (D17b).

Low θ_g with shallow WTD during the rainy season reduces soil O_2 transport, forces root O_2 uptake to rely more on $[O_{2r}]$ and hence on root O_2 transport determined by θ_{pr}. If this transport is inadequate, decline in $[O_{2r}]$ slows root O_2 uptake (C14c, d) and hence R_a (C14b), R_g (C17) and root growth (C20b). Increased θ_g with WTD drawdown during the dry season, however, facilitates rapid D_g which allows root O_2 demand to be almost entirely met from $[O_{2s}]$ (C14c, d).

3-2.1.4. Gross Primary Productivity

By reducing root O_2 uptake, shallow WTD slows root growth (C20b) and root nitrogen and phosphorus uptake (C23b, d, f). Root nitrogen and phosphorus uptake in this hydroperiod is further slowed by reductions in aqueous concentrations of NH_4^+, NO_3^- and $H_2PO_4^-$ (C23a, c, e) from slower mineralization of organic nitrogen and phosphorus as described in Sect. 3-2.1.2. Slower root nitrogen and phosphorus uptake in turn reduces concentrations of non-structural nitrogen and phosphorus products of root uptake (σ_N and σ_P) with respect to that of σ_C in leaves (C11), thereby slowing CO_2 fixation (C6) and hence GPP.

Increased availability of $[O_{2s}]$ with WTD drawdown during the dry season hastens root O_2 uptake and so enables more rapid root growth and nitrogen and phosphorus uptake as discussed in Sect. 3-2.1.3. Increased root growth and nitrogen and phosphorus uptake is further stimulated by increased aqueous concentrations of NH_4^+, NO_3^- and $H_2PO_4^-$ (C23a, c, e) from more rapid mineralization of organic nitrogen and phosphorus during this hydroperiod as described in Sect. 3-2.1.2. Greater root nitrogen and phosphorus uptake in turn increases concentrations of σ_N and σ_P with respect to σ_C in leaves (C11), thereby facilitating rapid CO_2 fixation (C6) and hence GPP.

With deeper WTD during the late dry season, GPP is less limited by root and microbial growth and nutrient uptake as discussed above. However, GPP in this hydroperiod can be adversely affected by water stress. When WTD deepens past a critical depth (Sect. 3-1), inadequate capillary rise (D9a) causes near-surface peat desiccation, reducing soil water potential (ψ_s) and increasing soil hydraulic resistance (Ω_s) (B9), forcing lower root, canopy and turgor potentials (ψ_r, ψ_c and ψ_t) (B4) and hence lower canopy stomatal conductance (g_c) (B2b) to be calculated when equilibrating plant water uptake with transpiration (T) (B14). Lower g_c in turn reduces CO_2 diffusion into the leaves thereby reducing CO_2 fixation (C6) and hence GPP during this hydroperiod.

Thus WTD effects on R_h, R_a and GPP in *ecosys* are not parameterized from ecosystem level observations, but instead are governed by basic processes of O_2 transport and uptake; root and microbial energy yields, growth and nutrient uptake; and stomatal regulation controlled by root water uptake parameterized from independent research.

3-2.2. Modelling experiment

3-2.2.1. Site conditions

The *ecosys* algorithms for simulating WTD effects on net ecosystem CO_2 exchange were tested against the measurements over Palangkaraya Peat Swamp Forest (PPSF), Central Kalimantan, Indonesia (2°20′42″ S and 114°2′11″ E). The site is a tropical bog peatland formed mainly by roots and remains of trees where the major source of water and nutrient inputs is through precipitation. Vegetation of these peatlands includes evergreen over-storey trees and dense under-storey of dominant tree seedlings with no mosses. These peatlands were drained by excavating drainage canals approximately 4 years before the measurements started in 2001 at a flux station established in PPSF. Peat depth around the flux tower site was about 4 m. Detailed

description of edaphic and vegetation characteristics as well as management history of the site can be found in Hirano et al. (2007), Hirano et al. (2009), Jauhiainen et al. (2005) and Jauhiainen et al. (2008).

3-2.2.2. Field datasets

CO_2 fluxes used for model validation in our study were measured by Hirano et al. (2007) at a flux station established in PPSF during November 2001. Hourly NEP (a negative sign represents an upward flux or a flux out of the ecosystem and a positive sign represents a downward flux or a flux into the ecosystem) over PPSF was estimated by a combination of eddy and storage CO_2 flux measured using a micro-meteorological approach Hirano et al. (2007). NEP along with latent heat and sensible heat fluxes were measured by using an open path CO_2/H_2O analyzer mounted at 41.3 m height, about 15 m above the forest canopy (Hirano et al. 2005, 2007). A CO_2 profile was also measured by using a closed path analyzer at six heights between 2.0 and 41.3 m. Hourly weather variables (e.g. incoming longwave and shortwave radiation, wind speed, relative humidity, air temperature, precipitation etc.) were also measured at the flux station. Soil moisture content (θ) at a depth from 0-0.2 m and soil temperature (T_s) at 0.05 m depth were measured in hummocks. Hourly WTD measurements at the site were started from April 2004. Ground reference point for WTD measurements was a hollow surface.

A u^* (friction velocity) threshold of 0.17 m s^{-1} was used to screen out the NEP in a calm night hour. However, no u^* threshold screening was performed for daytime NEP. NEP measured in the rain was also excluded (Hirano et al. 2012). Nighttime NEP that passed the quality control procedure was used as a measure of nighttime R_e. Daytime R_e was extrapolated by using nighttime R_e. GPP was then calculated by adding daytime R_e to daytime NEP that survived the quality screening.

Flux gaps due to quality control were filled by Hirano et al. (2007) through look up tables (LUT) created for four periods of 3 months each (November-January, February-April, May-July and August-October). Hourly measured θ, WTD and T_s were used to incorporate environmental controls in LUTs for filling nighttime NEP (=R_e) gaps. No hourly WTD measurement was available at the site before April 2004. Therefore, only θ was used as hydrological control in LUTs from January 2002-March 2004. To balance the number of original data in each cell, θ was grouped into six classes from below 0.23 m^3 m^{-3} to above 0.35 m^3 m^{-3} with an interval of 0.03 m^3 m^{-3}. T_s was also grouped into five classes from 25 to 30°C with an interval of 1°C. In filling GPP gaps, photosynthetic photon flux density (PPFD) and vapor pressure deficit (D) were used as environmental factors to create LUTs similar to those used for R_e. PPFD and D were grouped into eight classes from 5-250 to above 1750 μmol m^{-2} s^{-1} at intervals of 250 μmol m^{-2} s^{-1} and three classes of below 1.2, 1.2-1.8 and above 1.8 kPa, respectively. Finally, NEP gaps during daytime hours were calculated by the differences between gap-filled GPP and estimated daytime R_e.

Hirano et al. (2012) estimated uncertainties in annual EC-gap filled NEP estimates due to random errors in measurements and due to gap-filling throughout 2002-03 to 2008-09 over PPSF. However, systematic uncertainties in the nighttime NEP measurements due to u^* threshold and land breezes as well as in the gap-filling due to continuous data gaps (November 11-22, 2002, January 3-31, 2003, March 29-May 22, 2003, June 24-July 26, 2003 and September 14 to October 9, 2004) from instrumental failures were not quantified. A more detailed description of EC methodology; measurement techniques, quality control, partitioning and gap-filling of fluxes; and uncertainty estimation can be found in Hirano et al. (2007) and Hirano et al. (2012).

3-2.2.3. Model run

For our modelling experiment, the PPSF landscape was represented by one hummock and one hollow grid cell each of which had a dimension of 1 m × 1 m. Both of the grid cells had identical soil properties except that the hollow grid cell had a fibric layer thinner by 0.15 m than the hummock cell to represent the average site micro-topography described by Jauhiainen et al. (2008) (Table 3-1). Physical and hydrological characteristics of the PPSF peatland and their representation in our modelling study were described in Chapter 2. Very high carbon and nitrogen to phosphorus ratios with low pH are typical characteristics of tropical peatlands which were represented in our modelling experiment by inputs measured either at the same site or at similar surrounding sites (Table 3-1). Both hummock and hollow grid cells were seeded with evergreen tropical rainforest over- and under-storey vascular vegetation using the same plant functional types used in an earlier study on an Amazonian rainforest (Grant et al. 2009b), but selecting 0.2 for root porosity (θ_{pr}) used in root O_2 transport [D17d] to represent wetland plant adaptation (Visser et al. 2000). These peatlands under study are generally devoid of mosses and hence we did not simulate any moss species. The model was then run for 44 years (40 years of spin up and 4 years of simulation run) under repeating 4-year sequences of hourly weather data (solar radiation, air temperature, wind speed, humidity and precipitation) recorded at the site from 2002 to 2005. The spin up period allowed CO_2 exchange in the model to achieve stable values through successive weather sequences. Model results for the 4 years of simulation run were compared with measurements at PPSF from 2002-2005.

3-2.2.4. Model validation

Hourly CO_2 fluxes modelled over the hummock and the hollow were spatially averaged to represent 50:50 hummock-hollow ratios as described by Jauhiainen et al. (2008), and then

regressed on hourly measured EC CO_2 fluxes for each year from 2002-2005. Model performance was evaluated from regression intercepts ($a \rightarrow 0$), slopes ($b \rightarrow 1$) and coefficients of determination ($R^2 \rightarrow 1$) for each study year to test whether there was any systematic divergence between the modelled and EC measured as well as between modelled and gap-filled CO_2 fluxes. This test is very important since any small divergence between hourly modelled and EC measured as well as between hourly modelled and gap-filled CO_2 fluxes can result in a large divergence between modelled and EC-gap filled annual estimates.

3-2.2.5. Analyses of model results

To examine WTD effects on seasonal variations in NEP as proposed in hypotheses 1, 2 and 3 of our study, we chose daily modelled and EC-gap filled NEP for 30 days each from the three WTD hydroperiods, i.e. shallow, intermediate and deep, for 2002-2005. These 30 day periods were chosen based on the greatest availability of EC measured CO_2 fluxes that passed the quality control procedure described in Sect. 3-2.2.2. We then performed single factor analyses of variance (ANOVA) for the modelled and EC-gap filled NEP to test whether the means of daily NEP significantly differed among different hydroperiods. A significant difference in mean NEP between two particular hydroperiods meant the variation in mean NEP between those hydroperiods was larger than the day to day variation in NEP within each of those hydroperiods. This test would signify the consistency of seasonal variations in NEP as a result of WTD fluctuations.

3-2.2.6. Model sensitivity to drained vs. undrained WTD

WTD in the modelled grid cells in *ecosys* arises from water exchanges with the atmosphere in the forms of vertical water influxes (e.g. precipitation) and effluxes (e.g. evapotranspiration) through a surface boundary and in the forms of recharge and discharge with

an adjacent ecosystem through lateral boundaries. The distance (L_t) and hydraulic gradient between modelled WTD and a set external water table depth (WTD_x, representing mean WTD of the adjacent watershed) generally governs the rate of lateral recharge and discharge (D10, D10a). All modelled WTDs were spatially averaged for the hummock and the hollow grid cell with reference to the hollow surface. The WTD_x for the simulation in this study was set at 0.45 m below the hollow surface (i.e. 0.60 m below the hummock surface) so as to represent the average watershed WTD for our drained site (Rieley and Page 2005, Hirano et al. 2009). L_t was set to 400 m in all directions which was the nearest distance from the study site to the drainage canal (Hirano et al. 2012). Since drainage is a key disturbance reported to alter WTD and hence C balance of Southeast Asian peatlands (Couwenberg et al. 2010, Hooijer et al. 2010), we performed a parallel simulation with WTD_x raised from 0.45 m below the hollow surface to 0.15 m above the hollow surface (i.e. level with the hummock surface) with everything else unchanged to represent the undrained condition. The difference between the two WTD_xs was based on the maximum observed difference between mean annual WTDs over our drained site and a nearby similar undrained site as reported by Hirano et al. (2012). The purpose of this undrained simulation was to test the sensitivity of the modelled NEP to the difference in drained vs. undrained WTD. A more detailed description of how subsurface hydrology, water balance and surface energy exchange over PPSF was simulated can be found in Chapter 2.

3-3. Results

3-3.1. Modelled vs. measured ecosystem net CO_2 fluxes

Regressions of hourly modelled vs. measured net ecosystem CO_2 fluxes gave intercepts within 1.0 μmol m^{-2} s^{-1} of zero, and slopes within 0.1 of one, indicating minimal bias in modelled values for all years of the study except 2005 when modelled fluxes gave a positive bias slightly

greater than 1.0 μmol m^{-2} s^{-1} (Table 3-2). Values for coefficients of determination (R^2) and root mean square for errors (RMSE) were ~ 0.8 ($P < 0.0001$) and ~ 5.0 μmol m^{-2} s^{-1} (Table 3-2). Much of the unexplained variance in EC-measured CO_2 fluxes could be attributed to a random error of ca. 20% in EC methodology (Wesely and Hart 1985). This attribution was corroborated by root mean squares for random errors (RMSRE) in EC measurements, calculated for forests with similar CO_2 fluxes from Richardson et al. (2006) that were similar to RMSE. These similar values indicated that further constraint in model testing could not be achieved without further precision in EC measurements. Regressions of modelled vs. gap-filled CO_2 fluxes gave larger slopes than those of modelled vs. EC-measured CO_2 fluxes despite higher R^2 and lower RMSEs, indicating the diurnal variation of the modelled CO_2 fluxes was systematically larger than that of the gap-filled CO_2 fluxes (Table 3-2). Further investigation into hourly simulated vs. gap-filled and simulated vs. EC measured net ecosystem CO_2 fluxes suggested that modelled nighttime fluxes were systematically larger than the gap-filled nighttime fluxes particularly in the rainy season when valid EC measured data were scarce (Fig. 3-1). However, modelled nighttime fluxes showed good agreement with more available valid EC measured nighttime fluxes during the dry season (Fig. 3-1).

3-3.2. Seasonal variation in WTD and daily net ecosystem CO_2 exchange

WTD in PDPSF showed distinct seasonality in each year from 2002 to 2005 (Figs. 2-2 and 2-3). Observed WTDs were typically within 0.3 m of the hollow surface during the rainy season (November–April) increasing to 0.5–0.8 m below the hollow surface at the onset of the dry season (May–July) (Figs. 3-2 to 3-5). During late dry seasons (August–October) observed WTD fell below 1.0 m from the hollow surface (Figs. 3-2 to 3-5). Increasing amounts and

declining seasonality of precipitation caused the wet to dry season drawdown of WTD to be more and more gradual from the driest year 2002 to the wettest year 2005 (Figs. 3-2 to 3-5).

NEP (a negative sign represents C source and a positive sign represents C sink) modelled and measured over PDPSF showed a distinct seasonality, with negative values over shallow WTD (within 0.3 m below the hollow surface) during the rainy season, near zero or slightly positive values over intermediate WTD (0.5–0.8 m below the hollow surface) during the early dry season, and returning to negative values over deep WTD (> 1.0 m below the hollow surface) in the late dry season during each year from 2002 to 2005 (Figs. 3-2 to 3-5). These values indicated that the ecosystem was a C source when the WTD was shallow, became C neutral or a small sink when WTD receded to an intermediate position, and again became a large source of C when WTD further deepened (Figs. 3-2 to 3-5). Modelled and EC-gap filled NEP during intermediate WTD hydroperiods were significantly ($P < 0.01$) higher than those during shallow WTD hydroperiods during 2002–2003 (Fig. 3-6). Both the modelled and EC-gap filled NEP showed similar trend of increasing NEP from shallow to intermediate WTD hydroperiods during 2004–2005. However, only the increases in modelled NEP from shallow to intermediate WTD hydroperiods in those years were statistically significant ($P < 0.01$) (Fig. 3-6). Both modelled (in 2002–2004) and EC-gap filled (in 2002–2005) NEP during deep WTD hydroperiods was significantly ($P < 0.01$) lower than that during intermediate WTD hydroperiods (Fig. 3-6). This seasonal trend in NEP also varied interannually depending upon the duration and intensity of dry seasons. For instance, NEP during the deep WTD hydroperiod was more negative in a drier dry season (2002–2004, Figs. 3-2 to 3-4 and 3-6) than that in a wetter dry season (2005, Figs. 3-5 and 3-6).

In addition to the successful simulations of interannual variation in seasonal cycles of NEP, *ecosys* was adequately sensitive to the short-term variations in NEP caused by changes in weather. There were several short-term dips in EC-gap filled NEP, e.g. DOY 160–170 in 2002 (Fig. 3-2), DOY 258–262 in 2003 (Fig. 3-3), DOY 143–146 in 2004 (Fig. 3-4), DOY 259–262 in 2005 (Fig. 3-5) etc. caused by smaller CO_2 influxes and larger CO_2 effluxes on cloudy and rainy days. These dips were modelled from less CO_2 fixation under lower R_n and/or from flushes of soil CO_2 effluxes due to rewetting surface residues from a rainfall following a dry period (Grant et al. 2012a).

3-3.3. Seasonal variation in WTD and diurnal CO_2 exchange

To examine WTD effects on ecosystem diurnal net CO_2 exchange, we compared hourly modelled net CO_2 fluxes against EC-gap filled CO_2 fluxes binned for the three WTD hydroperiods, i.e. shallow, intermediate and deep from 2002–2005 (Fig. 3-7). During 2002–2003, modelled downward CO_2 fluxes were suppressed over shallow WTD during the rainy seasons, became larger over intermediate WTD during the early dry seasons, and again suppressed over deeper WTD during the late dry seasons, as were also apparent in EC-gap filled CO_2 fluxes (Fig. 3-7). During 2004, modelled downward fluxes followed the same seasonal pattern as in 2002–2003 but EC-gap filled fluxes showed clear suppression in only the deep WTD hydroperiod (Fig. 3-7). Both modelled and EC-gap filled downward CO_2 fluxes during 2005, however, increased with deepening WTD with no suppression during late dry season (Fig. 3-7). Suppressions of downward CO_2 fluxes during deep WTD periods varied interannually depending upon the duration and intensity of the hydroperiods. For instance, suppression of modelled and EC-gap filled downward CO_2 fluxes during the deep WTD hydroperiods was

stronger during the drier late dry seasons of 2002 and 2004, less strong in wetter late dry season of 2003 and absent in the wettest late dry season of 2005 (Fig. 3-7).

Limited precision and frequency of EC-measured nighttime CO_2 fluxes caused by insufficient nighttime turbulence made the comparison of modelled vs. EC-gap filled upward CO_2 fluxes more difficult than that for downward CO_2 fluxes. EC-gap filled upward CO_2 fluxes (= R_e) showed no significant change except a small decrease during 2003 with WTD drawdown from rainy to early dry seasons and marked increases with further deepening of WTD in late dry seasons during 2002–2005 (Fig. 3-7). These effects of seasonal WTD variation on upward CO_2 fluxes (= R_e) were reasonably well simulated except that the modelled decrease in upward CO_2 fluxes from shallow to intermediate WTD hydroperiod in 2003 was smaller than that in EC-gap filled fluxes (Fig. 3-7). Moreover, modelled upward CO_2 fluxes (= R_e) had a small decrease from rainy to dry season in 2005 which was not apparent in EC-gap filled fluxes (Fig. 3-7). Increase in EC-gap filled upward CO_2 fluxes (= R_e) from intermediate to deep WTD hydroperiod was not prominent in modelled upward fluxes during 2002 (Fig. 3-7).

Both modelled and EC-gap filled downward CO_2 fluxes increased from shallow to intermediate WTD hydroperiods during 2002, 2003 and 2005 while upward CO_2 fluxes (= R_e) decreased little or not at all, suggesting that GPP was raised by gradual drawdown of WTD from the rainy to early dry season (Fig. 3-7). An increase in R_n from the rainy to early dry season may have contributed to the increase in downward CO_2 fluxes during 2002 (Figs. 3-2b and 3-7). However, a similar increase in R_n from the rainy to early dry seasons during 2003 and 2004 did not coincide with a similar increase in downward flux, whereas no change in R_n between those hydroperiods during 2005 coincided with an increase in downward CO_2 fluxes (Figs. 3-3 to 3-5 and 3-7). Moreover, an increase in D from rainy to early dry season (Fig. 3-6f) did not cause a

decline in downward CO_2 fluxes during 2002– 2005 (Fig. 3-7). These confounding effects of R_n and D on modelled and EC-gap filled downward CO_2 fluxes further indicated that there was a consistent increase in GPP from shallow to intermediate WTD hydroperiods which was driven by eco-hydrology rather than micrometeorology. Larger declines in downward modelled and EC-gap filled CO_2 fluxes than the increases in upward CO_2 fluxes (= R_e) from intermediate to deep WTD hydroperiods during 2002–2004 indicated GPP suppression by deep WTD (Fig. 3-7). Higher D (e.g. during 2002–2004 in Fig. 3-6f) and lower R_n (e.g. due to smoke haze shading from surrounding forest and peat fires during 2002 in Fig. 3-2b as mentioned by Hirano et al., 2007) may have further contributed to GPP suppression during deep WTD hydroperiods (Fig. 3-7). However, interannual variation in the intensity of GPP suppression (Fig. 3-7) coincided with that in the duration and intensity of dry seasons irrespective of changes in D and R_n (Figs. 3-2 to 3-6), as described earlier, further suggested the significance of hydrological control over micrometeorological control in suppressing GPP during deep WTD hydroperiods.

Therefore, a gradual drawdown of WTD from rainy to early dry season resulted in higher NEP mainly by raising GPP with no change or little decrease in R_e (Figs. 3-2 to 3-7). Further drawdown of WTD during late dry season forced NEP to decline by a combination of reduced GPP and increased R_e (Figs. 3-2 to 3-7). This seasonal effect of WTD on NEP through its effects on GPP and R_e can also be corroborated by the quadratic curve fittings between monthly modelled and EC-derived NEP, GPP and R_e vs. monthly modelled and observed WTD. Such curve fittings between NEP and WTD yielded goodness of fits (R^2) of 0.61 (modelled NEP vs. modelled WTD) and 0.53 (EC-derived NEP vs. observed WTD) indicating a small increase in NEP from shallow to intermediate WTD hydroperiods and a remarkable decline in NEP from intermediate to deep WTD hydroperiods during 2002–2004 (Fig. 3-8). The quadratic

relationships between GPP and WTD (R^2 = 0.14 for modelled GPP vs. modelled WTD and R^2 = 0.10 for EC-derived GPP vs. observed WTD) indicated that increases in GPP from shallow to intermediate WTD hydroperiods contributed to increases in NEP and declines in GPP from intermediate to deep WTD hydroperiods contributed to declines in NEP (Fig. 3-8). R_e and WTD relationships (R^2 = 0.53 for modelled R_e vs. modelled WTD and R^2 = 0.60 for EC-derived R_e vs. observed WTD) indicated that no change or small decreases in R_e from shallow to intermediate WTD hydroperiods contributed little to increases in NEP, and large increases in R_e from intermediate to deep WTD hydroperiods contributed substantially to declines in NEP (Fig. 3-8). Though monthly modelled NEP values were similar to EC-gap filled NEP values, both monthly modelled GPP and R_e were systematically larger than EC-derived GPP and R_e (Fig. 3-8).

3-3.4. Interannual variation in WTD and NEP

Interannual variation in WTD over PDPSF from 2002 to 2005 was mainly caused by differences in annual precipitation. Increasing amount of annual precipitation from the driest year 2002 to the wettest year 2005 drove a gradually shallower average annual modelled and measured WTD from 2002 to 2005 (Table 3-3). Variation in annual estimates of neither modelled nor EC-gap filled evapotranspiration (*ET*) from 2002 to 2005 did correlate with that in average annual modelled or observed WTD (Table 3-3). However, modelled lateral discharge increased from 2002 to 2005 with decreasing WTD (Table 3-3). This interannual variation in WTD caused interannual variation in NEP over PDPSF from 2002 to 2005. A gradual rise in both modelled and EC-gap filled annual NEP was found from 2002 to 2004 with progressively shallower WTD (Table 3-3). However, modelled NEP was considerably lower than the EC-gap filled estimates of NEP in 2003 and 2004 (Table 3-3). The decreasing WTD from 2002 to 2005 reduced modelled annual GPP, R_a and R_h and hence R_e (Table 3-3), although this reduction could

not be corroborated from EC-derived estimates. In contrast, EC-derived annual GPP increased with decreasing WTD from 2002–2004 but EC-derived R_e showed no response (Table 3-3). Moreover, modelled annual GPP and R_e were consistently larger than the EC-derived estimates during 2002–2004 (Table 3-3). Similar declines in modelled GPP and R_a with shallower WTD left modelled NPP almost unchanged throughout the study period (Table 3-3). However, greater suppression of annual R_h by shallow WTD caused annual NEP to become gradually less negative from 2002 to 2005 (Table 3-3).

3-3.5. Seasonal and annual variations in simulated drained vs. undrained WTD and NEP

Large negative simulated and EC-gap filled annual NEP during 2002–2005 (Table 3-3) may reflect disturbance effects of drainage in 1996–1997 which increased WTD. To examine the drainage effects on modelled NEP, we performed a drained vs. undrained model sensitivity test as described in Sect. 3-2.2.6. During the rainy seasons (November–April) from 2002–2005, simulated undrained WTD was always above the hollow surface as opposed to the simulated drained WTD where water table never rose above the hollow surface (Fig. 3-9). The undrained WTD remained ~ 0.5 m shallower than the drained WTD, and so altered the timing and intensity of the different hydroperiods (Fig. 3-9). The seasonal variation in simulated undrained WTD followed that in a nearby similar undrained tropical peat swamp forest (Fig. 3-9).

NEP modelled in the undrained condition was higher (less negative) than that in the drained condition during the rainy seasons (November–April) but similar during the late dry seasons (August–October) (Fig. 3-10). However in 2004 and 2005, NEP modelled in the undrained simulation was higher than in the drained simulation during late dry season (Fig. 3-10). Large spikes of negative NEP were simulated in the undrained simulation at the end of the rainy seasons when WTD first declined below the hollow surface (Fig. 3-10). This decline

suddenly increased contact between atmosphere and aqueous CO_2 in the previously saturated soil, causing rapid degassing. Such spikes were not found in the drained simulation where WTD remained below the hollow surface.

On an annual basis, the undrained simulation produced a shallower average WTD by ~ 0.5 m than the drained simulation over four years i.e. 2002–2005. This reduction in WTD in undrained vs. drained simulation decreased GPP and R_a slightly, but decreased R_h much more, thereby increasing mean annual NEP throughout the study period (Table 3-4).

3-4. Discussion

3-4.1. Modelling hypotheses of WTD effects on seasonal variation in tropical peatland NEP

Reduction of NEP during both shallow and deep WTD hydroperiods with respect to that in the intermediate WTD hydroperiods was established during 2002–2005 in Sects. 3-3.2 and 3-3.3. Reduction of NEP during the shallow WTD hydroperiods was mainly attributed to reduction in GPP that was independent of changes in R_n and D (Sect. 3-3.3). Reduction of NEP during the deep WTD hydroperiods, however, was attributed to reduction in GPP irrespective of changes in R_n and D, and to increase in R_e irrespective of changes in temperature (variations in mean daily air temperature and mean daily soil temperature measured at 0.05 m depth of the hummocks were less than 3°C among the hydroperiods) (Sect. 3-3.3). The absence of a decline in GPP during the deep WTD hydroperiod in the wettest year 2005 also suggested that there was a considerable interannual variation in WTD effect on tropical peatland NEP that depended on the intensity and duration of dry vs. wet seasons (Sect. 3-3.3). Seasonal variation in WTD thus affected that in NEP through its effect on both GPP and R_e as mentioned above independent of variations in other micrometeorological controls such as R_n, D and temperature. These effects suggested that tropical peatland NEP was reduced by plant processes as affected by soil

processes influenced by both shallow and deep WTD. Since our modelling could reasonably simulate seasonal variation in WTD as well as its effects on that in NEP (Sects. 3-3.2 and 3-3.3), we hereby discuss the modelling hypotheses proposed at the beginning of our study to explain the underlying causes of these WTD effects on tropical peatland NEP.

3-4.1.1. Hypothesis 1: WTD and NEP during rainy season

A shallower aerobic zone (Fig. 3-11) and resulting lower [O_{2s}] modelled during the shallow WTD (within 0.3 m of the hollow surface) hydroperiod reduced rates of C oxidation by microbial populations (A13-A14) which limited microbial growth (A25) and hindered nutrient mineralization (A26). Moreover, low [O_{2s}] caused by shallow WTD forced [O_{2r}] to depend predominantly upon O_2 transport through root gaseous phase controlled by θ_{pr} as discussed in Sect. 3-2.1.3. Our input of 0.20 for θ_{pr} to represent peatland species adaptation (Visser et al., 2000), however, was not enough to maintain adequate [O_{2r}] during this hydroperiod. Lower [O_{2r}] supressed rates of C oxidation by root and mycorrhizal populations (C14a, b), slowing root and mycorrhizal growth (C20b) and hence plant nutrient (predominantly phosphorus) uptake (C23b, d, f). Root and mycorrhizal growth during this hydroperiod were largely confined to the shallow aerobic zone, thus limiting the soil volume from which phosphorus uptake could occur. Slow phosphorus uptake reduced σ_P with respect to σ_C in leaves (C11), thereby slowing CO_2 fixation (C6) and hence GPP in the model as discussed in Sect. 3-2.1.4. The suppression of productivity with shallow WTD was also apparent in higher modelled and measured Bowen ratios (β=H/LE) resulting from lower g_c required to conserve c_c:c_a ratios with slower CO_2 diffusion (Figs. 2-5d and 2-6b). Reduction of GPP in our undrained simulation compared to our drained simulation was also caused by greater phosphorus limitation under shallower WTD (Table 3-4).

In tropical peatlands, phosphorus uptake is likely to be most limiting to CO_2 fixation as indicated by foliar nitrogen to phosphorus ratios (mass based) ranging from 22:1 to 130:1 for different tree species growing in Indonesian peatlands (Tuah et al., 2000). A mass based foliar nitrogen to phosphorus ratio greater than 15:1 generally indicates phosphorus limitation to plant productivity (Townsend et al. 2007). This phosphorus limitation arises from high soil organic nitrogen to phosphorus ratios, low pH and high aluminum (Al) and iron (Fe) contents of these peats (Page et al. 1999, Rieley and Page 2005, Page et al. 2006). When site-specific inputs for soil pH, organic and inorganic nitrogen and phosphorus (Table 3-1), exchangeable Al (12 g Mg^{-1}) and Fe (21.6 g Mg^{-1}) were used in our modelling with site-independent algorithms for soil solute transformations (E1-E55) (Grant et al. 2009b), soil solution phosphorus concentrations and hence root phosphorus uptake were forced to very low values. Low plant phosphorus availability and uptake in the model was reflected in lower modelled foliar phosphorus content (~2.5 g kg^{-1} C) during shallow WTD hydroperiods. Such low plant phosphorus status in our modelling was corroborated by even lower foliar phosphorus contents (0.2-1.4 g kg^{-1} C in matured leaves, assuming that 50% of the dry matter was C) measured by Tuah et al. (1999) in the dominant species growing on our study site. Low foliar phosphorus contents in 150 tree species of tropical rain forests of Costa Rica and Brazil was also attributed to low phosphorus availability for plants growing on highly weathered phosphorus-deficient tropical soils (Townsend et al. 2007).

These results from the model are also consistent with those from Milner (2009) from a transect study on the effect of soil fertility on vegetation diversity of a tropical mixed swamp forest surrounding our study site. She found a reduction in basal area and tree growth in areas where the WTD was shallower by only ~0.10 m. She speculated that the reduced tree growth was

a result of low nutrient availability caused by anoxia under shallow WTD. Slow nutrient (phosphorus) mineralization in wet soils under shallow WTD may have reduced CO_2 diffusion and thereby fixation and productivity in her study site which supports the nutrient stress theory in our hypothesis 1. Moreover, a reduction in foliar phosphorus content during the rainy season with respect to mid-wet and dry seasons was also measured by Townsend et al. (2007) in tropical forest species of Costa Rica. Furthermore, tropical mangroves in Panama, Belize and Florida have shown significant increases in leaf CO_2 assimilation and plant growth with phosphorus enrichment indicating phosphorus stress to leaf gas exchange under anoxic conditions despite those species being well adapted to flooding stress (Lovelock et al. 2004, 2006a, 2006b, 2006c). Similar suppression of productivity caused by low nitrogen availability and uptake can also be found in boreal peatlands which are known to be nitrogen deficient as reported in experimental (Sulman et al. 2010, Flanagan and Syed 2011) and modelling studies (Sulman et al. 2010, Grant et al. 2012b) across northern boreal peatlands.

During shallow WTD in rainy seasons, [O_{2s}] below the water table was almost zero (Fig. 3-11) and well below the Michaelis-Menten constant (K_m) used for microbial, root and mycorrhizal uptake in *ecosys* (A17a, C14c) so that DOC oxidation coupled with O_2 reduction was strongly limited by [O_{2s}]. In these layers, DOC oxidation was coupled with DOC reduction by anaerobic heterotrophic fermenters, which yielded much less energy (4.4 vs. 37.5 kJ g C^{-1}) (A21) than did O_2 reduction and so resulted in slower microbial growth (A25) and R_h (A13) as discussed in Sect. 3-2.1.2. However, [O_{2s}] above the water table during shallow WTD hydroperiod was well above K_m (Fig. 3-11) used for simulated microbial, root and mycorrhizal O_2 uptake so that R_h in this zone was not limited by [O_{2s}]. Moreover, frequent precipitation throughout this hydroperiod kept the surface residue layer moist and maintained optimum

heterotrophic microbial concentrations for decomposition (A3, A5) and growth (A15), driving surface CO_2 flushes. This absence of suppression in modelled R_e during shallow WTD hydroperiods can further be corroborated by no significant decrease or even slight increase in nighttime EC gap-filled CO_2 fluxes during shallow compared to intermediate WTD hydroperiods (Fig. 3-7). Similar absence of suppression in soil respiration during shallow WTD hydroperiods compared to those in intermediate WTD hydroperiods were also measured by Sundari et al. (2012) in our study site and Jauhiainen et al. (2008) in a nearby drained tropical peatland.

Shallow WTD during the rainy season thus caused lower NEP (Figs. 3-2 to 3-6) to be modelled over PPSF through reducing GPP due to plant nutrient (phosphorus) stress and hence net CO_2 uptake (Figs. 3-7 to 3-8). This GPP suppression from nutrient stress during shallow WTD hydroperiod was well corroborated by EC-gap filled CO_2 fluxes (Fig. 3-7) (Table 3-2) as well as other biometric measurements (Townsend et al. 2007) and hence validated our hypothesis 1.

3-4.1.2. Hypothesis 2: WTD and NEP during early dry seasons

Increased availability of $[O_{2s}]$ with an intermediate WTD (0.5-0.8 m below the hollow surface) during the early dry season almost entirely met root O_2 demand and hence facilitated more rapid and deeper root growth (C20b) and hence phosphorus uptake (C23b, d, f). Uptake was further stimulated by more rapid mineralization of organic phosphorus (C23a, c, e) driven by more rapid microbial O_2 uptake (A17), C oxidation (A1, A2), growth (A25) and R_h (A13, A20) as described in Sects. 3-2.1.2 and 3-2.1.3. Greater root phosphorus uptake in turn increased $\sigma_P:\sigma_C$ in leaves (C11), thereby facilitating rapid CO_2 fixation (C6) and hence GPP as discussed in Sect. 3-2.1.4. Rapid CO_2 fixation from improved plant nutrient (phosphorus) status was also apparent in larger EC gap-filled downward net CO_2 fluxes during intermediate WTD

hydroperiods in 2002, 2003 and 2005 (Fig. 3-7). Rapid CO_2 fixation due to improved plant nutrient (phosphorus) status can further be corroborated by lower measured and modelled β resulting from greater g_c as described in Chapter 2.

Modelled foliar phosphorus content increased from ~2.5 g kg^{-1} C in the wet season to ~3 g kg^{-1} C in the early dry season indicating an improved plant nutrient status in the early dry season with intermediate WTD. This increase in modelled foliar phosphorus content by ~ 20% from rainy to early dry season was consistent with a 25% increase in foliar phosphorus content from wet to mid-wet and dry seasons measured by Townsend et al. (2007) in tropical forest species of Costa Rica. Similarly, higher foliar phosphorus content modelled in the drained simulation (~3 g kg^{-1} C) than in the undrained simulation (~2.5 g kg^{-1} C) during this hydroperiod raised GPP, further indicating improved nutrient status due to deeper WTD (Table 3-4). Increased productivity resulting from improved nutrient (phosphorus) availability with WTD drawdown has been found in field studies for Indonesian peatlands (Milner 2009), and Florida everglades wetlands (Saha et al. 2010). These field measurements further support our modelling hypothesis 2 of improved plant nutrient status with improved soil aeration which increased GPP and hence NEP during intermediate WTD hydroperiods. Increased GPP with WTD drawdown was also measured by Sulman et al. (2009) and Flanagan and Syed (2011) for northern boreal peatlands. However, in those nitrogen limited ecosystems, the drawdown of WTD could improve plant nitrogen rather than phosphorus availablity and uptake and hence productivity as modelled with *ecosys* by (Grant et al. 2012b).

A deeper aerobic zone and resulting increase in $[O_{2s}]$ during the intermediate WTD hydroperiod in the early dry season (Fig. 3-11) stimulated R_h (A13, A20) as described above. However, this increase in deeper R_h was fully, and sometimes more than fully, offset by

decreases in surface and near-surface R_h caused by near-surface peat desiccation which reduced microbial access to substrate for decomposition (A15) (Sect. 3-2.1.2). This enabled *ecosys* to simulate nighttime net CO_2 fluxes measured by EC during intermediate WTD hydroperiods that were similar to or lower than those in shallow WTD hydroperiods. This modelling hypothesis in *ecosys* was further corroborated by soil CO_2 effluxes measured with surface chambers by Sundari et al. (2012) over our study site and by Jauhiainen et al. (2008) over a nearby similar site during intermediate WTD hydroperiods that were similar or lower than those in shallow WTD hydroperiods. Declines in R_h due to near surface peat desiccation were also modelled by (Dimitrov et al. 2010a) and (Grant et al. 2012b) by using the same model *ecosys* over two contrasting northern boreal peatlands.

Intermediate WTD during the early dry season thus caused higher NEP (Figs. 3-2 to 3-6) over PPSF by a combination of increased GPP and unchanged or slightly decreased R_e (Figs. 3-7 to 3-8). This trend of increased GPP with improved nutrient (phosphorus) status and unchanged R_e due to offsetting effects of surface vs. deep respiration was well corroborated by EC-gap filled CO_2 fluxes (Fig. 3-7) (Table 3-2) and other field measurements in our study site and in similar ecosystems and hence validated our hypothesis 2.

3-4.1.3. Hypothesis 3: WTD and NEP during late dry seasons

GPP during the late dry season with deep WTD (> 1.0 m below the hollow surface) was limited not by plant nutrient status but by plant water stress. Inadequate recharge of near surface peat layers through a combination of less precipitation and slow capillary rise (D9a) during this hydroperiod reduced ψ_s and increased Ω_s (B9) in those layers where most of the plant roots were located (Fig. 2-10). These changes in turn forced higher Ω_r (B10), lower ψ_r, ψ_c, ψ_t (B4) and g_c (B2b) (Figs. 2-8 and 2-9) and hence slower CO_2 diffusion (C6) through stomata and

consequently less GPP (Sect. 3-2.1.4). GPP suppression due to plant water stress can further be corroborated by higher measured and modelled β resulting from lower g_c as described in Chapter 2. Similar reductions in GPP due to plant water stress were reported during the late dry season in Hirano et al. (2012) for a drained and burnt tropical peat swamp forest.

Deeper peat respiration during the deep WTD hydroperiod greatly increased due to abundant [O_{2s}] in the deeper aerobic zone (Fig. 3-11) and resulting rapid microbial O_2 uptake (A17), C oxidation (A1, A2), growth (A25) and R_h (A13, A20) as discussed in Sect. 3-2.1.2. This increase in deeper R_h was greater than the reduction in surface and near-surface microbial respiration due to desiccation as discussed in Sect. 3-4.1.2, which led to a net increase in R_e during this hydroperiod. This modelling hypothesis was further corroborated by larger soil CO_2 effluxes measured by Sundari et al. (2012) over our study site during the deep WTD hydroperiod than during the rest of the year. Cai et al. (2010) also measured a stimulation of respiration over a northern boreal peatland with deepening of WTD.

Deep WTD during the late dry season thus caused lower NEP (Figs. 3-2 to 3-6) by a combination of reduced GPP and increased R_e (Figs. 3-7 to 3-8). This trend of decreased GPP due to plant water stress and increased R_e due to enhanced deeper peat respiration during deep WTD hydroperiods was well corroborated by EC-gap filled CO_2 fluxes (Fig. 3-7) (Table 3-2) as well as by other field measurements over same site or similar ecosystems and hence validated our hypothesis 3.

3-4.2. Modelling WTD effects on annual tropical peatland C balance

3-4.2.1. Differences in annual EC-derived vs. modelled GPP, R_e and NEP

Modelled annual NEP was considerably lower than the EC gap-filled annual NEP in 2003 and 2004 (Table 3-3). These lower NEP estimates were mainly attributed to larger

modelled vs. gap-filled R_e predominantly in the rainy seasons (Fig. 3-1) which was consistent throughout the study period and yielded larger slopes from modelled vs. gap-filled net CO_2 flux regressions (Table 3-2). During the rainy seasons throughout the study period, modelled water table never rose above the hollow surface leaving the top 0.05 m of hollow and the entire hummock unsaturated even when the WTD was the shallowest (Figs. 3-2 to 3-5). This trend was consistent with the observed daily WTD (Figs. 3-4 to 3-5). Total porosity for the top 0.2 m of the modelled peat was 0.89 calculated from bulk density provided to the model (Fig. 2-1), consistent with field measurements in similar drained tropical peatlands (Takakai et al. 2006, Hooijer et al. 2012, Jauhiainen et al. 2012a, Couwenberg and Hooijer 2013). Therefore, when θ in the top 0.2 m rose from ~0.22 m^3 m^{-3} in the dry seasons to just above 0.30 m^3 m^{-3} in the rainy seasons, near surface peat in the model still had enough air filled porosity for soil respiration not to be suppressed (Fig. 3-1). Moreover, wet surface residue from frequent rainfall caused large flushes of modelled residue CO_2 effluxes during rainy seasons which were also apparent in soil respiration measurements by Sundari et al. (2012) at our study site. However, despite a similar rise in θ measured vs. modelled in the top 0.2 m, gap-filled CO_2 effluxes were much smaller than the modelled CO_2 effluxes during the rainy season (Fig. 3-1). Such smaller gap-filled vs. modelled nighttime NEP (Fig. 3-1) was consistent throughout the rainy seasons (November-April) of 2002-2005 as indicated by a slope of 1.24 from a regression of modelled on gap-filled net CO_2 fluxes (n = 13218). However, a slope of 0.98 from regression of modelled on EC-measured CO_2 fluxes (n = 4464) for the same hydroperiods indicated better model agreement with EC-measured fluxes. Since 75% of the total hourly CO_2 fluxes during rainy seasons of 2002-2005 were gap-filled, larger modelled vs. gap-filled CO_2 fluxes during these hydroperiods

could largely contribute to larger modelled vs. EC-derived annual R_e and hence lower modelled vs. EC-gap filled annual NEP estimates (Table 3-3).

Systematic uncertainties embedded in EC methodology were also thought to contribute to larger modelled vs. EC-derived monthly and annual R_e estimates (Fig. 3-8) (Table 3-3). Nighttime EC NEP decreased with u^* below 0.3 m s^{-1} in our study site (Hirano et al. 2007) indicating the dependence of nighttime CO_2 flux measurements on above-canopy turbulent mixing (Miller et al. 2004). However, biological production of CO_2 by plant and microbial respiration was independent of u^* in the model. Possible underestimation of nighttime NEP resultant of uncertainty related to low u^* threshold can be as large as ~ 45% of nighttime CO_2 fluxes estimated by Miller et al. (2004) for an Amazonian rainforest which would further contribute to larger modelled vs. EC-derived R_e estimates.

Larger modelled vs. gap-filled R_e contributed to larger modelled vs. gap-filled annual GPP (Fig. 3-8) (Table 3-3). In EC datasets, GPP was derived from extrapolated daytime R_e (Sect. 3-2.2.2) and hence smaller gap-filled vs. modelled nighttime R_e would cause smaller EC-derived GPP. A further cause of smaller EC-derived vs. modelled GPP could have been the incomplete (~80%) energy balance closure in EC measurements (Wilson et al. 2002) vs. complete energy balance closure in the model, which would reduce EC-derived *ET* and also possibly GPP (Table 3-3).

All of these above mentioned sources of larger modelled vs. EC-derived R_e and GPP estimates were related to EC methodology and gap-filling. These descrepencies between modelled and EC-derived R_e and GPP aggregates, however, could not be resolved in our modelling since, unlike EC datasets, every single mole of CO_2 that was modelled from fundamental ecosystem processes was counted in the modelled C budget.

3-4.2.2. Differences in annual WTD effects on EC derived vs. modelled GPP and R_e

At an annual time scale, reductions in both GPP and R_e with a gradually shallower WTD from 2002 to 2005 in *ecosys* were not corroborated by changes in GPP and R_e partitioned from EC-gap filled net CO_2 fluxes by Hirano et al. (2007) (Sect. 3-2.2.2) (Table 3-3) although monthly partitioned GPP and R_e showed the similar seasonal trends as those modelled (Fig. 3-8). Accumulation of above-mentioned discrepancies between modelled and EC gap-filled fluxes (Sect. 3-4.2.1) over a larger time scale (e.g. monthly vs. annual) obscured the agreement between the modelled and EC-gap filled trends in WTD effects on annual GPP and R_e. Furthermore, as opposed to EC-derived R_e that was used to calculate EC-derived GPP, modelled R_e (R_a+R_h) was driven by modelled GPP thereby contributing to deviation between WTD effects on modelled vs. EC-derived annual GPP and R_e. Modelled R_a was directly dependent on fixed C products during photosynthesis. Modelled R_h was also dependent on fixed C products in a diurnal time scale through root exudates as well as in a seasonal time scale through above and below ground litterfall.

Despite the above mentioned divergence between modelled vs. EC-derived R_e and GPP estimates, components of modelled annual C balance were comparable with biometric measurements and estimations from other studies on similar ecosystems. Modelled net primary productivity (NPP) was comparable with values estimated for Amazonian rainforests and oil palm plantations in tropical peatlands (Table 3-3). Modelled R_h was comparable with R_h measured for a mature *Acacia* plantation on drained Indonesian peatlands (Table 3-3).

3-4.3. Effects of WTD on modelled annual C balance in drained vs. undrained simulation

Reducing WTD by an average of 0.5 m in drained vs. undrained simulation increased mean NEP by 270 g C m^{-2} yr^{-1} (Table 3-4). This modelled trend was corroborated by an increase

in EC gap-filled NEP for a nearby undrained peatland of 154 ± 204 g C m^{-2} yr^{-1} over that for the drained peatland measured by Hirano et al. (2012). This rise in NEP was modelled through greater suppressions of R_a and R_h than of GPP with decreasing WTD (Table 3-4).

Apart from net vertical CO_2 exchange, drainage of tropical peatlands can also trigger substantial C losses through lateral transport of dissolved organic C (DOC). Moore et al. (2013) measured a drainage-induced additional C loss of 20 g C m^{-2} yr^{-1} through the export of DOC in our study area. We, however, simulated a negligible additional increase in C losses through export of DOC (1-2 g C m^{-2} yr^{-1}) due to drainage in this modelling study. Since transport of DOC heavily depends upon total amount of catchment discharge (Moore et al. 2013) this discrepancy between our point scale study and their watershed scale measurements on DOC transport is reasonable. However, up scaling our modelling to watershed scale might be a potential opportunity to examine the effects of drainage on C losses through export of DOC in drained tropical peatlands.

Even in the undrained simulation, NEP for 2002-2004 indicated substantial C losses from PPSF (Table 3-4). Similarly large C losses were estimated by EC-gap filled NEP from 2004-05 to 2008-09 by Hirano et al. (2012) over a nearby similar undrained peat swamp forest. They also predicted from a simple linear regression analysis of NEP on WTD that maintaining a mean annual WTD within 0.03 m below the hollow surface could bring the undrained peatland ecosystem to C neutrality. In line with their simple prediction, a much more sophisticated process-based undrained simulation by *ecosys* in our study resulted in a near C neutral NEP during the wettest year 2005 with a mean annual WTD of 0.10 m above the hollow surface (Table 3-4).

C losses modelled in the undrained simulation and observed in the undrained peat swamp forest, however, may be a recent phenomenon since a long term apparent C accumulation study showed that Central Kalimantan peatlands have been accumulating C at a rate of 31 g C m^{-2} yr^{-1} for last ~ 12,000 years (Dommain et al. 2011) and that the peatlands around our study site have been accumulating C at a rate of 56 g C m^{-2} yr^{-1} for last ~ 20,000 years (Page et al. 2004). One of the main reasons behind the modelled negative NEP even in the undrained simulation may be that the precipitation within our study period (2002-2005) was less than the long term average, which led to deeper WTD than the long term mean. The wettest year in our study period (2005) experienced a total annual precipitation which was considered as 'normal' annual precipitation (2570 mm yr^{-1}) measured over Indonesian Borneo during 1994-2004 (Takahashi et al. 2004). The year 1999 was the wettest within their measurement period with an annual precipitation of 3788 mm that caused the water table to remain above the ground throughout the year (Wösten et al. 2008). This speculation of large C losses due to reduced precipitation and consequent deeper WTD in recent years can be further corroborated by the cessation of Central Kalimantan peat growth during last ~ 5000 years as reported by Dommain et al. (2011) due to WTD drawdowns caused by increased El Niño frequency and intensity.

3-5. Conclusions

Ecosys successfully simulated the reduction of tropical peatland NEP during shallow and deep WTD hydroperiods with respect to those in intermediate WTD hydroperiods for four years i.e. 2002-2005 over PPSF (Figs. 3-2 to 3-5) (Table 3-2). Reduction of NEP during shallow WTD was modelled mainly through reduced GPP and that during deep WTD hydroperiods was modelled by a combination of reduced GPP and increased R_e (Figs. 3-6 to 3-8). Seasonal variation in NEP that was apparent in the measurements was thought to be caused by the

following key responses that were modelled using following alogrithms of WTD effects on GPP and R_e from basic independent research fed by site specific inputs (Sect. 3-2.2.3):

1) Shallow WTD during rainy seasons reduced modelled NEP by explicitly simulating slower convective-dispersive O_2 transport through soils and roots and hence slower root O_2 uptake, slower soil nutrient (phosphorus) transformations (A26), slower root nutrient (phosphorus) uptake and growth (C23), and consequently lower leaf nutrient (phosphorus) status (C11) and slower CO_2 fixation (C6) (Sect. 3-4.1.1).
2) WTD drawdown during early and late dry seasons in the model increased deeper peat respiration due to better aeration by explicitly simulating higher [O_{2s}] (A17) from more rapid O_2 transport through soils, and hence more rapid microbial and root oxidation-reduction reactions (A3, A5), greater microbial O_2 uptake and energy yields (A20) driving more rapid microbial growth (A25) and respiration (A13, A14, A20) (Sects. 3-4.1.2. and 3-4.1.3).
3) Deeper WTD during late dry seasons in the model reduced NEP through plant water stress by explicitly simulating declines in g_c and their effects on CO_2 fixation from hydraulically driven water transport along soil-plant-atmosphere water potential gradients (B1-B14) (Sect. 3-4.1.3).

Though our modelling effort reasonably well simulated seasonal WTD effects on NEP of the tropical peatland under study, the modelled GPP and R_e aggregates were systematically larger than the EC-derived estimates (Fig. 3-8) (Table 3-3). The possible reasons for these discrepancies are discussed in Sect. 3-4.2. Despite the modelled vs. EC-derived divergence in monthly and annual R_e and GPP aggregates, this study showed for the first time the application of detailed process based modelling in capturing non-linear WTD-tropical peatland CO_2

exchange interactions, as recommended by Murdiyarso et al. (2010). The findings of this study showed that the duration and intensity of the dry season with deeper WTD had profound effects on tropical peatland CO_2 emissions irrespective of disturbance (e.g. drainage). This has an important implication in terms of the fate of tropical peatland C storage under future climate change scenarios since Li et al. (2007) predicted a general drying trend and consequent WTD drawdown over Southeast Asian peatlands during this century using 11 land surface models. Moreover, the response of tropical peatland CO_2 exchange to disturbance (e.g. drainage) was also investigated by our model sensitivity test for drained vs. undrained condition. Insights gained from our modelling effort thus can improve our predictive capacity for the effects of WTD fluctuations arising from interactions between seasonality in precipitation and artificial drainage on tropical peatland C balance.

Our point scale modelling reasonably delineated WTD effects on NEP over a homogeneous patch of tropical peatland in terms of plant functional type (PFT) and land use (i.e. drained forest). However, this modelling can be up scaled to an ecosystem level by model inputs of weather data (Sect. 3-2.2.3); soil physical, hydrological, chemical and biological properties (Sect. 3-2.2.3) (Table 3-1) (Fig. 2-1); PFT (e.g. moss vs. vascular plants, coniferous vs. broad leaved species, evergreen vs. deciduous); and disturbance (e.g. drainage as discussed in Sect. 3-2.2.6, fire, logging etc.) representing a particular peatland ecosystem. Such up scaling could provide us with improved predictive capacity on management opportunities (e.g. undrained vs. drained, reforestation/afforestation vs. deforestation, unburnt vs. burnt) for reducing C emissions. This capacity might be very important for planning long term tropical peatland rehabilitation projects and mapping peat C sequestration for current REDD+ (Reducing Emissions from Deforestation and forest Degradation) scheme.

Table 3-1: Key soil properties as *ecosys* inputs to represent a tropical peatland at Palangkaraya Peat Swamp Forest, Indonesia

D_{humm} (m)	D_{holl} (m)	TOC (g kg^{-1})	TON (g Mg^{-1})	TP (g Mg^{-1})	pH	CEC (cmol+ kg^{-1})
0.01				256		
0.05				238		
0.15			18000	192	3.78	
0.16	0.01					
0.20	0.05			143		
0.25	0.10					
0.40	0.25					
0.60	0.45	500		115		37.5
0.80	0.65					
1.00	0.85					
1.20	1.05		14000		3.71	
1.40	1.25			49		
1.60	1.45					
1.80	1.65					
4.00	3.85					

D_{humm} = depth from hummock surface, D_{holl} = depth from hollow surface, TOC = Total organic C (maximum limit of input for TOC concentration in *ecosys* is used from an average of TOC values for a 4 m deep tropical peat column measured by Page et al. (2004)), TON = Total organic nitrogen and TP = total phosphorus (Values obtained from Page et al. (1999)), pH and CEC = Cation exchange capacity (Values obtained from Sayok et al. (2007)).

Table 3-2: Modelled vs. measured net ecosystem CO_2 fluxes, Palangkaraya Peat Swamp Forest, Indonesia

Year	Precipitation (mm yr^{-1})	*n*	*a*	*b*	R^2	RMSE	RMSRE
Modelled vs. eddy covariance CO_2 fluxes measured at $u^* > 0.17$ m s^{-1}							
2002	1852	3007	0.82	1.03	0.77	5.7	5.5
2003	2291	2595	0.11	1.05	0.83	4.9	5.9
2004	2560	3299	0.61	1.01	0.83	4.9	5.8
2005	2620	3164	1.09	1.01	0.81	5.2	5.6
Modelled vs. gap-filled CO_2 fluxes							
2002	1852	5753	0.23	1.19	0.93	2.5	
2003	2291	6165	-0.51	1.14	0.92	2.8	
2004	2560	5485	-0.76	1.08	0.92	2.6	
2005	2620	5494	-0.35	1.10	0.93	2.3	

(*a, b*) from simple linear regressions of modelled on measured. R^2 = coefficient of determination and RMSE = root mean square for errors from simple linear regressions of measured on simulated. RMSRE= root mean square for random errors in eddy covariance (EC) measurements calculated by inputting EC CO_2 fluxes recorded at u^* (friction velocity) > 0.17 m s^{-1} into algorithms for estimation of random errors due to EC CO_2 measurements developed for forests by Richardson et al. (2006).

Table 3-3: Simulated (*sim*) and observed (*obs*) annual water and C balance, Palangkaraya Peat Swamp Forest, Indonesia

	Units	Year								Values from other studies
		2002		2003		2004		2005		
		sim	*obs*	*sim*	*obs*	*sim*	*obs*	*sim*	*obs*	
Precipitation			1852		2291		2560		2620	
ET	mm yr^{-1}	1485	1325	1607	1366	1545	1324	1558	1310	
Q		390		708		918		1067		
Avg. WTD	m	-0.77		-0.73	-0.56	-0.59	-0.52	-0.45	-0.52	
GPP		4201	3254	4164	3466	4109	3631	4040		
R_a		2909		2823		2760		2778		
NPP	g C m^{-2} yr^{-1}	1292		1341		1349		1262		900[a] 1200[b]
R_h		1901		1918		1777		1635		2182[c]
R_e		4810	3848	4741	3844	4537	3907	4413		
NEP		**-609**	**-594**	**-577**	**-378**	**-428**	**-276**	**-373**		

ET = evapotranspiration, observed *ET* for each year was calculated from EC-gap filled hourly latent heat fluxes measured by Hirano et al. (2005); *Q* = total lateral discharge; WTD = water table depth, simulated and observed WTDs are averages of data used in Figs. 3-2c, 3-3c, 3-4c and 3-5c for 2002, 2003, 2004 and 2005 respectively, observed mean WTD for 2002 was not calculated due to the lack of field observations for the first six months (Fig. 3-2c), negative values of WTD represent depth below the hollow surface; GPP = gross primary productivity, observed GPP for each year was partitioned from eddy covariance (EC)-gap filled net ecosystem productivity estimates as found in Hirano et al. (2007); R_a = autotrophic respiration; NPP = net primary productivity (NPP=GPP-R_a); R_h = heterotrophic respiration; R_e = ecosystem respiration, observed R_e for each year was partitioned from EC-gap filled net ecosystem productivity estimates as found in Hirano et al. (2007); and NEP = net ecosystem productivity (NEP=NPP-R_h), observed NEP for each year was calculated from hourly EC-gap filled CO_2 flux data mentioned by Hirano et al. (2007).

[a] for Amazonian rainforest (Chambers et al. 2004).

[b] for oil palm plantations in tropical peatlands of Malaysia (Melling et al. 2008).

[c] for a mature Acacia plantation in a drained Indonesian peatland with an average WTD of 0.8 m below the hummock surface (Jauhiainen et al. 2012a).

Table 3-4: Sensitivity of modelled annual C balance to drainage, Palangkaraya Peat Swamp Forest, Indonesia

	Units	Year									
		2002		2003		2004		2005		Mean	
		dr	*undr*	*dr*	*undr*	*dr*	*undr*	*dr*	*undr*	*dr*	*undr*
WTD	m	-0.77	-0.22	-0.73	-0.17	-0.59	-0.11	-0.45	0.10	-0.59	-0.10
GPP		4201	3578	4164	3780	4109	3695	4040	3665	4123	3680
R_a		2909	2412	2823	2455	2760	2431	2778	2396	2818	2423
NPP	g C	1292	1166	1341	1325	1349	1264	1262	1269	1311	1256
R_h	m^{-2} yr^{-1}	1901	1595	1918	1636	1777	1382	1635	1320	1808	1483
R_e		4810	4007	4741	4091	4537	3813	4413	3716	4625	3907
NEP		**-609**	**-429**	**-577**	**-311**	**-428**	**-118**	**-373**	**-51**	**-497**	**-227**

dr = drained simulation; *undr* = undrained simulation (Sect. 3-2.2.6); WTD = water table depth, values are the annual means of simulated WTD data in Fig. 3-9, the positive value represents WTDs above hollow surface and negative values represent WTD below the hollow surface; GPP = gross primary productivity; R_a = autotrophic respiration; NPP = net primary productivity (NPP=GPP-R_a); R_h = heterotrophic respiration; R_e = ecosystem respiration; and NEP = net ecosystem productivity (NEP=NPP-R_h).

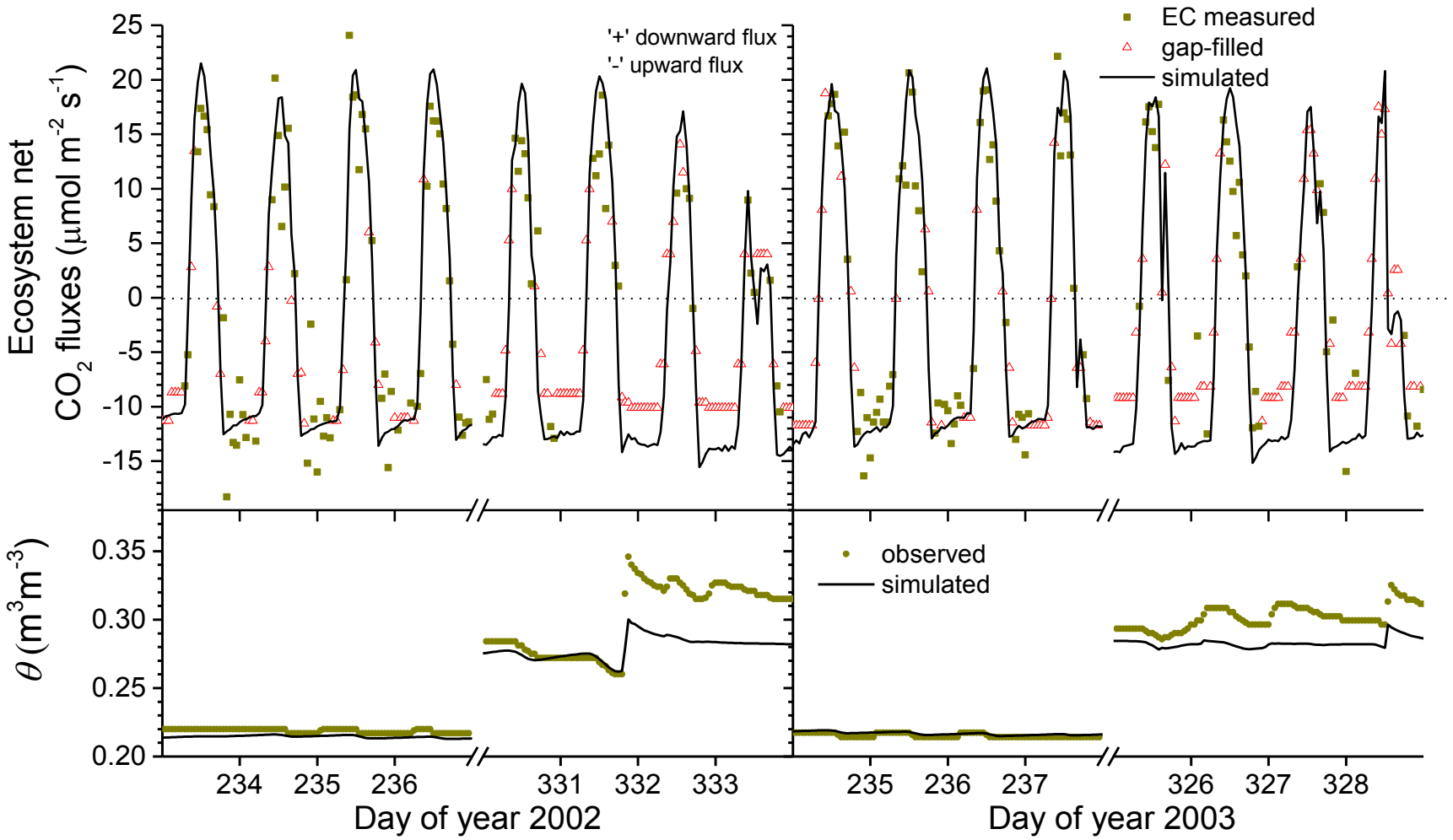

Fig. 3-1. Hourly EC measured, gap-filled and simulated net ecosystem CO_2 fluxes and observed and simulated soil water content (θ) from 0-0.20 m depth of the hummock during 2002 and 2003 over a tropical peatland at Palangkaraya Peat Swamp Forest, Indonesia

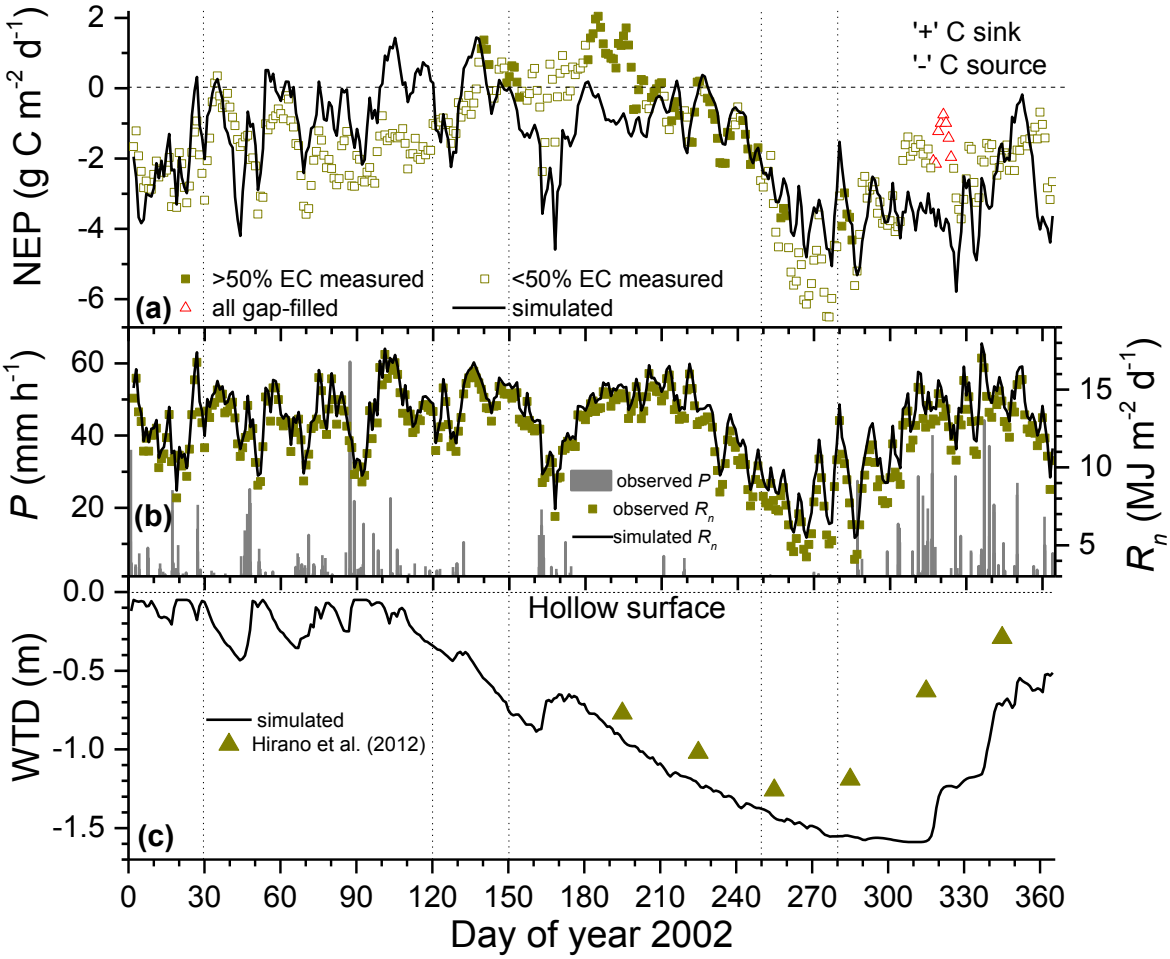

Fig. 3-2. (a) Three day moving averages of simulated and EC-gap filled estimates of net ecosystem productivity (NEP). Closed squares indicate sums of 24 values more than ½ of which were recorded at u^* (friction velocity) > 0.17 m s^{-1}, open squares indicate sums of 24 values more than ½ of which were gap-filled, and open triangles indicate sums of 24 values all of which were gap-filled); (b) hourly measured precipitation (P) and three day moving averages of simulated and measured net radiation (R_n); and (c) monthly measured (values digitally obtained from Hirano et al. (2012)) and daily modelled water table depths (WTD) from hollow surface during 2002 over a tropical peatland at Palangkaraya Peat Swamp Forest, Indonesia. Negative values of WTD mean depths below the hollow surface

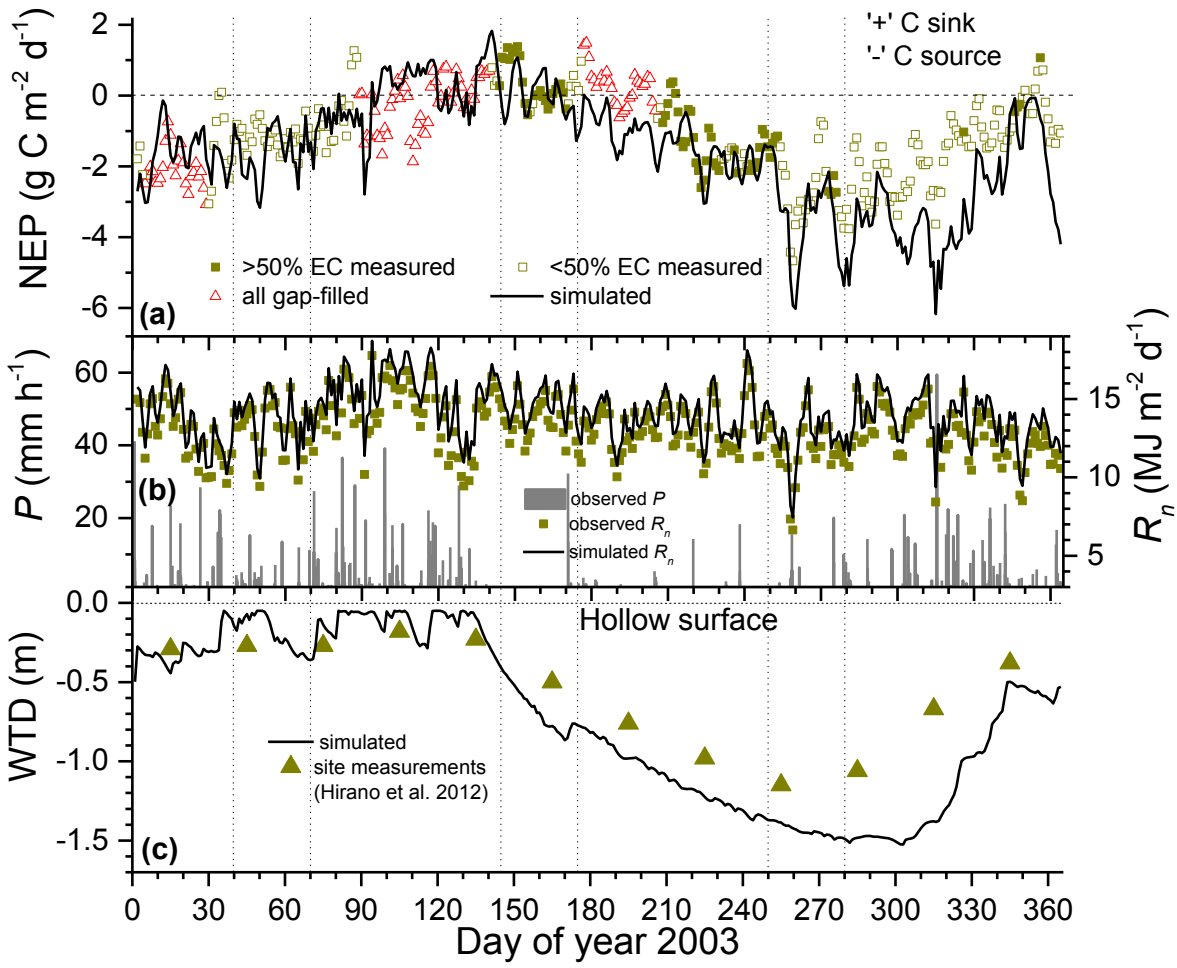

Fig. 3-3. (a) Three day moving averages of simulated and EC-gap filled estimates of net ecosystem productivity (NEP). Closed squares indicate sums of 24 values more than ½ of which were recorded at u^* (friction velocity) > 0.17 m s^{-1}, open squares indicate sums of 24 values more than ½ of which were gap-filled, and open triangles indicate sums of 24 values all of which were gap-filled); (b) hourly measured precipitation (P) and three day moving averages of simulated and measured net radiation (R_n); and (c) monthly measured (values digitally obtained from Hirano et al. (2012)) and daily modelled water table depths (WTD) from hollow surface during 2003 over a tropical peatland at Palangkaraya Peat Swamp Forest, Indonesia. Negative values of WTD mean depths below the hollow surface

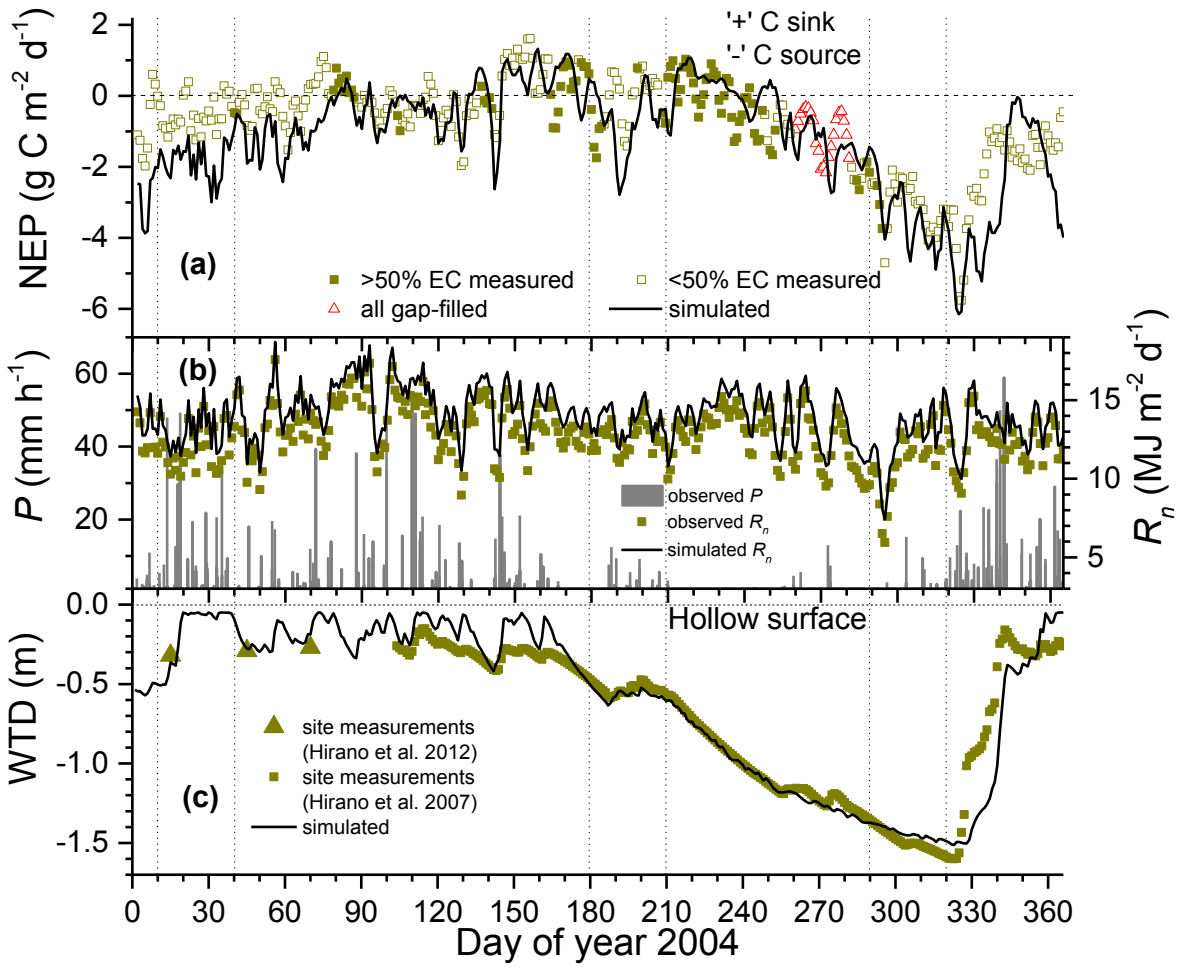

Fig. 3-4. (a) Three day moving averages of simulated and EC-gap filled estimates of net ecosystem productivity (NEP). Closed squares indicate sums of 24 values more than ½ of which were recorded at u^* (friction velocity) > 0.17 m s^{-1}, open squares indicate sums of 24 values more than ½ of which were gap-filled, and open triangles indicate sums of 24 values all of which were gap-filled); (b) hourly measured precipitation (P) and three day moving averages of simulated and measured net radiation (R_n); and (c) monthly measured (values digitally obtained from Hirano et al. (2012)), daily measured (site measurements mentioned in Hirano et al. (2007)) and daily modelled water table depths (WTD) from hollow surface during 2004 over a tropical peatland at Palangkaraya Peat Swamp Forest, Indonesia. Negative values of WTD mean depths below the hollow surface

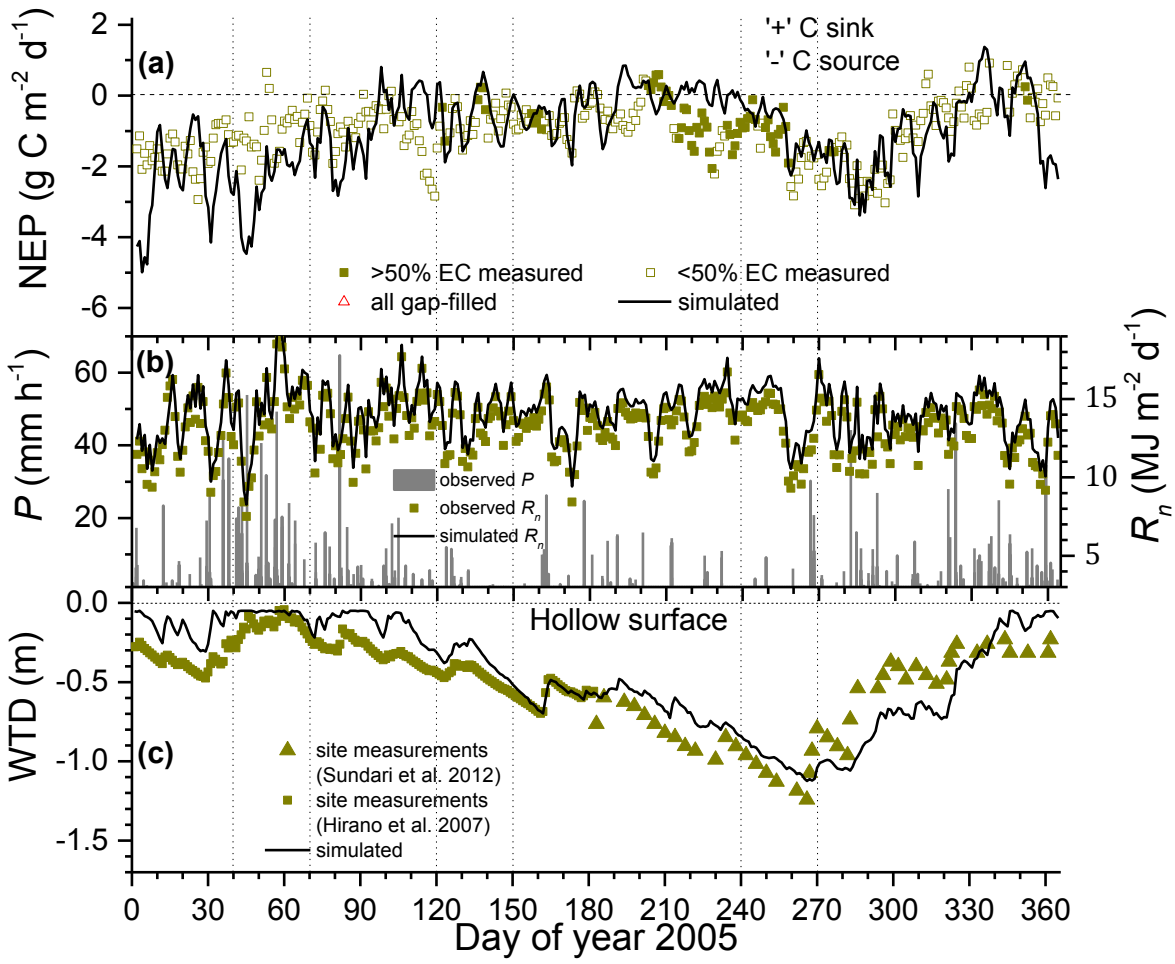

Fig. 3-5. (a) Three day moving averages of simulated and EC-gap filled estimates of net ecosystem productivity (NEP). Closed squares indicate sums of 24 values more than ½ of which were recorded at u^* (friction velocity) > 0.17 m s^{-1} and open squares indicate sums of 24 values more than ½ of which were gap-filled); (b) hourly measured precipitation (P) and three day moving averages of simulated and measured net radiation (R_n); and (c) daily measured (values digitally obtained from Sundari et al. (2012) and measured *in situ* as mentioned in Hirano et al. (2007)) and modelled water table depths (WTD) from hollow surface during 2005 over a tropical peatland at Palangkaraya Peat Swamp Forest, Indonesia. Negative values of WTD mean depths below the hollow surface

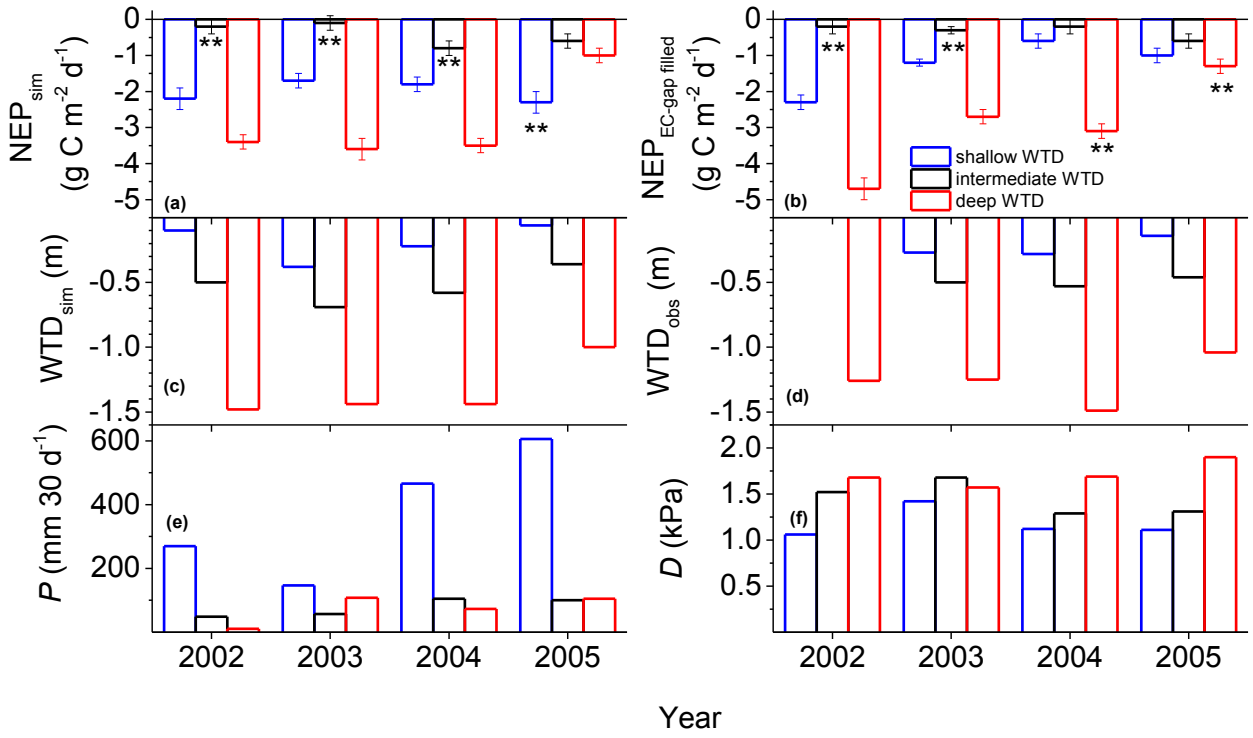

Fig. 3-6. (a) Average simulated daily net ecosystem productivity (NEP_{sim}) (b) average EC-gap filled daily net ecosystem productivity ($NEP_{EC\text{-}gap}$) (c) average simulated water table depths (WTD_{sim}) (d) average observed water table depths (WTD_{obs}) (e) total observed precipitation (P), and (f) average mid-day (10:00-14:00 local time) vapor pressure deficit (D) over 30 days each of shallow (DOY 1-30, 41-70, 11-40 and 41-70 during 2002, 2003, 2004 and 2005 respectively), intermediate (DOY 121-150, 146-175, 181-210 and 121-150 during 2002, 2003, 2004 and 2005 respectively) and deep (DOY 251-280, 251-280, 291-320 and 241-270 during 2002, 2003, 2004 and 2005 respectively) WTD hydroperiods (delineated by vertical dotted lines in Figs. 3-2 to 3-5) in a tropical peatland at Palangkaraya Peat Swamp Forest, Indonesia. Bars represent standard errors of means. Asterisks (**) on the top of a column represent significant ($P < 0.01$) difference from the adjacent column(s). Negative values of WTD mean depths below the hollow surface

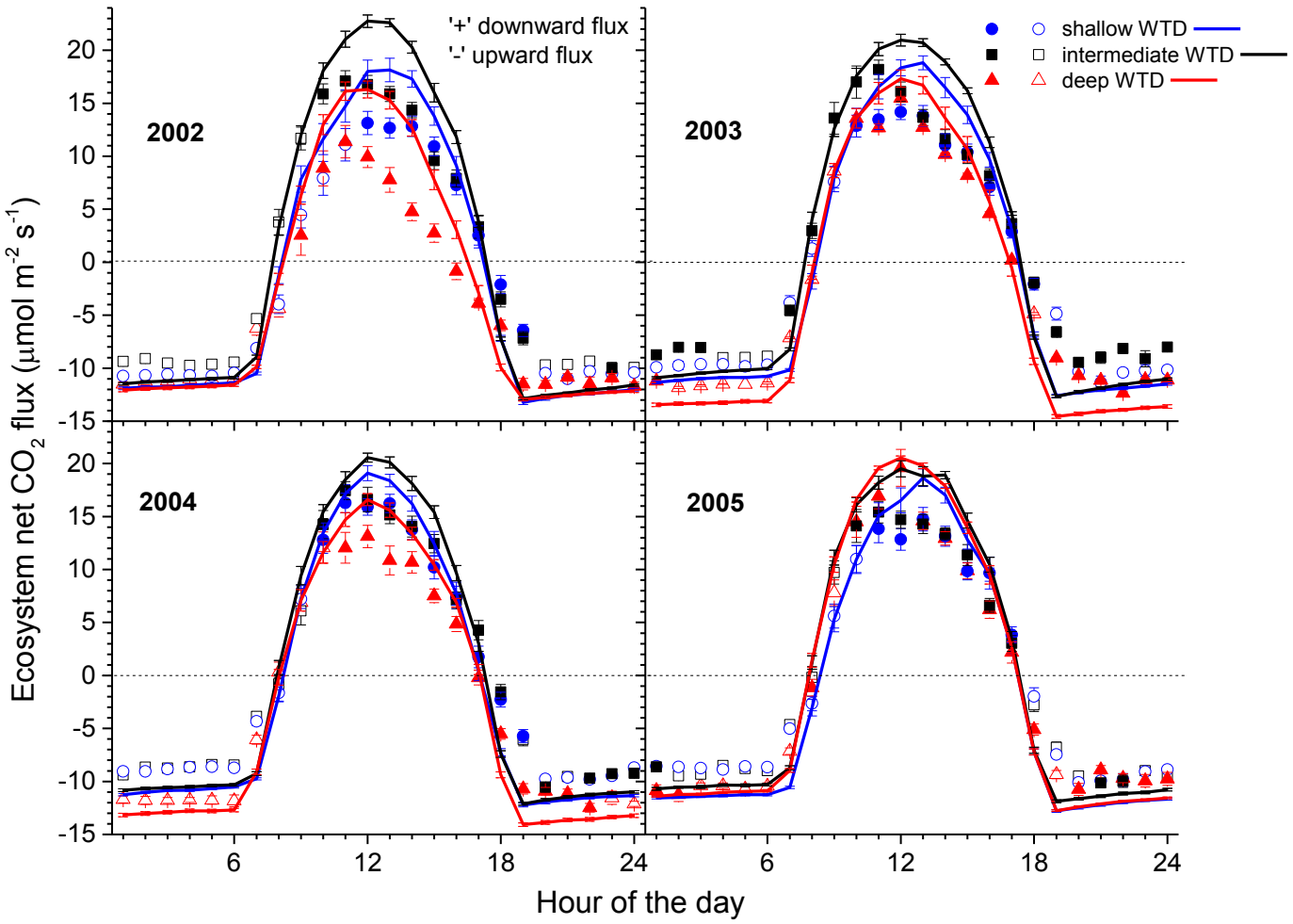

Fig. 3-7. Hourly binned simulated (lines) and EC-gap filled (symbols) ecosystem net CO_2 fluxes during shallow (DOY 1-30, 41-70, 11-40 and 41-70 during 2002, 2003, 2004 and 2005 respectively), intermediate (DOY 121-150, 146-175, 181-210 and 121-150 during 2002, 2003, 2004 and 2005 respectively) and deep (DOY 251-280, 251-280, 291-320 and 241-270 during 2002, 2003, 2004 and 2005 respectively) water table depth (WTD) hydroperiods (delineated by vertical dotted lines in Figs. 3-2 to 3-5) over a tropical peatland at Palangkaraya Peat Swamp Forest, Indonesia. Closed symbols are averages of 30 hourly values more than 1/3 of which were EC measured CO_2 fluxes recorded at u^* (friction velocity) > 0.17 m s^{-1}. Open symbols are averages of 30 hourly values less than 1/3 of which were EC measured CO_2 fluxes recorded at u^* > 0.17 m s^{-1}

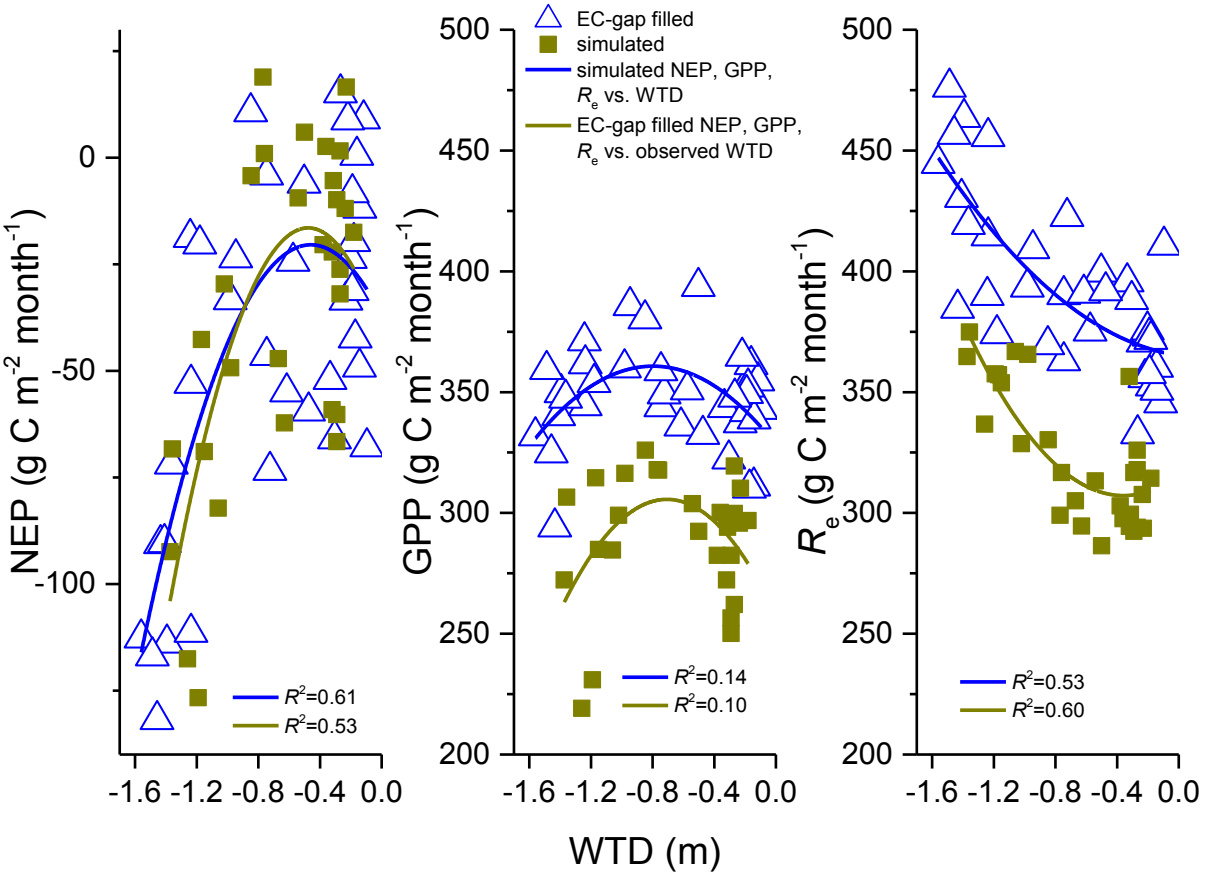

Fig. 3-8. Relationships between monthly simulated net ecosystem productivity (NEP), gross primary productivity (GPP) and ecosystem respiration (R_e), and monthly averaged simulated water table depths (WTD) (from Figs. 3-2c, 3-3c and 3-4c for 2002, 2003 and 2004 respectively); and monthly EC-derived NEP (derived from EC-gap filled hourly CO_2 fluxes), GPP and R_e (calculated from monthly averaged daily values digitally obtained from Hirano et al. (2007)), and monthly averaged observed WTDs (from Figs. 3-2c, 3-3c and 3-4c for 2002, 2003 and 2004 respectively) during 2002-2004 over a tropical peatland at Palangkaraya Peat Swamp Forest, Indonesia. Negative values of WTD mean depths below the hollow surface

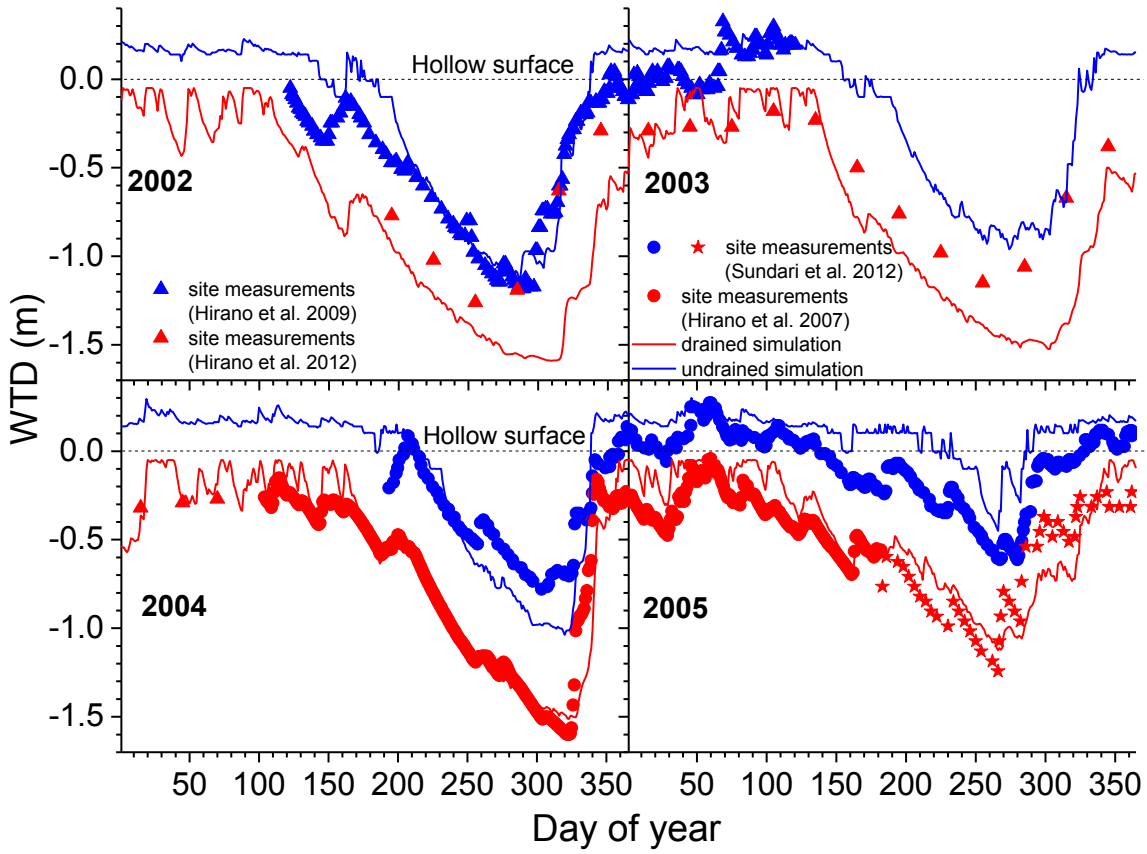

Fig. 3-9. Simulated daily drained vs. undrained water table depths (WTD) (Sect. 3-2.2.6) during 2002-2005 over a tropical peatland at Palangkaraya Peat Swamp Forest, Indonesia. Drained WTDs are the same as those in Figs. 3-2c, 3-3c, 3-4c and 3-5c for 2002, 2003, 2004 and 2005 respectively. Negative values of WTD mean depths below the hollow surface and positive values mean depths above the hollow surface

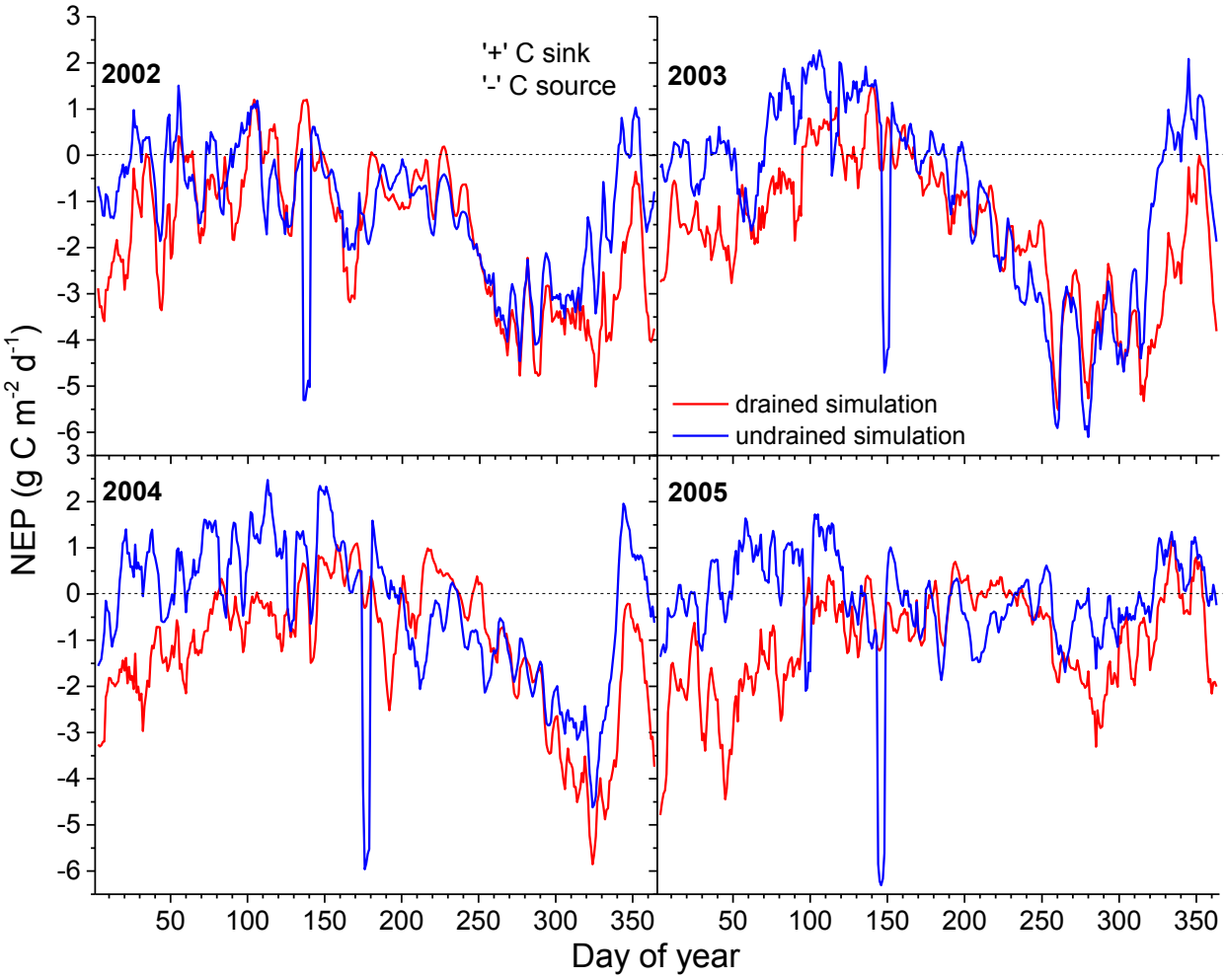

Fig. 3-10. Five-day moving averages of simulated daily net ecosystem productivity (NEP) for drained vs. undrained conditions (Sect. 3-2.2.6) during 2002-2005 over Palangkaraya Peat Swamp Forest, Indonesia. Drained values are the same as those in Figs. 3-2 to 3-5

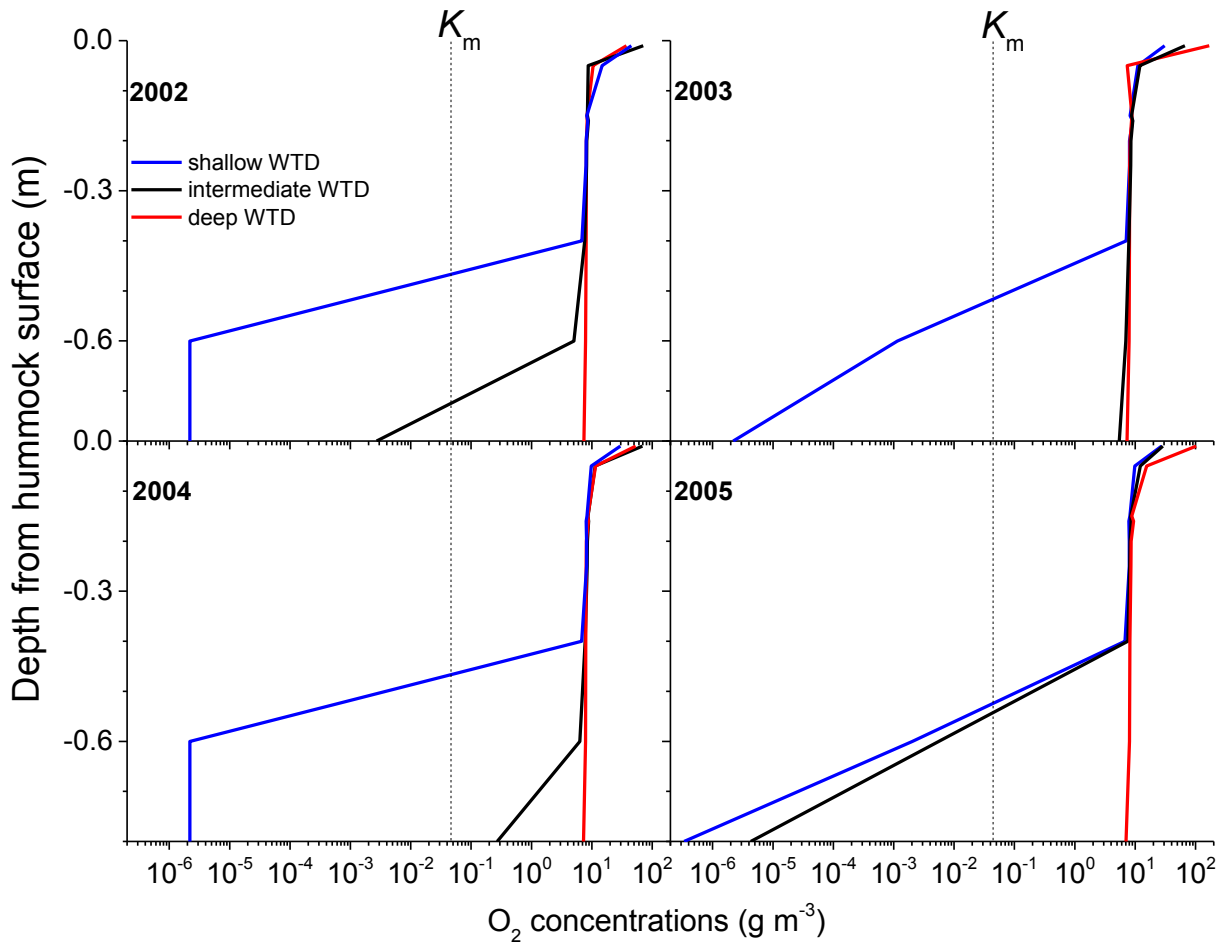

Fig. 3-11. Vertical profile distributions of peat soil aqueous oxygen concentrations simulated under hummock surface during shallow water table depth (WTD) hydroperiods (DOY 15, 55, 25 and 55 of 2002, 2003, 2004 and 2005 respectively), intermediate WTD hydroperiods (DOY 135, 160, 195 and 135 of 2002, 2003, 2004 and 2005 respectively), and deep WTD hydroperiods (DOY 265, 265, 305 and 255 of 2002, 2003, 2004 and 2005 respectively) over a tropical peatland at Palangkaraya Peat Swamp Forest, Indonesia. K_m = Michaelis-Menten constant (0.064 g m^{-3}) for microbial, root and mycorrhizal uptake (A17a, C14c) in *ecosys*

Chapter 4 : Modelling Hydrological Controls on Peat Water Content, Water Table Depth and Surface Energy Exchange of a Boreal Western Canadian Peatland

4-1. Introduction

Northern boreal and sub-arctic peatlands comprise 75-80% of total global peatland area (Frolking et al. 2011) and have been accumulating soil carbon at a rate of 19-24 g m^{-2} yr^{-1} (Flanagan and Syed 2011) over more than 6,000 years (Zoltai and Vitt 1990). These peatlands have formed mainly due to slow decomposition in saturated soils under shallow or above-ground water table (WT). However, these peatlands are projected to shift from carbon sinks to sources as a result of water table depth (WTD) drawdown due to increased frequency and intensity of droughts over the upcoming millennium (Frolking et al. 2011). Deeper WT along with warmer weather can cause rapid aerobic decomposition in these peatlands and hence can further contribute to atmospheric CO_2 (Cai et al. 2010). Moreover, WTD drawdown can hinder evapotranspiration (*ET*) due to drying of peat surfaces, bryophytes (e.g. moss) and/or vascular plant water stress (Dimitrov et al. 2011). Intensive drying of mosses as well as vascular plant water stress can in turn cause reductions in gross primary productivity (GPP) of these peatlands thereby impeding peat accumulation (Lafleur et al. 2005, Dimitrov et al. 2011, Peichl et al. 2014).

Seasonal and interannual variations in northern peatland WTD arise from variable balance among precipitation (*P*), *ET*, and lateral water fluxes in the forms of surface run-on/run-offs and sub-surface recharge/discharge. However, these WTD variations are not only affected by *ET* but also can affect peatland *ET*. The WTD-*ET* interaction is largely mediated by the moisture retention characteristics of a peat and its interaction with the peat forming vegetation. Peats with low moisture holding capacity can be rapidly drained with WTD drawdown. When

WTD falls below a certain threshold level in these peats, capillary rise from WT becomes inadequate to supply moisture to the shallow rhizoids of the mosses which causes a reduction in moss evaporation (*E*). This WTD threshold depends upon moisture supplying capacity of a particular peat through capillary rise. Vascular plant roots, however, can penetrate much deeper than the moss rhizoids and thus are expected to sustain water uptake and hence transpiration (*T*) during deeper WT periods. If the reduction in moss *E* due to this near surface peat desiccation cannot be offset by vascular *T*, the peatland *ET* declines (Dimitrov et al. 2011). However, drawdown of WT beyond the root zone of the vascular plants can cause a reduction in vascular water uptake and hence canopy stomatal conductance (g_c), *T* and GPP (Lafleur et al. 2005, Peichl et al. 2014). Unlike these peats with low moisture holding capacity, those with high moisture holding capacity can supply adequate moisture to the mosses through capillary rise and can hold adequate moisture for vascular uptake. Consequently these peatland ecosystems do not experience water stress and hence reductions in *ET* and GPP due to similar drawdown of WTD (Parmentier et al. 2009, Wu et al. 2010). Therefore, the effects of WTD on *ET* vary across peatlands depending upon the interaction of WTD, peat specific soil moisture retention and rooting depths of peat forming vegetation.

WTD variations also determine the transition between aerobic and anaerobic zones and govern the O_2 status and energy yields for microbial and root respirations through its effects on peat moisture retention and hence aeration. Peats that have low moisture holding capacity at deeper WTD periods can be drained rapidly with WTD drawdown that improves soil O_2 status and hence stimulates peat respiration (Sulman et al. 2009, Cai et al. 2010, Sulman et al. 2010). However, some peats can retain very high moisture content at deeper WTD periods thus

resulting in poorer peat drainage and O_2 status and hence less increase or no response of peat respiration to deeper WTD (Parmentier et al. 2009, Sonnentag et al. 2010).

Therefore, to better apprehend how these northern boreal peatlands would behave under future drier and warmer climates and hence to assess the need to restore and sustain the carbon sinks of these peatlands, it is imperative to have improved predictive capacity for the seasonal and interannual variations in the interactions between peatland hydrological and biogeochemical processes. To acquire this capacity, significant efforts have been made in developing and testing process-based models of eco-hydrological interactions in these peatlands (Sulman et al. 2012). However, most of these models still have some key limitations that prevent them from adequately simulating WTD effects on GPP and ecosystem respiration (R_e) (Sulman et al. 2012). One of the key limitations in most of the existing process-based peatland models is the lack of a prognostic WTD simulation from vertical and lateral water fluxes (Frolking et al. 2002, Zhang et al. 2002, Van Huissteden et al. 2006, Kurbatova et al. 2009, St-Hilaire et al. 2010). This hinders those models' ability to simulate a continuous anaerobic zone below WTD in which R_e is suppressed resulting in peat formation (Sulman et al. 2012).

Prognostic WTD dynamics in process-based peatland models can be simulated from hydraulically driven vertical and lateral water fluxes. However, northern peatlands differ between two major classes i.e. fens and bogs, in terms of lateral water exchange (Tarnocai et al. 2006). Fens are known to receive water laterally from surrounding mineral soil WT whereas bogs are entirely precipitation fed. So, process-based modelling of fen WTD variation poses an additional challenge in accounting for lateral water inflow from adjacent upland ecosystems. Bond-Lamberty et al. (2007) accounted for this lateral inflow as a function of P while simulating site-specific lateral water gain in a poorly drained forest of Manitoba, Canada. However, a more

universal solution of hydraulically driven lateral water transfer scheme based on Darcy's law in a process-based ecosystem model *ecosys* reasonably well simulated lateral water exchange of a northern boreal fen peatland (Grant et al. 2012b), and a boreal peat-mineral soil transitional ecotone (Dimitrov et al. 2014).

WTD variation can affect seasonal and interannual variation in peat moisture content. The effects of WTD on peat moisture contents are mediated by peat moisture retention characteristics. The peat moisture retention characteristic in current process-based peatland models is predominantly simulated from numerical solution of soil moisture content as a function of height above the WT (i.e. soil matric water potential) using either a linear (Zhang et al. 2002) or a Campbell (Campbell 1974) type power function (Frolking et al. 2002, St-Hilaire et al. 2010). These models, however, do not simulate a prognostic WTD, and hence uses WTD as inputs from site measurements in these numerical solutions (Frolking et al. 2002, Zhang et al. 2002, Kurbatova et al. 2009, St-Hilaire et al. 2010). A more complex process-based model *ecosys* simulates a prognostic WTD dynamic that affects soil moisture retention through a log-transformed Campbell model (defined as a modified Campbell model or MCM hereafter) which enabled the model to reasonably well simulate peat moisture retention in a northern boreal peatland (Dimitrov et al. 2010b). The Campbell type (Campbell 1974) function or its modification(s) (e.g. MCM in *ecosys*) usually results in a hyperbolic relationship (*J*-shape) between soil moisture content (θ) and soil matric water potential (ψ_m) while simulating soil moisture desorption with decreasing ψ_m (Fig. 4-1). However, many peats have moisture retention characteristics that follow sigmoidal (*S*-shape) logistic curves (Päivänen 1973, Weiss et al. 1998, Gnatowski et al. 2010, Dettmann et al. 2014) with inflection points (ψ_{in}) (Fig. 4-1). Application of desorption equation like Campbell model or its modification(s) in simulating these types of

peat moisture retention could thus lead to a significant underestimation of near saturation peat water contents (Fig. 4-1). This in turn can cause a substantial overestimation of peat aeration and hence respiration in those peatlands. A van Genuchten type (Van Genuchten 1980) soil moisture retention function can address this challenge by simulating sigmoidal or *S*-shape moisture desorption curves with regressing ψ_m (Fig. 4-1). The van Genuchten model (VGM) is in fact the most commonly used soil moisture retention equation in current hydrological modelling of mineral soils (Dettmann et al. 2014). This equation also well simulates a wide range of measured peat moisture retention curves from *J*-shape (Silins and Rothwell 1998, Weiss et al. 1998) to *S*-shape (Päivänen 1973, Weiss et al. 1998, Gnatowski et al. 2010) and hence is suggested to be the most suitable one for moisture retention modelling across peatlands (Dettmann et al. 2014). Despite the advantages, VGM has not been very commonly used thus far in peatland models in simulating seasonal and interannual variations of peat θ as affected by WTD variations. In fact, Schwärzel et al. (2006) performed the only modelling so far by using hydrological model HYDRUS in a drained German peatland that showed VGM can successfully be used in simulating seasonal and interannual variations of peat θ in a 1D soil-plant-atmosphere moisture scheme. So, investigating the applicability of VGM in simulating peat θ variations while coupled with a detailed 3D soil-plant-atmosphere moisture scheme in *ecosys* would further improve our predictive capacity of seasonal and interannual variations in peat moisture retention.

Variation in θ as affected by variation in WTD can affect peatland *ET* and hence GPP. The effects of peat moisture retention on peatland *ET* and GPP in most of the process-based peatland models are currently computed by using scalar functions to account for moisture limitations to *ET* and GPP under either very dry or wet soil conditions (Frolking et al. 2002, Zhang et al. 2002, Bond-Lamberty et al. 2007, St-Hilaire et al. 2010, Sulman et al. 2012). This

approach has its own limitation because soil-vegetation-climate moisture feedbacks vary across peatlands depending upon the interaction between peat moisture retention and peat forming vegetation as discussed above and so these scalar functions need to be parameterized for every site. So, to improve our predictive capacity of variable WTD feedbacks to *ET* across peatlands we need a more universal solution of peatland *ET* while equilibrating vegetation-atmosphere moisture exchange with vegetation water uptake in a soil-plant-atmosphere hydraulic scheme. Instead of using site specifically parameterized scalar functions, this hydraulic scheme can equilibrate atmospheric *ET* demand from surface and canopy energy balances with moisture supply by vegetation as mediated by (1) rooting profiles resulting from root-WTD interactions and (2) a series of water potentials (e.g. soil, root and canopy water potentials) and hydraulic resistances (soil, root, canopy surface and/or stomatal resistances).

4-1.1. Objectives and rationale

Given the importance of interactions among WTD, peat moisture retention and peat forming vegetation in modelling WTD effects on *ET* and GPP across peatlands, the present study aims at using a process-based ecosystem model *ecosys* to (1) examine the applicability of the van Genuchten model in improving simulation of peat moisture desorption, and (2) simulate seasonal and interannual variations of WTD by coupling vertical and lateral water fluxes determined by the improved moisture retention and water exchange through vertical and lateral model boundary, and (3) simulate and thereby better understand the effects of seasonal and interannual variations in soil moisture and WTD on surface energy exchange while modelling process-based feedbacks between hydrology and ecology of a Western Canadian boreal fen peatland (Syed et al. 2006, Flanagan and Syed 2011) in Alberta, Canada.

Improvement of peat moisture simulation in this study would be accomplished by replacing the existing moisture retention function (MCM) in *ecosys* with the VGM and testing the VGM vs. MCM daily outputs for θ against daily site measurements. With the improved moisture retention function, *ecosys* outputs of hourly WTD and energy fluxes (e.g. latent and sensible heat fluxes) would then be tested against site measurements to examine how well *ecosys* would simulate seasonal and interannual variations in WTD and surface energy exchange of Western Canadian peatland (WPL) site. After the testing of modelled outputs against measurements, comparative studies of modelled and measured WTD and surface energy exchange would be performed between shallow and deep WTD hydroperiods to examine and explain WTD effects on surface energy exchange of WPL. This rigorous testing of model outputs against measurements as well as examination of contrasting responses of surface energy exchange between different WTD periods is likely to improve our predictive capacity and insights of how the northern boreal peatlands' eco-hydrology would be affected by future drier climates.

4-1.2. Hypotheses

Soil moisture retention in *ecosys* is simulated by numerical solution of soil water matric potential (ψ_m) as a function of θ in a log-transformed Campbell model (MCM) (Fig. 4-1). This enabled *ecosys* to successfully simulate near surface peat θ in a tropical (Fig. 2-2) and a boreal (Dimitrov et al. 2010b) bog peatland. However, those peats had low near saturation moisture holding capacity and hence exhibited rapid pore drainage immediately below saturation thereby matching the *J*-shaped moisture retention curve in MCM when simulating decreasing θ with declining ψ_m (Fig. 4-1). Measurements of peat θ in the fen peatland at WPL by Cai et al. (2010) and Long et al. (2010), however, showed that unlike those bog peats, fen peats retained high θ

near saturation and then drained rapidly when declining WTD caused ψ_m to decrease below a threshold (i.e. air entry potential, ψ_e) thereby producing a sigmoidal (*S*-shape) moisture retention curve. Since VGM simulates sigmoidal moisture desorption curves we, therefore, hypothesize that substituting MCM with VGM in *ecosys* would better simulate peat θ measured in WPL. This test of VGM vs. MCM in *ecosys* for simulating peat θ would improve our predictive capacity of peat moisture retention across peatlands.

Variation in peat θ is also affected by changes in site hydrology that affect variation in WTD that in turn affects peat matric water potential (ψ_m). Flanagan and Syed (2011) measured a gradual drawdown of growing season (May-August) WTD from the wettest growing season of 2004 to the driest growing season of 2009 at the WPL. This gradual drawdown of WTD provided us with an opportunity to test the robustness of the model hypothesis that *ecosys* would simulate this gradual WTD drawdown from gradually decreasing vertical influx (*P*) to efflux (*ET*) and lateral influx (recharge) to efflux (discharge) ratios.

The gradual WTD drawdown from wetter to drier growing seasons at the WPL also caused ecosystem drying as evaluated by actual to potential *ET* (ET_a/ET_p) (Flanagan and Syed 2011). A decrease in growing season (May-August) ET_a/ET_p was apparent from eddy covariance (EC) measurements by Flanagan and Syed (2011) when average growing season WT fell below a threshold level during drier growing seasons of 2008 and 2009 compared to other growing seasons (e.g. 2004-2007). We hypothesize that *ecosys* would be able to model this threshold WTD response to *ET* in the WPL by simulating feedbacks between WTD and *ET* as mediated by vertical water fluxes controlled by the interaction between plant water relations and soil moisture retention improved with the use of VGM.

4-2. Methods

4-2.1. Model development

Ecosys is a process-based general purpose terrestrial ecosystem model that successfully simulated 3D water, energy, carbon and nutrient (N, P) cycles across peatlands (Dimitrov et al. 2010b, Grant et al. 2012b, Sulman et al. 2012) (Chapters 2-3). *Ecosys* algorithms that govern simulations of soil moisture retention, WTD and surface energy exchange which are related to our hypotheses are described below. The equations that are listed in the appendices A to H at the end of the chapter are cited in the text within round brackets with a letter representing a particular appendix followed by the equation number.

4-2.1.1. Water table depth (WTD)

The WTD in *ecosys* is calculated at the end of each time step as the depth to the top of the saturated zone below which air-filled porosity is zero (C1). This WTD is the depth at which lateral water flux is in equilibrium with the difference between vertical influxes (P) and effluxes (ET). The lateral water flux in *ecosys* is governed by the lateral sub-surface boundary condition. This lateral sub-surface boundary condition in *ecosys* is defined by a specified external WTD (WTD_x) and a specified lateral distance (L_t) over which lateral sub-surface water flow occurs (Fig. 4-2). This WTD_x represents average WTD of the surrounding watershed with which modelled boundary grid cells exchange water. The lateral water fluxes are governed by the hydraulic gradient between the WTD within the modelled grid cell and WTD_x over L_t in a Darcy's equation, and by macropore and matrix hydraulic conductivity of the soil layer in which these fluxes occur (Fig. 4-2). Thus when WTD within modelled grid cells is shallower than WTD_x, discharge through the model lateral boundary occurs and when WTD falls below WTD_x recharge into the modelled grid cells occurs (Fig. 4-2). The WTD in *ecosys* is thus not

prescribed, but rather controls, and is controlled by, vertical and lateral surface and sub-surface water fluxes (A1-A7, B1-B5, B18-B24).

4-2.1.2. Vertical water fluxes

Vertical surface boundary influxes from *P* are provided as inputs to the model, as are solar radiation, air temperature, humidity and wind speed used to drive energy balance calculations. These calculations drive vertical surface boundary effluxes of *ET* from vascular canopy surfaces (E2-E3), and of evaporation (*E*) from non-vascular canopy (E2), residue (A6) and soil surfaces (A7). These effluxes are coupled with subsurface water transfers through root (F1-F6) and soil (B1-B5, B18-B24) profiles within the modelled grid cells. Both lateral and vertical subsurface water flows through soil matrices within the modelled grid cells (B2) are calculated from the Richard's equation using total soil water potentials (ψ_s) (matric + osmotic + gravimetric) of adjacent cells if both source and destination cells are either saturated or unsaturated (B3), or from the Green-Ampt equation using ψ_s beyond the wetting front of the unsaturated cell if either cell is saturated (B4-B5) (Grant et al. 2004). Vertical and lateral subsurface water flows can also occur within the soil profiles through macropores using Hagen-Poiseuille's theory for laminar flow in tubes (B18-B21), depending on inputs for macropore volume fraction (B22) (Dimitrov et al. 2010b).

Vertical surface boundary effluxes from vascular *T* (E3) are governed by canopy conductance (g_c) (=1/r_c, where r_c = canopy stomatal resistance) determined by equilibrating plant water uptake (U_w), calculated from gradients of soil, root and canopy water potentials (ψ_s, ψ_r and ψ_c) regulated by soil and root hydraulic resistances (Ω_s and Ω_r) in each rooted soil layer, with *T* calculated from canopy energy exchange within a soil-plant-atmosphere continuum (F6). Since

non-vascular plants lack stomatal regulation, E from non-vascular canopy is predominantly determined by vapor pressure gradient between the canopy and adjacent air (E3) and a specified fixed canopy surface resistance to E (E6). Non-vascular U_w is modelled similarly to the vascular canopy-root-soil hydraulic scheme.

Root/rhizoidal growth used to calculate Ω_s and Ω_r in each plant population is calculated from its assimilation of the non-structural C product of CO_2 fixation (σ_C) (G8). Assimilation is driven by growth respiration (R_g) (G7) remaining after subtracting maintenance respiration (R_m) (G6) from autotrophic respiration (R_a) (G1) driven by oxidation of σ_C (G2-G5). This oxidation in roots/rhizoids may be limited by root/rhizoidal O_2 reduction (G3), required to sustain C oxidation and nutrient uptake (G5). Reduction is driven by root/ rhizoid O_2 demand, and constrained by root/rhizoidal O_2 uptake controlled by concentrations of aqueous O_2 in the soil ($[O_{2s}]$). Values of $[O_{2s}]$ are maintained by convective-dispersive transport of O_2 through soil gaseous and aqueous phases (H3, H5) and by dissolution of O_2 from soil gaseous to aqueous phases (H1). Root O_2 uptake in vascular plants is also controlled by concentrations of aqueous O_2 in roots ($[O_{2r}]$) (G4). Values of $[O_{2r}]$ in vascular plants are maintained by convective-dispersive transport of O_2 through the root gaseous phase (H4) and by dissolution of O_2 from root gaseous to aqueous phases (H2). This transport depends on species-specific values used for root air-filled porosity (aerenchyma) (θ_{pr}) (H5). *Ecosys*, however, does not simulate atmosphere to rhizosphere O_2 transport through non-vascular rhizoids ($\theta_{pr} = 0$).

Slower production of σ_C in under-storey non-vascular plants (e.g. mosses) is modelled in *ecosys* from inter-specific competition for light and nutrients (N, P) with over-storey vascular plants and from intra-specific competition for those resources due to large moss population (G9).

This slower σ_C production in the moss canopy causes less shoot-rhizoid transfer of σ_C and hence slower rhizoid growth respiration (R_g) (G7) and growth by individual moss plants. This in turn results in shallower moss rhizoids. Absence of aerenchyma in moss rhizoids hinders rhizoid O_2 uptake and hence oxidation of σ_C that further slows moss rhizoid R_g and growth in wet deeper peat layers where $[O_{2s}]$ is inadequate for σ_C oxidation (G9-G10). This limits moss rhizoids mostly to near surface peat layers that are frequently unsaturated. When WTD deepens past a certain point, inadequate capillary rise causes near-surface peat desiccation (B2-B5), reducing ψ_s and increasing Ω_s (F3) of those layers. This in turn causes a reduction in moss canopy water potential (ψ_c) while equilibrating moss E with U_w (F6).

Deeper rooting by larger vascular plants in *ecosys*, on the other hand, is facilitated by greater root growth stimulated by greater assimilation and consequent rapid shoot-root transfer of σ_C due to more access to light and less intra-specific competition with lower populations than mosses, as well as O_2 transfer through root aerenchyma into wet deeper peat layers (G2-G5, H2, H4-H5). This deeper rooting pattern and consequent increased U_w from the wetter deeper layers enables those vascular plants to offset the suppression of U_w from desiccated near surface layers. Those vascular plants can therefore limit the reduction in ψ_c and g_c and can sustain T (E3, E6) during deeper WTD.

4-2.1.3. Lateral water fluxes

Lateral surface runoff within the modelled grid cells and across lower surface boundaries is modelled using Manning's equation (A2) with surface water velocity (A3) calculated from surface geometry (A4) and slope (A5), and with surface water depth (A2) calculated from surface water balance (A1) using kinematic wave theory. Lateral flows through subsurface

boundaries are controlled by WTD_x, used to represent watershed effects on landscape hydrology, and L_t (Fig. 4-2). Lateral subsurface flows from saturated boundary grid cells are calculated from their lateral hydraulic conductivities, external hydraulic gradients determined by elevation differences between these grid cells and the WTD_x and L_t (B23-B24). These lateral fluxes thus both determine, and are determined by WTD, which in turn determines surface fluxes.

4-2.1.4. van Genuchten (VGM) model vs. modified Campbell model (MCM) in simulating vertical and lateral water fluxes

The rates of vertical and lateral fluxes through soil matrices in *ecosys* are governed by hydraulic gradients and unsaturated hydraulic conductivities in Richard's or Green-Ampt equations that are affected by soil matrix moisture retention. Soil matrix moisture retention in *ecosys* is currently simulated by log-transforming a Campbell equation (Eq. 4-1) (Campbell 1974) in two segments, one above field capacity (Eqs. 4-3b and 4-4b) and the other below (Eqs. 4-3a and 4-4a) instead of using a parameter value for *b* representing peat soil texture as suggested by Letts et al. (2000) (Frolking et al. 2002, St-Hilaire et al. 2010).

$$\psi_m(\theta) = \psi' \left(\frac{\theta}{\theta_s} \right)^{-b} \tag{4-1}$$

Log-transforming equation (1) we had,

$$\psi_m(\theta) = \exp\left[\ln\psi' + b\left(\ln\theta_s - \ln\theta \right) \right] \tag{4-2}$$

Splitting the curve derived from equation (2) into two sub-curves at field capacity we had,

$$\begin{aligned} \psi_m(\theta) &= \exp[\ln\psi_{fc} + b\left(\ln\theta_{v,fc} - \ln\theta \right)] (\text{if } \theta < \theta_{v,fc}) \\ &= \exp\left[\ln\psi' + b\left(\ln\theta_s - \ln\theta \right) \right] (\text{if } \theta \geq \theta_{v,fc}) \end{aligned} \tag{4-3a, b}$$

In equation 4-3(a, b) b was calculated as,

$$b = \frac{\ln\psi_{fc} - \ln\psi_{wp}}{\ln\theta_{v,fc} - \ln\theta_{v,wp}} (\text{if } \theta < \theta_{v,fc}) \\ = \frac{\ln\psi' - \ln\psi_{fc}}{\ln\theta_{s} - \ln\theta_{v,fc}} (\text{if } \theta \geq \theta_{v,fc}) \quad (4\text{-}4a, b)$$

Where, $\psi_m(\theta)$= soil water matric potential (-MPa) as a function of θ; θ=ambient soil moisture content ($m^3\ m^{-3}$); ψ'=soil water matric potential at air-entry/saturation (-MPa); θ_s=soil moisture content at saturation ($m^3\ m^{-3}$); b=dimensionless parameter representing influence of soil texture on slope of moisture retention curve; ψ_{fc} and $\theta_{v,fc}$=soil water potential (-MPa) and soil moisture content ($m^3\ m^{-3}$) at field capacity; ψ_{wp} and $\theta_{v,wp}$=soil water potential (-MPa) and soil moisture content ($m^3\ m^{-3}$) at wilting point.

This modification of Campbell model (Eqs. 4-3 to 4-4) enabled *ecosys* to take advantage of available measurements of field capacity and wilting point that have physical meanings. Total porosity of a grid cell is calculated from dry bulk density (ρ_b) input and is used as θ_s for that grid cell. ψ_{fc} and ψ_{wp} are user defined (ψ_{fc}=-0.01 MPa and ψ_{wp}=-1.5 MPa for peat soils) and $\theta_{v,fc}$ and $\theta_{v,wp}$ are model inputs based on site measurements.

Simulation of peat moisture desorption by the MCM in *ecosys* has been tested only against the measurements from peat soils with low near saturation moisture holding capacity (Dimitrov et al. 2010b) (Chapter 2). In those studies, the peat θ started dropping sharply right below ψ' and consequently were well modelled by the MCM in *ecosys*. However, MCM could underestimate θ of peats that retain high moisture near ψ' and rapidly drain below a threshold (i.e. air entry potential, ψ_e) (Fig. 4-1). The Van Genuchten model (VGM) (Van Genuchten 1980)

(Eqs. 4-5 and 4-6) can better model this type of retention by simulating higher θ near saturation, with sharp declines in θ when ψ_m declines below ψ_e (Fig. 4-1).

$$S_e = \frac{\theta - \theta_r}{\theta_s - \theta_r} \tag{4-5}$$

$$\psi_m(\theta) = \frac{\left(S_e^{-\frac{1}{m}} - 1\right)^{\frac{1}{n}}}{\alpha}; \text{where } m = 1 - 1/n \tag{4-6}$$

where, S_e=relative degree of saturation (Fig. 4-1); θ_r=residual soil moisture content (m^3 m^{-3}); n =van Genuchten parameter that describes the mean slope of the desorption curve or the range of pore size distribution; α= equivalent to the inverse of the pressure head at ψ_e (i.e. $\alpha \approx 1$/air entry potential) that governs the shape of desorption curve ($-MPa^{-1}$).

A higher value of α in VGM (Eq. 4-6) can simulate larger θ at a given ψ_m compared to MCM (Fig. 4-1). However, an accompanying higher n value would also simulate rapid pore drainage once the ψ_m falls below the ψ_e (Fig. 4-1). Values for the VGM parameters θ_r, n and α (Eqs. 4-5 and 4-6) are usually derived from inverse optimization by using least square method while fitting sets of measured θ and corresponding ψ_m (Van Genuchten et al. 1991). However, substitution of MCM with VGM in *ecosys* requires use of a simpler method for this parameter optimization to make use of the existing input structure of *ecosys* that only requires inputs for commonly measured soil physical and hydrologic parameters such as ρ_b to calculate θ_s, $\theta_{v,fc}$ and $\theta_{v,wp}$. This simple parameter optimization in VGM version of *ecosys* is thus performed by solving B8-B15 using a maximum of 19000 iterations up to the point at which the squares of the differences between observed and simulated $\theta_{v,fc}$, and $\theta_{v,wp}$ approaches $\leq 10^{-6}$. To obtain a unique set of the VGM parameters from a particular optimization, an additional input for ψ_{in} (B10) for each soil

layer is required (Fig. 4-1). This ψ_{in} represents the point of the sign inversion on the *S*-shaped semi-logarithmic VGM desorption curve and can be estimated from measured soil moisture retention curves (Fig. 4-1). The inputs for ψ_{in} would affect the values of α in VGM curves (B10) and thus would govern the extent of moisture retention close to saturation water potential. For instance, a lower ψ_{in} input would result in a higher α (B10) and a consequent lower ψ_e (since $\alpha \approx 1/\psi_e$) and hence a higher moisture retention at lower matric potentials and vice-versa (Fig. 4-1).

4-2.1.5. Snowpack and freezing-thawing

Snowpack hydrology and freeze-thaw dynamics of snowpack, surface residue and soil are integral parts of northern boreal peatland water balances. *Ecosys* simulates snowpack as a single layer. Depth of the snowpack is calculated by dividing bulk volume of snow, water and ice in the snowpack by the basal area of the snowpack (D5). The snow density (D5) increases over time with melting of snow to water and refreezing as ice (D6). The snowpack exchanges heat with the atmosphere (D1), residue and soil surface through conduction and vapor convection (D2, D4). Snowmelt water directly infiltrates into residue and soil surface and can run-off when the rate of snowmelt exceeds that of infiltration.

Freezing and thawing are calculated when snowpack, surface residue or a soil layer temperature falls below or rise above the freezing point of the snowpack, surface residue or that soil layer. Freezing point of the snowpack is considered the same as freezing point of free water while for each soil and residue layer it is calculated from freezing point depression equation using ψ_s (D3). The rate of freezing or thawing is calculated from a 3D general heat balance

equation governed by bulk heat capacity, vertical and lateral heat fluxes, and the difference between ambient and freezing temperature of each of snowpack, residue or soil layers (D2).

4-2.2. Modelling experiment

4-2.2.1. Study site

The eco-hydrology algorithms in *ecosys* are tested in this study against measurements of peat water content, WTD and ecosystem energy fluxes from 2003 to 2009 in a flux station of Fluxnet-Canada Research Network established at the WPL (latitude: 54.95°N, longitude: 112.47°W). The study site is a moderately nutrient rich treed fen peatland within the Central Mixed-wood Sub-region of Boreal Alberta, Canada. Peat depth around the flux station was about 2 m. This peatland is dominated by stunted trees of black spruce (*Picea mariana*) and tamarack (*Larix laricina*) with an average canopy height of 3 m. High abundance of a shrub species *Betula pumila* (dwarf birch), and the presence of a wide range of mosses e.g. *Sphagnum* spp., feather moss, and brown moss characterize the under-storey vegetation of WPL. The topographic, climatic, edaphic and vegetative characteristics of this site were described in more details by Syed et al. (2006).

4-2.2.2. Field data sets

Ecosys model inputs of half hourly weather variables i.e. incoming shortwave and longwave radiation, air temperature, wind speed, precipitation and relative humidity during 2003-2009 were measured at the micrometeorological station established at WPL (Syed et al. 2006). Ecosystem net radiation (R_n) was calculated by Syed et al. (2006) from measured incoming and outgoing shortwave and longwave radiation. Modelled outputs of hourly WTD and daily θ were tested against site measured WTD (with respect to average hummock surface) and θ (at 0.075, 0.1 and 0.125 m depths from hummock surface) to test adequacy of WTD and peat

moisture retention simulation in *ecosys* (Flanagan and Syed 2011). Since snowpack hydrology is an important component of WPL water balance, modelled outputs of hourly snowpack depth were also tested against measured snowpack depths. To examine how well *ecosys* simulated the surface energy exchange and hence vertical boundary water effluxes, hourly modelled latent heat (*LE*) and sensible heat (*H*) fluxes were tested against eddy covariance (EC) measurements of *LE* and *H* by Flanagan and Syed (2011) and Syed et al. (2006). Along with *LE* and *H* fluxes, net ecosystem CO_2 fluxes were also measured by using EC micro-meteorological approach in Flanagan and Syed (2011) and Syed et al. (2006). Erroneous EC *LE*, *H* and CO_2 measurements due to stable air condition were screened out by using a friction velocity (u^*) of 0.15 m s^{-1} (Syed et al. 2006). The resultant data gaps were filled by extrapolation of valid measurements using moving windows of 15 day periods (Wever et al. 2002, Syed et al. 2006). Net CO_2 fluxes partitioned into gross primary productivity (GPP) and ecosystem respiration (R_e) by using Fluxnet-Canada Research Network standard protocol except the application of an energy balance closure adjustment (Syed et al. 2006). More details about site measurements, screening, gap-filling and partitioning of EC fluxes can be found in Flanagan and Syed (2011), Syed et al. (2006), and Wever et al. (2002).

4-2.2.3. Model runs

One model run for each of the MCM and VGM versions of *ecosys* was set up. Each of these runs had a hummock and a hollow grid cell of 1m×1m which exchanged water, heat, carbon and nutrients (N, P) (Fig. 4-2). The hollow grid cell in each run had near surface peat layer that was 0.3 m thinner than the hummock cell representing a hummock-hollow surface difference of 0.3 m observed in the field (Long 2008a) (Fig. 4-2). Any depth with respect to the

modelled hollow surface would thus be 0.3 m shallower than the depth with respect to the modelled hummock surface.

Dry bulk density (ρ_b) input for each soil layer was obtained from empirical relationships between ρ_b and peat depth in Flanagan and Syed (2011) constructed from measurements at the WPL (Fig. 4-2). Input values for θ at field capacity ($\theta_{v,fc}$) and wilting point ($\theta_{v,wp}$) for each of the layers were derived from generalized empirical equations of $\theta_{v,fc}$ and $\theta_{v,wp}$ as functions of ρ_b developed by (1969, 1970), Päivänen (1973) and Szymanowski (1993) for northern boreal peatlands (Fig. 4-2). Input values for matric potential at inflection point (ψ_{in}) for the top 0.19 m of the VGM run were derived from moisture retention curves constructed by using θ measurements at corresponding depths of WPL and the height of those measurement depths above the water table (Fig. 4-2). ψ_{in} inputs for the remaining layers were derived from generalized moisture retention curves by Boelter (1969, 1970), Päivänen (1973) and Szymanowski (1993).

Due to the lack of pore-size distribution measurements in WPL, we could not use measured values for macropore volume fractions (θ_{mac}) in the model. Instead we used an analogy similar to that of Silins and Rothwell (1998) and Wösten et al. (2008) who calculated peat macroporosity as the fraction of total porosity drained at matric water potentials very close to saturation. This matric potential however, varied from -0.0004 to -0.004 MPa in those studies. We therefore assumed the fraction of total porosity drained at a water potential of -0.003 MPa as θ_{mac} for a particular layer and used those values as model inputs (Fig. 4-2). Higher moisture retention in the two layers 0.065-0.085 and 0.085-0.115 m compared to the layer below was indicated by soil moisture content measurements at depths corresponding to the mid-points of

those layers. This was accordingly represented in our model runs by higher inputs of ρ_b, $\theta_{v,fc}$, and $\theta_{v,wp}$ and lower inputs of θ_{mac} in those two layers compared to the layer below (Fig. 4-2).

Macropore saturated hydraulic conductivities in the model were calculated from the θ_{mac} inputs by using Hagen-Poiseuille's equation (B18-B22) (Dimitrov et al. 2010b). However, saturated hydraulic conductivities for the remaining soil matrices ($K_{s,mat}$) were given as model inputs (Fig. 4-2). Since the soil matrix in our modelling represented the fraction of bulk soil excluding macropores, we used $K_{s,mat}$ values measured by Boelter (1969) for well decomposed peat layers in a northern peatland. Lateral saturated hydraulic conductivity of the macropore and the soil matrix fraction of each layer were assumed to be equal to its macropore and soil matrix vertical saturated conductivity.

Both the VGM and the MCM model versions were run for a spin up period of 1961-2002 under repeating 7-year sequences of hourly weather data (solar radiation, air temperature, wind speed, humidity and precipitation) recorded at the site from 2003 to 2009. Since measurements of these weather variables at the site stopped at the end of September in 2009, we filled October-December weather sequence in 2009 by those measured for the same period in 2008 to complete the 7-year weather sequences in the spin up run. This spin up period allowed energy and CO_2 exchanges in the model to achieve stable values through successive weather sequences.

To accommodate effects of catchment hydrology on fen peatland WTD, we set the WTD_x at different levels based on the annual wetness of weather e.g. shallow WTD_x for wetter years, intermediate WTD_x for regular years, and deep WTD_x for drier years (Fig. 4-2). This scheme simulates larger hydraulic gradients between modelled WTD and the WTD_x for lateral recharge than discharge resulting in net lateral water gains in wetter years and net losses in drier years (Fig. 4-2). The WTD_x for the spin up runs was thus set at 0.19, 0.35, and 0.72 m below the

hummock surface (0.11 m above and 0.05 and 0.42 m below the hollow surface) following shallowest measured WTD in 2003-2005, average measured WTD in 2006-2007, and deepest measured WTD in 2008-2009 representing a gradual drying trend in overall watershed hydrology (Fig. 4-2). L_t was set to a fixed 100 m in all directions for all years (Fig. 4-2). The lower boundary condition in each of our model runs was defined such that there was no exchange of water to represent the presence of clay sediment with very low permeability underlying the peat (Syed et al. 2006) (Fig. 4-2).

At the beginning of the spin up run, the hummock grid cells were seeded with evergreen needle leaf and deciduous needle leaf over-storey plant functional types (PFT) to represent the black spruce and tamarack trees at the WPL. The modelled hollow grid cells were seeded only with the deciduous needle leaf over-storey PFT (to represent tamarack) since the black spruce at the site was found to grow only in the raised areas or hummocks. Each of the modelled hummock and the hollow was also seeded with a deciduous broadleaved vascular (to represent dwarf birch) and a non-vascular (to represent mosses) under-storey PFTs. These PFTs are the same as those in earlier studies with *ecosys* in northern boreal ecosystems (Grant et al. 2009a, Dimitrov et al. 2011, Grant et al. 2012b). The planting density was such that the population density of the evergreen needle leaf and the deciduous needle leaf PFT was 0.16 and 0.14 m^{-2} at the end of the spin up run after accounting for annual mortality, thereby representing the site measured population of the two dominant over-storey species during the study period (Syed et al. 2006). The under-storey deciduous broadleaved and the moss PFTs had population densities of 0.3 and 500 m^{-2} at the end of the spin up run. To include wetland adaptation, we selected a value of 0.1 for root porosity (θ_{pr}) used in calculating root O_2 transport through aerenchyma (H6) in the two over-storey PFTs. A higher θ_{pr} value of 0.3 for the under-storey vascular PFT was selected

to simulate better wetland adaptation in the under-storey vegetation at the WPL. We did not use any porosity for non-vascular moss rhizoids and hence did not simulate O_2 transport through mosses. These input values for vascular θ_{pr} fall within the range of root porosities (0.01-0.34) measured for various plants taken from northern temperate and boreal bogs, fens and reed swamps (Cronk and Fennessy 2001). θ_{pr} in wetland adapted species can also vary with intensity of waterlogging (Cronk and Fennessy 2001). However, current versions of *ecosys* used the set input for θ_{pr} to simulate O_2 transport from atmosphere to rhizosphere through roots which did not vary with intensity in waterlogging.

When the modelled ecosystem had attained dynamic energy and carbon equilibria at the end of the spin up run, we continued the spin up run from 2003 to 2009 for each of the MCM and VGM versions of *ecosys* by using a real-time weather sequence. We tested our outputs from 2004-2009 of the simulation runs against the available site measurements of peat water contents, WTD and energy exchange over those years.

4-2.2.4. Model validation

Daily measured soil water contents at 0.075, 0.1 and 0.125 m depths were used to corroborate daily modelled MCM and VGM soil water content outputs from the layers whose mid-points corresponded to the measurement depths. Hourly modelled WTD was first averaged 50:50 over the modelled hummock and the modelled hollow for both MCM and VGM runs and then tested against the hourly measured WTD. Comparative model performance of MCM vs. VGM was examined by comparing R^2, and RMSE from regressions of modelled on measured and measured on modelled soil water contents and WTDs (with respect to the hollow surface) respectively. A higher R^2 and a lower RMSE would mean a better performance in simulating peat moisture desorption and WTD. Since soil moisture content and WTD data do not always

follow a normal distribution, an additional analysis of comparative model performance was done based on an index of agreement (*d*) proposed for model performance comparison by (Willmott 1981, 1982) and Willmott and Wicks (1980) (Eq. 4-7).

$$d = 1 - \left[\frac{\sum_{i=1}^{n} (P_i - O_i)^2}{\sum_{i=1}^{n} (|P_i'| - |O_i'|)^2} \right];\ 0 \le d \le 1;\ P_i' = P_i - \overline{O};\ O_i' = O_i - \overline{O} \qquad (4\text{-}7)$$

Where, *n*=number of observations; *P*=predicted value; *O*=observed value; $\overline{O}$=mean of the observed values. The nearer the *d* value to 1 the better would be the model performance. The model that performs better between the two (MCM vs. VGM) based on the above mentioned modelled vs. measured statistics of soil water contents and WTD would be used for further analyses in the course of the study. The outputs from the remaining run would not be used any further in this paper.

Hourly R_n, *LE* and *H* fluxes modelled by the version selected from the above test were averaged 50:50 over the hummock and the hollow and then regressed on hourly measured EC fluxes. Model performance in simulating those energy fluxes was evaluated from regression intercepts ($a \rightarrow 0$), slopes ($b \rightarrow 1$) and coefficients of determination ($R^2 \rightarrow 1$).

4-2.2.5. Analyses of model results

Model performance in simulating effects of WT deepening on surface drying of the northern boreal peatland at WPL was evaluated by comparing modelled and measured Bowen ratios (β) (=*H*/*LE*). To examine the short-term effects on WTD drawdown on β, hourly modelled vs. half-hourly measured mid-day (2 hours before and after solar noon i.e. 1700-2100 local time) β was compared for 3 hydroperiods of 3 days each with gradually deeper WTD. These hydroperiods were chosen in mid-August of 2005, 2008 and 2009 on the basis of comparable

weather conditions i.e. R_n and vapor pressure deficit (D) in similar days and therefore distinguished from each other predominantly by the WTD. To further examine the consistency of the short-term effects of WTD drawdown on β over longer time scales, we also studied the effects of WTD drawdown on average β over late (mid-July to mid-August) and whole (May-August) growing seasons. Since atmospheric drivers like R_n and D can also affect β we therefore had to control for the effects of R_n and D in examining the net effects of WTD on β. To control for R_n effects on β, only the mid-day βs that were measured and modelled under clear sky condition i.e. incoming solar radiation >700 W m^{-2} were selected and averaged over the late and/or whole growing seasons. Effects of D on β were screened out by selecting three D classes for both late (e.g. D=0.8-1, 1-1.2 and 1.2-1.4 kPa) and the whole growing season (e.g. D=1-1.5, 1.5-2 and 2-2.5 kPa) and by studying WTD effects on average β in each of those three D classes. The consistency of WTD effects on β in each of those D classes would further ensure the consistency of WTD effects irrespective of the effects of D on late and/or whole growing season β. Those D classes were selected on the basis of the highest availability of measurements across D classes over the specified period (e.g. late or whole growing season) throughout 2004-2009.

In *ecosys* complete energy balance closure is achieved while solving for canopy, soil, residue and snow surface temperature (D1, E1) following energy and mass conservation theory, whereas in the EC measurements, ecosystem energy fluxes e.g. LE and H can be underestimated due to the lack of adequate convection and hence can yield incomplete energy balance closure (Wilson et al. 2002). This difference in energy balance closure between the modelled outputs and the EC measurements can also contribute to the divergence between modelled and measured WTD effects on β. To examine this divergence we compared modelled vs. EC measured energy balance closure for each year from 2004-2009. This energy balance closure was calculated as the

slope of regression of $H+LE$ on R_n-G (ground heat flux) for both modelled and EC measured (u^*>0.15 m s^{-1}) energy fluxes. Since, G was not measured in the field we assumed G as 10% of R_n as suggested by Kellner (2001).

Increases in GPP and ET across Canadian peatlands have been found to be closely associated with each other, i.e. increases in GPP were positively correlated to increases in ET (Brümmer et al. 2012). We thus compared modelled and measured water use efficiencies (WUEs) calculated from modelled and EC derived GPP and ET (Eq. 4-8) to further evaluate agreement or disagreement between modelled vs. measured ET.

$$\mathrm{WUE}_{\mathrm{modelled}}=\frac{\mathrm{GPP}_{\mathrm{modelled}}}{ET_{\mathrm{modelled}}};\mathrm{WUE}_{\mathrm{EC\text{-}gapfilled}}=\frac{\mathrm{GPP}_{\mathrm{partitioned}}}{ET_{\mathrm{EC\text{-}gap\ filled}}} \quad (4\text{-}8)$$

Where, $\mathrm{WUE}_{\mathrm{modelled}}$ and $\mathrm{WUE}_{\mathrm{EC\text{-}gap\ filled}}$=modelled and EC-gap filled WUE (g C kg^{-1} H_2O); $\mathrm{GPP}_{\mathrm{modelled}}$ and $\mathrm{GPP}_{\mathrm{partitioned}}$=modelled GPP and partitioned GPP derived from EC-gap filled net CO_2 fluxes (g C m^{-2} h^{-1}) (Syed et al. 2006); ET_{modelled} and $ET_{\mathrm{EC\text{-}gap\ filled}}$=$ET$ calculated from modelled and EC-gap filled LE fluxes (kg H_2O m^{-2} h^{-1}).

4-3. Results

4-3.1. Peat moisture retention simulation by van Genuchten model (VGM) vs. modified Campbell (MCM) model

The VGM version of *ecosys* better simulated peat θ at 0.075, 0.1 and 0.125 m depths from the hummock surface at the WPL than did the MCM version (Fig. 4-3a). This was apparent in higher average modelled vs. measured R^2 (Figs. 4-4d, g, j) and d (Figs. 4-4e, h, k), and lower average measured vs. modelled RMSE (root mean square for errors) by 0.05 m^3 m^{-3} (Figs. 4-4f, i, l) in the VGM than in the MCM simulation of θ at all depths in all years. Despite this large divergence in θ simulations, the two model versions simulated the measured WTD at WPL

almost equally well (Fig. 4-3b). This was apparent in very low differences in average modelled vs. measured R^2 (0.08) (Fig. 4-4a) and d (0.09) (Fig. 4-4b) and measured vs. modelled RMSE (<0.01 m^3 m^{-3}) (Fig. 4-4c) between the VGM and the MCM versions of *ecosys* for WTD in all years.

This improved simulation of peat θ by the VGM version of *ecosys* was achieved by computing higher moisture retention compared to the MCM version when θ was close to θ_s above the WT. For instance, VGM simulated θ at 0.075, 0.1 and 0.125 m depths from the hummock surface at the onset of springs in 2005-2007 which were very close to the measured θ and >0.5 m^3 m^{-3} higher than the MCM simulated θ at the same depths when both the modelled and measured WTD was within 0.1 m below the hollow surface (within 0.4 m below the hummock surface) (Fig. 4-3a). However, at the end of May in 2006, when WTD fell below 0.1 m from the hollow surface (below 0.4 m from the hummock surface), VGM simulated a gradual drop in θ at all 3 depths that corresponded well with the measurements (Figs. 4-3a, b). The drop in θ with the similar drop in WTD simulated by MCM occurred from a much lower initial θ and about a month earlier than the measured (Figs. 4-3a, b). During 2007 measured θ remained close to 0.7 m^3 m^{-3} until the end of June when WTD fell below 0.1 m from the hollow surface (Figs. 4-3a, b). This trend was well captured by VGM but was completely missed by MCM (Figs. 4-3a, b). Much earlier and more rapid drainage of peat pore in MCM during 2007 yielded more rapid discharge and hence deeper WTD compared to the measurements (Fig. 4-3b). This trend of greater modelled vs. measured WTD divergence in the MCM simulation also continued in 2008 and 2009 as apparent in lower MCM modelled vs. measured d compared to VGM (Fig. 4-4b).

Since substituting MCM with VGM in *ecosys* substantially improved θ simulation, we hereafter use the outputs from *ecosys* modelling by using VGM to test the rest of the hypotheses in this study.

4-3.2. Seasonal and interannual variations in modelled vs. measured WTD and θ

Seasonal and interannual variation in WTD measured at the WPL were modelled by *ecosys* from the balance between vertical and lateral water influxes (*P* and lateral recharge) and effluxes (*ET* and lateral discharge). During the growing season (May-August) of 2004, *P* frequently exceeded *ET* resulting in a modelled WT that remained above the hollow surface for most of the growing season (Figs. 4-5c and 4-6). This trend was also apparent in the site measured WTD and the cumulative difference between *P* and EC-gap filled *ET* (P-$ET_{\text{EC-gap filled}}$) (Figs. 4-5c and 4-6). The shallow WTD was sustained by a shallow WTD_x (=0.19 m) (Fig. 4-2) that created a hydraulic gradient that simulated net recharge during 2004 (Fig. 4-7c) which stabilized the modelled WTD at the shallowest position in 2004 compared to that of 2005-2009 (Figs. 4-5c, f, i, l, o, r and 4-7a). This shallow WTD also enabled *ecosys* to simulate higher near surface θ (>0.5 m^3 m^{-3}) at 0.075, 0.1 and 0.125 m depths below the hummock surface throughout the growing season of 2004 (Fig. 4-5b). Short term drops in *P* to *ET* ratio during late June-early July and late August resulted in a transient fall of modelled WTD below the hollow surface that was apparent in WTD measurements (Fig. 4-5c). This transient drop of WTD caused a short-term drop in near surface modelled θ (Fig. 4-5a).

The WTD_x (= 0.19 m) in 2005 was set the same as that in 2004 (Fig. 4-2). However, a lower *P* and a consequently lower *P* to *ET* ratio during the growing season of 2005 caused *ecosys* to simulate a deeper growing season WTD than in 2004 (Figs. 4-5f, 4-6 and 4-7a, b). This trend

was also apparent in WTD measurements and the cumulative P-$ET_{\text{EC-gap filled}}$ at the WPL (Figs. 4-5f, 4-6 and 4-7a). A deeper modelled WTD with respect to WTD_x in 2005 than in 2004 caused a larger hydraulic gradient that simulated more rapid lateral recharge in 2005 than in 2004 (Figs. 4-2, 4-5f and 4-7c). This more rapid lateral recharge in 2005 caused WTD to remain less than 0.1 m below the hollow surface which enabled the modelled near surface peats to retain high θ that was well corroborated by the measurements (Fig. 4-5e).

The WTD_x in 2006 (= 0.35 m) was deeper than that in 2005 and 2004 (= 0.19 m) (Fig. 4-2) which created a smaller hydraulic gradient between modelled WTD and WTD_x in 2006 that generated less recharge (Figs. 4-5i and 4-7a). Less recharge along with declining P to ET ratio caused a gradual drawdown of WTD from early June to August in 2006 that in turn caused modelled θ to gradually fall from ~0.7 to ~0.45 $m^3\ m^{-3}$at 0.1 m depth and from ~0.7 to 0.3 $m^3\ m^{-3}$ at 0.075 and 0.125 m depths (Fig. 4-5h). This modelled trend of gradual WTD drawdown and the declines in near surface θ due to reduction in P to ET ratio was also apparent in WTD, θ and P-$ET_{\text{EC-gap filled}}$ measured at the WPL (Figs. 4-5i, 4-6 and 4-7c). Smaller P to ET ratio along with less recharge during the growing season of 2006 stabilized modelled WTD in the growing season of 2006 at a deeper position than in 2005 (Figs. 4-5i, 4-6 and 4-7a, b, c).

The WTD_x (= 0.35 m) in 2007 was the same as that in 2006 (Fig. 4-2). However, P in excess of ET during May 2007 caused modelled WTD to rise above WTD_x creating a hydraulic gradient which generated lateral discharge and eventually stabilized modelled WTD at a position where the residual between P and ET equilibrated with the discharge (Figs. 4-2, 4-5l, 4-6 and 4-7c). This early growing season discharge in 2007, however, ceased by the end of May when ET exceeded P and the modelled WTD gradually receded thereafter and consequently WTD fell below WTD_x causing a hydraulic gradient that simulated lateral recharge (Fig. 4-2, 4-5l and 4-

7c). This gradual decline in modelled WTD also caused a gradual decline in near surface θ from late May to the end of the year (Figs. 4-5l, 4-6 and 4-7a, c). This gradual decline in WTD and hence near surface θ in 2007 was similar to that in 2006 but unlike in 2006 it did not start until late June in 2007 due to higher May-June precipitation in 2007 than in 2006 (Figs. 4-5g, h, i in 2006 vs. 4-5j, k, l in 2007). This modelled interannual variation between 2006 and 2007 in declines of WTD and θ was also well corroborated by site measurements (Fig. 4-5).

The WTD_x in 2008 (= 0.72 m) was deeper than that in 2007 (= 0.35 m) (Fig. 4-2). This was deeper than the modelled WTD during April-June in 2008 and generated a hydraulic gradient that drove a larger lateral discharge than in 2007 (Figs. 4-2, 4-5o and 4-7c). This lateral discharge caused a gradual drawdown of WTD from late-May to July in 2008 which in turn caused a gradual decline in near surface θ (Fig. 4-5n).This lateral discharge, however, ceased as growing season progressed (Fig. 4-7c). Larger lateral discharge and lower P to ET ratio stabilized the modelled WTD at a deeper position in the growing season of 2008 than in 2007 (Figs. 4-5o, 4-6 and 4-7a, c). A large rainfall event in mid-August caused the near surface θ to increase by almost two-fold which was reasonably well modelled by *ecosys* (Fig. 4-5n). This rainfall event also caused a rise in both modelled and measured WTs (Fig. 4-5o). Although the modelled seasonal trend in WTD and θ in 2008 was well corroborated by the measured WTD and θ, cumulative $P\text{-}ET_{\text{EC-gap filled}}$ diverged from the cumulative difference between P and modelled ET ($P\text{-}ET_{\text{sim}}$) (Figs. 4-5o, 4-6 and 4-7a).

The WTD_x (= 0.72 m) in 2009 was same as in 2008 (Fig. 4-2). During the early growing season (April-May) in 2009, a modelled WTD was less than WTD_x causing a hydraulic gradient that drove lateral discharge (Fig. 4-7c). This lateral water loss through discharge caused *ecosys* to

simulate the lowest early growing season near-surface θ during 2009 as measured at the WPL (Figs. 4-5p, q and 4-7b). This lateral discharge in the model, however, ceased when modelled WTD fell below the WTD_x as dry season progressed and then the resultant hydraulic gradient drove lateral recharge (Figs. 4-2, 4-5r and 4-7c). Besides, further reduction in *P* and a consequent reduction in *P* to *ET* ratio during the growing season of 2009 caused the modelled WTD to stabilize at a deeper position than in 2008 where the difference between *ET* and *P* was in equilibrium with the lateral recharge (Figs. 4-5r, 4-6 and 4-7a). This modelled trend was well corroborated by the measured growing season WTD in 2009 vs. 2008 at the WPL (Figs. 4-5r, 4-7a). However, like in 2008, $P\text{-}ET_{sim}$ in 2009 also significantly diverged from $P\text{-}ET_{EC\text{-}gap\ filled}$ (Fig. 4-6).

4-3.3. Sensitivity of modelled WTD to lateral boundary condition

The rates of the lateral water exchange in *ecosys* were largely affected by the hydraulic gradients between the modelled WTD and the WTD_x (B23). The inputs of WTD_x in the model thus affected the rates of modelled lateral water exchange and hence the seasonal and interannual variations in modelled WTD. To test the adequacy of these WTD_x inputs in the current simulation, we performed three other runs by inputting constant WTD_x of 0.19, 0.35 and 0.72 m from the hummock surface for all years instead of using these WTD_x in different years as in the current run. A constant WTD_x of 0.19 m created hydraulic gradients that generated larger lateral recharge and smaller lateral discharge than the current simulation and hence modelled shallower WTD than measured for the growing seasons of 2006 to 2009. A constant WTD_x of 0.35 m simulated less recharge than the current simulation in 2004 and 2005 and hence modelled deeper WTD than the measured in those years. This also simulated smaller discharge and larger recharge than the current simulation in 2008 and 2009 and hence modelled shallower WTD than

the measured for the growing seasons in those years. A constant WTD_x of 0.72 m simulated greater lateral discharge and hence modelled deeper WTD than the measured for the growing seasons of 2004 to 2007. Thus accurate modelling of WTD required changes in WTD_x during the model run.

Like WTD_x, inputs for L_t also governed the rates of lateral water recharge and discharge and hence the variations in modelled WTD. To test the adequacy of the input for L_t in our current simulation, we performed two other runs by inputting 10 m and 200 m in all directions instead of 100 m in the current simulation run leaving everything else unchanged. L_t = 10 m in all directions simulated faster lateral discharge/recharge than the current model run and hence smaller seasonal fluctuations in WTD than measured. L_t = 200 m simulated slower lateral discharge/recharge than the current model run and hence larger seasonal fluctuations in WTD than measured. Therefore, these sensitivity tests suggested that, for the given input of saturated hydraulic conductivity of each peat layer, the lateral boundary condition defined by the combination of inputs for WTD_x (0.19 m for 2004-2005, 0.35 m for 2006-2007 and 0.72 m for 2008-2009) and L_t (100 m in all directions) in our current simulation best simulated the balance between lateral recharge and discharge and hence the seasonal and interannual variations in WTD as measured at the WPL.

4-3.4. Modelled vs. measured snowpack and freeze-thaw

The depth and the timing of snowpack accumulation and soil freezing-thawing were also important components of hydrology in seasonally frozen peats at the WPL. Measured snowpack depth throughout the winter, timing of snowmelt during the spring, and the initiation of the snowpack accumulation at the onset of winter were well simulated by *ecosys* throughout the study period (Figs. 4-5a, d, g, j, m, p). However, the modelled snowpack depth was about 0.1 m

thicker than the measured during January-March of 2005-2009 (Figs. 4-5a, d, g, j, m, p). Consequently the disappearance of the snowpack in the model was on an average 10 days later than that measured (Figs. 4-5a, d, g, j, m, p). The timing and rates of thawing in near surface peats was also well modelled by *ecosys* as corroborated by measured θ during thawing periods of 2006, 2008 and 2009 (Figs. 4-5g, n, q).

4-3.5. Modelled vs. measured ecosystem energy fluxes

Ecosystem energy fluxes (R_n, *LE* and *H*) control vertical water exchange between the ecosystem and the atmosphere. Agreement between modelled and measured energy fluxes thus indicated the adequate simulation of drying effects on *ET* as WT recedes. *Ecosys* reasonably well simulated the diurnal and seasonal variations in ecosystem surface energy fluxes. Regressions of hourly modelled vs. measured R_n, *LE* and *H* gave intercepts within 20 W m^{-2} of zero, and slopes within 0.1 of one, indicating minimal bias in modelled values for all years of the study except 2008 and 2009 when *LE* was overestimated (Table 4-1). Larger values for R^2 (> 0.8) and smaller values for RMSEs (~20 W m^{-2}) further indicated that *ecosys* well simulated the diurnal and seasonal variations in energy fluxes at the WPL (Table 4-1). Much of the unexplained variance in EC *LE* and *H* could be attributed to a random error of *ca.* 20% in EC methodology (Wesely and Hart 1985). This attribution was corroborated by root mean squares for random error (RMSRE) in EC measurements over forests calculated from Richardson et al. (2006) that were similar to RMSE, indicating that further constraint in model testing could not be achieved without further precision in EC measurements. Modelled vs. measured ecosystem energy flux divergence may also have been affected by incomplete energy balance closures of about 75% in the EC measurements for 2004-2007 and about 65% for 2008-2009 as opposed to complete energy balance closure in the model (Table 4-1).

4-3.6. Seasonal variation in modelled vs. measured surface energy exchange

The WPL ecosystem experienced strong seasonality in temperature and radiation that affected the seasonality in surface energy exchange. EC-gap filled daily *ET* gradually rose from the onset of the spring till the end of summer with the increase in temperature and hence vapor pressure deficit (*D*) and R_n before it gradually started falling off in the fall with declining *D* and R_n from 2004-2009 (Fig. 4-8). *Ecosys* simulated this seasonality in *ET* reasonably well as suggested by modelled vs. EC-gap filled daily *ET* from 2004-2009 (Fig. 4-8). This seasonality in *ecosys* was modelled by adequately simulating (1) *D* from the inputs of air temperature and humidity and (2) R_n (Figs. 4-8b, e, h, k, n, q) from the inputs of incoming solar radiation and by calculating comparative radiation interception, absorption and reflection by and from vegetation and peat surface. R_n at the vegetation surface was simulated from adequate modelling of seasonality in leaf area index (LAI) for the evergreen and the deciduous PFTs. This simulation was further corroborated by reasonable agreement between modelled vs. measured peak LAI during July 2004, the only year in which measurements were carried out. Modelled peak LAI of 2.43 m^2 m^{-2} for all the three vascular PFTs and 1.04 m^2 m^{-2} for the non-vascular (moss) PFT were comparable with 1.76 m^2 m^{-2} for the trees, shrubs and herbs, and 0.85 m^2 m^{-2} for the mosses measured optically by Syed et al. (2006) at the WPL.

Although *ecosys* reasonably well simulated the diurnal and seasonal variations in EC-gap filled *ET* throughout 2004-2007, it overestimated daily *ET* during May-June of 2008 and 2009 (Figs. 4-8g-r). This was also apparent in larger modelled vs. measured hourly *LE* flux regression slopes (Table 4-1) as well as larger divergence between $P\text{-}ET_{\text{Ec-gap filled}}$ and $P\text{-}ET_{\text{sim}}$ (Fig. 4-6) during 2008-2009 compared to other years.

4-3.7. Modelled vs. measured effects of interannual variations in WTD on surface energy exchange

Beside the seasonal variation in surface energy exchange as affected by seasonality in R_n and D, the interannual variation in surface energy balance at the WPL was also affected by that in the WTD. Shallow WTD (less than 0.1 m below the hollow surface) during the 3-day period in mid-August (Sect. 4-2.2.5) of 2005 caused greater LE than H fluxes as also apparent from diurnal EC flux measurements (Figs. 4-9 and 4-10a). WTD drawdown to about 0.32 m below the hollow surface during the similar period with comparable weather conditions (in terms of R_n and D) in 2008 caused a reduction in EC-measured LE fluxes with respect to H fluxes (Figs. 4-9 and 4-10a). Further recession of WTD to about 0.38 m in the same period of 2009 with comparable R_n and D further reduced EC-measured LE with respect to H fluxes thus yielding a surface energy balance dominated by H fluxes (Figs. 4-9 and 4-10a). This shift of surface energy balance from LE-dominated in 2005 to H-dominated in 2009 under comparable R_n and D indicated ecosystem surface drying with a deepening of WTD from about 0.1 to 0.4 m below the hollow surface (Figs. 4-9 and 4-10a). This was corroborated by increases in EC-gap filled mid-day (2 hours before and after solar noon) β from about 0.5 in 2005 to above 1 in 2009 which was well simulated by *ecosys* (Figs. 4-9 and 4-10a). This ecosystem dryness in *ecosys* was modelled predominantly by reductions in moss canopy water potentials (ψ_c) (Fig. 4-10c) that reduced evaporation (E) from mosses. *Ecosys* also simulated a smaller reduction in vascular ψ_c during deeper WTD periods of 2008 and 2009, but not enough to cause a decline in mid-day canopy g_c and hence T from the vascular canopies (Fig. 4-10b).

These WTD effects on surface energy balance also contributed to a WTD threshold effect on interannual variations in late growing season (mid-July to mid-August) surface energy

exchange. A sharp reduction in EC-gap filled *ET* and a concurrent shift in EC-gap filled mid-day β under clear sky condition (shortwave radiation >700 Wm^{-2}) (Sect. 4-2.2.5) from below to above unity (Fig. 4-11b) from late growing season of 2007 to that of 2008 and 2009 (Fig. 4-11a) was caused when the WTD fell more than ~0.35 m below the hollow surface (Fig. 4-11c). However, β in drier growing seasons can also increase with increasing *D*. But the shift in mid-day β from below to above 1 with WTD drawdown from the late growing seasons of 2007 to 2008 and 2009 was consistent for a given *D* as indicated by WTD effects on β across three *D* classes (Fig. 4-11b) (Sect. 4-2.2.5). *Ecosys* well simulated this late growing season threshold WTD effects on *ET* and β (Figs. 4-11a, b, c). However, a similar WTD threshold effect on β was also apparent in EC-gap filled *ET* and β during the whole growing season (May-August) which was not simulated by *ecosys* (Figs. 4-11d, e). Though *ecosys* well simulated a gradual drawdown of WTD from the growing season of 2004 to that of 2009, it missed the sharp reduction in EC-gap filled *ET* and a concurrent increase in mid-day β from the growing season of 2007 to that of 2008 (Figs. 4-11d, e, f). *Ecosys*, however, simulated a reduction in *ET* and a concurrent increase in mid-day β with further WTD increase in the growing season of 2009 (Figs. 4-11d, e, f). This divergence between modelled and EC-gap filled whole growing season *ET* and β was mainly caused by the deviation between modelled and EC-gap filled *LE* fluxes during May-June of 2008 and 2009 (Figs. 4-8m, p) (Table 4-1).

4-4. Discussion

4-4.1. Modelling peat moisture retention by van Genuchten model (VGM) vs. modified Campbell model (MCM)

The VGM moisture desorption function (Eqs. 4-5 and 4-6) better simulated water retention at ψ_m near saturation than did the MCM (Eqs. 4-3 and 4-4) due to its use of sigmoidal

moisture retention curves that retain higher θ near ψ_m (Fig. 4-1). This ability in VGM was imparted by the shape parameter α (Eq. 4-6) that was absent in the MCM (Eq. 4-4) (Fig. 4-1). Moreover, different combinations of the slope parameter n and the shape parameter α that arise from the differences in ρ_b and hence θ_s, $\theta_{v,fc}$ and $\theta_{v,wp}$ enabled VGM to simulate differential soil moisture desorption at different peat depths that was not well simulated by MCM (Figs. 4-1, 4-2 and 4-3b). For instance, a smaller n and a larger α for the layer at 0.085-0.115 m depth compared to those for the layers at 0.065-0.085 and 0.115-0.135 m depths in VGM represented higher moisture retention in the former layer and consequently simulated more gradual moisture desorption in that layer with increasing WTD than in the latter layers (Figs. 4-1 and 4-2). This enabled the VGM version of *ecosys* to simulate more gradual pore drainage and consequent higher θ at 0.1 m than at 0.075 and 0.125 m. This trend was also corroborated by the higher θ measured at 0.1 m depth than at 0.075 and 0.125 m depths of a hummock at the WPL (Fig. 4-3b). This suggests that the VGM is a better model of water retention in peats than is MCM, but at the cost of two additional parameters that require fitting to observations of water desorption.

Peats at 0.075, 0.1 and 0.125 m were not saturated even when observed θ at those layers remained consistently high (>0.65 m^3 m^{-3}) during most of 2005 and April-June of 2007 (Figs. 4-3a and 4-4e, k). This lack of saturation was modelled by adequately simulating rapid infiltration through macropores (B18-B22) thus indicating significance of preferential flow in modelling northern peatland moisture retention.

4-4.2. Modelling WTD variations in a boreal fen

Decreasing vertical water influx (*P*) vs. efflux (*ET*) along with decreasing lateral water influx (recharge) and increasing lateral water efflux (discharge) enabled *ecosys* to simulate the

gradual WTD drawdown from 2004 to 2009 that was measured at the WPL (Figs. 4-6 and 4-7). Lateral water gain from upland ecosystems during the wetter years is typical for fen hydrology and was also observed by Flanagan and Syed (2011) at the WPL site. We did not have any direct hourly or daily site measurements of lateral inflow or outflow of water to corroborate the simulated recharge or discharge. However, reasonably accurate simulation of changes in soil water storage (ΔWTD and $\Delta\theta$) and vertical water transfer (ET) indicated adequate simulation of lateral inflow/outflow of water at the WPL.

4-4.3. Modelling WTD threshold effects on surface energy exchange

A WTD threshold effect on late growing season (mid-July to mid-August) surface energy exchange was apparent in EC measurements at the WPL. When WTD fell below ~0.35 m from the hollow surface (below 0.65 m from the hummock surface), EC-gap filled surface energy balance shifted from LE to H flux dominated and concurrently mid-day EC-gap filled β rose from below to above unity (Figs. 4-9, 4-10a and 4-11a, b, c). *Ecosys* successfully simulated this WTD threshold effect on interannual variations in late growing season surface energy exchange by simulating different patterns of vertical rooting and water uptake between vascular (trees and shrubs) and non-vascular (moss) vegetation. Root growth in *ecosys* was simulated for individual plant which was then scaled to the population. Moss population were larger (Sect. 4-2.2.3) and hence intra-specific competition was greater so that individual moss plants and hence the downward growth of rhizoid were smaller (G9). This resulted in a shallow modelled moss rhizoid depth of 0.115 m below the hummock surface and 0.05 m below the hollow surface. Reduced availability of $[O_{2s}]$ in deeper wet peat layers and lack of O_2 transport through aerenchyma further limited simulated moss rhizoid growth to near surface peat layers (G9). When WTD fell below ~0.35 m from the hollow surface (~0.65 m from the hummock surface),

the near surface peats drained from the VGM desorption curve in Fig. 4-1, thereby decreasing θ, ψ_m (Eq. 4-6) and hence ψ_s, soil matrix hydraulic conductivity (K_{mat}) (B16) and increasing soil hydraulic resistance (Ω_s) (F3) in those layers. Reduced K_{mat} hindered recharge of those layers through capillary rise (B2-B5) from the WT below thereby further reducing ψ_s and increasing Ω_s in those layers. Reductions in ψ_s combined with increase in Ω_s thus reduced rhizoid U_w (F2) that forced a reduction in moss canopy water potential (ψ_c) (Fig. 4-10c) and hence E from moss surface while equilibrating rhizoid U_w with moss E (F6).

Unlike the moss PFT, the three vascular PFTs in *ecosys* could grow their roots into the wet deeper peat layers immediately above the WT. Deeper rooting in those vascular PFTs was simulated from enhanced root mass growth and elongation (G8-G9) facilitated by greater root growth respiration (G4-G5, G7) that was modelled from a combination of less intra-specific competition within lower populations (G9) and by improved root O_2 status ($[O_{2r}]$) in the deeper wet layers from O_2 transport through aerenchyma facilitated by root porosity (θ_{pr}) inputs of 0.1 and 0.3 (G3-G5, G7, G9) (Sect. 4-2.2.3). The near surface peat drying under WTD below ~0.35 from the hollow surface (~0.65 m from the hummock surface) also increased vascular root Ω_r and Ω_a and hence reduced vascular U_w from those layers (F2, F4-F5) as for mosses. However, deeper rooting enabled *ecosys* to simulate root U_w from those deeper layers with high θ and ψ_s and low Ω_s, Ω_r, and Ω_a (F2-F5) that offset the reduction in near surface root U_w. This offset enabled negligible reductions in vascular ψ_c and canopy g_c (Fig. 4-10) and hence sustained vascular T when WTD was deeper than ~0.35 from the hollow surface (~0.65 m from the hummock surface). However, this sustained vascular T could not offset the suppression of moss E when WTD fell below this threshold level of ~0.35 from the hollow surface (~0.65 m from the

hummock surface). This caused a reduction in modelled late growing season *ET* thereby shifting the modelled energy balance from *LE* to *H* flux dominated that was well corroborated by late growing season EC measurements at the WPL (Figs. 4-9, 4-10a and 4-11a, b, c).

Lafleur et al. (2005) found a similar WTD threshold effect on *ET* in a boreal bog peatland at Mer Bleue bog, Canada. In this study, a reduction in *ET* was observed when WTD fell below ~0.65 m from the hummock surface. This WTD threshold effect on *ET* and hence GPP over that site was also modelled by Dimitrov et al. (2011) using the same model *ecosys* as in our study. Similar threshold type effects of WTD on *ET* and hence GPP were also measured over northern boreal fen peatlands in Saskatchewan, Canada and northern Sweden by Sonnentag et al. (2010) and Peichl et al. (2014) respectively. However, the WTD threshold below which they found reductions of g_c, *ET* and hence GPP was much shallower than that of the Canadian fen peatland in this study (i.e. ~0.4 and ~0.3 m for the Canadian and the Swedish fen). Findings from all of those studies suggested that this WTD threshold effect on *ET* and hence GPP was mediated by (1) reductions in moss *E* when capillary rise from the deeper WT was inadequate to support moss canopy water potentials, and/or (2) reductions in vascular g_c when WTD fell beyond the maximum vascular rooting depth. The threshold WTD for reductions in *ET* and hence GPP across those peatlands thus varied depending upon the maximum depth at which capillary rise could support moss water transport as well as the maximum rooting depths of vascular plant communities. The maximum height of capillary rise is again controlled by the peat soil moisture retention properties thereby yielding greater capillary rise from deeper WT in peats with high rather than low moisture holding capacity.

4-4.4. Divergence between modelled vs. measured growing season energy exchange

Although *ecosys* successfully simulated late growing season (mid-July to mid-August) reduction in *ET* and concurrent rise in mid-day β when WTD fell below a threshold value of ~0.35 m from the hollow surface (~0.65 m from the hummock surface), it could not simulate the large drop in growing season (May-August) *ET* and a concurrent rise in β from 2007 to 2008 and 2009 with a similar drop of growing season WTD below the threshold (Figs. 4-8 and 4-11). This modelled overestimation of *ET* in 2008 and 2009 was also apparent in larger slopes from modelled vs. EC measured hourly *LE* fluxes compared to other years (Table 4-1). This overestimation of *ET* was mainly contributed by larger modelled vs. measured *ET* during May-June in 2008 and 2009 compared to other years (Figs. 4-8m, p). A slightly higher *D* (Table 4-2) and R_n (Figs. 4-8k, l, n, o) during June 2007 and 2008 suggested that the potential *ET* would be greater in June 2008 than in June 2007. Consequently the modelled actual *ET* was larger in June 2008 than in June 2007, but the EC-gap filled actual *ET* in June 2008 was about 45% less than that in June 2007 (Fig. 4-8). Modelled near surface θ (>0.3 m^3 m^{-3} at 0.075 m depth from the hummock surface) (Fig. 4-5n) and shallow WTD (within 0.2 m below the hollow surface) (Fig. 4-5o) were well corroborated by measured θ and WTD, and provided adequate moisture to sustain larger modelled *ET* during June 2008. Moreover, smaller EC-gap filled June *ET* in 2008 than in 2007 was not associated with a decreased EC-derived GPP. This caused a great difference in EC-derived WUE (=GPP/*ET*) between these two periods whereas the modelled WUE was almost the same (Table 4-2). GPP to *T* ratio for a vascular species (Larcher 2003) or GPP to *E* ratio for a moss species (Williams and Flanagan 1996) is normally stable for a given range of *D*. Brümmer et al. (2012) showed that a reduction or an increase in EC-derived GPP was associated with a commensurate increase or decrease in EC-gap filled *ET* over WPL during

2003-2006 thereby yielding a consistent WUE (GPP/*ET* = ~3 g C kg^{-1} H_2O). As in those studies, an increase in our modelled growing season (May-August) GPP by 32 g C m^{-2} from 2007 to 2008 was also associated with an increase in modelled growing season *ET* by 6 mm (Fig. 4-11a). On the contrary, an increase in EC-derived growing season GPP by 54 g C m^{-2} from 2007 to 2008 was associated with a substantial decrease in EC-gap filled growing season *ET* by 68 mm (Fig. 4-11a).

4-5. Conclusions

Our first objective was to examine whether *ecosys* could better simulate peat moisture retention in a northern boreal fen peatland when MCM was replaced by VGM. Our results showed that the higher near saturation peat moisture retention can be better modelled by using the VGM desorption function that simulates sigmoidal (*S*-shape) moisture retention curves (Figs. 4-1 and 4-3). We also examined whether the lateral boundary condition in a site scale simulation in *ecosys* as defined by a specified external WTD (WTD_x) to some distance (L_t) can simulate lateral inflow and/or outflow of water and hence seasonal and interannual variations in a northern boreal fen WTD. Our results showed that hydraulically driven lateral water transfer using Darcian flow with the specified WTD_x and L_t could reasonably well simulate the seasonal and interannual variations in WTD at the WPL as long as WTD_x was adjusted to represent larger watershed scale effects of fen hydrology (Figs. 4-5 and 4-7). Lastly we examined whether *ecosys* could simulate and hence explain the ecosystem drying as manifested by changes in surface energy exchange with WTD drawdown in a boreal fen. Differential vascular vs. non-vascular rooting profiles enabled *ecosys* to simulate a reduction in late growing season (mid-July to mid-August) *ET* and a concurrent rise in β that was measured at the WPL indicating ecosystem drying when WTD fell below a threshold (~0.35 m below the hollow or ~0.65 m below the hummock

surface) (Fig. 4-11). However, our modelling could not explain a large decline in growing season (May-August) ET and a concurrent rise in β from 2007 to 2008 as a similar WTD threshold effect (Fig. 4-11) (Table 4-2).

The algorithms used to simulate these eco-hydrological interactions in this boreal fen represented fundamental soil physical and biological processes that were derived from basic independent research. Hence these processes would be replicable across other fen peatlands if informed by site-specific eco-hydrological inputs (Fig. 4-2) (Sect. 4-2.2.3). Such modelling can also be scaled up with regional, continental or global level inputs of those parameters. Since hydrology largely governs the balance between peat production and decomposition and hence between peat aggradation and degradation, these eco-hydrological process level modelling would thus be important to predict hydrological effects on boreal fen peatlands' carbon balance. The insights and the improved predictive capacity of simulating eco-hydrological interactions in fen peatlands could therefore be used to predict how those peatlands would behave under future warmer and drier climates.

Table 4-1: Statistics from modelled vs. measured regressions of ecosystem energy fluxes at a Western Canadian fen peatland

Year	2004	2005	2006	2007	2008	2009
Modelled vs. observed ecosystem net radiation (R_n)						
n	8704	8752	8758	8752	8758	6872
a	10	10	8	10	8	10
b	0.97	0.96	0.96	0.95	0.95	0.96
R^2	0.99	0.99	0.99	0.99	0.99	0.99
RMSE (Wm^{-2})	10	15	17	17	17	19
Modelled vs. eddy covariance (EC) measured ($u^* > 0.15$ m s^{-1}) ecosystem latent heat fluxes (*LE*)						
n	7142	5983	6033	6075	6789	3886
a	-3	-2	-3	-4	-2	-2
b	1.06	1.05	1.06	1.04	1.46	1.41
R^2	0.92	0.9	0.9	0.86	0.90	0.91
RMSE (Wm^{-2})	14	18	20	23	14	13
RMSRE (Wm^{-2})	14	14	15	15	12	12
Modelled vs. EC measured ($u^* > 0.15$ m s^{-1}) ecosystem sensible heat fluxes (*H*)						
n	7143	5978	6031	6026	6135	3686
a	-11	-16	-14	-17	-14	-11
b	1.17	1.17	1.10	1.19	1.23	1.21
R^2	0.85	0.85	0.82	0.82	0.81	0.84
RMSE (Wm^{-2})	25	29	31	29	31	31
RMSRE (Wm^{-2})	12	12	12	12	12	12
Energy balance closure [slopes of regressions of *H*+*LE* fluxes over R_n-*G* (ground heat flux)]						
EC-gap filled	0.77	0.77	0.78	0.75	0.66	0.64
Modelled	1.00	1.00	1.00	1.00	1.00	1.00

(*a, b*) from simple linear regressions of modelled on measured. R^2 = coefficient of determination and RMSE = root mean square for errors from simple linear regressions of measured on simulated. RMSRE= root mean square for random errors in EC measurements calculated by inputting EC *LE* and *H* fluxes recorded at u^* (friction velocity) > 0.15 m s^{-1} into algorithms for estimation of random errors in EC *LE* and *H* measurements developed for forests by Richardson et al. (2006). Since *G* was not measured, we assumed *G* as 10% of R_n in calculating energy balance closure (Kellner 2001) (Sect. 4-2.2.5).

Table 4-2: Average eddy covariance (EC)-gap filled and modelled water use efficiency (WUE), vapor pressure deficit (D), air temperature (T_a), relative humidity (RH) and energy balance closure between June 2007 and June 2008 at a Western Canadian peatland

Year		June 2007	June 2008
WUE (g C kg^{-1} H_2O)	EC-gap filled	3.82±0.08	6.71±0.13
	Modelled	4.17±0.07	4.69±0.09
D (kPa)	Observed	0.87±0.02	0.99±0.02
T_a (°C)	Observed	16.37±0.12	17.61±0.12
RH (%)	Observed	59±1	57±1
Energy balance closure	EC-gap filled	0.73	0.66
	Modelled	1.00	1.00

WUE were calculated from the ratio of gross primary productivity (GPP) and evapotranspiration (ET). Details of both WUE and energy balance closure calculations are in Sect. 4-2.2.5. ± standard error of mean.

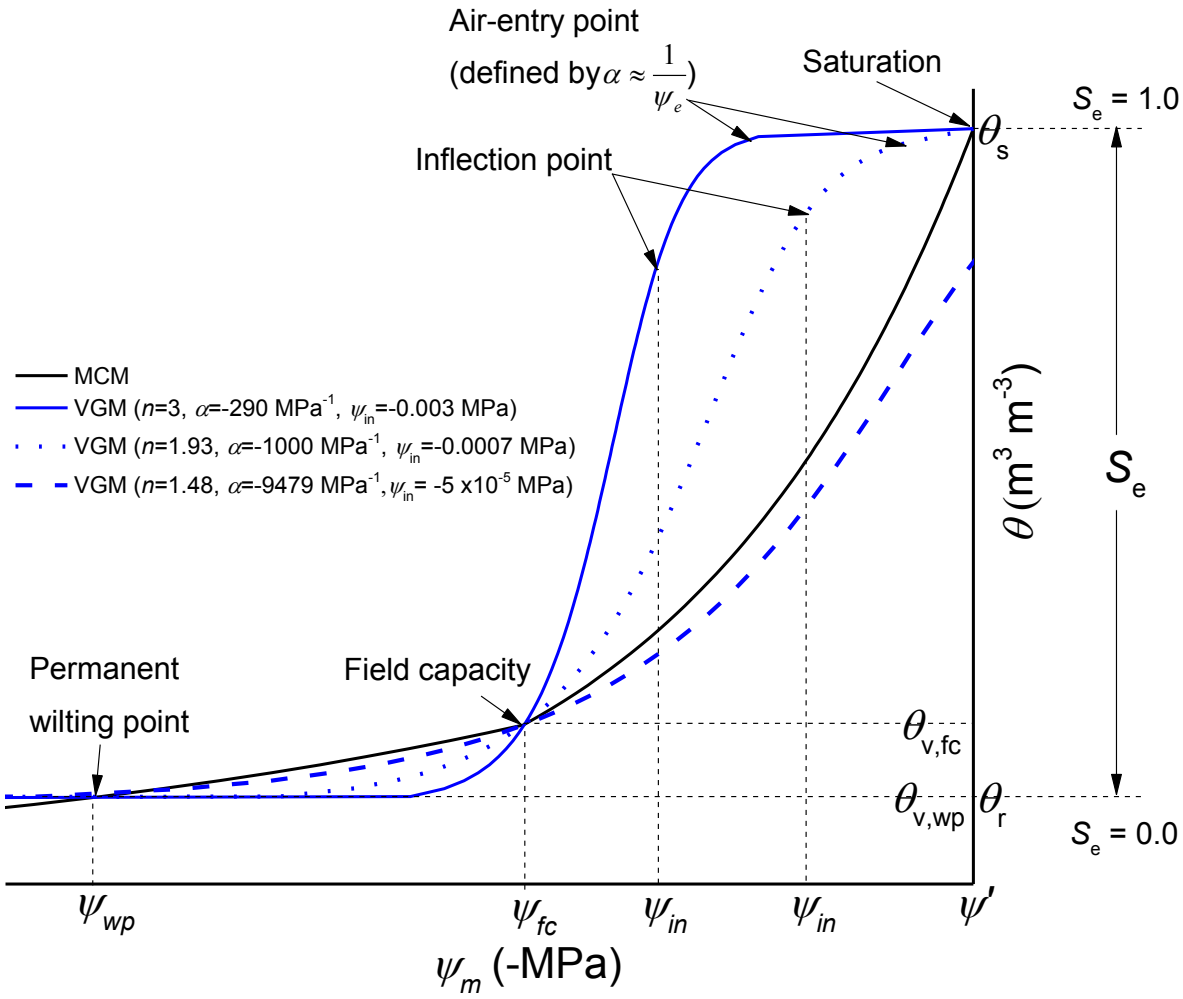

Fig. 4-1. Hypothetical curves for van Genuchten (VGM) and modified Campbell (MCM) soil moisture desorption functions. S_e=relative degree of saturation; θ=ambient volumetric soil water content; θ_s = volumetric soil water content at saturation; $\theta_{v,fc}$ = volumetric soil water content at field capacity; $\theta_{v,wp}$ = volumetric soil water content at wilting point; θ_r = residual soil water content; ψ_m= soil matric water potential; ψ'= ψ_m at saturation; ψ_e= air-entry potential; ψ_{in}= ψ_m at the inflection point; ψ_{fc}= ψ_m at field capacity; ψ_{wp}= ψ_m at wilting point; n and α=VGM shape parameters

D_{humm} (m)	D_{holl} (m)	ρ_b (Mg m^{-3})	$\theta_{v,fc}$ (m^3 m^{-3})	$\theta_{v,wp}$ (m^3 m^{-3})	$K_{s,mat}$ (mm h^{-1})	θ_{mac} (m^3 m^{-3})	ψ_{in} (MPa)	θ_r (m^3 m^{-3})	n (-)	α (MPa^{-1})
0.010		0.010	0.091	0.074		0.29	-0.0046	0.073	5.84	-211
0.065										
0.085		0.015	0.124	0.091		0.26	-0.0051	0.090	5.61	-189
0.115		0.020	0.157	0.102		0.22	-0.0056	0.100	5.51	-172
0.135		0.010	0.091	0.074		0.29	-0.0051	0.073	5.84	-211
0.190										
0.295		0.057	0.314	0.061	18.00	0.00	-0.0020	0.059	1.98	-350
0.305	0.005									
0.350	0.050									
0.540	0.240									
0.650	0.350									
0.720	0.420	0.076	0.393	0.083		0.00	-0.0010	0.064	1.58	-529
0.900	0.600									
1.100	0.800									
2.000	1.700									

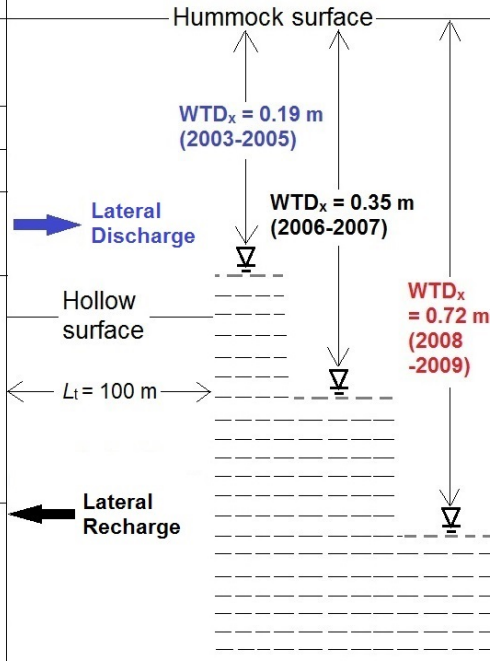

Fig. 4-2. Layout for *ecosys* model run to represent physical and hydrological characteristics of a Western Canadian fen peatland. Figure is not drawn to scale. D_{humm} = depth to the bottom of a layer from the hummock surface; D_{holl} = depth to the bottom of a layer from the hollow surface; ρ_b = dry bulk density (Flanagan and Syed 2011); $\theta_{v,fc}$ = volumetric soil water content at field capacity (-0.01 MPa) and $\theta_{v,wp}$ = volumetric soil water content at wilting point (-1.5 MPa) (Boelter 1969, 1970, Päivänen 1973, Szymanowski 1993); $K_{s,mat}$ = saturated hydraulic conductivity of soil matrix (Boelter 1969); θ_{mac} = volumetric macropore fractions; WTD_x = external reference water table depth representing average water table depth of the adjacent ecosystem; L_t = distance from modelled grid cells to the adjacent watershed over which lateral discharge / recharge occurs; ψ_{in}= matric water potential at the inflection point; θ_r = residual soil water content; n and α=van Genuchten model (VGM) shape parameters

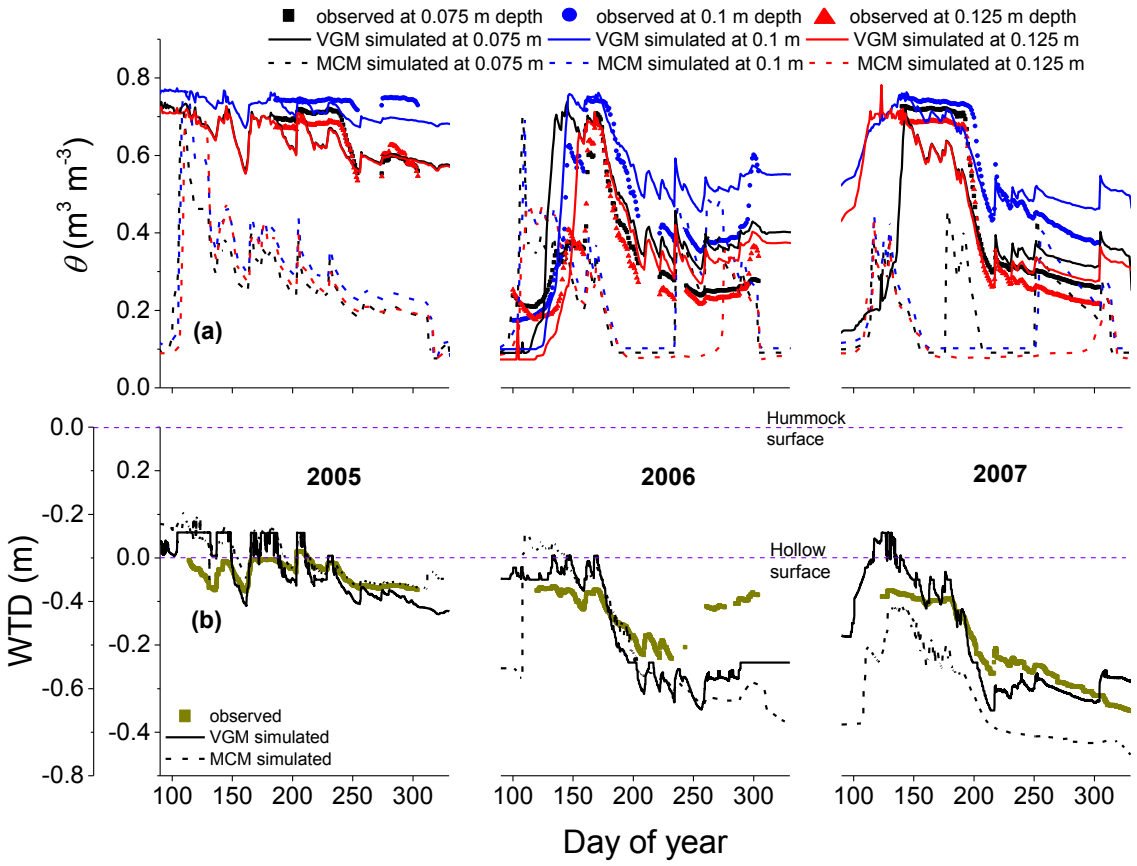

Fig. 4-3. (a) Daily soil water contents (θ) simulated with *ecosys* using Van Genuchten model (VGM) and modified Campbell model (MCM), and measured θ at 0.075, 0.1 and 0.125 m depths (Syed et al. 2006, Cai et al. 2010, Long et al. 2010, Flanagan and Syed 2011) from the hummock surface, and (b) hourly water table depth (WTD) simulated with *ecosys* using VGM and MCM, and measured half hourly WTD (Syed et al. 2006, Cai et al. 2010, Long et al. 2010, Flanagan and Syed 2011) during March-November 2005-2007 at a Western Canadian fen peatland. A negative WTD represents a depth below hummock/hollow surface and a positive WTD represents a depth below hummock/hollow surface

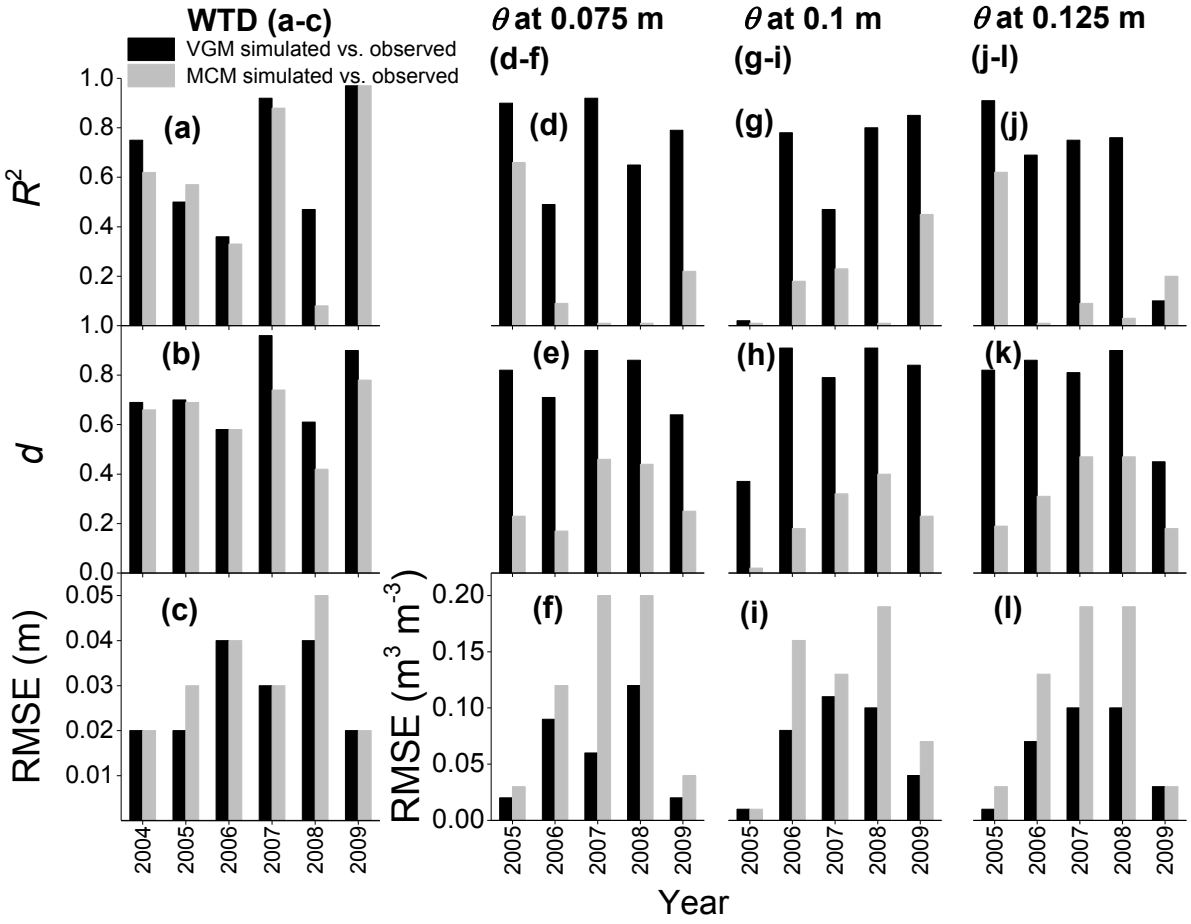

Fig. 4-4. (a, d, g, j) Coefficients of determination (R^2) from regressions of modelled on measured; (b, e, h, k) index of agreement (d) (Sect. 4-2.2.5) between modelled and measured; and (c, f, i, l) root mean squares for errors (RMSE) from regressions of measured on modelled water table depth (WTD) from hollow surface; and soil water contents (θ) at 0.075, 0.1 and 0.125 m depths from the hummock surface respectively during 2004-2009 at a Western Canadian fen peatland

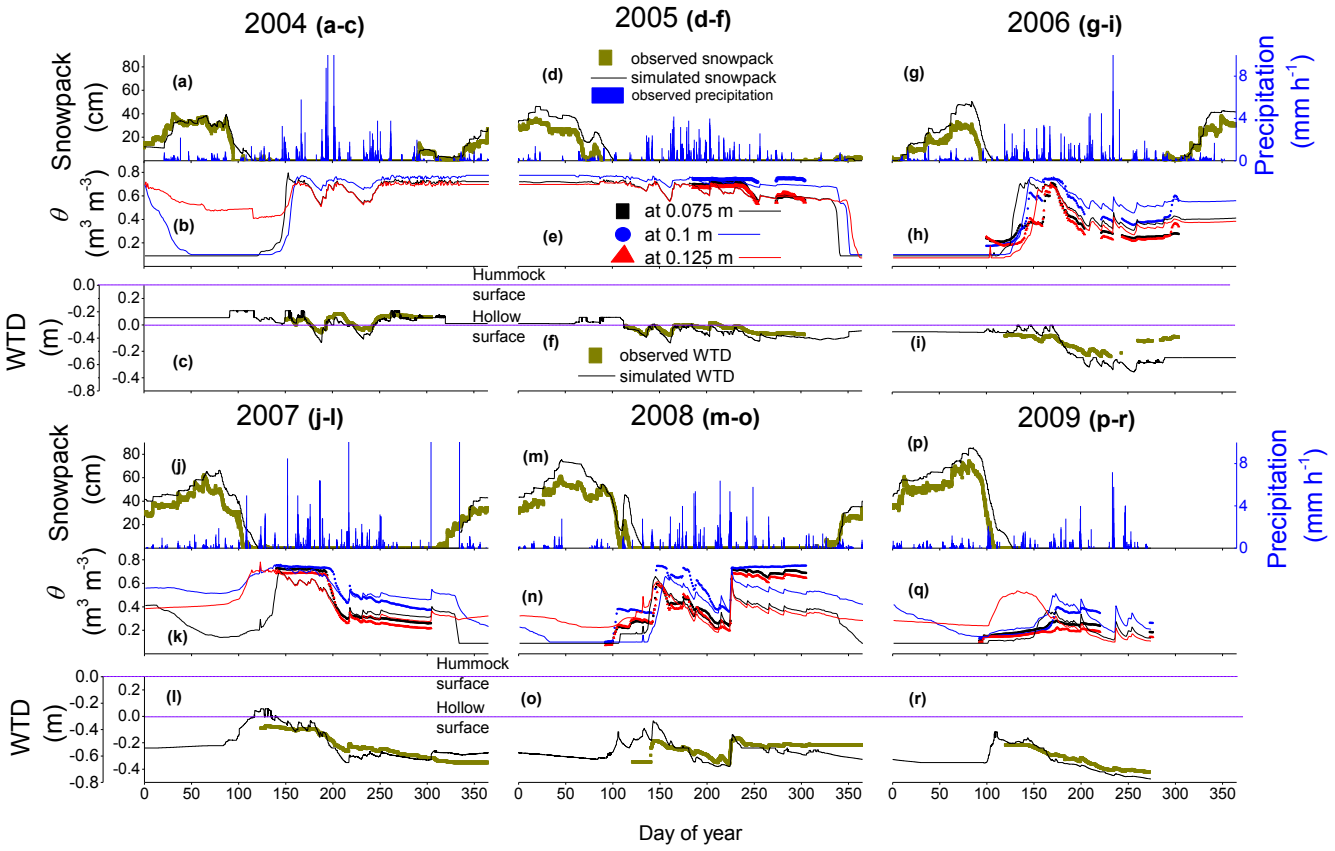

Fig. 4-5. (a, d, g, j, m, p) Half hourly measured and hourly modelled snowpack depth (on the left y-axes) (Flanagan and Syed, 2011; Syed et al., 2006) and half hourly measured precipitation (on the right y-axes); (b, e, h, k, n, q) daily modelled and measured soil water contents (θ) at 0.075, 0.1 and 0.125 m depths (Syed et al. 2006, Cai et al. 2010, Long et al. 2010, Flanagan and Syed 2011) from the hummock surface; and (c, f, i, l, o, r) half hourly measured and hourly modelled water table depth (WTD) (Syed et al. 2006, Cai et al. 2010, Long et al. 2010, Flanagan and Syed 2011) from 2004-2009 at a Western Canadian fen peatland. A negative WTD represents a depth below hummock/hollow surface and a positive WTD represents a depth below hummock/hollow surface

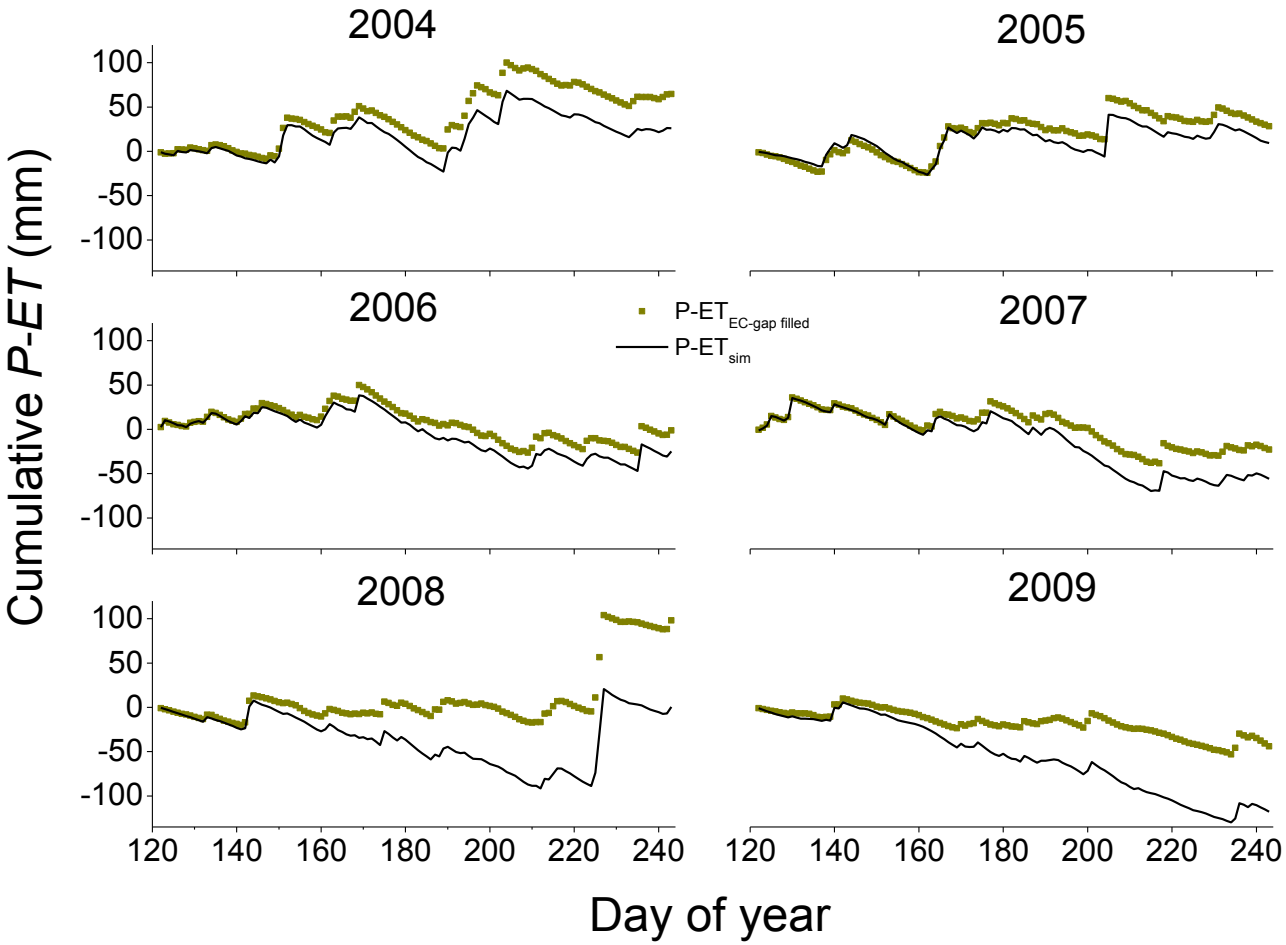

Fig. 4-6. Cumulative differences between observed precipitation (*P*) and eddy covariance (EC)-gap filled evapotranspiration (*ET*) (*P-ET*$_{\text{EC-gap filled}}$) (Syed et al. 2006, Flanagan and Syed 2011) and between observed *P* and simulated *ET* (*P-ET*$_{\text{sim}}$) during 2004-2009 at a Western Canadian fen peatland

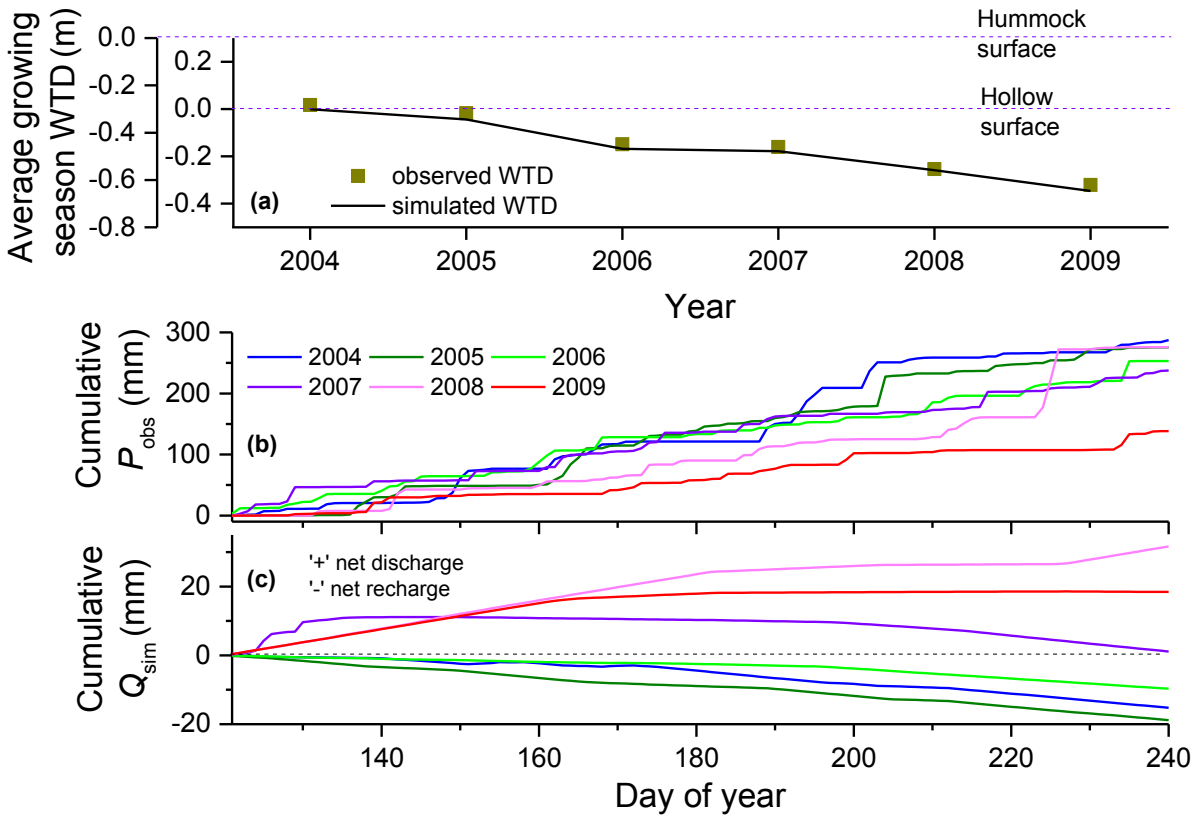

Fig. 4-7. (a) Modelled and measured average water table depth (WTD) (b) cumulative observed precipitation (P_{obs}) over the growing season (Syed et al. 2006, Flanagan and Syed 2011), and (c) simulated cumulative lateral recharge / discharge (Q_{sim}) over the growing season (May-August) of 2004-2009 at a Western Canadian fen peatland. A negative WTD represents a depth below hummock/hollow surface and a positive WTD represents a depth below hummock/hollow surface

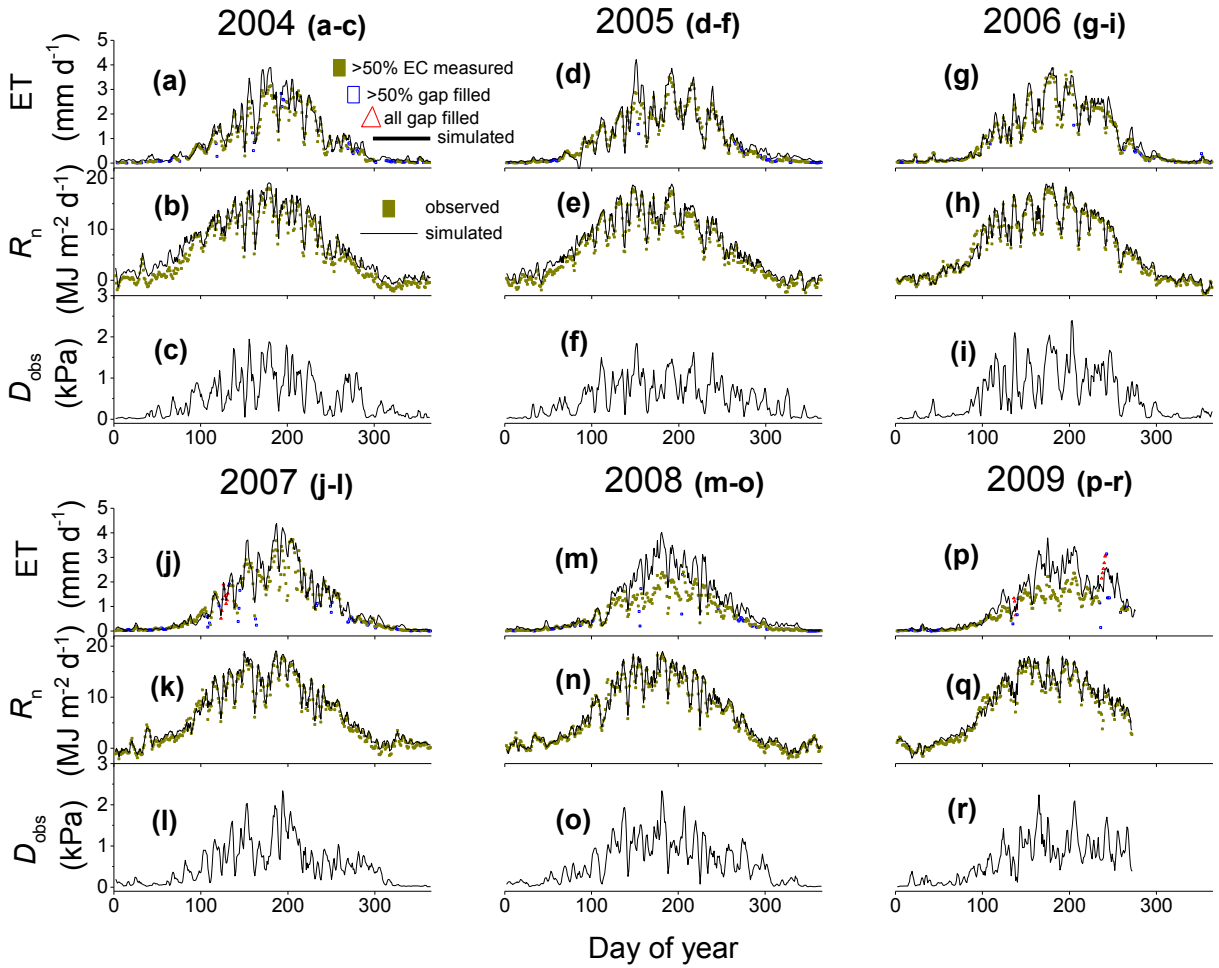

Fig. 4-8. Three-day moving averages for (a, d, g, j, m, p) eddy covariance (EC)-gap filled (Syed et al. 2006, Flanagan and Syed 2011) and modelled evapotranspiration (*ET*); (b, e, h, k, n, q) observed and modelled net radiation (R_n); and (c, f, i, l, o, r) observed vapour pressure deficit (D_{obs}) (Syed et al. 2006, Flanagan and Syed 2011) during 2004-2009 at a Western Canadian fen peatland

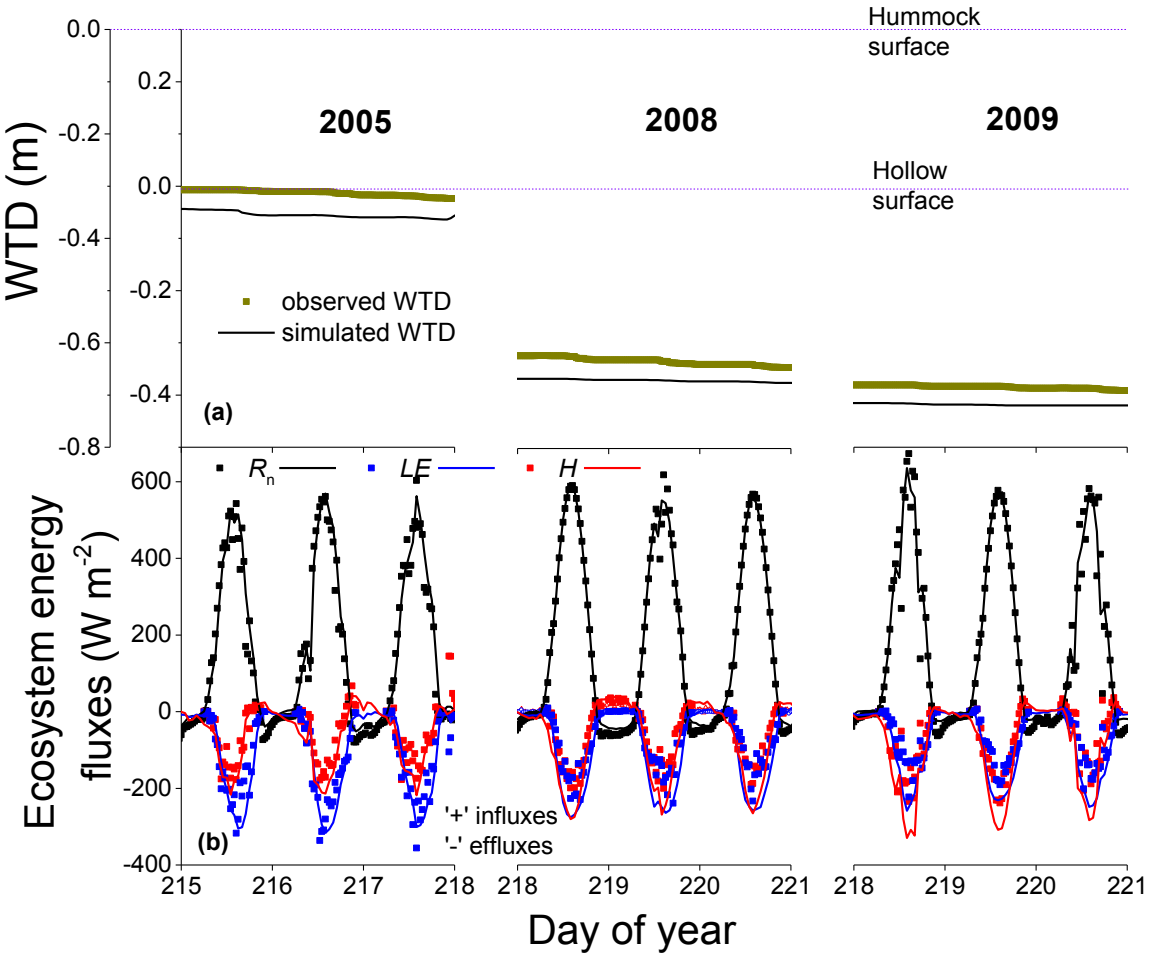

Fig. 4-9. (a) Half hourly measured and hourly modelled water table depth (WTD), and (b) half hourly eddy covariance (EC) measured (u^* (friction velocity) > 0.15 m s^{-1}) (Syed et al. 2006, Flanagan and Syed 2011) and modelled ecosystem energy fluxes (R_n=net radiation, *LE*=latent heat and *H*=sensible heat flux) during August 2005, 2008 and 2009 at a Western Canadian fen peatland. Positive values for fluxes represent downward fluxes or fluxes into the ecosystem and negative values for fluxes represent upward fluxes or fluxes out of the ecosystem. A negative WTD represents a depth below hummock/hollow surface and a positive WTD represents a depth below hummock/hollow surface

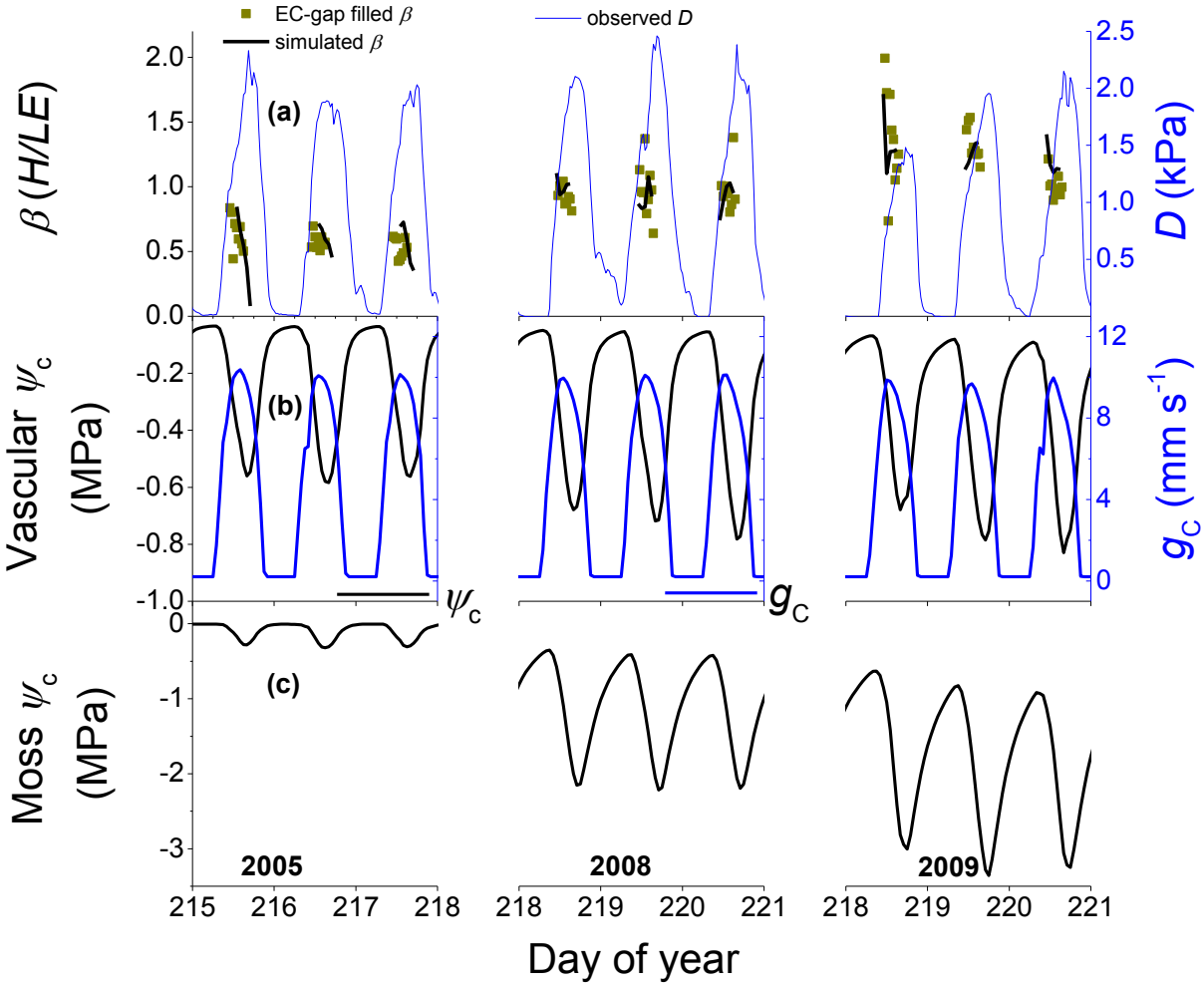

Fig. 4-10. (a) Half hourly eddy covariance (EC)-gap filled (Syed et al. 2006, Flanagan and Syed 2011) and hourly modelled mid-day (2 hours before and after solar noon) Bowen ratio (β) (b) hourly modelled vascular canopy water potential (ψ_c) (on the left y-axes) and canopy stomatal conductance (g_c) (on the right y-axes), and (c) hourly modelled moss (non-vascular) ψ_c during August 2005, 2008 and 2009 at a Western Canadian fen peatland

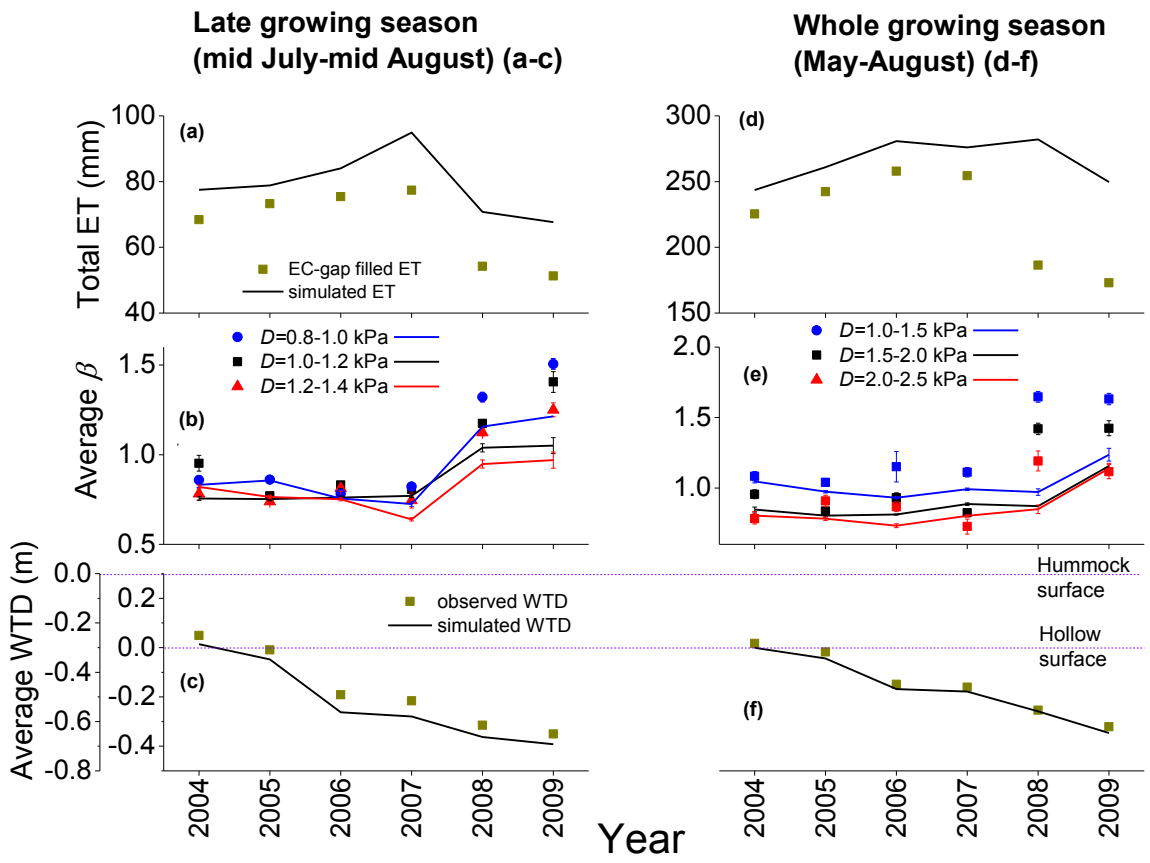

Fig. 4-11. (a, d) Modelled and eddy covariance (EC)-gap filled (Syed et al. 2006, Flanagan and Syed 2011) total late growing season (mid-July to mid-August) and whole growing season (May-August) evapotranspiration (*ET*); (b, e) modelled and EC-gap filled (Syed et al. 2006, Flanagan and Syed 2011) average late and whole growing season mid-day (2 hours before and after solar noon) Bowen ratio (β) under clear sky condition (incoming shortwave radiation > 700 W m^{-2}) for three different vapour pressure deficit (*D*) classes for each period (i.e. *D*=0.8-1, 1-1.2 and 1.2-1.4 kPa for late growing season and *D* 1-1.5, 1.5-2 and 2-2.5 kPa for whole growing season); and (c, f) average modelled and measured late and whole growing season water table depth (WTD) during 2004-2009 at a Western Canadian fen peatland. A negative WTD represents a depth below hummock/hollow surface and a positive WTD represents a depth below hummock/hollow surface

Appendices

Appendix A: Surface water flux

$$\frac{\Delta(d_w A)}{\Delta t} = \sum_i Q_{w,in_i} + \sum_i Q_{w,out_i} + P - E_{res} - E_{surf} \text{ ; kinematic wave theory of overland flow} \quad \text{(A1)}$$

$$Q_{w_i} = v_i \left(d_w - d_{sw}\right) L_i \quad \text{(A2)}$$

$$v_i = \frac{R^{0.67} S_i^{0.5}}{z_r} \quad \text{(A3)}$$

$$R = \frac{s_r d_{mw}}{s_r^2 + 1} \quad \text{(A4)}$$

$$S_i = \frac{2abs[\left(Z + d_{sw} + d_{mw}\right)_{s_i} - \left(Z + d_{sw} + d_{mw}\right)_{d_i}]}{L_{s_i} + L_{d_i}} \quad \text{(A5)}$$

$$E_{res} = \frac{e_{air} - e_{res}(\psi_{res} T_{res})}{r_{a_{res}} + r_{s_{res}}} \quad \text{(A6)}$$

$$E_{surf} = \frac{e_{air} - e_{surf}(\psi_{surf} T_{surf})}{r_{a_{surf}} + r_{s_{surf}}} \quad \text{(A7)}$$

Where, subscripts i=dimensions (i=x, y), s=source cell, d=destination cell, in=flow into the grid cells, and out=flow out of the grid cells; d_w=depth of surface water (m); A=area of landscape position (m^2); t=time (h); Q_w=surface water flux (m^3 m^{-2} h^{-1}); P=precipitation flux (m^3 m^{-2} h^{-1}); E_{res}=evaporation flux from surface residue (m^3 m^{-2} h^{-1}); E_{surf}=evaporation flux from soil surface (m^3 m^{-2} h^{-1}); v=velocity of surface water flow (m h^{-1}); ; d_{sw}= maximum depth of surface water storage (m); L=length of grid cells (m); R=ratio of cross-sectional area to perimeter of surface flow (m); S=slope (m m^{-1}); z_r=Manning's roughness coefficient (=0.01 m$^{-1/3}$ h); s_r=slope of channel sides during surface flow (m m^{-1}); Z=surface elevation (m); d_{sw}= maximum depth of surface water storage (m); d_{mw}=depth of mobile surface water (m); e_{air}=atmospheric vapour density (g m^{-3}); e_{res}=vapour density at surface residue (g m^{-3}) at current residue water potential (ψ_{res}) and temperature (T_{res}); $r_{a_{res}}$ =boundary layer resistance to evaporation from surface residue (h m^{-1}); $r_{s_{res}}$ =surface resistance to evaporation from surface residue (h m^{-1}); e_{surf}=vapour density at soil surface (g m^{-3}) at current soil surface water potential (ψ_{surf}) and temperature (T_{surf}); $r_{a_{surf}}$ =boundary layer resistance to evaporation from soil surface (h m^{-1}); and $r_{s_{surf}}$ =surface resistance to evaporation from soil surface (h m^{-1}).

Appendix B: Sub-surface water flux

$$\frac{\Delta\theta_w}{\Delta t} = \sum_i (Q_{w_{mat,in_i}} + Q_{w_{mac,in_i}} - Q_{w_{mat,out_i}} - Q_{w_{mac,out_i}}) + \sum_j \left(Q_{w_{b,mat,in_j}} + Q_{w_{b,mac,in_j}} - Q_{w_{b,mat,out_j}} - Q_{w_{b,mac,out_j}} \right) + Q_f - U_w$$; 3D continuity equation for water balance of each soil layer (B1)

$Q_{w_{mat_i}} = K'_{mat_i}(\psi_{s_s} - \psi_{s_d})$; soil matrix water flow (B2)

$K'_{mat_i} = \frac{2K_{mat_{s_i}} K_{mat_{d_i}}}{K_{mat_{s_i}} L_{d_i} + K_{mat_{d_i}} L_{s_i}}$; when both the source and destination grid cells are either saturated or unsaturated (Richard's equation) (B3)

$K'_{mat_i} = \frac{2K_{mat_{s_i}}}{L_{s_i} + L_{d_i}}$; when the source cell is saturated and the destination cell is unsaturated (Green-Ampt equation) (B4)

$K'_{mat_i} = \frac{2K_{mat_{d_i}}}{L_{s_i} + L_{d_i}}$; when the source cell is unsaturated and the destination cell is saturated (Green-Ampt equation) (B5)

$K_{mat_i} = K_{s,mat} \left(\frac{q-p+1}{q} \right) \left[\frac{\sum_{p=1}^{p=q} \frac{2p-1}{\psi_p^2}}{\sum_{r=p}^{r=q} \frac{2r+1-2p}{\psi_r^2}} \right]$; Green and Corey (1971) model used in MCM version of *ecosys* (B6)

$p = \text{Int} \left[q \frac{(\theta_s - \theta_p)}{\theta_s} \right] + 1$ (B7)

$n(k) = 1 + 0.001k$ (B8)

$m(k) = 1 - \frac{1}{n(k)}$ (B9)

$\alpha(k) = \frac{m(k)^{1-m(k)}}{\psi_{in}}$ (van Genuchten 1978) (B10)

$S_{e_{fc,sim}}(k) = \left[1 + (\alpha(k)\psi_{fc})^{n(k)} \right]^{-m(k)}$ (Van Genuchten 1980) (B11)

$S_{e_{wp,sim}}(k) = \left[1 + (\alpha(k)\psi_{wp})^{n(k)} \right]^{-m(k)}$ (Van Genuchten 1980) (B12)

$$\theta_r(k) = \max\left[0, \frac{\theta_s - \theta_{v,fc} + \theta_{v,wp}}{S_{e_{fc,sim}}(k) - S_{e_{wp,sim}}(k)}\right] \quad \text{(B13)}$$

$$\theta_{v,fc_{sim}}(k) = \theta_r(k) + \left[\theta_s - \theta_r(k)\right] S_{e_{fc,sim}}(k) \text{ (Van Genuchten 1980)} \quad \text{(B14)}$$

$$\theta_{v,fc_{sim}}(k) = \theta_r(k) + \left[\theta_s - \theta_r(k)\right] S_{e_{fc,sim}}(k) \text{ (Van Genuchten 1980)} \quad \text{(B15)}$$

$$K_{mat_i} = K_{s,mat} S_e^{0.5}\left[1 - \left(1 - S_e^{\frac{1}{m}}\right)^m\right]^2 \text{; where } S_e = \frac{\theta - \theta_r}{\theta_s - \theta_r} = \left[1 + \left(\alpha\psi_m\right)^n\right]^{-m} \text{; Mualem-van Genuchten}$$

model (Mualem 1976, Van Genuchten 1980) used in VGM version of *ecosys* (B16)

$$K_{mat_i} = K_{s,mat} S_e^{0.5}\left[\frac{1 - \left(1 - (S_e S_c)^{\frac{1}{m}}\right)^m}{1 - \left(1 - S_c^{\frac{1}{m}}\right)^m}\right]^2 \text{; where } S_e = \frac{1}{S_c}[1 + (\alpha\psi_m)^n]^{-m} \text{ and } S_c = [1 + (\alpha\psi_e)^n]^{-m} \text{;}$$

modified Mualem-van Genuchten model (Ippisch et al. 2006) used when $n \leq 2$ used in VGM version of *ecosys* (B17)

$$Q_{w_{mac\ i}} = K'_{mac_i}(\psi_{g_s} - \psi_{g_d}) \text{; soil macropore water flow} \quad \text{(B18)}$$

$$K'_{mac} = \frac{2K_{mac_s}K_{mac_d}}{K_{mac_s}L_{d_i} + K_{mac_d}L_{s_i}} \quad \text{(B19)}$$

$$K_{mac} = N_{mac}K^*_{mac} \quad \text{(B20)}$$

$$K^*_{mac} = \frac{\pi R^4}{8\eta} \text{; Hagen-Poiseuille's theory of laminar flow in tubes} \quad \text{(B21)}$$

$$N_{mac} = \theta_{mac}\pi R^2 \quad \text{(B22)}$$

$$Q_{w_{b,mat_j}} = \frac{K_{b,mat_j}\left[\psi'_b - \psi_{s_b} + 0.01\left(d_{z_b} - WTD_x\right)\right]}{L_{t_j}} \text{; lateral discharge occurs when}$$

$d_{z_b} < WTD_x$ and $\psi_{s_b} > \psi'_b + 0.01\left(d_{z_b} - WTD_x\right)$ and lateral recharge occurs when

$$d_{z_b} > WTD_x \quad \text{(B23)}$$

$$Q_{w_{b,mac_j}} = \frac{K_{b,mac_j} 0.01\left[d_{z_b} - L_{z_b}\left(\theta_{w,mac} - 0.5\right) - WTD_x\right]}{L_{t_j}}$$; lateral discharge occurs when $d_{z_b} < WTD_x$ and lateral recharge occurs when $d_{z_b} > WTD_x$ (B24)

Where, subscripts i=dimensions (i=x, y, z), j=dimensions (j=x, y), s=source cell, d=destination cell, *in*=flow into the grid cells, and *out*=flow out of the grid cells; b=boundary grid cell; *mat*=soil matrix/micropore; *mac*=soil macropore; θ_w=soil water content (m^3 m^{-3}); Q_w=sub-surface water flux (m^3 m^{-2} h^{-1}); Q_f=freeze-thaw flux (a positive flux represents thaw and a negative flux represents freeze) (m^3 m^{-2} h^{-1}); U_w=total root water uptake flux (m^3 m^{-2} h^{-1}); K=hydraulic conductance (m MPa^{-1} h^{-1}); ψ_s=total soil water potential (MPa); K=hydraulic conductivity (m^2 MPa^{-1} h^{-1}); L=length of the grid cells (m); $K_{s,mat}$=saturated soil matrix hydraulic conductivity (m^2 MPa^{-1} h^{-1}); p=individual pore class [1,2,3,…..q; where q=total number of pore classes (=100)]; ψ_p=matric potential of pore class p; ψ_p=matric potential of pore class r (r=p→q); n =van Genuchten parameter that describes the mean slope of the desorption curve or the range of pore size distribution; α= the inverse of the pressure head at the air-entry value (i.e. $\alpha \approx 1$/air entry potential) that governs the shape of van Genuchten desorption curve ($-MPa^{-1}$); k=number of iteration (1,2,3…..19000); ψ_{in}=matric potential at inflection point (-MPa); $S_{e_{fc,sim}}$ = simulated relative degree of saturation at field capacity; ψ_{fc}=matric potential at field capacity (-MPa); $S_{e_{wp,sim}}$ = simulated relative degree of saturation at wilting point; ψ_{wp}=matric potential at wilting point (-MPa); θ_r =residual soil water content (m^3 m^{-3}); θ_s =soil water content at saturation (m^3 m^{-3}); $\theta_{v,fc}$ =observed input for soil water content at field capacity (m^3 m^{-3}); $\theta_{v,wp}$ =observed input for soil water content at wilting point (m^3 m^{-3}); $\theta_{v,fc_{sim}}$ =simulated soil water content at field capacity (m^3 m^{-3}); $\theta_{v,wp_{sim}}$ =simulated soil water content at wilting point (m^3 m^{-3}); θ=ambient soil water content (m^3 m^{-3}); ψ_m=matric potential as a function of θ (-MPa); ψ_e=matric potential very close to saturation (=-0.0001 MPa); ψ_g=gravitational soil water potential (MPa); N_{mac}=number of macropore channels (m^{-2}); K^*_{mac}=individual macropore hydraulic conductivity (m^4 MPa^{-1} h^{-1} macropore $channel^{-1}$); η=dynamic viscosity of water (MPa h); θ_{mac}=volumatric macropore fraction (m^3 m^{-3}); R=radius of a macropore channel (m); ψ'=soil water potential at saturation (MPa)(=0 and -0.005 MPa for van Genuchten and modified Campbell model respectively); d_z=depth of the mid-point of a grid cell from the surface (m); L_z=vertical thickness of a grid cell (m); WTD_x=depth of the water table depth at the adjacent watershed with which modelled grid cells exchange water laterally (m); and L_t=lateral distance over which lateral discharge/recharge occurs (m).

Appendix C: Water table depth

$$WTD = -[d_{z,sat} - L_{z,sat}(1 - \frac{\theta_g}{\theta_g^*})]$$; negative sign represents depth below the surface of the a particular grid cell (C1)

Where, WTD=water table depth (m); $d_{z,sat}$=depth to the bottom of the layer immediately above the uppermost saturated layer (m); $L_{z,sat}$=vertical thickness of the layer immediately above the uppermost saturated layer (m); θ_g=current air-filled porosity of the layer immediately above the

uppermost saturated layer (m^3 m^{-3}); and θ_g^*=air-filled porosity at air-entry potential of the layer immediately above the uppermost saturated layer (m^3 m^{-3}).

Appendix D: Heat flux

$R_n + LE + H + G = 0$; energy balance for each of the canopy, snow, residue and soil surface (D1)

$\sum G_{c,in_i} - \sum G_{c,out_i} + L_v Q_f + c(T - T_{frz}) = 0$; 3D general heat flux equation in snowpack, surface residue and soil layers (D2)

$$T_{frz} = \frac{\text{-9.095895} \times 10^4}{\psi_m - 333} (\text{for residue layer}) = \frac{\text{-9.095895} \times 10^4}{\psi_m + \psi_o - 333} (\text{for soil layers}) = T'_{frz} (\text{for snowpack}) \quad \text{(D3)}$$

$$G_{c_i} = \frac{2\kappa_{s,d_i}(T_s - T_d)}{L_{s_i} + L_{d_i}} + c_{w_s} T_s Q_{w_i} \quad \text{(D4)}$$

$$D_{snowpack} = \frac{V_{sweq}\frac{\rho_w}{\rho_{oldsnow}} + V_{ice} + V_{water}}{A_{snowpack}} \quad \text{(D5)}$$

$$\rho_{oldsnow} = \min(0.5, \rho_{freshsnow} + 0.25\frac{V_{snow}}{A_{snowpack}}) \quad \text{(D6)}$$

Where, subscripts *i*=dimensions (*i*=*x*, *y, z*), *s*=source cell, *d*=destination cell, *in*=flow into the grid cells, and *out*=flow out of the grid cells; R_n=net radiation (Wm^{-2}); *LE*=latent heat flux (Wm^{-2}); *H*=sensible heat flux (Wm^{-2}); and *G*=ground heat flux (Wm^{-2}); G_c=conductive heat flux (MJ m^{-2} h^{-1}); L_v=latent heat of evaporation (=2460 MJ m^{-3}); Q_f=freeze-thaw flux (a positive flux represents thaw and a negative flux represents freeze) (m^3 m^{-2} h^{-1}); *c*=heat capacity of residue/soil layers (solid + liquid + void) or the snowpack (snow + ice + water) (MJ m^{-2} K^{-1}); *T*=ambient temperature of soil/residue layers or the snowpack (K); T_{frz}=freezing temperature of soil/residue layers or the snowpack (K); ψ_m=matric water potential of residue/soil layers (-MPa); ψ_o=osmotic potential of soil layers (-MPa); T'_{frz} =freezing temperature of free water (=273.15 K); κ=thermal conductivity (MJ m^{-1} h^{-1} K^{-1}); *L*=length of the residue layer/ a soil layer/ the snowpack (m); c_w=heat capacity of water (=4.19 MJ m^{-2} K^{-1}) ; Q_w=water flux (m^3 m^{-2} h^{-1}); $D_{snowpack}$=depth of snowpack (m); V_{sweq}=volume of snow water equivalent (m^3); ρ_w=density of water (=1 Mg m^{-3}); $\rho_{oldsnow}$=density of settled snow (Mg m^{-3}); V_{ice}=volume of ice in snowpack (m^3 m^{-3}); V_{water}=volume of water in snowpack (m^3 m^{-3}); $A_{snowpack}$=snowpack basal area (m^2); $\rho_{freshsnow}$=density of freshly fallen snow (=0.083 Mg m^{-3}); V_{snow}=volume of snow in the snowpack (m^3)

Appendix E: Canopy transpiration

$$R_{nc_i} + LE_{c_i} + H_{c_i} + G_{c_i} = 0 \text{; canopy energy balance} \quad \text{(E1)}$$

$$LE_{c_i} = \frac{L_v\left[e_a - e_{c_i}\left(T_{c_i}, \psi_{c_i}\right)\right]}{r_{a_i}} \text{; } LE \text{ from canopy evaporation} \quad \text{(E2)}$$

$$LE_{c_i} = \frac{L_v\left[e_a - e_{c_i}\left(T_{c_i}, \psi_{c_i}\right)\right]}{r_{c_i} + r_{a_i}} - LE_{c_i} \text{from}\left(\text{E2}\right) \text{; } LE \text{ from canopy transpiration} \quad \text{(E3)}$$

$$H_{c_i} = \frac{\rho C_p (T_a - T_{c_i})}{r_{a_i}} \quad \text{(E4)}$$

$$r_{cmin_i} = \frac{0.64(C_b - C'_{i_i})}{V_{c'_i}} \text{; } r_c \text{ driven by rates of carboxylation vs. diffusion} \quad \text{(E5)}$$

$$r_{c_i} = r_{cmin_i} + \left(r_{cmax_i} - r_{cmin_i}\right)e^{\left(-\beta\psi_{t_i}\right)} \text{(for vascular species)} \\ = r_{cmax_i} \text{(for non-vascular species)} \text{; } r_c \text{ constrained by water stress in vascular plants} \quad \text{(E6)}$$

$$\psi_{t_i} = \psi_{c_i} - \psi_{\pi_i} \quad \text{(E7)}$$

Where, subscript i=species or plant functional type (PFT); R_{nc}=net radiation at canopy surface (Wm^{-2}); LE=latent heat flux at canopy surface (Wm^{-2}); H=sensible heat flux at canopy surface (Wm^{-2}); G=canopy storage heat flux (Wm^{-2}); L_v=latent heat of evaporation (=2460 Jg^{-1}); e_a= atmospheric vapour density (g m^{-3}) at ambient T_a and relative humidity; e_c= canopy vapour density (g m^{-3}) at T_c and ψ_c; r_a=boundary layer resistance to evaporation and transpiration from canopy (s m^{-1}); r_c=canopy stomatal resistance (s m^{-1}) to transpiration (=$1/g_c$; g_c=canopy stomatal conductance in m s^{-1}); ρC_p=volumatric heat capacity of air (=1250 J m^{-3} °C^{-1}); T_a=air temperature (°C); T_c=canopy temperature (°C); r_{cmin}=minimum r_c at ψ_c=0 MPa (s m^{-1}); C_b=[CO_2] in canopy air (μmol mol^{-1}); C'_i=[CO_2] in canopy leaves at ψ_c=0 MPa (μmol mol^{-1}); V'_c=potential canopy CO_2 fixation rate at ψ_c=0 MPa (μmol m^{-2} s^{-1}); r_{cmax}=canopy cuticular resistance to vapour flux (=5.0×10^3 s m^{-1}) (Larcher 2003); β=stomatal resistance shape parameter (=-5 MPa^{-1}) (Grant and Flanagan 2007); ψ_t=canopy turgor potential (MPa); ψ_c=canopy water potential (MPa); and ψ_π=canopy osmotic potential (MPa).

Appendix F: Root/rhizoid/mycorrhizal water uptake

$$U_{w_i} = \sum_l \sum_r U_{w_{i,r,l}} \quad \text{(F1)}$$

$$U_{w_{i,r,l}} = \sum_l \sum_r \frac{\psi'_{c_i} - \psi'_{s_i}}{\Omega_{s_{i,r,l}} + \Omega_{r_{i,r,l}} + \sum_x \Omega_{a_{i,r,l,x}}} \quad \text{(F2)}$$

$$\Omega_{s_{i,r,l}} = \ln\left[\frac{\left(\frac{d_{i,r,l}}{r_{i,r,l}}\right)}{\left(\frac{2\pi L_{i,r,l}}{\kappa_{r_{i,r,l}}}\right)}\right]\frac{\theta_{P_l}}{\theta_{w_l}} \quad \text{(F3)}$$

$$\Omega_{r_{i,r,l}} = \frac{\Omega'_{r_{i,r}}}{L_{i,r,l}} \quad \text{(F4)}$$

$$\Omega_{a_{i,r,l,x=1}} = \frac{\Omega_{a_{i,r}} Z_l}{\left[n_{i,r,l,1}\left(\frac{r_{i,r,l,1}}{r'_{i,r}}\right)^4\right]} + \gamma\Omega'_{a_{i,r}}\left[\frac{Z_{b_i}}{n_{i,r,l,1}\left(\frac{r_{b_i}}{r'_{b_i}}\right)^4}\right]\left[\frac{\sum_{i,r,l} M_{i,r,l}}{M_{i,r,l}}\right] \quad \text{(F5)}$$

$$\frac{\left[e_a - e_{c_i}\left(T_{c_i}, \psi_{c_i}\right)\right]}{r_{c_i} + r_{a_i}} = \sum_l \sum_r \frac{\psi'_c - \psi'_s}{\Omega_{s_{i,r,l}} + \Omega_{r_{i,r,l}} + \sum_x \Omega_{a_{i,r,l,x}}} + X_{c_i}\frac{\Delta\psi_{c_i}}{\Delta t} \quad \text{(F6)}$$

Where, subscripts i=species or plant functional type (PFT), r=root/rhizoid/mycorrhizae, l=soil/canopy layer, x=1, 2 (1=primary root/rhizoid/mycorrhizae, 2=secondary root/rhizoid/mycorrhizae); U_w=water uptake by root/rhizoid/mycorrhizal surfaces ($m^3\ m^{-2}\ h^{-1}$); ψ_c=canopy water potential (MPa); ψ'_c=ψ_c + canopy gravitational potential (MPa); ψ'_s=soil water potential (ψ_s)+ soil gravitational potential (MPa); Ω_s = radial resistance to water transport from soil to surface of root/rhizoid/mycorrhizae (MPa h m^{-1}); Ω_r = radial resistance to water transport from surface to axis of root/rhizoid/mycorrhizae (MPa h m^{-1}); Ω_a = axial resistance to water transport along axes root/rhizoid/mycorrhizae (MPa h m^{-1}); d= half distance between adjacent root/rhizoid/mycorrhizae (m); r=radius of root/rhizoid/mycorrhizae at ambient root/rhizoid/mycorrhizal water potential (ψ_r); L=length of root/rhizoid/mycorrhizae (m); κ_r = hydraulic conductivity between soil and root/rhizoid/mycorrhizal surface (m^2 MPa^{-1} h^{-1}); θ_P=total soil porosity ($m^3\ m^{-3}$); θ_w=soil water content ($m^3\ m^{-3}$); Ω'_r = radial resistivity to water transport from surface to axes of root/rhizoid/mycorrhizae (MPa h m^{-2}) (1.0×10^4) (Doussan et al. 1998); Z_l=depth of soil layer l from soil surface (m); n= number of root/rhizoid/mycorrhizal axes; r' = radius root/rhizoid/mycorrhizae at ψ_r=0 MPa; Ω'_a = axial resistivity to water transport along root/rhizoid/mycorrhizal axes (MPa h m^{-4}) (4.0×10^9 for deciduous) (Larcher 2003); Z_b= length of bole from soil surface to top of canopy (m); r_b=radius of bole at ambient ψ_c; r'_b=radius of bole at ψ_c=0 MPa; M= mass of root/rhizoid/mycorrhizae (g m^{-2}); e_a= atmospheric vapour density (g m^{-3}) at ambient T_a and relative humidity; e_c= canopy vapour density (g m^{-3}) at T_c and ψ_c; r_a=boundary layer resistance to evaporation and transpiration from canopy (s m^{-1}); r_c=canopy stomatal resistance (s m^{-1}) to transpiration; T_a=air temperature (°C); T_c=canopy temperature (°C); ψ_c=canopy water potential (MPa); X_c= canopy capacitance ($m^3\ m^{-2}$ MPa^{-1}) ; and t=time (h).

Appendix G: Root/rhizoid/mycorrhizal respiration and growth

$$R_a = \sum_i \sum_j \left(R_{c_{i,j}} + R_{s_{i,j}} \right) + \sum_i \sum_l \sum_z (R_{c_{i,r,l}} + R_{s_{i,r,l}}) + E_{N,P}(U_{NH_4\,i,r,l} + U_{NO_3\,i,r,l} + U_{PO_4\,i,r,l}) \quad \text{(G1)}$$

$$R_{c_{i,j}} = R_c' \sigma_{C_{i,j}} f_{Ta_i} \quad \text{(G2)}$$

$R_{c_{i,r,l}} = R_c' \sigma_{C_{i,r,l}} f_{T_{a_i}} \frac{U_{O_2\,i,r,l}}{U_{O_2}'_{i,r,l}}$; O_2 constraint on root/rhizoid/mycorrhizal respiration from active uptake (G3)

$U_{O_2\,i,r,l} = U_{O_2}'_{i,r,l} \frac{\left[O_{2r_{i,r,l}}\right]}{\left[O_{2r_{i,r,l}}\right] + K_{O_2}} = U_{w_{i,r,l}} \left[O_{2s_l}\right] + 2\pi L_{i,r,l} D_{s_{O_2}} \left(\left[O_{2s_l}\right] - \left[O_{2r_{i,r,l}}\right] \right)$; active O_2 uptake $ln\left[\frac{r_{s_l} + r_{r_{i,r,l}}}{r_{r_{i,r,l}}}\right] + 2\pi L_{i,r,l} D_{r_{O_2}} \left(\left[O_{2q_{i,r,l}}\right] - \left[O_{2r_{i,r,l}}\right] \right) ln\left[\frac{r_{q_{i,r,l}}}{r_{r_{i,r,l}}}\right]$ by root /mycorrhizae coupled with diffusion of O_2 through root/mycorrhizal aerenchyma (G4)

$$U_{O_2}'_{i,r,l} = 2.67 R_a'_{i,r,l} \quad \text{(G5)}$$

$$R_{m_{i,j}} = \sum_z N_{i,j,z} R_m' f_{Tm_i} \quad \text{(G6)}$$

$$R_{g_{i,j}} = \left(R_{c_{i,j}} - R_{m_{i,j}} \right) \left(\psi_{t_i} - \psi_t' \right); \text{growth when } R_m < R_c \text{and } \psi_{t_i} > \psi_t' \quad \text{(G7)}$$

$\frac{\Delta M_{R_{i,r,l}}}{\Delta t} = \left[R_{g_{i,r,l}} \frac{1 - Y_{g_{i,r}}}{Y_{g_{i,r}}} \right] - R_{s_{i,r,l}} - l_{C_{i,r,l}}$; root/rhizoid/mycorrhizal growth driven by R_g (G8)

$\frac{\Delta L_{i,r,l,1}}{\Delta t} = \frac{\frac{\Delta M_{R_{i,r,l,1}}}{\Delta t}}{y_i} \frac{\nu_r}{\rho_r \pi r_{r_{i,r,l,1}}^2 \left(1 - \theta_{pr_{i,r}}\right)}$; extension of primary root/rhizoid/mycorrhizal axis driven by root/rhizoid/mycorrhizal mass growth (G9)

$\frac{\Delta L_{i,r,l,2}}{\Delta t} = \frac{\Delta M_{R_{i,r,l,2}}}{\Delta t} \frac{\nu_r}{\rho_r \pi r_{r_{i,r,l,2}}^2 (1 - \theta_{pr_{i,r}})}$; extension of secondary root/rhizoid/mycorrhizal axis driven by root/rhizoid/mycorrhizal mass growth (G10)

Where, subscripts *i*=species or plant functional type (PFT), *j*=branch/tiller, *l*=soil or canopy layer, *z*=organ (root/rhizoid/mycorrhizae (*r*), canopy, stem, mycorrhizae); R_a= total autotrophic respiration (g C m^{-2} h^{-1}); R_c= autotrophic respiration of σ_C (g C m^{-2} h^{-1}), *1*=primary

root/rhizoid/mycorrhizal axis, *2*=secondary root/rhizoid/mycorrhizal axis; R_s=respiration from remobilization of leaf carbon (g C m^{-2} h^{-1}); $E_{N,P}$=energy cost of nutrient uptake (=2.15 g C g N^{-1} or P^{-1}) (Veen 1981); U_{NH_4}=NH_4^+ uptake by root/rhizoid/mycorrhizae (g N m^{-2} h^{-1}); U_{NO_3} = NO_3^- uptake by root/rhizoid/mycorrhizae (g N m^{-2} h^{-1}); U_{PO_4} = $H_2PO_4^-$ uptake by root/rhizoid/mycorrhizae (g P m^{-2} h^{-1}); R'_c=specific autotrophic respiration of σ_C at 25°C (=0.015 g C g C^{-1} h^{-1}); σ_C= non-structural C product of CO_2 fixation (g C g C^{-1}); f_{Ta}=temperature effect on R_a; U_{O_2} = O_2 uptake by root/rhizoid/mycorrhizae under ambient O_2 (g O m^{-2} h^{-1}); U'_{O_2} = O_2 uptake by root/rhizoid/mycorrhizae under non-limiting O_2 (g O m^{-2} h^{-1}); [O_{2r}]= aqueous O_2 concentration at root/rhizoid/mycorrhizal surfaces (g m^{-3}); K_{O_2} = Michaelis-Menten constant for root/rhizoid/mycorrhizal O_2 uptake (=0.064 g m^{-3}) (Griffin 1972); U_w= root/rhizoid/mycorrhizal water uptake flux (m^3 m^{-2} h^{-1}); [O_{2s}]= aqueous O_2 concentration is soil (g m^{-3}); L= root/rhizoid/mycorrhizal length (m m^{-2}); $D_{s_{O_2}}$=aqueous diffusivity of O_2 from soil to root/rhizoid/mycorrhizal surfaces (m^2 h^{-1}); r_s= thickness of soil water films (m); r_r= root/rhizoid/mycorrhizal radius (=1.0 × 10^{-4} m); $D_{s_{O_2}}$ =aqueous diffusivity of O_2 from root/mycorrhizal aerenchyma to root/ mycorrhizal surfaces (m^2 h^{-1}); [O_{2q}]=aqueous O_2 concentration in root/mycorrhizal aerenchyma (g m^{-3}); r_q= radius of root/mycorrhizal aerenchyma (m); R_a' = R_a under non-limiting O_2 (g C m^{-2} h^{-1}); R_m= above-ground maintenance respiration (g C m^{-2} h^{-1}); N=number of species, or branch/tiller or organs; R_m'= specific maintenance respiration of σ_C at 25°C (=0.0115 g C g N^{-1} h^{-1}) (Barnes et al. 1997); f_{Tm}= temperature effect on R_m (Q_{10}=2.25); R_g=growth respiration (g C m^{-2} h^{-1}); ψ_t= canopy turgor potential (MPa); ψ_t'=canopy turgor potential (MPa) at ψ_c=0 MPa; M_R=; t=time (h); Y_g= fraction of σ_C used for growth expended as R_g by organ z (g C g C^{-1}) [0.28 (z = leaf), 0.24 (z = root/rhizoid/mycorrhizae and other non-foliar), 0.20 (z = wood)] (Waring and Running 1998); l_C=carbon litter fall from leaf or root/rhizoid/mycorrhizae (g C m^{-2} h^{-1}) ; y=plant population (m^{-2}); v_r= specific volume of root/rhizoid/mycorrhizal biomass (m^3 g^{-1}); and θ_{pr}= root/mycorrhizal porosity representing aerenchyma fraction (m^3 m^{-3}).

Appendix H: Gas flux

$$Q_{ds\gamma_s} = \alpha_{gs_s} D_{d\gamma} \left(S'_\gamma f_{T_{d\gamma_s}} \left[\gamma_{gs}\right]_s - \left[\gamma_{ss}\right]_s \right);$$ volatilization-dissolution between aqueous and gaseous phases in soil (H1)

$$Q_{dr\gamma_s} = \alpha_{gr_s} D_{d\gamma} \left(S'_\gamma f_{T_{d\gamma_s}} \left[\gamma_{gr}\right]_s - \left[\gamma_{sr}\right]_s \right);$$ volatilization-dissolution between aqueous and gaseous phases in roots (H2)

$$Q_{gs\gamma_i} = -Q_{w_i} \left[\gamma_{gs}\right]_s + \frac{2D_{gs\gamma_i} \left(\left[\gamma_{gs}\right]_s - \left[\gamma_{gs}\right]_d \right)}{L_{s_i} + L_{d_i}};$$ 3D convective-conductive gas flux between two adjacent grid cells (H3)

$$Q_{gr\gamma_{i=z}} = \frac{D_{gr\gamma_{i=z}}\left(\left[\gamma_{gr}\right]_d - \left[\gamma_a\right]\right)}{\sum_{1,i=z} L_{d_{i=z}}}$$; convective-conductive gas flux between root and the atmosphere (H4)

$$D_{gs\gamma_i} = \frac{D'_{g\gamma} f_{T_{g_s}} \left[0.5\left(\theta_{g_s} + \theta_{g_d}\right)\right]^2}{\theta_{P_s}^{0.67}}$$; 3D gaseous diffusivity between two adjacent grid cells as functions of air-filled porosities in those cells (H5)

$$D_{gr\gamma_{i=z}} = \frac{D'_{g\gamma} f_{T_{g_s}} \theta_{pr_s}^{1.33} A_{r_s}}{A_{i=x,y}}$$; gaseous diffusivity as a function of air-filled porosity in the roots/mycorrhizae (H6)

Where, subscripts i=dimensions (i=*x, y, z*), s=source cell, d=destination cell; $Q_{ds\gamma}$=volatilization – dissolution of gas γ between aqueous and gaseous phases in soil (g m^{-2} h^{-1}); α_{gs}=air-water interfacial area in soil (m^2 m^{-2}); $D_{d\gamma}$= volatilization - dissolution transfer coefficient for gas γ (m^2 h^{-1}); S'_γ=Ostwald solubility coefficient of gas γ at 30°C (0.0293 for $\gamma = O_2$) (Wilhelm et al. 1977); $f_{T_{d\gamma}}$ =temperature dependence of S'_γ (Wilhelm et al. 1977); [γ_{gs}]=gaseous concentration of gas γ in soil (g m^{-3}); [γ_{ss}]= aqueous concentration of gas γ in soil (g m^{-3}); $Q_{dr\gamma}$= volatilization – dissolution of gas γ between aqueous and gaseous phases in root/rhizoid (g m^{-2} h^{-1}); α_{gr}= air-water interfacial area in root/mycorrhizae (m^2 m^{-2}) (Skopp 1985); [γ_{gr}]= gaseous concentration of gas γ in root/mycorrhizae (g m^{-3}); [γ_{sr}]= aqueous concentration of gas γ in root/rhizoid/mycorrhizae (g m^{-3}); $Q_{gs\gamma}$= gaseous flux of gas γ in soil (g m^{-2} h^{-1}); Q_w=sub-surface water flux (m^3 m^{-2} h^{-1}); $D_{gs\gamma}$=gaseous diffusivity of gas γ in soil (m^2 h^{-1}) (Millington and Quirk 1960); L=length of grid cells (m); $Q_{gr\gamma}$=gaseous flux of gas γ between root/mycorrhizae and the atmosphere (m^2 h^{-1}); $D_{gr\gamma}$=gaseous diffusivity of gas γ in root/mycorrhizae (m^2 h^{-1}) (Luxmoore et al. 1970a, b); [γ_a]=atmospheric concentration of gas γ (g m^{-3}); $D'_{g\gamma}$ =diffusivity of gas γ in air at 0°C (m^2 h^{-1}) (6.43×10^{-2} m^2 h^{-1} for γ=O_2) (Campbell 1985); f_{T_g} =temperature dependence of $D'_{g\gamma}$ (Campbell 1985); θ_g=air-filled porosity (m^3 m^{-3}); θ_P=total porosity of soil (m^3 m^{-3}); θ_{pr}= root/mycorrhizal porosity representing aerenchyma fraction (m^3 m^{-3}); A_r= root cross-sectional area (m^2); and A=area of landscape position (m^2).

Chapter 5 : Process-based Modelling of Effects of Interannual Variation in Water Table Depth on Net CO_2 Exchange of a Western Canadian Boreal Fen

5-1. Introduction

Northern boreal peatlands have been accumulating carbon (C) at a rate of about 20-30 g yr^{-1} over several thousand years (Gorham 1991, Turunen et al. 2002, Flanagan and Syed 2011, Yu 2012). This long-term C accumulation has been sustained by decomposition slower than net primary productivity (NPP) as a result of wet hydrologic conditions under shallow and/or above-ground water table (WT). Drier and warmer future climates, however, can affect the permanence of these C sinks and the resilience of these C stocks by lowering WT. This deepening of water table depth (WTD) can result in decomposition greater than NPP and hence can halt or even reverse these C accumulations (Limpens et al. 2008, Dise 2009, Frolking et al. 2011). To maintain the C sequestration potentials of these peatlands and to protect these from possible degradation we need an improved predictive capacity of how these C stocks would behave under future drier and warmer climates. However, northern peatland C processes are currently under-represented in global C models mainly due to inadequate understanding and consequent inability to simulate hydrologic feedbacks to northern boreal peatland C cycles (St-Hilaire et al. 2010, Sulman et al. 2012, Waddington et al. 2015). This inability can, however, be overcome by (1) improving our understanding of process-based interactions among hydrology, ecology and biogeochemistry of these peatlands, (2) integrating these understandings into spatially and temporally high resolution process models tested against site measurements and (3) scaling up the most important feedbacks into larger spatial and temporal scale C models (Waddington et al. 2015).

The hydrologic feedbacks to northern boreal peatland C processes are highly non-linear and largely mediated by WTD variation and its effects on peat-microbe-plant-atmosphere exchanges of C, energy, water and nutrients. WTD drawdown can reduce net ecosystem productivity (NEP) of northern boreal peatlands by raising ecosystem respiration (R_e). WTD drawdown can cause peat pore drainage and hence can improve peat aeration that in turns enhances microbial O_2 availability, energy yields, growth and decomposition that eventually increases ecosystem respiration (R_e) (Ise et al. 2008, Sulman et al. 2009, Cai et al. 2010, Sulman et al. 2010, Flanagan and Syed 2011, Peichl et al. 2014). The rate of increase in R_e due to the WTD drawdown, however, may vary with peat moisture retention and quality of peat forming substrates. For instance, peats with low moisture retention exhibit more rapid pore drainage and hence aeration than those with high moisture retention thus causing more increase in R_e for similar WTD drawdowns (Parmentier et al. 2009, Sulman et al. 2009, Cai et al. 2010, Sulman et al. 2010). Peats formed from *Sphagnum* mosses degrade at rates slower than those formed from remains of vascular plants (Moore and Basiliko 2006). So for similar WTD drawdowns, moss peats would generate less increase in microbial decomposition (Updegraff et al. 1995) and hence R_e than would sedge, reed or woody peats. Continued WTD drawdown can, however, cause near surface peat desiccation from inadequate recharge through capillary rise from deeper WT. This desiccation can cause a reduction in microbial decomposition that can partially or fully offset the increased decomposition in the deeper peat layers thereby yielding indistinct net effects of WTD drawdown on R_e (Dimitrov et al. 2010a).

Beside R_e, WTD can also affect gross primary productivity (GPP) and hence NEP of northern boreal peatlands. The interactions between WTD and GPP are also non-linear and vary depending upon peat forming vegetation. For instance, increased aeration due to WTD

drawdown enhances root O_2 availability and hence growth in vascular plants. This enhanced root growth in deeper WTD hydroperiods is further associated with greater root nutrient availability and uptake due to more rapid mineralization facilitated by greater microbial energy yields, growth and decomposition. Greater root nutrient uptake in turns increases the rate of vascular CO_2 fixation and hence gross primary productivity (GPP) (Sulman et al. 2009, Cai et al. 2010, Sulman et al. 2010, Flanagan and Syed 2011, Peichl et al. 2014). This WTD drawdown, however, does not affect the non-vascular (e.g. moss) GPP in the same way it does the vascular GPP. These non-vascular plants usually have very shallow rhizoids and mostly depend upon the available water for uptake in the near surface peat layers. These layers can drain quickly with WTD drawdown and thus have to depend on moisture supply through capillary rise from deeper WT. If recharge through the capillary rise is not adequate, near surface peat desiccation occurs which in turn slows rhizoid water uptake and eventual drying of mosses that reduces moss GPP (Lafleur et al. 2005, Riutta 2008, Sonnentag et al. 2010, Sulman et al. 2010, Dimitrov et al. 2011, Kuiper et al. 2014, Peichl et al. 2014). This near surface peat desiccation caused by WTD drawdown also suppresses vascular root water uptake from those desiccated layers. However, enhanced root growth and elongation facilitated by improved O_2 status in the newly aerated deeper peat layers during the deeper WTD hydroperiods enables vascular roots to uptake water from these wetter deeper layers. If this deeper root water uptake offsets the reduction in water uptake from desiccated near surface layers, vascular transpiration (T), canopy stomatal conductance (g_c) and hence GPP are sustained during deep WTD hydroperiods. But if the WT falls below certain threshold level below which this deeper root water uptake can no longer sustain vascular T, reductions in g_c and hence vascular GPP occur (Wu et al. 2010, Dimitrov et al. 2011).

Therefore, WTD variation can affect northern boreal peatland NEP through its effects on peat moisture and aeration and consequent root and microbial oxidation-reduction reactions and energy yields. So to better understand how these peatlands would behave under future drier and warmer climates, a peatland C model needs to have adequate representation of WTD dynamics that determine the boundary between aerobic and anaerobic zones thereby controlling peat biogeochemistry. However, most of the current process-based C models that simulate peatland C balance (1) either do not have prognostic WTD dynamics that prevent these models from simulating a continuous anaerobic zone below WT (e.g. Baker et al. 2008, Schaefer et al. 2008, Tian et al. 2010), or (2) do not simulate peat saturation since any water in excess of field capacity is drained in these models (e.g. Gerten et al. 2004, Krinner et al. 2005, Weng and Luo 2008). Moreover, instead of explicitly simulating the above-described hydrological and biological interactions between peat aeration and biogeochemistry, most of these models use scalar functions of soil moisture contents to inhibit R_e and GPP in low or high moisture conditions (e.g. Frolking et al. 2002, Zhang et al. 2002, Bond-Lamberty et al. 2007, St-Hilaire et al. 2010, Sulman et al. 2012). Consequently, these peatland C models failed to simulate decrease in GPP and R_e due to shallow WTD periods while modelling WTD effects on peatland C processes across Northern US and Canadian peatlands (Sulman et al. 2012). Furthermore, the approach of using scalar functions to simulate moisture limitations to GPP and R_e requires site-specific parameterization of these functions thereby making this approach less suitable when scaling up across different peatlands.

5-1.1. Objective and rationale

Unlike those peatland C models mentioned above, the general purpose process-based terrestrial ecosystem model *ecosys* includes a prognostic, dynamic WTD and soil moisture

retention that are coupled with (1) microbial oxidation-reduction reactions, energy yields, decomposition, growth and uptake for different substrate qualities (e.g. labile vs. recalcitrant) and (2) root oxidation-reduction reactions, growth and uptake in soil-plant-atmosphere water, C and nutrient (N, P) schemes. This coupling of hydrology with physiology and biogeochemistry enabled *ecosys* to successfully simulate WTD effects on net ecosystem CO_2 exchange of two contrasting bog peatlands e.g. a northern boreal bog at Mer Bleue, Ontario, Canada (Dimitrov et al. 2011) and a tropical bog at Palangkaraya, Central Kalimantan, Indonesia (Chapter 3) and a northern boreal fen peatland at Lost Creek, Wisconsin, USA (Grant et al. 2012b). This testing of *ecosys* algorithms representing hydrological, biological and ecological feedbacks against site measurements across those contrasting peatlands provided an excellent opportunity for rigorous testing of the versatility of those feedbacks in a process-based C model in simulating WTD effects on C balance across peatlands. Since these WTD feedbacks to peatland C processes are highly site-specific, this high spatial resolution testing of these feedbacks in *ecosys* across contrasting peatlands would thus provide an important platform for scaling up simulations of those feedbacks across peatlands at larger spatial scales i.e., national, regional, continental or global which is currently not available. Waddington et al. (2015) in their reviews of conceptual modelling of feedbacks among key peatland processes also suggested a similar approach as ours to develop a generalized process model to simulate peatland eco-hydrology on a regional/global scale. As an extension of this endeavour, the present study aims at deploying *ecosys* in simulating effects of WTD variation on NEP of a Western Canadian boreal fen peatland (WPL) (Syed et al. 2006) in Alberta, Canada. This study would use similar coupling of hydrological, biological and ecological feedback algorithms as in those previous studies along with an improved soil moisture retention function (Chapter 4) fed by site specific inputs measured at the

WPL. The modelled outputs for net ecosystem CO_2 exchange and WTD would be tested against site measurements at the WPL o rigorously examine the accuracy with which *ecosys* simulates diurnal, seasonal and interannual variations in net CO_2 exchange as affected by variations in WTD. Gradually declining WT at the WPL from 2004-2009 as observed by Flanagan and Syed (2011) provided an opportunity to test the robustness of *ecosys* algorithms of peatland eco-hydrology under changing WTD. The tested modelled outputs would be further examined to explain the WTD effects on C processes at this northern boreal fen.

Ecosys previously simulated WTD effects on C processes of a northern boreal fen peatland at Lost Creek, USA (Grant et al. 2012b). However, the fen peatland in the current study differs from the Lost Creek peatland in peat forming vegetation, peat substrate and peat depth that can yield contrasting WTD feedbacks to net CO_2 exchange between these two northern boreal fen peatlands. WPL peatland is co-dominated by trees, shrubs and mosses (Syed et al. 2006) as opposed to the Lost Creek peatland that is co-dominated by shrubs and sedges (Sulman et al. 2009). The presence of both vascular and non-vascular plant functional types (PFTs) at the WPL thus might produce contrasting WTD effects on vascular vs. non-vascular GPP that was absent in the Lost Creek peatland due to the absence of non-vascular PFT. Moreover, the peat substrate at the WPL originates from a mixture of remains of *Sphagnum* mosses, trees and shrubs as opposed to the shrub and sedge originated substrate at the Lost Creek peatland. This differences in the peat substrates might yield differential WTD feedback to peat decomposition and hence R_e between these two peatlands. Furthermore, peat deposition in the Lost Creek peatland is much shallower (~0.25-0.50 m) (Sulman et al. 2009) than that in the WPL (~2 m) (Syed et al. 2006). This difference might also contribute to the contrasting WTD effects on GPP and/or R_e and hence NEP between these two peatlands since the autotrophic and heterotrophic

processes in the rhizosphere of Lost Creek peatland is more frequently affected by the mineral soil processes than those in the WPL. So the above-discussed differences in the interactions between hydrology, biogeochemistry and ecology between these two fen peatlands would further provide us with an opportunity to test the adequacy of *ecosys* algorithms representing these interactions in simulating WTD effects on net ecosystem CO_2 exchange across contrasting northern boreal fen peatlands.

5-1.2. Hypotheses

In a field study using eddy covariance (EC) micro-meteorological approach, Flanagan and Syed (2011) found no net effect of WTD drawdown from 2004-2009 caused by progressively drier and warmer weather on NEP of WPL. From the regressions of EC-derived GPP and R_e on site measured WTD, they inferred that the absence of a net effect on NEP was caused by similar increases in GPP and R_e with WTD drawdown. We hypothesize that a prognostic, dynamic WTD driven by equilibrium between vertical and lateral water fluxes that determines root and microbial redox reactions and energy yields, microbial decomposition, root and microbial growth and uptake in *ecosys* would be able to simulate these effects of WTD drawdown on GPP and R_e and hence NEP at the WPL. For this purpose we formulate the following four modelling hypotheses to simulate WTD effects on R_e and GPP of WPL:

(1) WTD drawdown in *ecosys* would cause peat pore drainage and improve peat aeration that in turns would increase the energy yields from aerobic vs. anaerobic microbial decomposition and hence would increase R_e in the modelled WPL ecosystem.

(2) Enhanced microbial activity due to WTD drawdown in *ecosys* would also cause more rapid nutrient mineralization and consequent greater root nutrient availability and uptake, greater leaf nutrient concentrations and hence increased GPP.

(3) But when the WT falls below a certain threshold level, inadequate recharge of the near surface peat layers through capillary rise would cause desiccation of those layers. This drying of near surface peat layers as well as the surface residue can reduce near surface and surface peat respiration that can partially offset the increase in deeper peat respiration due to aeration in hypothesis 1.

(4) This near surface peat desiccation would also reduce peat water potential and hydraulic conductivity and hence root and rhizoid water uptake from those near surface layers. Since rhizoids are shallow and depend mainly on those near surface peat layers for moisture supply, reduction in rhizoid water uptake would thus cause a reduction in non-vascular (moss) water potential and hence moss GPP. Suppression of root water uptake by deeper rooted vascular PFTs from those near surface layers during this deeper WTD hydroperiod would, however, be offset by increased root water uptake from newly aerated deeper peat layers with higher water potentials and hence would sustain vascular canopy water potential (ψ_c), canopy stomatal conductance (g_c) and GPP.

5-2. Methods

5-2.1. Model development

Ecosys is a process-based general purpose terrestrial ecosystem model that successfully simulated 3D water, energy, carbon and nutrient (N, P) cycles in different peatlands (e.g. Dimitrov et al. 2011, Grant et al. 2012b, Sulman et al. 2012) (Chapters 2 and 3). *Ecosys*

algorithms that govern the effects of WTD variations on ecosystem net CO_2 exchange which are related to our hypotheses are described below. The equations that are listed in the supplementary material are cited in the text within round brackets with a letter representing a particular appendix followed by the equation number.

5-2.1.1. Water table depth (WTD)

The WTD in *ecosys* is the depth at which the residual between lateral water influx (recharge) and efflux (discharge) is in equilibrium with that between vertical influx (precipitation) and efflux (evapotranspiration). This WTD is thus not prescribed, but rather controls, and is controlled by, vertical and lateral surface and sub-surface water fluxes (D1-D10). The WTD in *ecosys* is calculated at the end of each time step as the depth to the top of the saturated zone below which air-filled porosity is zero. The lateral water flux in *ecosys* is governed by the lateral sub-surface boundary condition. This lateral sub-surface boundary condition in *ecosys* is defined by a specified external WTD (WTD_x) and a specified lateral distance (L_t) over which lateral sub-surface water flow occurs (Fig. 5-1). This WTD_x represents average WTD of the surrounding watershed with which modelled boundary grid cells exchange water. The rates of the lateral water fluxes are governed by the hydraulic gradient between the WTD within the modelled grid cell and WTD_x over L_t in a Darcy's equation, and by macropore and matrix hydraulic conductivity of the soil layer in which these water transfers occur (D10, D10a). Thus when WTD within modelled grid cells is shallower than WTD_x, discharge through the model lateral boundary occurs (D10) and when WTD falls below WTD_x recharge into the modelled grid cells occurs (D10a) (Fig. 5-1). Fen peatlands are known to gain water from upland ecosystems through lateral recharge. To accommodate this effect of catchment hydrology on fen peatland WTD, we set the WTD_x at different levels based on the annual wetness of weather e.g.

shallow WTD_x for wetter years, intermediate WTD_x for regular years, and deep WTD_x for drier years (Fig. 5-1). This scheme simulates hydraulic gradients between modelled WTD and the WTD_x for larger lateral recharge than discharge resulting in net lateral water gain in wetter years and vice-versa (Fig. 5-1) (D10, D10a).

5-2.1.2. Heterotrophic respiration and WTD

WTD fluctuation in *ecosys*, which arises from variations in the balance between vertical and lateral fluxes, determines the boundary between and hence the extent of aerobic vs. anaerobic soil zones. These in turn affect organic oxidation-reduction transformations and hence microbial energy yields, which drive microbial growth, hence substrate decomposition and uptake (A1-A30). Organic transformations in *ecosys* occur in a residue layer and in each of the soil layers within five organic matter-microbe complexes i.e. coarse woody litter, fine non-woody litter, animal manure, particulate organic C and humus. Each of these complexes has three decomposition substrates i.e. solid organic C, sorbed organic C and microbial residue C; the decomposition agent i.e. microbial biomass; and the decomposition product i.e. dissolved organic C (DOC). Rates of the decomposition and resulting DOC production in each of these complexes is a first-order function of the fraction of substrate colonized by active biomasses (M) of diverse microbial functional types (MFTs). These MFTs in *ecosys* are obligate aerobes (bacteria and fungi), facultative anaerobes (denitrifiers), obligate anaerobes (fermenters), heterotrophic (acetotrophic) and autotrophic (hydrogenotrophic) methanogens, and aerobic and anaerobic heterotrophic diazotrophs (non-symbiotic N_2 fixers) (A1, A2, A4). Biomass (M) growth of each of these MFTs (A25) is calculated from their DOC uptake (A21). The rate of M growth is driven by energy yield from growth respiration (R_g) (A20) that is calculated by subtracting maintenance respiration (R_m) (A18) from heterotrophic respiration (R_h) (A11). The

values of R_h are driven by oxidation of DOC (A13). This oxidation may be limited by microbial O_2 reduction (A14) driven by microbial O_2 demand (A16) and constrained by O_2 diffusion calculated from aqueous O_2 concentrations in soil ($[O_{2s}]$) (A17). Values of $[O_{2s}]$ are maintained by convective-dispersive transport of O_2 from the atmosphere to gaseous and aqueous phases of the soil surface layer (D15), by convective-dispersive transport of O_2 through gaseous and aqueous phases in adjacent soil layers (D16, D19), and by dissolution of O_2 from gaseous to aqueous phases within each soil layer (D14a).

Shallow WTD in *ecosys* can cause lower air-filled porosity (θ_g) due to the higher moisture content in the peat layers above the WT. This reduces O_2 diffusivity in the gaseous phase (D_g) (D17) and hence gaseous O_2 transport (D16) in these layers. However, the peat layers below the WT have zero θ_g that prevents gaseous O_2 transport in these layers. So during shallow WTD hydroperiods, $[O_{2s}]$ relies more on O_2 transport through the slower aqueous phase (D19) which causes a decline in $[O_{2s}]$. This decline slows O_2 uptake (A17) and hence R_h (A14), R_g (A20) and growth of M (A25). Lower M in turn slows decomposition of organic C (A1, A2) and production of DOC which further slows R_h (A13), R_g and growth of M. Although some MFTs can sustain DOC oxidation by reducing alternative electron acceptors (e.g. methanogens reducing acetate or CO_2 to CH_4, and denitrifiers reducing NO_x to N_2O or N_2), lower energy yields from these reactions reduce R_g (A21), and hence M growth, organic C decomposition and subsequent DOC production. Slower decomposition of organic C under low $[O_{2s}]$ also causes slower decomposition of organic nitrogen and phosphorus (A7) and production of dissolved organic nitrogen (DON) and phosphorus (DOP), which causes slower uptake of microbial nitrogen and phosphorus (A22) and hence growth of M (A29). This slower growth causes slower mineralization (A26), and hence lowers aqueous concentrations of NH_4^+, NO_3^- and $H_2PO_4^-$.

WTD drawdown can cause peat pore drainage and hence an increase in θ_g that results in greater D_g (D17) and hence more rapid gaseous O_2 transport. A consequent rise in [O_{2s}] increases O_2 uptake (A17) and hence R_h (A14), R_g (A20) and growth of M (A25). Larger M in turn hastens decomposition of organic C (A1, A2) and production of DOC which further hastens R_h (A13), R_g and growth of M. More rapid decomposition of organic C under adequate [O_{2s}] in this period also causes more rapid decomposition of organic nitrogen and phosphorus (A7) and production of DON and DOP, which increases uptake of microbial nitrogen and phosphorus (A22) and hence growth of M (A29). This rapid growth causes rapid mineralization (A26), and hence greater aqueous concentrations of NH_4^+, NO_3^- and $H_2PO_4^-$.

However, when WTD recedes below a certain threshold level, capillary rise from the WT (D9a) can no longer support adequate recharge of the near surface peat layers and the surface litter. This causes desiccation of the residue and the near surface peat layers thereby causing a reduction in water potential (ψ_s) and hence an increase in aqueous microbial concentrations [M] (A15) in each of these layers. The increased [M] caused by the peat desiccation reduces microbial access to the substrate for decomposition in each of these layers and hence reduces R_h (A13). This reduction in R_h is calculated in *ecosys* from competitive inhibition of microbial exo-enzymes with increasing concentrations (A4) (Lizama and Suzuki 1991).

5-2.1.3. WTD effects on vascular gross primary productivity

WTD variation effects on vascular gross primary productivity (GPP) in *ecosys* is simulated from the effects of WTD variation on root O_2 and nutrient availability and hence root growth and uptake, and plant water relations in a hydraulically driven soil-plant-atmosphere water scheme. Root growth in each vascular plant population in *ecosys* is calculated from its assimilation of the non-structural C product of CO_2 fixation (σ_C) (C20). Assimilation is driven

by R_g (C17) remaining after subtracting R_m (C16) from autotrophic respiration (R_a) (C13) driven by oxidation of σ_C (C14). This oxidation in roots may be limited by root O_2 reduction (C14b) which is driven by root O_2 demand to sustain C oxidation and nutrient uptake (C14e), and constrained by O_2 uptake controlled by concentrations of aqueous O_2 in the soil ($[O_{2s}]$) and roots ($[O_{2r}]$) (C14d). Values of $[O_{2s}]$ and $[O_{2r}]$ are maintained by convective-dispersive transport of O_2 through soil gaseous and aqueous phases and root gaseous phase (aerenchyma) respectively and by dissolution of O_2 from soil and root gaseous to aqueous phases (D14b, D16, D17, D19). O_2 transport through root aerenchyma depends on species-specific values used for root air-filled porosity (θ_{pr}) (D17b). Shallow WTD and resultant high peat moisture content in *ecosys* can cause low θ_g that reduces soil O_2 transport, forcing root O_2 uptake to rely more on $[O_{2r}]$ and hence on root O_2 transport determined by θ_{pr}. If this transport is inadequate, decline in $[O_{2r}]$ slows root O_2 uptake (C14c, d) and hence R_a (C14b), R_g (C17) and root growth (C20b) and root nitrogen and phosphorus uptake (C23b, d, f). Root nitrogen and phosphorus uptake in this hydroperiod is further slowed by reductions in aqueous concentrations of NH_4^+, NO_3^- and $H_2PO_4^-$ (C23a, c, e) from slower mineralization of organic nitrogen and phosphorus as described in Sect. 5-2.1.2. Slower root nitrogen and phosphorus uptake in turn reduces concentrations of non-structural nitrogen and phosphorus products of root uptake (σ_N and σ_P) with respect to that of σ_C in leaves (C11), thereby slowing CO_2 fixation (C6) and hence GPP.

WTD drawdown facilitates rapid D_g which allows root O_2 demand to be almost entirely met from $[O_{2s}]$ (C14c, d) and so enables more rapid root growth and nitrogen and phosphorus uptake (C23b, d, f). Increased root growth and nutrient uptake is further stimulated by increased aqueous concentrations of NH_4^+, NO_3^- and $H_2PO_4^-$ (C23a, c, e) from more rapid mineralization of organic nitrogen and phosphorus during this hydroperiod as described in Sect. 5-2.1.2. Greater

root nitrogen and phosphorus uptake in turn increases concentrations of σ_N and σ_P with respect to σ_C in leaves (C11), thereby facilitating rapid CO_2 fixation (C6) and hence GPP. However, when WTD falls below a certain threshold, inadequate capillary rise (D9a) causes near-surface peat desiccation, reducing soil water potential (ψ_s) and increasing soil hydraulic resistance (Ω_s) (B9), forcing lower root water uptake (U_w) from these desiccated layers (B6). But deeper rooting facilitated by increased [O_{2s}] in this period can sustain U_w (B6) from wetter deeper peat layers with higher ψ_s and lower Ω_s (B9). If this U_w from the deeper wetter layers cannot offset the suppression in U_w from desiccated near surface layers, the resultant net decrease in U_w causes a reduction in root, canopy and turgor potentials (ψ_r, ψ_c and ψ_t) (B4) and hence g_c (B2b) in *ecosys* when equilibrating U_w with transpiration (T) (B14). Lower g_c in turn reduces CO_2 diffusion into the leaves thereby reducing CO_2 fixation (C6) and hence GPP (C1) during this hydroperiod.

5-2.1.4. WTD effects on non-vascular gross primary productivity

Effects of WTD drawdown on non-vascular (e.g. moss) GPP in *ecosys* is simulated from the interaction between shallow moss rhizoid depth and peat moisture supplying capacity through capillary rise from the WT to adequately recharge these shallow peat layers to sustain rhizoid U_w. Shallow moss rhizoid depth in *ecosys* is simulated from intra-specific competition for light and nutrients (N, P) among small plants with large populations because root and rhizoid growth are simulated for individual plants and then scaled to the population. *Ecosys* model input for moss population is usually larger and hence intra-specific competition is greater so that individual moss plant and the downward growth of rhizoid is smaller (C21b). Absence of aerenchyma in moss rhizoids further hinders rhizoid O_2 status and hence oxidation of σ_C that further slows moss rhizoid growth respiration (R_g) and growth in wet deeper peat layers where [O_{2s}] is inadequate for σ_C oxidation (C14, C17). This limits moss rhizoids mostly to near surface

peat layers that are frequently unsaturated. When WT deepens past a threshold level, inadequate capillary rise (D9a) causes near-surface peat desiccation, thereby reducing ψ_s and increasing Ω_s (B9) of those layers. This in turns causes a reduction in moss canopy water potential (ψ_c) while equilibrating moss E with U_w (B6). Reduced moss ψ_c causes a reduction in moss carboxylation rate (C3, C6a) and hence moss GPP (C1).

5-2.2. Modelling experiment

5-2.2.1. Study site

The algorithms for effects of WTD variations on ecosystem net CO_2 exchange in *ecosys* are tested in this study against measurements of WTD and ecosystem net CO_2 fluxes from 2003 to 2009 at a flux station of the Fluxnet-Canada Research Network established at the WPL (latitude: 54.95°N, longitude: 112.47°W). The study site is a moderately nutrient-rich treed fen peatland within the Central Mixed-wood Sub-region of Boreal Alberta, Canada. Peat depth around the flux station was about 2 m. This peatland is dominated by stunted trees of black spruce (*Picea mariana*) and tamarack (*Larix laricina*) with an average canopy height of 3 m. High abundance of a shrub species *Betula pumila* (dwarf birch), and the presence of a wide range of mosses e.g. *Sphagnum* spp., feather moss, and brown moss characterize the under-storey vegetation of WPL. The topographic, climatic, edaphic and vegetative characteristics of this site were described in more details by Syed et al. (2006).

5-2.2.2. Field data sets

Ecosys model inputs of half hourly weather variables i.e. incoming shortwave and longwave radiation, air temperature, wind speed, precipitation and relative humidity during 2003-2009 were measured by Syed et al. (2006) and Flanagan and Syed (2011) at the

micrometeorological station established at WPL. To test the adequacy of WTD simulation in *ecosys*, modelled outputs of hourly WTD were tested against WTD measured at the WPL with respect to average hummock surface by Flanagan and Syed (2011). To examine how well *ecosys* simulated net ecosystem CO_2 exchange at the WPL, we tested hourly modelled net ecosystem CO_2 fluxes against those measured by using eddy covariance (EC) micro-meteorological approach by Syed et al. (2006) and Flanagan and Syed (2011). Each of these EC-measured net CO_2 fluxes consisted of an eddy flux and a storage flux (Syed et al. 2006). Erroneous flux measurements due to stable air conditions were screened out by Syed et al. (2006) and Flanagan and Syed (2011) with the use of a minimum friction velocity (u^*) threshold of 0.15 m s^{-1}. The data gaps resulting from this quality control were filled to estimate annual NEP. The resultant EC measured and gap-filled NEP were again partitioned to derive GPP and R_e. These gap-filling and partitioning of NEP were done by Syed et al. (2006) and Flanagan and Syed (2011) who followed standard procedure of Fluxnet-Canada research network described by Barr et al. (2004) except for energy balance closure adjustment.

Soil CO_2 fluxes measured by automated chambers can provide a valuable supplement to EC CO_2 fluxes in testing modelled respiration by providing more continuous measurements than EC. So, we also tested our modelled outputs against half-hourly automated chamber measurements by Cai et al. (2010) at the WPL. These CO_2 flux measurements were carried out over both hummocks and hollows by using a total of 9 steady-state transparent chambers (Cai et al. 2010). Apart from soil respiration these chamber CO_2 fluxes thus included fixation and autotrophic respiration from dwarf shrubs, herbs and mosses (Cai et al. 2010). Therefore we compared modelled fixation and autotrophic respiration from understorey PFTs (e.g. shrub and moss) combined with modelled soil respiration against these chamber net CO_2 fluxes measured

at the WPL. For this purpose net CO_2 flux measurements from all of those chambers were averaged and compared against average soil and understorey CO_2 fluxes modelled over the hummock and the hollow.

5-2.2.3. Model runs

The *ecosys* model run to simulate WTD effects on net CO_2 exchange of WPL had a hummock and a hollow grid cell of 1 m × 1 m intended to represent site micro-topography (Fig. 5-1). These two modelled grid cells exchanged water, heat, carbon and nutrients (N, P) between them and with surrounding vertical and lateral boundaries. The hollow grid cell had near surface peat layer that was 0.3 m thinner than the hummock cell representing a hummock-hollow surface difference of 0.3 m observed in the field (Long 2008b) (Fig. 5-1). Any depth with respect to the modelled hollow surface would thus be 0.3 m shallower than the depth with respect to the modelled hummock surface.

Peat organic properties at the WPL were represented in *ecosys* by inputs of total organic C, total nitrogen (N) and total phosphorus (P) measured at the site by Flanagan and Syed (2011) that were averaged for less decomposed layers within 0-0.19 m from the hummock surface and for relatively more decomposed layers underneath (0.19-2.0 m of the hummock) (Fig. 5-1). Input for pH represented relatively high pH measured at the WPL that classified this peatland as a moderately nutrient rich fen (Syed et al. 2006). CEC input in *ecosys* represented high CEC characteristic of moss-derived Albertan peats as measured by Rippy and Nelson (2007). N to P ratios less than 15 in top 0.19 m suggested that the vegetation in WPL was more N limited than P limited (Flanagan and Syed 2011). Moreover, nutrient gain through lateral water inflow in the fen peatland at WPL was also reported by Syed et al. (2006). However, we did not have any site measurement for this lateral nutrient gain to use as inputs in *ecosys*, so we used background wet

deposition rates of 0.5 mg ammonium-N, 0.25 mg nitrate-N and 0.075 mg phosphate-P per litre of precipitation water to simulate this additional source of nutrient input.

Ecosys was run for a spin up period of 1961-2002 under repeating 7-year sequences of hourly weather data (shortwave and longwave radiation, air temperature, wind speed, humidity and precipitation) recorded at the site from 2003 to 2009. Since measurements of these weather variables at the site stopped at the end of September in 2009, we filled October-December weather in 2009 by those measured for the same period in 2008 to complete the 7-year weather sequences in the spin up run. This spin up period allowed CO_2 exchange in the model to achieve stable value through successive weather sequences. The WTD_x for the spin up run was set at 0.19, 0.35, and 0.72 m below the hummock surface (0.11 m above and 0.05 and 0.42 m below the hollow surface) following the shallowest measured WTD in 2003-2005, average measured WTD in 2006-2007, and the deepest measured WTD in 2008-2009 representing a gradual drying trend in overall watershed hydrology (Fig. 5-1). L_t was set to a fixed 100 m in all directions for all years (Fig. 5-1). The lower boundary condition was defined such that there was no exchange of water to represent the presence of clay sediment with very low permeability underlying the peat deposition (Syed et al. 2006) (Fig. 5-1). Further details about *ecosys* model set up to represent the physical and hydrological characteristics of WPL can be found in Chapter 4.

At the beginning of the spin-up run, the hummock grid cell was seeded with evergreen needle leaf and deciduous needle leaf over-storey plant functional types (PFT) to represent the black spruce and tamarack trees at the WPL. The hollow grid cell was seeded with only the deciduous needle leaf over-storey PFTs (to represent tamarack over-storey) excluding the evergreen needle leaf since the black spruce trees were observed to grow only on the raised areas at the WPL. Each of the modelled hummock and the hollow was also seeded with a deciduous

broadleaved vascular (to represent dwarf birch) and a non-vascular (to represent mosses) under-storey PFTs. These PFTs are the same as those in earlier studies with *ecosys* in northern boreal ecosystems (e.g. Grant et al. 2009a, Dimitrov et al. 2011, Grant et al. 2012b). The planting density was such that the population density of the evergreen needle leaf and the deciduous needle leaf PFT was 0.16 and 0.14 m^{-2} at the end of the spin up run after accounting for annual mortality, thereby representing the site-measured population of the two dominant over-storey species during the study period (Syed et al. 2006). The under-storey deciduous broadleaved and moss PFTs had population densities of 0.3 and 500 m^{-2} at the end of the spin up run. To include wetland adaptation, we selected a value of 0.1 for root porosity (θ_{pr}) used in calculating root O_2 transport through aerenchyma (H6) in the two over-storey PFTs. A higher θ_{pr} value of 0.3 for the under-storey vascular PFT was selected to simulate better wetland adaptation in the under-storey vegetation at the WPL. We did not use any porosity for non-vascular moss rhizoids and hence did not simulate O_2 transport through mosses. These input values for vascular θ_{pr} fall within the range of root porosities (0.01-0.34) measured for various plants taken from northern temperate and boreal bogs, fens and reed swamps (Cronk and Fennessy 2001). θ_{pr} in wetland adapted species can also vary with intensity of waterlogging (Cronk and Fennessy 2001). However, the current version of *ecosys* used the set input for θ_{pr} to simulate O_2 transport from atmosphere to rhizosphere through roots which did not vary with intensity in waterlogging. Non-symbiotic N_2 fixation through association of cyanobacteria and mosses are also reported for Canadian boreal forests (Markham 2009). This was represented in *ecosys* as N_2 fixation by non-symbiotic heterotrophic diazotrophs (A27) in the moss canopy.

When the modelled ecosystem attained dynamic carbon equilibrium at the end of the spin-up run, we continued the spin up run from 2003 to 2009 by using a real-time weather

sequence. We tested our outputs from 2004-2009 of the simulation runs against the available site measurements of WTD, net EC CO_2 fluxes and net chamber CO_2 fluxes over those years.

5-2.2.4. Model validation

To examine the adequacy of modelling WTD effects on canopy, root and soil CO_2 fluxes which were summed for net ecosystem CO_2 exchange at the WPL, we spatially averaged hourly net CO_2 fluxes modelled over the hummock and the hollow to represent a 50:50 hummock-hollow ratio and then regressed against hourly EC measured net ecosystem CO_2 fluxes for each year from 2004-2009 with varying WTD. Each of these hourly EC measured net ecosystem CO_2 fluxes used in these regressions is an average of two half-hourly net CO_2 fluxes measured at a friction velocity (u*) greater than 0.15 m s^{-1}. Model performance was evaluated from regression intercepts ($a \rightarrow 0$), slopes ($b \rightarrow 1$) and coefficients of determination ($R^2 \rightarrow 1$) for each study year to test whether there was any systematic divergence between the modelled and EC measured CO_2 fluxes. Similar regressions of modelled vs. gap-filled net CO_2 fluxes were also performed to test for any divergence between the modelled and gap-filled CO_2 fluxes. These regressions based tests are very important since any small divergence between hourly modelled and EC measured as well as between hourly modelled and gap-filled CO_2 fluxes can result in a large divergence between modelled and EC-gap filled annual estimates.

5-2.2.5. Analyses of model results

After comparing modelled CO_2 fluxes against the measured values (Sect. 5-2.2.4) we interpreted the modelled outputs to examine WTD effects on net CO_2 exchange at the WPL. WTD fluctuation can affect peatland net CO_2 exchange by affecting root and microbial oxidation-reduction reactions and energy yields and hence root and microbial decomposition, growth and uptake thereby affecting GPP and R_e. The effects of WTD drawdown on diurnal CO_2

exchange of WPL was examined by comparing hourly modelled net CO_2 fluxes against half hourly measured EC fluxes over three 10-day periods in late growing seasons (mid-August) of 2005, 2006 and 2008. These periods had comparable weather conditions i.e. temperature and radiation that affected GPP and R_e, so that those three periods mostly differed from each other in their WTD. These three periods were selected based on the highest availability of night-time valid EC CO_2 flux measurements for comparison with modelled fluxes. Further examination of this WTD drawdown effect in these three periods was facilitated by comparing modelled soil and understorey CO_2 fluxes averaged over the hummock and the hollow against net chamber CO_2 fluxes measured by Cai et al. (2010) at the WPL (Sect. 5-2.2.2).

To examine the consistency of short-term WTD effects on CO_2 exchange at the WPL over a longer time scale, we compared modelled vs. EC-derived growing season (May-August) and annual sums of NEP, GPP and R_e for modelled vs. measured interannual variations in average growing season and May-October (ice free period) WTD from 2004-2009.

5-2.2.6. Sensitivity of modelled peatland CO_2 exchange to artificial drainage

Large areas of northern boreal peatlands in Canada have been drained primarily for increased forest and agricultural production since plant productivity in pristine peatlands are known to be constrained by shallow WTD (Choi et al. 2007). However, drainage and resultant WTD drawdown can affect both GPP and R_e on a short-term basis and the vegetation composition on a longer time scale thereby changing overall net CO_2 exchange trajectories of a peatland. To predict short-term effects of drainage on WTD and hence ecosystem net CO_2 exchange of WPL, we extended our simulation run (Sect. 5-2.2.3) by two 7-yr cycles using repeated weather sequences of 2003-2009. During this extension, we forced a stepwise drawdown in WTD_x from that simulated under current conditions at WPL (Fig. 5-1) by 1.0 and

2.0 m in the first (drainage cycle 1) and the second cycle (drainage cycle 2) respectively. This projection run would give us a further insight about how the northern boreal peatland of Western Canada would be affected by further WTD drawdown as a result of drier and warmer weather as well as a disturbance such as drainage. This projection would also provide us with a test of how sensitive the modelled C processes were to the changes in model lateral boundary condition as defined by WTD_x in *ecosys*.

5-3. Results

5-3.1. Model performance in simulating diurnal variations in ecosystem net CO_2 fluxes

Variations in weather variables like precipitation can cause change in WTD and hence variation in diurnal net CO_2 exchange across years. *Ecosys* reasonably well simulated diurnal net CO_2 fluxes measured each year from 2004 to 2008 with varying precipitation (Table 5-1). Regressions of hourly modelled vs. measured net ecosystem CO_2 fluxes gave intercepts within 0.1 μmol m^{-2} s^{-1} of zero, and slopes within 0.1 of one, indicating minimal bias in modelled values during each year from 2004-2008 (Table 5-1). However, regressions of modelled vs. measured fluxes over the growing seasons (May-August) with varying precipitation from 2004-2009 yielded larger positive intercepts for all of these years (Table 5-2). These larger intercepts were predominantly caused by modelled overestimation of growing season day-time CO_2 fluxes. This overestimation was, however, offset by modelled overestimation of night-time CO_2 fluxes during the winter thus yielding smaller intercepts from whole year regressions of modelled vs. EC measured fluxes (Tables 5-1 and 5-2). We could not do a modelled vs. EC measured regression for the entire year of 2009 due to the lack of flux measurements from September to December in that year (Table 5-1). Values for coefficients of determination (R^2) were ~ 0.8 ($P < 0.001$) for all years from both whole year and growing season regressions (Tables 5-1 and 5-2). Root mean

squares for errors (RMSEs) were < 2.0 and ~2.5 μmol m^{-2} s^{-1} for whole year regressions from 2004 to 2008 (Table 5-1) and for growing season regressions from 2004 to 2009 (Table 5-2) respectively. Much of the variations in EC measured CO_2 fluxes that was not explained by the modelled fluxes could be attributed to a random error of ~20% in EC methodology (Wesely and Hart 1985). This attribution was further corroborated by root mean squares for random errors (RMSRE) in EC measurements, calculated for forests with similar CO_2 fluxes from Richardson et al. (2006) that were similar to RMSE (Table 5-1). The similar values of RMSE and RMSRE also indicated that further constraint in model testing could not be achieved without further precision in EC measurements.

Regressions of modelled vs. gap-filled CO_2 fluxes gave slopes and R^2 were similar to, and RMSEs were smaller than those from modelled vs. EC-measured CO_2 fluxes for most of the years except for the whole year regressions in 2004 and 2006 when the slopes were larger (Tables 5-1 and 5-2). The intercepts from modelled vs. gap filled CO_2 fluxes were, however, consistently more negative than those from modelled vs. EC measured fluxes for both whole year (Table 5-1) and growing season (Table 5-2) regressions. These more negative intercepts were mainly caused by larger modelled than gap filled night-time CO_2 effluxes.

5-3.2. Seasonality in WTD and net ecosystem CO_2 exchange

Seasonality in WTD measured at the WPL showed interannual variation from 2004 to 2009 which was reasonably well modelled by *ecosys* (Figs. 5-2b, d, f, h, j, l). This interannual variation in seasonality of WTD was modelled by accurate simulation of the balance between vertical water fluxes i.e. *P* vs. *ET* and lateral water fluxes i.e. recharge vs. discharge (Figs. 4-6 to 4-8). Larger *P* to *ET* ratio throughout 2004 caused the shallowest modelled WTD which remained above the hollow surface throughout most of the year (Fig. 5-2b). WTD_x (=0.19 m)

(Fig. 5-1) shallower than the modelled WTD in 2004 created a hydraulic gradient that caused net lateral recharge and hence further sustained the shallow modelled WTD. A smaller *P* to *ET* ratio in 2005 than in 2004 caused slightly deeper WTD that remained at the hollow surface or within 0.1 m below the hollow surface (Fig. 5-2d). During this year, WTD_x (=0.19 m) (Fig. 5-1) shallower than the modelled WTD caused net lateral recharge and hence further sustained WTD close to the hollow surface. Declines in the *P* to *ET* ratio over the growing seasons of 2006 and 2007 caused modelled WTD drawdown to levels where the differences between *ET* and *P* equilibrated with net lateral recharge caused by hydraulic gradients yielded from WTD_x (=0.35 m) (Fig. 5-1) which was deeper than the modelled WTD in both years (Figs. 5-2f, h). Continued declines in growing season *P* to *ET* ratio in 2008 and 2009 caused further deepening of the WT (Figs. 5-2j, l). A WTD_x (=0.72 m) (Fig. 5-1) deeper than the modelled WTD in these growing seasons generated hydraulic gradients that caused net lateral discharge which further deepened WTD. These modelled interannual variations in seasonality of WTD from 2004 to 2009 were well corroborated by site measured half hourly WTD at the WPL (Figs. 5-2b, d, f, h, j, l).

Seasonality in net CO_2 exchange at the WPL was predominantly governed by that in temperature which controlled the seasonality in phenology and hence GPP as well as that in R_e. *Ecosys* reasonably well simulated these seasonalities in phenology and hence GPP and R_e during a gradual growing season WTD drawdown from 2004 to 2009 which was apparent by good agreements between modelled vs. EC-gap filled daily NEPs (Fig. 5-2) and hourly net CO_2 fluxes (Tables 5-1 and 5-2) for all these years. Modelled NEPs throughout the winters of most of the years were, however, more negative than the EC-gap filled NEPs indicating larger modelled than EC-gap filled winter CO_2 effluxes (Fig. 5-2). This trend was also indicated by negative intercepts from regressions of modelled vs. gap-filled CO_2 fluxes (Table 5-1) (Sect. 5-3.1). The onset of

photosynthesis at the WPL also varied interannually depending upon spring temperature which was well modelled by *ecosys*. For instance, 2004 with a cooler spring produced smaller early growing season (May) GPP and hence NEP than 2005 with a warmer spring which was apparent in daily EC-gap filled and modelled NEPs (shaded areas in figs. 5-2a, c).

5-3.3. WTD effects on diurnal net CO_2 exchange

WTD variation can affect diurnal net CO_2 exchange by affecting peat O_2 status and consequently root and microbial O_2 and nutrient availability, growth and uptake thereby influencing CO_2 fixation (GPP) and/or respiration (R_e). To examine modelled vs. measured WTD effects on diurnal net CO_2 exchange at the WPL, we examined three 10-day periods with comparable weather conditions (radiation and air temperature) that differed predominantly in their WTDs during late growing seasons (August) of 2005, 2006 and 2008 (Fig. 5-3) (Sect. 5-2.2.5). A WTD drawdown from late growing season of 2005 to that of 2006 in *ecosys* caused a reduction in peat water contents (Fig. 4-5) and a consequent increase in O_2 influxes from atmosphere into the peat that eventually caused an increase in modelled soil CO_2 effluxes (Fig. 5-4c). These increased modelled soil CO_2 effluxes in mid-August of 2006 contributed to the larger modelled ecosystem CO_2 effluxes (R_e) as apparent in larger modelled night-time fluxes in the late growing season of 2006 than in that of 2005 which was well corroborated by night-time EC CO_2 fluxes during those periods (Fig. 5-4a). This R_e stimulation by WTD drawdown was further corroborated by larger sums of night-time soil CO_2 fluxes and understorey autotrophic respiration (R_a) as measured by Cai et al. (2010) using automated chambers and modelled by *ecosys* in late growing season of 2006 with deeper WTD than in that of 2005 with shallower WTD (Fig. 5-4b).

Further WTD drawdown into the late growing season of 2008 (Fig. 5-3b) caused improved peat oxygenation and hence larger soil CO_2 effluxes in the model (Fig. 5-4c). This contributed to similarly larger modelled night-time CO_2 fluxes in the late growing seasons of 2006 and 2008 than in 2005 that were also well corroborated by EC measured night-time fluxes during those periods (Fig. 5-4a). Consequently, the sums of modelled night-time soil CO_2 fluxes and understorey R_a in late growing season of 2008 were similarly larger as in 2006 with respect to those in that period of 2005 (Fig. 5-4b). We, however, did not have any chamber measurements available for 2008 to corroborate this trend. However, despite larger night-time modelled and EC CO_2 fluxes in the late growing season of 2008 than in 2005, the day-time influxes in 2008 were also similar to those in 2005 (Fig. 5-4a). This indicated a greater late growing season CO_2 fixation with WTD drawdown from 2005 to 2008. WTD drawdown thus stimulated both the night-time and the day-time net CO_2 fluxes as apparent in both the modelled outputs and in EC flux measurements during the three hydroperiods mentioned above thereby indicating increases in both R_e and GPP with the deepening of WT.

Apart from WTD, temperature variation could also profoundly affect ecosystem net CO_2 exchange at the WPL. For a given WTD condition, warmer weather caused increases in R_e at the WPL (Figs. 5-3 and 5-4a, b). Larger night-time modelled, EC-gap filled and chamber CO_2 fluxes in warmer nights of day 214, 220 and 222 than the cooler nights of day 221, 224 and 218 in 2005, 2006 and 2008 respectively indicated this trend of increased R_e with warming under similar WTD condition (Figs. 5-3a and 5-4a, b). However, at similar temperature conditions, modelled and EC-gap filled night-time ecosystem CO_2 fluxes as well as modelled and automated chamber measured sums of night-time soil CO_2 fluxes and understorey R_a under deeper WTD conditions in 2006 and 2008 were larger than those in 2005 under shallower WTD (denoted by

the shaded areas in Figs. 5-3 and 5-4). This indicated that WTD drawdown stimulated R_e at the WPL irrespective of temperature condition (Figs. 5-3 and 5-4). This further corroborated the net effects of WTD drawdown on R_e and hence on net ecosystem CO_2 exchange as discussed above.

The degree of stimulation in R_e at the WPL due to warming was also influenced by WTD conditions. To study this effect we further examined three 4-day warming events in late July and August of 2005, 2006 and 2008 with gradually deeper WTD (Figs. 5-5a to 5-5f). The warming events in early August of 2006 and in mid-August of 2008 with deeper WTD than in 2005 caused gradual increases in R_e as apparent from gradually larger modelled and EC-gap filled night-time ecosystem CO_2 effluxes (Figs. 5-5h, i). These increases in R_e due to warming during deeper WTD conditions were also apparent in gradually larger sums of modelled and automated chamber-measured (Cai et al. 2010) night-time soil CO_2 fluxes and understorey R_a in 2006 and modelled understorey and soil CO_2 fluxes in 2008 (Figs. 5-5k, l). These increases in R_e due to warming under deeper WTD contributed to declines in modelled and EC-gap filled July-August net ecosystem productivity (NEP) during 2006 and 2008 (Figs. 5-2e, i). Unlike in 2006 and 2008, a late-July warming event in 2005 with shallower WTD than in 2006 and 2008 did not yield a similarly evident stimulation of either modelled or EC-gap filled R_e and either modelled or chamber measured (Cai et al. 2010) soil and understorey respiration (Figs. 5-5g, j). This lack of stimulation in R_e with warming under shallower WTD in 2005 resulted in the absence of decline in July-August NEP as occurred in 2006 and 2008 (Figs. 5-2c vs. 5-2e, i). These findings showed that the stimulation of R_e due to warming was greater with deeper WTD thereby further indicating importance of WTD in mediating potential future warming effects on NEP of northern boreal peatlands.

5-3.4. Interannual variations in WTD and net ecosystem productivity

The effects of WTD drawdown on modelled and EC-gap filled diurnal net ecosystem CO_2 exchange as discussed in the previous section (Fig. 5-4) contributed to the effects of interannual variation in WTD on that of NEP. However, these WTD effects on growing season modelled and EC-derived GPP, R_e and hence NEP might also be affected by changes in temperature (Fig. 5-5). *Ecosys* simulated a gradual drawdown of average growing season (May-August) WTD from 2004 to 2009 from gradually declining growing season *P* to *ET* ratio and lateral water gain through recharge (Fig. 5-6d). This simulated WTD drawdown was corroborated by site measurements at the WPL (Fig. 5-6d). Deeper WT in 2005 than in 2004 caused larger growing season GPP in *ecosys* that was corroborated by EC-derived GPP (Fig. 5-6b). This increase in GPP from 2004 to 2005 was also contributed by larger GPP in warmer May of 2005 than 2004. WTD drawdown from 2004 to 2005, however, did not cause an increase in either modelled or EC-derived growing season R_e (Fig. 5-6c). This was because June and July in 2005 was more than 2°C cooler than in 2004, causing cooler soil which reduced R_e. This reduction in June and July R_e due to cooler soil more than fully offset the increase in R_e due to WTD drawdown and resulted in decreased growing season modelled and EC-derived R_e in 2005 than in 2004 (Fig. 5-6c). Larger GPP and smaller R_e hence caused a larger growing season NEP in 2005 than in 2004 (Figs. 5-2a, c and 5-6a). WTD drawdown in *ecosys* from 2005 to 2006 caused increases in both modelled growing season GPP and R_e that was corroborated by EC-derived GPP and R_e (Figs. 5-6b, c). This trend of increases in both GPP and R_e was also apparent in modelled vs. EC-gap filled and chamber diurnal net CO_2 fluxes (Figs. 5-4 and 5-5).

The effects of increasing WTD on NEP changed after 2005. A warmer growing season in 2006 than in 2005 (Fig. 5-6d) caused warmer soil that further contributed to the increase in

modelled and EC-derived growing season R_e from 2005 with shallower WTD to 2006 with deeper WTD (Figs. 5-4, 5-5 and 5-6c, d). Therefore, a larger increase in growing season R_e than in GPP caused modelled and EC-derived growing season NEP to decrease from 2005 to 2006 (Figs. 5-2c, e and 5-6a). Continued growing season WTD drawdown from 2006 to 2008 caused similar increases in modelled growing season GPP and R_e that caused no significant changes in modelled growing season NEP (Figs. 5-2e, i, 5-3, 5-4 and 5-6a, b, c, d). Like the modelled estimates, EC-derived growing season GPP and R_e also increased with WTD drawdown from 2006 to 2008 (Figs. 5-6a, b, c, d). However, the rate of increase in EC-derived growing season R_e was smaller than that in modelled growing season R_e thereby contributing to a larger growing season EC-gap filled NEP in 2008 than in 2006 which was not apparent in modelled estimates (Figs. 5-6a, b, c). A further drawdown in WTD from the growing season of 2008 to 2009 caused reductions in both modelled and EC-derived growing season GPP and R_e (Figs. 5-6a, b, c, d). These reductions in GPP and R_e from 2008 to 2009 could also be contributed by lower T_a in 2009 than in 2008 that caused cooler canopies and soil (Figs. 5-6b, c, d). The reduction in EC-derived growing season GPP was larger than that in EC-derived growing season R_e thereby causing a decrease in growing season EC-gap filled NEP from 2008 to 2009 (Figs. 5-6a, b, c). On the contrary, the reduction in modelled growing season GPP from 2008 to 2009 was less than that in the EC-derived GPP thereby causing an increase in modelled growing season NEP from 2008 to 2009 (Figs. 5-6a, b, c).

Despite these counteracting and offsetting effects of WTD and T_a on GPP and R_e, larger modelled and EC-derived estimates of growing season GPP and R_e in 2009 than in 2004 with similar mean T_a suggested that both modelled and EC-derived growing season GPP and R_e increased with the deepening of average growing season WTD at the WPL (Figs. 5-6a, b, c, d).

This trend was further corroborated by polynomial regressions of modelled growing season estimates of GPP and R_e on modelled average growing season WTD and similar regressions of EC-derived growing season GPP and R_e on measured average growing season WTD (Figs. 5-7a, b, c). These regressions showed that there were increases in modelled and EC-derived growing season GPP and R_e with deepening of the growing season WT from 2004 to 2008 after which further WTD drawdown in 2009 started to cause slight declines in both GPP and R_e (Figs. 5-7b, c). However, neither modelled nor EC-gap filled estimates of growing season NEP yielded significant regressions when regressed on modelled and measured growing season WTD respectively (Fig. 5-7a). This indicated that counteracting effects of WTD and T_a and similar increases in modelled and EC-derived growing season estimates of GPP and R_e with deepening of WT left no net effects of WTD drawdown on either modelled or EC-derived growing season NEP (Figs. 5-6 and 5-7a).

These WTD effects on growing season GPP and R_e and hence NEP from 2004 to 2009 as measured at the WPL and modelled by *ecosys* were also consistent at an annual time scale from 2004 to 2008 (Figs. 5-6e, f, g, h). Similar to the growing season trend, drawdown of both measured and modelled WTD averaged over the ice free periods (May-October) from 2004 to 2008 stimulated annual modelled and EC-derived GPP (Figs. 5-6f, h and 5-7e). This WTD drawdown also raised modelled and EC-derived annual R_e from 2005 to 2008 as was in the case of growing season R_e vs. WTD (Figs. 5-6g, h and 5-7f). Similar increases in both modelled and EC-derived annual GPP and R_e with WTD drawdown left no net WTD effects on modelled and EC-gap filled annual NEP (Fig. 5-7d). We did not include GPP, R_e and NEP from 2009 in this study of interannual WTD variation effect on these C balance components due to the lack of EC CO_2 flux measurements from September to December in 2009. These WTD effects on GPP, R_e

and hence NEP simulated by *ecosys* were well corroborated by EC-derived GPP, R_e and EC-gap filled NEP at both growing season and annual time scales. However the modelled growing season and annual GPP and R_e was consistently higher than the EC-derived estimates of those for all growing seasons and all the years from 2004 to 2009 (Figs. 5-6 and 5-7).

Increased GPP with WTD drawdown (Figs. 5-6b, f and 5-7b, e) was modelled predominantly through increased root growth and uptake of nutrients and consequently improved leaf nutrient status and hence more rapid CO_2 fixation in vascular PFTs (Sect. 5-2.1.3). Under shallow WTD during the growing season of 2004, roots in modelled black spruce PFT hardly grew below 0.35 m from the hummock surface (black spruce was not planted in the hollow) and the roots in modelled tamarack PFT were mostly confined to 0.35 m from the hummock surface and 0.05 m from the hollow surface. Modelled root densities of both black spruce and tamarack were, however, higher by 2-3 orders of magnitude in the top 0.19 m of the hummock (data not shown). A WTD drawdown from ~0.05 m above the hollow surface (~0.25 m below the hummock surface) in the growing season of 2004 to ~0.35 m below the hollow surface (~0.65 m below the hummock surface) in the growing season of 2009 caused an increase in maximum modelled rooting depth from 0.35 to 0.65 m below the hummock surface in black spruce and from 0.35 to 0.65 m below the hummock and from 0.05 to 0.35 m below the hollow surface in the tamarack PFT. This increased root growth in modelled vascular PFTs increased root surface area for nutrient uptake (Sect. 5-2.1.3) during deeper WTD periods in the growing season of 2009 than in 2004. The increased root surface area along with increased nutrient availability due to more rapid mineralization with improved aeration (Sect. 5-2.1.3) accompanying WTD drawdown caused improved root nutrient uptake in modelled vascular PFTs. Increased root growth, nutrient availability and hence uptake due to WTD drawdown from the growing season

of 2004 to that of 2009 in *ecosys* caused an increase in modelled foliar N concentrations in black spruce, tamarack and dwarf birch PFTs from 14, 32, and 37 g N kg^{-1} C to 17, 37 and 45 g N kg^{-1} C respectively, driving the increases in GPP (C1, C3, C6, C7, C11) modelled over this period (Figs. 5-6b, f and 5-7b, e). These foliar N concentrations in the growing season of 2004 were well corroborated by the foliar N concentrations of 12, 33 and 41 g N kg^{-1} C for black spruce, tamarack and dwarf birch measured by Syed et al. (2006) during summer 2004 at our study site.

5-3.5. Simulated drainage effects on WTD and NEP

Disturbance such as artificial drainage can drastically alter the WTD in a peatland that in turn can cause dramatic changes in peatland NEP by shifting the balance between GPP and R_e. To predict drainage effects on WTD and hence C balance of WPL, we performed a projected drainage simulation with two additional 7-year weather cycles by *ecosys* (Sect. 5-2.2.6). Increasing WTD_x by 1 and 2 m in the drainage cycles 1 and 2 (Sect. 5-2.2.6) deepened growing season WT by ~0.5 m and ~0.55 m respectively from those in the real-time simulation in all the years from 2004 to 2009 (Fig. 5-8a).

This drawdown of modelled growing season WTD caused changes in modelled growing season NEP, GPP and R_e. Modelled growing season GPP increased with drainage-induced WTD drawdown up to ~0.5 m below the hollow surface (~0.8 m below the hummock surface) below which GPP decreased (Figs. 5-8c, f). However, this WTD drawdown affected modelled vascular and non-vascular growing season GPP quite differently. Modelled growing season vascular GPP increased with WTD drawdown before it plateaued and eventually decreased when WTD fell below 0.6 m from the hollow surface (0.9 m below the hummock surface) (Figs. 5-9a, c, e). On the contrary, modelled non-vascular growing season GPP continued to decrease with WTD

drawdown below 0.1 m from the hollow surface (0.4 m below the hummock surface) (Figs. 5-9a, b, d).

WTD drawdown due to simulated drainage not only affected modelled growing season GPP but also affected, and was affected by, the change in *ET* associated with this change. Deeper WTD_x in drainage cycle 1 caused larger hydraulic gradients and hence greater lateral discharge thereby deepening the WT with respect to that in the real-time simulation (Figs. 5-8a) (Sect. 5-2.2.6). Larger GPP throughout the growing seasons of 2004-2007 in the drainage cycle 1 than in the real-time simulation caused a greater vertical water loss through *ET* that further contributed to this deepening of WTD (Fig. 5-8b). However, greater lateral water discharge in drainage cycle 2 caused by deeper WTD_x (Sect. 5-2.2.6) did not deepen the modelled growing season WTD much below that in cycle 1 (Fig. 5-8a). The larger lateral water loss through discharge in drainage cycle 2 than in cycle 1 was mostly offset by slower vertical water losses through *ET* as indicated by smaller GPP in the drainage cycle 2 (Fig. 5-8b). These changing feedbacks between WTD and GPP and hence *ET* in *ecosys* also indicated the ability of the model to simulate hydrological self-regulation which is an important characteristic of peatland eco-hydrology (Dise 2009).

Modelled growing season R_e continued to increase with deepening of modelled WT due to drainage (Figs. 5-8d, g). However, reductions in modelled growing season R_e from drainage cycle 1 to 2 in 2006-2009 indicated R_e inhibition due to desiccation of near surface peat layers and surface residues (Fig. 5-8d). Overall larger increases in GPP than those in R_e with initial WTD drawdown in the drainage simulation slightly increased modelled growing season NEP (Figs. 5-8 b, e). However, continued WTD drawdown in the drainage simulation caused declines in GPP particularly in model years 2008 and 2009 while causing greater R_e or a smaller decline

in R_e than in GPP, thereby causing decline in NEP (Fig. 5-8). This projected drainage simulation effect on WTD and NEP in *ecosys* may reflect short-term drainage effects and hence may be transient. Long-term manipulation of WTD through drainage may produce different trajectories of WTD effects on C processes and plant water relations in northern boreal peatlands via vegetation adaptation and succession (Strack et al. 2006, Munir et al. 2014).

5-4. Discussion

5-4.1. Modelling WTD effects on northern boreal peatland NEP

Modelled and EC-gap filled diurnal, seasonal and annual NEP, GPP and R_e vs. modelled and observed WTD in Sect. 5-3 (Figs. 5-2 to 5-7) suggested that WTD drawdown increased both GPP and R_e. However, offsetting effects of T_a and WTD and similar increases in GPP and R_e with WTD drawdown yielded no net effect on NEP at the WPL during 2004-2009. The simulated drainage experiment in *ecosys* also suggested that this increase in GPP would diminish and eventually shift to a decrease in GPP should WT fall further below a threshold of about 0.45 m from the hollow surface, particularly during drier years (Figs. 5-8c, f and 5-9). This decrease in GPP would also be accompanied by increased R_e thereby causing a decrease in NEP should the deepening of WT continue at the WPL (Figs. 5-8b, d, e, g). These effects of WTD on GPP, R_e and hence NEP in *ecosys* were modelled from algorithms representing basic processes determining hydrologic effects on peat biogeochemistry and ecology of peat forming vegetation that were derived from independent research. These *ecosys* algorithms were, however, fed by site specific but measureable inputs to represent hydrology, biology and ecology of the northern boreal fen peatland at the WPL (Figs. 4-2 and 5-1) (Sects. 4-2.2.3 and 5-2.2.3) . Our hypotheses that describe how *ecosys* would simulate these WTD effects on R_e, GPP and hence NEP at the WPL are discussed in the following sections of 5-4.1.1 to 5-4.1.4.

5-4.1.1. Hypothesis 1: Increase in R_e with WTD drawdown

Shallow WTD in *ecosys* caused shallow aerobic zone above WT and thicker anaerobic zone below the WT. In the shallow aerobic zone, peat O_2 concentration [O_{2s}] was well above the Michaelis-Menten constant for O_2 reduction (K_m = 0.064 g m^{-3}) and hence DOC oxidation and consequent microbial uptake and growth in *ecosys* (A17a, C14c) was not much limited by [O_{2s}]. However, [O_{2s}] in the thicker anaerobic zone below the WT in this period was well below K_m so that DOC oxidation was coupled with DOC reduction by anaerobic heterotrophic fermenters, which yielded much less energy (4.4 kJ g^{-1} C) than did DOC oxidation coupled with O_2 reduction (37.5 kJ g^{-1} C) (A21). Lower energy yields in this thicker anaerobic zone hence resulted in slower microbial growth (A25) and R_h (A13) as discussed in Sect. 5-2.1.2. Since the anaerobic zone in *ecosys* was thicker than the aerobic zone under shallow WTD, lower modelled R_h in the anaerobic zone contributed to reduced modelled soil respiration and hence R_e that was corroborated by EC measurements at the WPL (Figs. 5-4 to 5-8). WTD drawdown in *ecosys* caused peat pore drainage and increased θ_g thereby deepening of the aerobic zone. This in turn raised D_g (D17) and hence increased O_2 influxes into the peat (Fig. 5-4c) (D16). Increased O_2 influxes enhanced [O_{2s}] and stimulated R_h (A13, A20) and hence soil respiration and R_e (Figs. 5-4 to 5-8). Rapid mineralization of DON and DOP due to improved [O_{2s}] under deeper WTD also raised aqueous concentrations of NH_4^+, NO_3^- and $H_2PO_4^-$ (C23a, c, e) that in turns increased microbial nutrient availability, uptake (A22) and growth (A29) and hence further enhanced R_e (Figs. 5-4 to 5-8).

This modelling hypothesis of increased R_e stimulated by improved peat oxygenation due to WTD drawdown can be corroborated by other field, laboratory and modelling studies on similar northern boreal fen peatlands. Automated chamber measurements by Cai et al. (2010) at

our study site showed increased soil respiration with deeper WT thereby further corroborating our hypothesis (Figs. 5-4b and 5-5j, k, l). Kotowska (2013) found through a combination of automated chamber measurements and a laboratory incubation study that increases in aerobic microbial decomposition stimulated by WTD drawdown contributed to increased R_e in a moderately rich fen very close to our study site. Mäkiranta et al. (2009) also found increased rates of microbial decomposition in a Finish peatland due to thicker aerobic zone and consequently larger amounts of decomposable organic matter exposed to aerobic oxidation. However, the modelled increase in R_e of 0.26 μmol CO_2 m^{-2} s^{-1} per 0.1 m of WTD drawdown was greater than the EC-derived R_e increase of 0.16 μmol CO_2 m^{-2} s^{-1} per 0.1 m WTD drawdown reported by Flanagan and Syed (2011) for WPL over the growing seasons of 2004-2009 (Figs. 5-6c, d). The modelled rate of increasing R_e was, however, comparable with that of ~0.3 μmol m^{-2} s^{-1} per 0.1 m of WTD drawdown estimated by Peichl et al. (2014) from EC-derived R_e over the growing seasons of 2001-2012 in a Swedish fen. Ballantyne et al. (2014) also reported an increase in EC-derived R_e of ~0.33 μmol m^{-2} s^{-1} per 0.1 m of WTD drawdown from a WTD manipulation study in a Michigan peatland thereby further corroborating our modelling hypothesis of increased R_e due to WTD drawdown.

Apart from WTD, peat warming in *ecosys* also increased rates of decomposition (A1) through an Arrhenius function (A6) and hence increased R_h and R_e (Figs. 5-3 to 5-6). However, this warming effect in *ecosys* was also modified by WTD. For a similar warming, greater thermal diffusivity in peat with deeper WTD and consequent smaller water contents caused greater peat warming (D12). This enabled *ecosys* to simulate larger increases in R_e during warming periods in 2006 and 2008 with deeper WTD than in 2005 (Figs. 5-3 to 5-5). This trend of increased stimulation of peat decomposition by warming under deeper WTD was also modelled by Grant

et al. (2012b) using the same model *ecosys* over a northern fen peatland at Wisconsin, USA and by Ise et al. (2008) using a land surface scheme ED-RAMS coupled with a soil biogeochemical model across several shallow and deep peat deposits in Manitoba, Canada. These simulations and findings have important consequences since increased peat decomposition and consequent increased CO_2 emission due to WTD drawdown would be further aggravated by increased temperature under future drier and warmer climates.

5-4.1.2. Hypothesis 2: Increase in GPP with WTD drawdown

WTD variations affected GPP in *ecosys* by affecting root and microbial O_2 availability, energy yields, root and microbial growth and decomposition, rates of mineralization and hence root nutrient availability and uptake (Sect. 5-2.1.3). Wet soils under shallow WTD caused low O_2 diffusion (Fig. 5-4c) (D16) into the peat and consequent low [O_{2s}] meant that root O_2 demand had to be mostly met by [O_{2r}]. *Ecosys* inputs for root porosity (θ_{pr} = 0.1) that governed O_2 transport through aerenchyma (D17d) and hence maintained [O_{2r}] was not enough to meet the root O_2 demand in saturated soil by the two over-storey tree PFTs i.e. black spruce and tamarack, causing shallow root systems to be simulated in these two tree PFTs under shallow WTD (Sect. 5-3.4). The under-storey shrub PFT (dwarf birch), however, had a higher root porosity (θ_{pr}=0.3) and hence had deeper rooting under shallow WTD than the two tree PFTs (Sect. 5-2.1.3). Shallow rooting in the tree PFTs thus reduced root surface area for nutrient uptake. However, root nutrient uptake (C23b, d, f) in all of these three PFTs was also constrained by low nutrient availability due to smaller aqueous concentrations of NH_4^+, NO_3^- and/or $H_2PO_4^-$ (C23a, c, e) resulting from slower mineralization (A26) of DON and DOP (A7) because of low [O_{2s}] in the wet soils under shallow WTD (Sect. 5-2.1.2). Slower root growth and nutrient uptake caused

lower foliar σ_N and/or σ_P with respect to foliar σ_C (C11) that slowed the rates of carboxylation (C6) and hence reduced vascular GPP (C1) during shallow WTD hydroperiods (Sect. 5-2.1.3).

WTD drawdown enhanced O_2 diffusion (Fig. 5-4c) (D16) and raised $[O_{2s}]$ so that root O_2 demand in all the three vascular PFTs was almost entirely met by $[O_{2s}]$ (Sect. 5-2.1.3). Consequently roots in these three PFTs could grow deeper which increased the root surface for nutrient uptake (Sect. 5-3.4). This increment in modelled root growth due to WTD drawdown could be corroborated by the increase in maximum rooting depth in black spruce and tamarack from 0.2-0.3 to 0.6 m with a WTD drawdown from 0.14 to 0.9 m as a result of artificial drainage in a similar fen peatlands in Central Alberta as measured by Lieffers and Rothwell (1987). Murphy et al. (2009) also found a significant increase in tree fine root production with WTD drawdown from ~0.1 to ~0.25 m during a WTD manipulation study in a Finish peatland. Beside improved root growth, greater $[O_{2s}]$ under deeper WTD also enhanced rates of mineralization (A26) of DON and DOP (A7) that raised aqueous concentrations of NH_4^+, NO_3^- and/or $H_2PO_4^-$ and hence facilitated root nutrient availability and uptake. Enhanced root nutrient uptake increased foliar σ_N and/or σ_P with respect to foliar σ_C (C11) that hastened the rates of carboxylation (C6) and hence raised vascular GPP (C1) during deeper WTD hydroperiods.

The three modelled vascular PFTs were predominantly N limited as indicated by mass-based modelled foliar N to P ratios of 6.6:1, 5.2:1 and 4.8:1 for black spruce, tamarack and dwarf birch during the shallow WTD in the growing season of 2004 that are also well corroborated by mass-based foliar N to P ratios of 7.1:1 and 6.3:1 for black spruce and tamarack measured by Syed et al. (2006) at our site during the summer of 2004. Mass-based foliar N to P ratio less than 16:1 usually indicates that the particular vegetation is more N than P limited (Aerts and Chapin III 2000). Since these modelled PFTs were predominantly N limited, increases in foliar N

concentrations (Sect. 5-3.4) as a result of improved root nutrient availability, growth and nutrient uptake with WTD drawdown enhanced carboxylation rates and hence GPP in these PFTs. Choi et al. (2007) in a WTD manipulation study found an increase in peat NO_3^- -N due to enhanced mineralization and nitrification stimulated by a WTD drawdown from 0.24 to 0.7 m below the surface that caused increases in foliar N concentrations from ~21 to ~27 g kg^{-1} C (assuming 50% of dry matter as organic C) in black spruce and ~41 to ~66 g kg^{-1} C in tamarack in a Central Albertan fen peatland. These increases in foliar N concentrations due to enhanced root nutrient availability and uptake with WTD drawdown in their study also caused significantly greater radial tree growth (Choi et al. 2007). Macdonald and Lieffers (1990) in a WTD manipulation study also found that WTD drawdown by ~0.45 m raised foliar N concentrations from ~19 to ~21 g kg^{-1} C (assuming 50% of dry matter as organic C) in black spruce and ~36 to ~42 g kg^{-1} C in tamarack trees that enhanced net photosynthetic C assimilation rates by those tree species in an Albertan moderately rich fen. These rates of increases in foliar N concentrations and consequent increases in CO_2 fixation in black spruce and tamarack trees due to WTD drawdown in similar peatlands are comparable with similar increases in our modelled outputs for these same parameters (Sect. 5-3.4).

Our modelled growing season GPP increased by 0.39 μmol CO_2 m^{-2} s^{-1} per 0.1 m WTD drawdown which was greater than the EC-derived GPP increase of 0.22 μmol CO_2 m^{-2} s^{-1} per 0.1 m WTD drawdown as reported by Flanagan and Syed (2011) for the WPL over the growing seasons of 2004-2009. However, the modelled GPP increase with WTD drawdown was comparable with the range of 0.28 to 0.4 μmol CO_2 m^{-2} s^{-1} per 0.1 m WTD drawdown reported by Peichl et al. (2014) and Ballantyne et al. (2014) for northern boreal fen peatlands in Michigan and Sweden.

5-4.1.3. Hypothesis 3: Microbial water stress on R_e due to WT deepening below a threshold WTD

When WT in *ecosys* dropped below a threshold level of ~0.3 m from the hollow surface (~0.6 m below the hummock surface), near surface peat desiccation reduced microbial access to substrate for decomposition (A15) (Sect. 5-2.1.2) which enabled *ecosys* to simulate reduction in near surface R_h. When this reduction in near surface R_h more than fully offset the increase in deeper R_h, net ecosystem R_h decreased. This offsetting effect on R_h partly contributed to simulated decrease in growing season R_e (=R_h+R_a) from 2008 to 2009 with WTD drawdown that was corroborated by a similar decrease in EC-derived R_e (Fig. 5-6c). Greater reductions in R_h in desiccated near surface peat layers also caused the reductions in growing season R_e in drainage cycle 2 from those in cycle 1 during 2007-2009 in our simulated drainage study (Fig. 5-8d). As in our modelling study, Peichl et al. (2014) found reductions in R_e when WTD fell below a threshold of ~0.3 m from the peat surface in a Swedish fen which could be partially attributed to reduction in near surface R_h due to desiccation. Dimitrov et al. (2010a) in a modelling study using *ecosys* also showed that a decrease in desiccated near surface peat respiration partially offset increased deeper peat respiration when WT deepened below a threshold of ~0.6-0.7 m from the hummock surface.

5-4.1.4. Hypothesis 4: Plant water stress on GPP due to WT deepening below a threshold WTD

This deepening of WT below a threshold level also caused rapid peat pore drainage (D9) and hence low moisture contents in the near surface peat layers which were colonized by most of the vascular root systems and all of the non-vascular (moss) rhizoids. When WTD fell below ~0.1 m from the hollow surface (~0.4 m below the hummock surface), vertical recharge through

capillary rise from the WT was not adequate to maintain near surface peat moisture, and hence peat water potential (ψ_s) in these layers declined, increasing peat hydraulic resistance (Ω_s) (B9). Reduction in ψ_s and simultaneous increase in Ω_s supressed root and rhizoid water uptake (U_w) (B6) from these near surface peat layers. Since shallow (0.115 m deep in the hummock and 0.05 m deep in the hollow) moss rhizoid (Sect. 5-2.1.4) U_w entirely depended upon moisture supply from these near surface layers, reduction in U_w from these desiccated layers caused reduction in moss canopy water potential (ψ_c) (Fig. 4-10) and hence moss GPP (C1, C4). Reduction in root U_w from desiccated near surface layers during this period, however, was offset by increased root U_w (B6) from deeper wetter layers with higher ψ_s and lower Ω_s due to deeper root growth facilitated by enhanced aeration as discussed above. This enabled the vascular PFTs in *ecosys* to sustain ψ_c, canopy turgor potential (ψ_t) (B4), stomatal conductance (g_c) (Fig. 4-10) (B2, C4) and hence increased GPP (C1) due to higher root nutrient availability and uptake. The increased vascular GPP due to enhanced plant nutrient status more than fully offset the suppression in moss GPP due to moss water limitations and thus caused a net increase in modelled GPP with WTD drawdown (Figs. 5-6b and 5-9b, c). This indicated increased vascular dominance over moss with deepening of WT in the model. This modelled trend can be corroborated by various WTD manipulation studies (e.g. Munir et al., 2014; Moore et al., 2013) in similar northern boreal peatlands that reported increased tree, shrub and herb growth over mosses with WTD drawdown. However, gains in modelled vascular GPP halted and eventually vascular GPP started to decline when WT fell below ~0.6 m from the hollow surface (~0.9 m below the hummock surface) in our drainage simulation. This was because below this threshold WTD, deeper root U_w (B6) could no longer offset suppression of near-surface root U_w thereby causing lower ψ_c, ψ_t (B4), g_c (B2, C4) and slower CO_2 fixation (C6) (Figs. 5-9d, e).

Similar to our modelling study, Riutta et al. (2007) measured a reduction in moss productivity due to water limitation when WTD fell below ~0.15 m from the surface in a Finish fen peatland. However, vascular GPP during that period was sustained in their study indicating no vascular water stress (Riutta et al., 2007). Peichl et al. (2014), however, measured reduction in moss GPP due to water limitation when WTD fell below ~0.3 m from the surface in a Swedish fen. They inferred that the peat in their study had the sufficient moisture supplying capacity through capillary rise to sustain moss U_w when the WTD was within ~0.3 m from the surface (Peichl et al., 2014). Reductions in moss GPP due to decreased moss canopy water potentials were also modelled by Dimitrov et al. (2011) using the same model *ecosys* when WTD fell below ~0.3 m from the hummock surface of a Canadian bog. However, in their modelling Dimitrov et al. (2011) found no vascular plant water stress and hence no reduction in vascular GPP during that period. Similarly, Kuiper et al. (2014) found reductions in moss productivity with peat drying while vascular productivity was sustained in a simulated drought experiment on a Danish peat.

Continued deep WTD, however, can also cause vascular plant water stress and hence reductions in vascular GPP as modelled in our study (Figs. 5-9c, e). This trend in our modelling can also be corroborated by field measurements across various northern boreal fen peatlands in Canada and Sweden. Sonnentag et al. (2010) found a reduction in canopy stomatal conductance (g_c) and hence vascular GPP when WT fell below ~0.4 m from the ridge surface at a fen peatland in Saskatchewan. The dominant vascular vegetation in their study included tamarack and dwarf birch, two of the three vascular PFTs in our modelling thereby further corroborating the projected vascular water stress. Peichl et al. (2014) also found a reduction in vascular GPP due to plant water stress when WTD fell below ~0.3 m from the surface in a Swedish fen peatland. The

WTD threshold for reductions in vascular GPP in those two field studies were, however, shallower than that in our modelled projection i.e. ~0.6 m from the hollow surface (~0.9 m below the hummock surface) (Figs. 5-9a, c, e) thereby indicating different vertical rooting patterns determined by specific interactions between hydrologic properties and rooting. However Lafleur et al. (2005) and Schwärzel et al. (2006) found much deeper WTD thresholds for reductions in vascular transpiration that could negatively affect vascular GPP over a Canadian pristine peatland and a German drained peatland. Those WTD thresholds were ~0.65 and ~0.9 m below the surface for pristine and drained peatland respectively, further indicating the importance of root-hydrology interactions and the resultant root adaptations, growth and uptake in determining WTD effects on vascular GPP across peatlands.

5-4.2. Divergences between modelled and EC-derived annual GPP, R_e and NEP

Modelled annual NEP was consistently lower than the EC gap-filled annual NEP in 2005-2008 (Fig. 5-6e). These lower NEP estimates were mainly caused by larger modelled vs. gap-filled R_e which was also apparent in negative intercepts from modelled on gap-filled net CO_2 flux regressions (Fig. 5-6g) (Table 5-1). The gap-filling for night-time CO_2 fluxes (=R_e) was done by Syed et al. (2006) using empirical relationships between EC CO_2 measurements and soil temperature (T_s) measured at 0.05 m depth at the WPL. During night-time and the winter, peat at this shallow depth (0.05 m) could have rapidly cooled down and thus yielded smaller night-time gap-filled CO_2 fluxes (e.g. Figs. 5-2, 5-4 and 5-5). On the contrary, modelled CO_2 fluxes in those periods depended on the temperatures of not only these shallow peat layers but also the deeper peat profiles that were warmer than the shallower layers and hence simulated larger CO_2 effluxes than the gap-filled (e.g. Fig. 5-5). CO_2 fluxes measured by automated chamber in cooler nights, however, did not decline as rapidly as did the gap-filled CO_2 fluxes as night progressed further

corroborating this reasoning for larger modelled vs. gap-filled R_e during night-time and the winter (e.g. Figs. 5-4 and 5-5).

Systematic uncertainties embedded in EC methodology could also contribute to larger modelled vs. EC-derived annual and growing season R_e estimates (Figs. 5-6c, g). The major uncertainty in the EC methodology is the possible underestimation of nighttime EC CO_2 flux measurements due to poor turbulent mixing under stable air conditions. These uncertainties are usually addressed by screening out those measurements when friction velocity (u^*) is less than a threshold and filling the resulting data gaps in the EC datasets (Goulden et al. 1997). Syed et al. (2006) used a u^* threshold of 0.15 m s^{-1} to screen out the possibly underestimated fluxes from the EC datasets measured at the WPL. However, R_e estimates derived from these EC datasets could be subjected to a possible underestimation due to selecting of a lower u^* threshold (Goulden et al. 1997, Miller et al. 2004). On the contrary, biological production of CO_2 by plant and microbial respiration was independent of u^* in the model which would thus contribute to larger modelled than EC-derived R_e estimates.

Larger modelled vs. gap-filled R_e also contributed to larger modelled vs. gap-filled growing season and annual GPP (Figs. 5-6b, f). In EC datasets, GPP was derived from R_e (Sect. 5-2.2.2) and hence smaller gap-filled vs. modelled R_e would cause smaller EC-derived vs. modelled GPP. A further cause of smaller EC-derived vs. modelled GPP could have been the incomplete (~75%) (Table 4-1) energy balance closure in EC measurements vs. complete energy balance closure in the model, which would cause a smaller EC-derived vs. modelled evapotranspiration (Fig. 4-11d) and possibly GPP (Figs. 5-6b, f). Furthermore, as opposed to EC-derived R_e that was used to calculate EC-derived GPP, modelled R_e ($=R_a+R_h$) was driven by modelled GPP thereby further contributing to deviation between modelled vs. EC-derived

growing season and annual R_e estimates (Figs. 5-6c, g). Modelled R_a was directly dependent on fixed C products during photosynthesis. Modelled R_h was also dependent on fixed C products in a diurnal time scale through root exudates as well as in a seasonal time scale through above and below ground litter fall.

All of these sources of larger modelled vs. EC-derived R_e and GPP estimates were related to EC methodology and gap-filling. These discrepancies between modelled and EC-derived R_e and GPP aggregates, however, could not be resolved in our modelling since, unlike EC datasets, every single mole of CO_2 that was modelled from basic ecosystem processes for fixation and respiration was counted in the modelled C budget.

Besides, annual NEP from 2004-2008 as modelled in our study and as derived by Flanagan and Syed (2011) from EC-gap filled net CO_2 fluxes are considerably higher than the long term C accumulation rates i.e. 19-24 g C m^{-2} yr^{-1} at the WPL estimated by Flanagan and Syed (2011) from peat core studies. This discrepancy can be attributed to recent (for last 50 years) colonization of WPL by tamarack trees that caused higher GPP and hence NEP as opposed to long-term less productive mosses at the WPL (Flanagan and Syed 2011). This recent increase in NEP has also been contributed by increased black spruce GPP in last 60 years as evident from a boost in black spruce basal area at the WPL around 60 years ago signifying peat surface stability to support tree growth (Flanagan and Syed 2011).

5-5. Conclusions

WTD drawdown in *ecosys* from 2004 to 2009 caused a similar increase in R_e and GPP and hence caused no significant change in NEP at the modelled northern boreal fen peatland representing WPL. EC-derived NEP, R_e and GPP by Syed et al. (2006) and Flanagan and Syed (2011) and automated chamber measured NEP and R_e by Cai et al. (2010) showed the similar

trend of increased R_e and GPP with deepening of WT that left no net WTD effect on NEP at the WPL. These effects of WTD drawdown on R_e and GPP was modelled in *ecosys* by the algorithms representing following processes:

(1) Improved [O_{2s}] facilitated by rapid O_2 diffusion (D16) under deeper WTD raised microbial energy yields while oxidizing DOC coupled with O_2 reduction (A21) and hence caused increases in R_e. Increased mineralization rates of DON and DOP due to improved [O_{2s}] also increased aqueous concentrations of NH_4^+, NO_3^- and $H_2PO_4^-$ (C23a, c, e) that in turns facilitated microbial nutrient availability, uptake (A22) and growth (A29) and hence further enhanced R_e (Sects. 5- 2.1.2. and 5-4.1.1).

(2) Increased nutrient availability due to rapid mineralization with WTD drawdown as mentioned above hastened root nutrient (mainly N) availability and uptake (C23b, d, f). Root nutrient availability and uptake in *ecosys* were further facilitated by increased root growth stimulated by improved [O_{2s}] during deeper WTD periods. Greater root growth and uptake thus caused improved foliar σ_N with respect to σ_C thereby enhancing CO_2 fixation (C6) and vascular GPP (C1). When WTD fell below ~0.1 m from the hollow surface (~0.4 m below the hummock surface) vertical recharge of near surface peat layers through capillary rise from WT was not enough to sustain moss water uptake thereby causing reductions in moss canopy water potentials (Fig. 4-10c) and hence moss GPP (C1, C4) (Sects. 5-2.1.3, 5-2.1.4 and 5-4.1.2). However, sustained increases in vascular GPP due to root water uptake from deeper wetter layers more than fully offset this suppression of moss GPP thereby causing a net increase in GPP with WTD drawdown (Figs. 5-6b and 5-9b, c).

These modelling hypotheses were corroborated by reasonably good agreements between hourly modelled net ecosystem CO_2 fluxes and WTD vs. hourly EC net ecosystem CO_2 fluxes and half hourly WTD measured by Syed et al. (2006) and Flanagan and Syed (2011) during each year from 2004 to 2009 at the WPL (Fig. 5-2) (Table 5-1). These hypotheses were also corroborated by automated chamber soil respiration and understorey CO_2 fluxes measured by Cai et al. (2010) at the WPL (Fig. 5-4b). Various field, laboratory and modelling studies over similar northern boreal peatlands throughout the world also corroborated the responses of GPP and R_e to WTD driven by the key processes in our modelling hypotheses that determined WTD effects on R_e and GPP and hence on NEP (Sect. 5-4.1). Moreover, a projected drainage simulation showed that the increase in vascular GPP due to improved plant nutrient status caused by WTD drawdown would only sustain while WTD remained above a threshold level i.e. ~0.6 m below the hollow surface (~0.9 m below the hummock surface). When WTD fell below this threshold, vascular GPP in our drainage projection started to decrease with further WTD drawdown thereby causing reductions in ecosystem GPP. Similar WTD threshold effects on vascular GPP were also found in other studies (Sect. 5-4.1.2) in similar peatlands.

Our modelling showed that adequate coupling of algorithms representing feedbacks among peatland hydrological and C processes in the process based model *ecosys* successfully simulated WTD effects on R_e, GPP and hence NEP of a northern boreal fen peatland at the WPL. Our projected drainage simulation showed that continued WTD could alter ecosystem C balance of this northern boreal peatland by decreasing GPP and sustaining increased R_e thereby causing declines in NEP. These findings provide us with important insights into how these northern boreal peatland C stocks would be affected by likely WTD drawdown under future drier and warmer climates. This modelling is also reproducible in other peatlands when the model is fed by

required physical, hydrological, chemical, biological and ecological inputs those are measurable at the sites (Figs. 4-2 and 5-1) (Sects. 4-2.2.3 and 5-2.2.3). Successful simulation of hydrological effects on peatland C processes by *ecosys* for a northern boreal fen peatland in this study along with simulations of feedbacks between hydrology and ecology by the same model *ecosys* across other contrasting peatlands (e.g. Dimitrov et al. 2011, Grant et al. 2012b) (Chapters 3 and 4), therefore, provide us with an important platform to launch an scaling up of such studies across regions, continents and/or the globe.

Table 5-1: Statistics from regressions between modelled and EC-gap filled net ecosystem CO_2 fluxes throughout the years of 2004-2008 at a Western Canadian fen peatland

Year	Total annual precipitation (mm)	*n*	*a*	*b*	R^2	RMSE (μmol m^{-2} s^{-1})	RMSRE (μmol m^{-2} s^{-1})
Modelled vs. eddy covariance CO_2 fluxes measured at $u^* > 0.15$ ms^{-1}							
2004	553	5034	0.08	1.10	0.81	1.58	1.92
2005	387	5953	0.07	1.03	0.82	1.68	1.99
2006	465	6012	0.07	1.08	0.79	1.68	1.98
2007	431	5385	0.06	0.99	0.79	1.83	2.09
2008	494	5843	-0.01	0.98	0.84	1.63	2.02
Modelled vs. gap-filled CO_2 fluxes							
2004	553	3750	-0.13	1.20	0.89	0.64	
2005	387	2807	-0.49	1.03	0.76	0.82	
2006	465	2748	-0.48	1.15	0.81	0.58	
2007	431	3375	-0.36	0.97	0.74	1.23	
2008	494	2941	-0.54	1.05	0.79	0.95	

(*a, b*) from simple linear regressions of modelled on measured. R^2 = coefficient of determination and RMSE = root mean square for errors from simple linear regressions of measured on simulated. RMSRE= root mean square for random errors in eddy covariance (EC) measurements calculated by inputting EC CO_2 fluxes recorded at u^* (friction velocity) > 0.15 m s^{-1} into algorithms for estimation of random errors due to EC CO_2 measurements developed for forests by Richardson et al. (2006).

Table 5-2: Statistics from regressions between modelled and EC-gap filled net ecosystem CO_2 fluxes during the growing seasons of 2004-2009 at a Western Canadian fen peatland

Year	Total growing season precipitation (mm)	*n*	*a*	*b*	R^2	RMSE (μmol m^{-2} s^{-1})	RMSRE (μmol m^{-2} s^{-1})
Modelled vs. eddy covariance CO_2 fluxes measured at $u^* > 0.15$ ms^{-1}							
2004	287	2043	0.55	1.05	0.78	2.27	2.55
2005	276	2200	0.82	0.98	0.79	2.50	2.74
2006	253	2107	0.48	1.06	0.78	2.36	2.76
2007	237	1822	0.65	0.93	0.75	2.91	3.06
2008	276	2070	0.32	0.96	0.82	2.45	2.85
2009	138	1870	0.76	1.01	0.81	2.27	2.83
Modelled vs. gap filled CO_2 fluxes							
2004	287	837	-0.01	1.21	0.87	1.22	
2005	276	680	-0.57	1.07	0.75	1.26	
2006	253	773	-1.70	0.95	0.73	0.78	
2007	237	1058	-0.51	0.98	0.76	1.88	
2008	276	810	-1.04	1.02	0.79	1.62	
2009	138	1010	-0.02	0.98	0.87	1.20	

(*a, b*) from simple linear regressions of modelled on measured. R^2 = coefficient of determination and RMSE = root mean square for errors from simple linear regressions of measured on simulated. RMSRE= root mean square for random errors in eddy covariance (EC) measurements calculated by inputting EC CO_2 fluxes recorded at u^* (friction velocity) > 0.15 m s^{-1} into algorithms for estimation of random errors due to EC CO_2 measurements developed for forests by Richardson et al. (2006).

D_{humm} (m)	D_{holl} (m)	TOC (g kg^{-1})	TN (g Mg^{-1})	TP (g Mg^{-1})	pH	CEC (cmol+ kg^{-1})
0.010		463	10100	700	6.2	139
0.065						
0.085						
0.115						
0.135						
0.190						
0.295		462	13600	400		
0.305	0.005					
0.350	0.050					
0.540	0.240					
0.650	0.350					
0.720	0.420					
0.900	0.600					
1.100	0.800					
2.000	1.700					

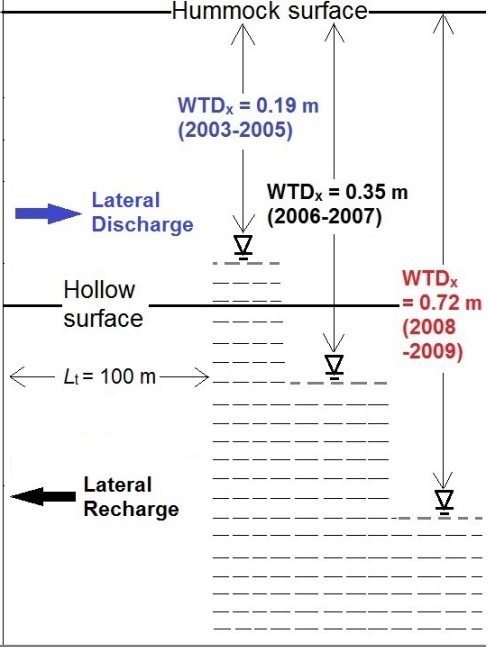

Fig. 5-1. Layout for *ecosys* model run to represent biological, chemical and hydrological characteristics of a Western Canadian fen peatland. Figure is not drawn to scale. D_{humm} = depth to the bottom of a layer from the hummock surface; D_{holl} = depth to the bottom of a layer from the hollow surface; TOC = total organic C (Flanagan and Syed 2011); TN = total nitrogen (Flanagan and Syed 2011); TP = total phosphorus (Flanagan and Syed 2011); CEC = Cation exchange capacity (Rippy and Nelson 2007); the value for pH was obtained from Syed et al. (2006); WTD_x = external reference water table depth representing average water table depth of the adjacent ecosystem; L_t = distance from modelled grid cells to the adjacent watershed over which lateral discharge / recharge occurs

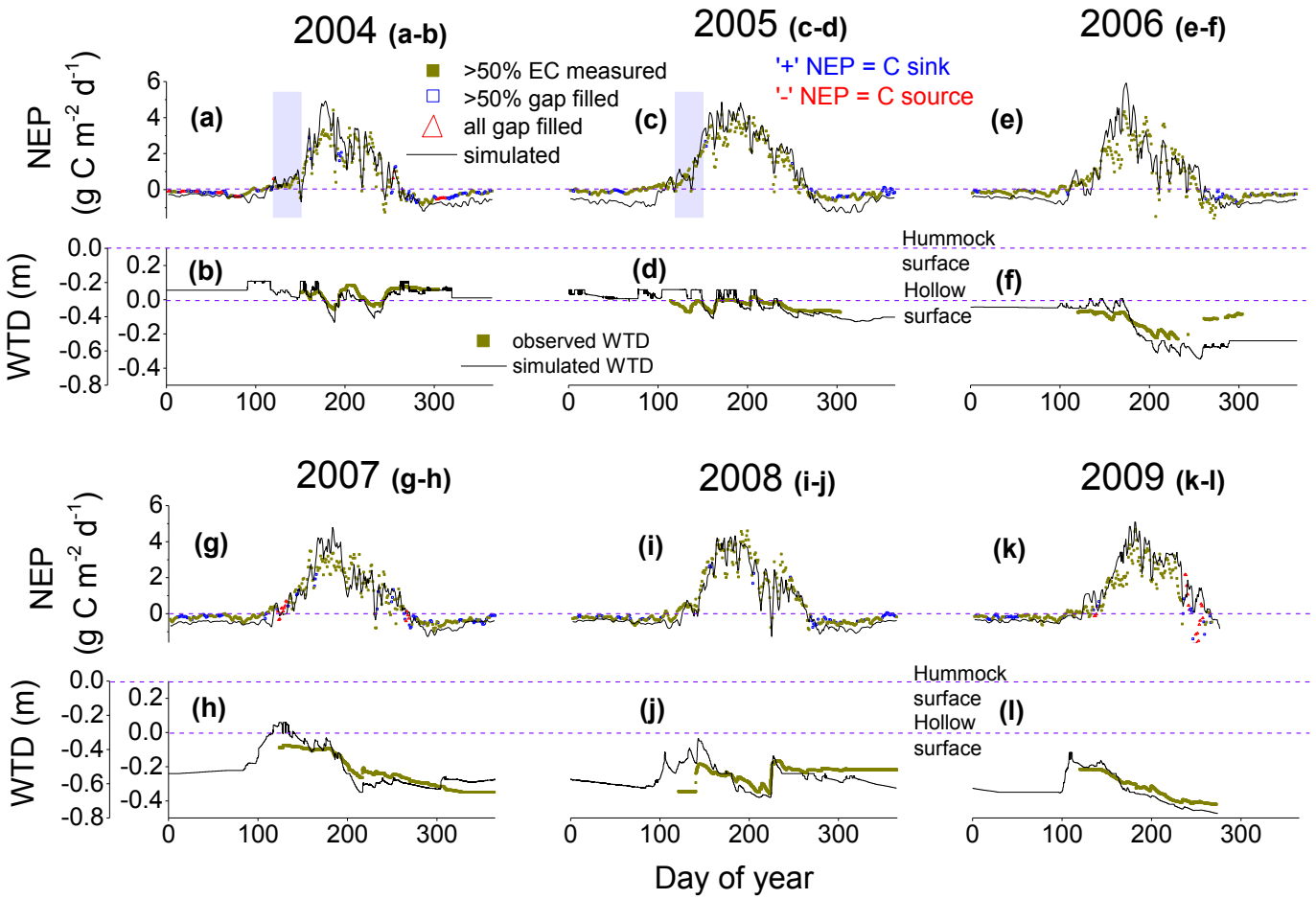

Fig. 5-2. (a, c, e, g, i, k) 3-day moving averages of modelled and EC-gap filled net ecosystem productivity (NEP) (Flanagan and Syed 2011) and (b, d, f, h, j, l) hourly modelled and half hourly measured water table depth (WTD) (Syed et al. 2006, Cai et al. 2010, Long et al. 2010, Flanagan and Syed 2011) from 2004-2009 at a Western Canadian fen peatland. A positive NEP means the ecosystem is a C sink and a negative NEP means the ecosystem is a C source. A negative WTD represents a depth below hummock/hollow surface and a positive WTD represents a depth above hummock/hollow surface

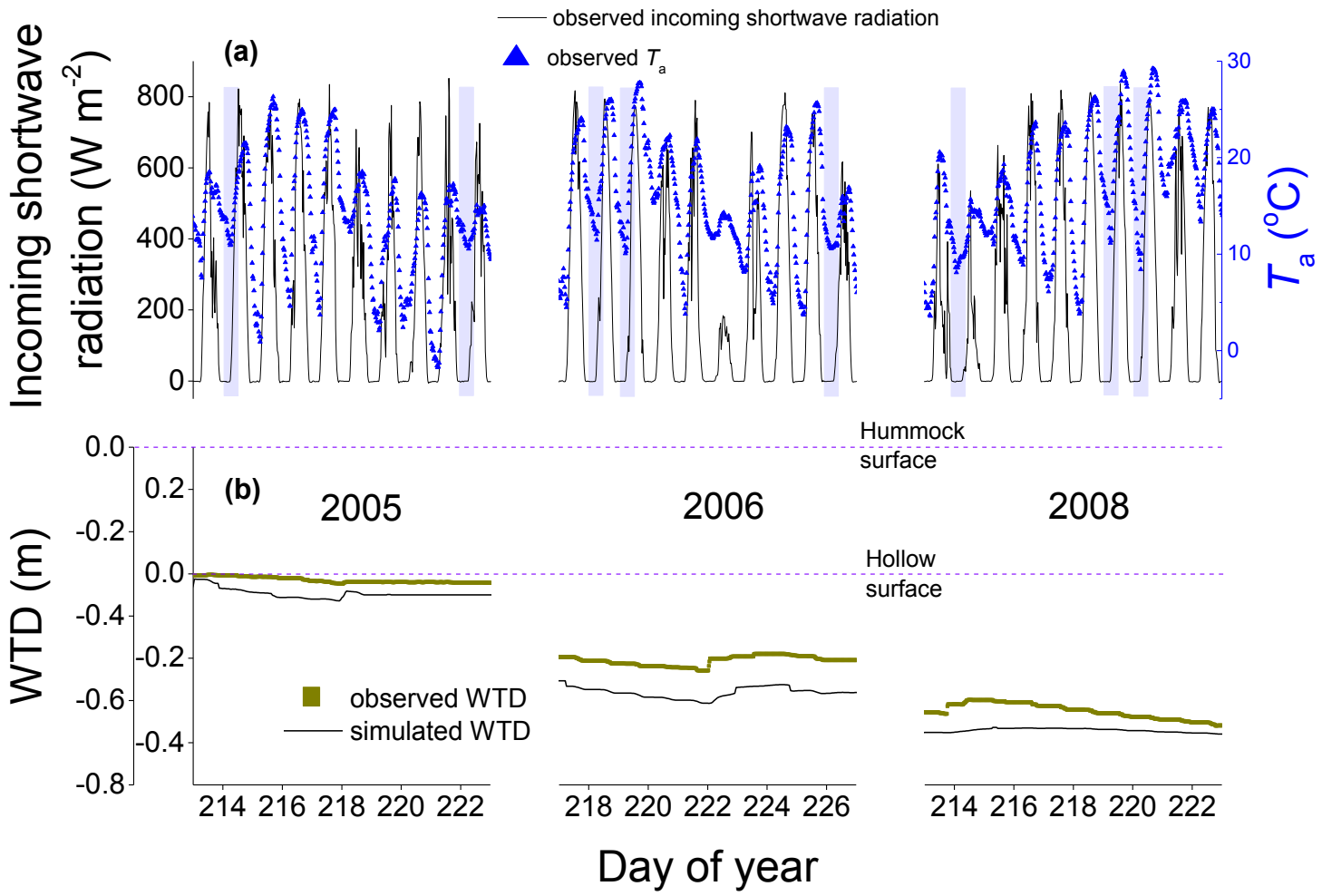

Fig. 5-3. (a) Half hourly measured incoming shortwave radiation and air temperature (T_a) and (b) hourly modelled and half hourly measured water table depth (WTD) (Syed et al. 2006, Cai et al. 2010, Long et al. 2010, Flanagan and Syed 2011) during August 2005, 2006 and 2008 at a Western Canadian fen peatland. A negative WTD represents a depth below hummock/hollow surface and a positive WTD represents a depth above hummock/hollow surface

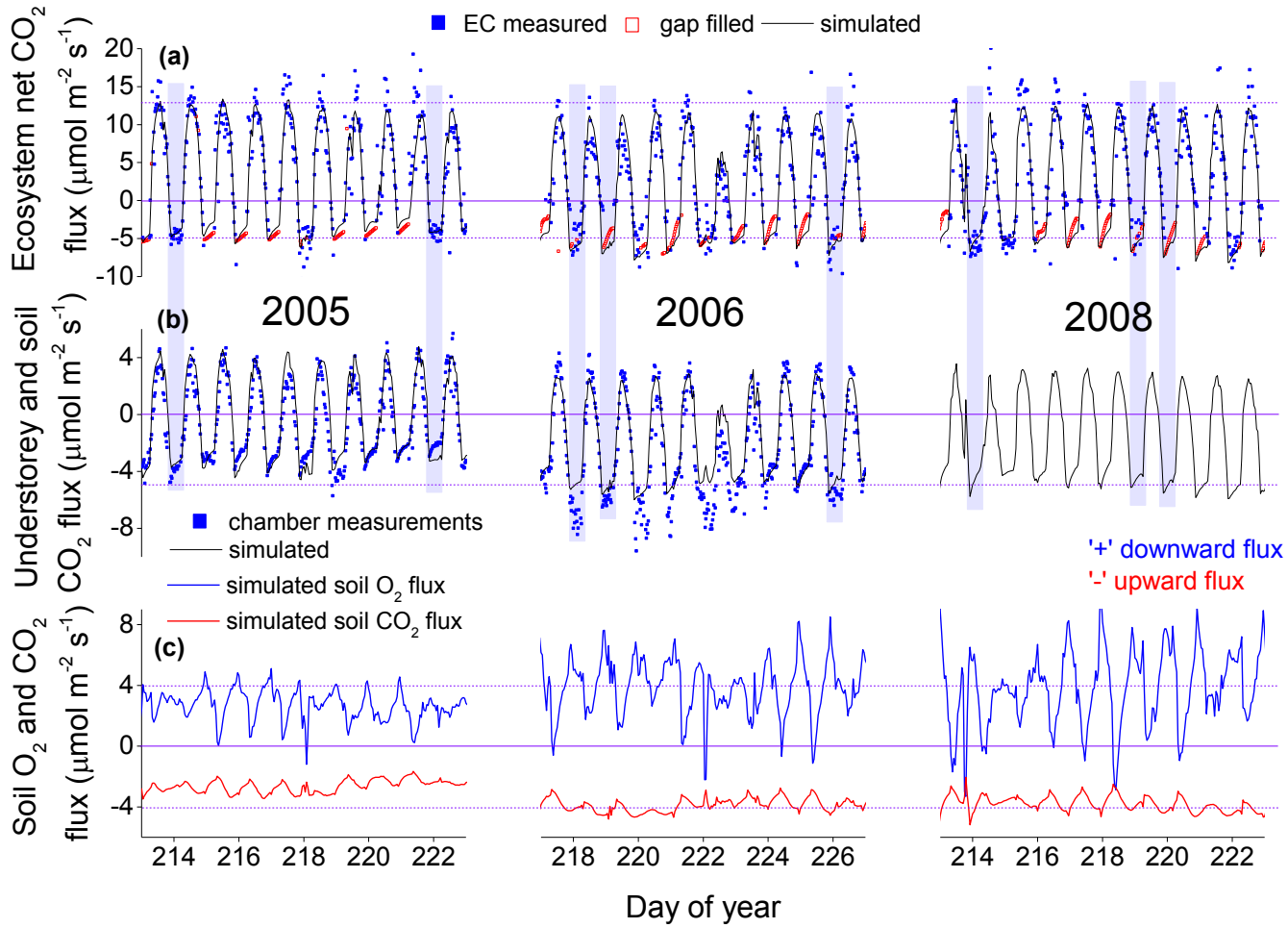

Fig. 5-4. (a) Half hourly EC-gap filled (Flanagan and Syed 2011) and hourly modelled ecosystem net CO_2 fluxes, (b) half hourly automated chamber measured (Cai et al. 2010) and hourly modelled understorey and soil CO_2 fluxes, and (c) hourly modelled soil CO_2 and O_2 fluxes during August 2005, 2006 and 2008 at a Western Canadian fen peatland. A negative flux represents an upward flux or a flux out of the ecosystem and a positive flux represents a downward flux or a flux into the ecosystem

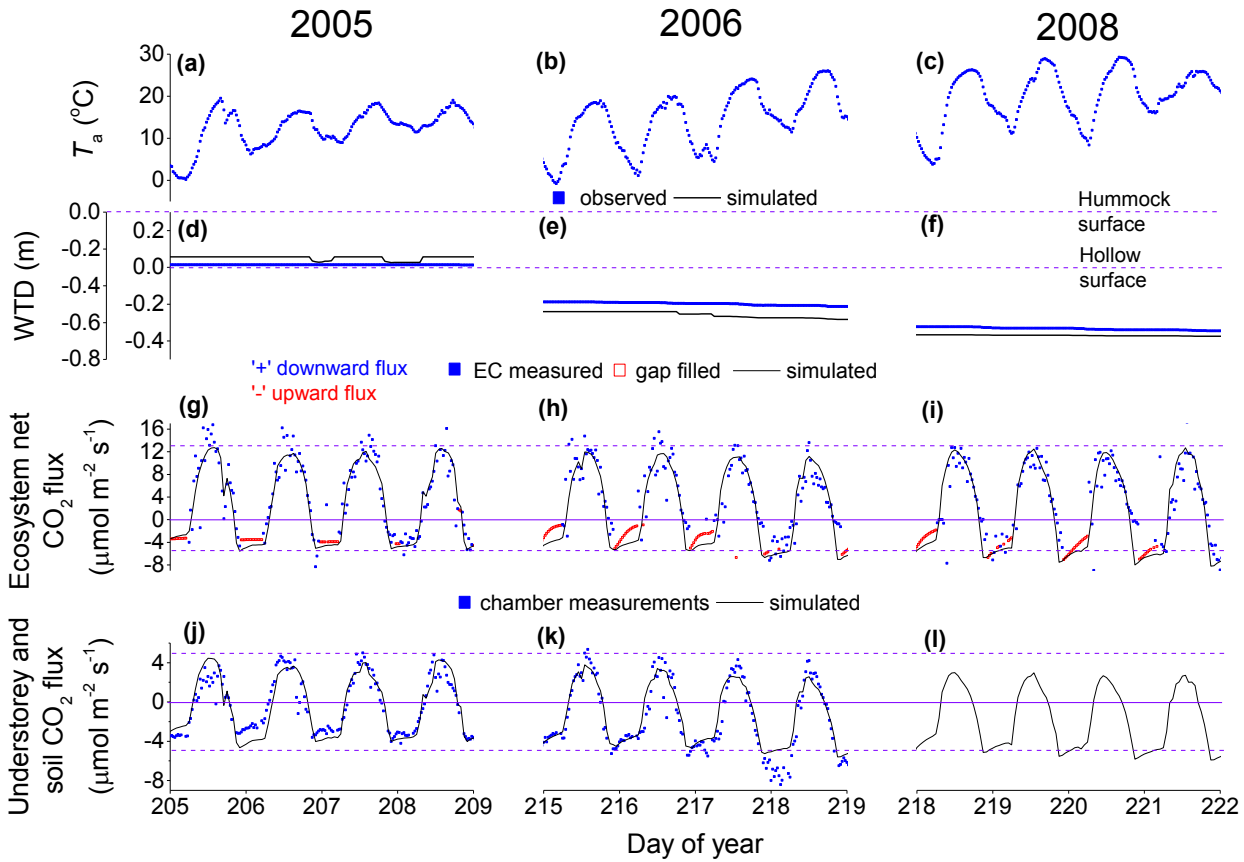

Fig. 5-5. (a-c) Half hourly observed air temperature (T_a), (d-f) hourly modelled and half hourly observed water table depth (WTD), (g-i) half hourly EC-gap filled (Flanagan and Syed 2011) and hourly modelled ecosystem net CO_2 fluxes, (j-l) half hourly automated chamber measured (Cai et al. 2010) and hourly modelled understorey and soil CO_2 fluxes during July-August 2005, 2006 and 2008 at a Western Canadian fen peatland. A negative flux represents an upward flux or a flux out of the ecosystem and a positive flux represents a downward flux or a flux into the ecosystem. A negative WTD represents a depth below hummock/hollow surface and a positive WTD represents a depth above hummock/hollow surface

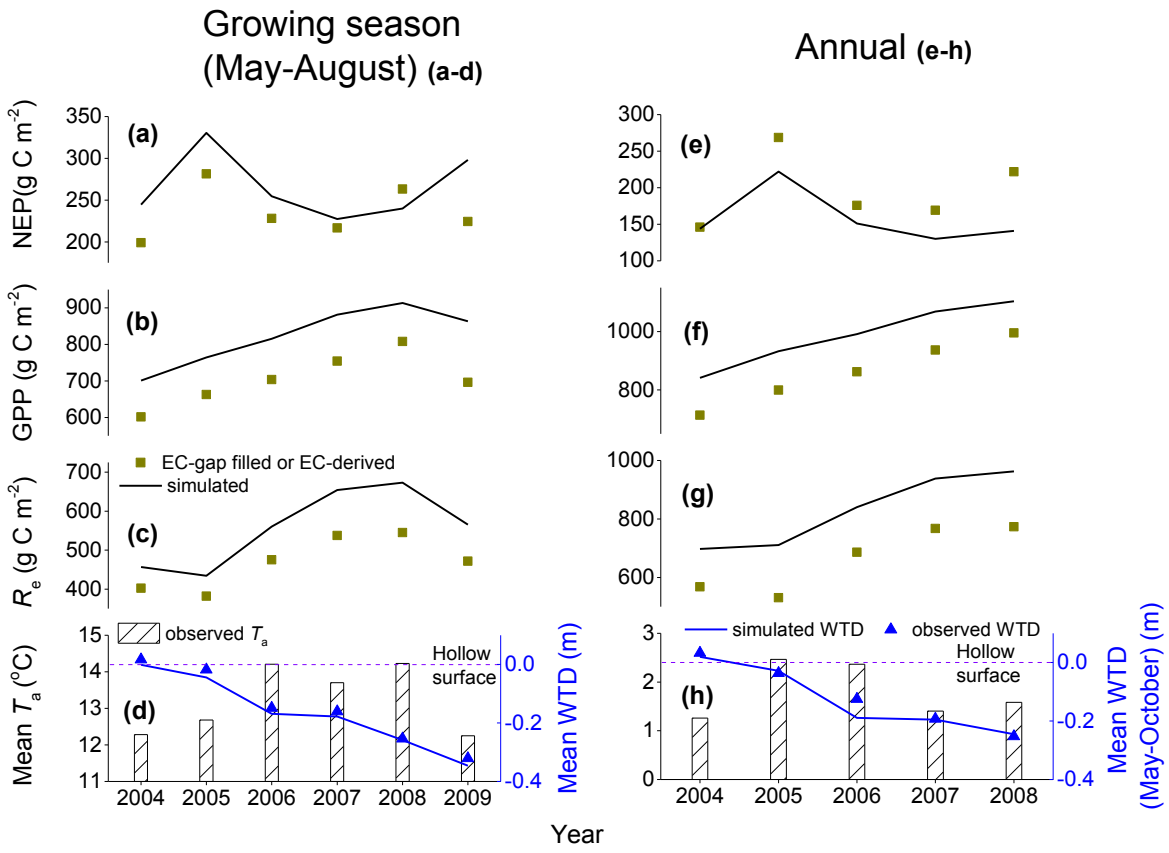

Fig. 5-6. Modelled and EC-derived (Flanagan and Syed 2011) growing season (May-August) sums of (a) net ecosystem productivity (NEP), (b) gross primary productivity (GPP), and (c) ecosystem respiration (R_e) during 2004-2009; (d) observed mean growing season air temperature (T_a) and measured and modelled average growing season water table depth (WTD) during 2004-2009; Modelled and EC-derived (Flanagan and Syed 2011) annual sums of (e) NEP, (f) GPP, and (g) R_e during 2004-2008; and (h) observed mean annual T_a and measured and modelled average WTD during ice free periods (May-October) of 2004-2008 at a Western Canadian fen peatland. A negative WTD represents a depth below hollow surface and a positive WTD represents a depth above hollow surface. A positive NEP means the ecosystem is a C sink and a negative NEP means the ecosystem is a C source

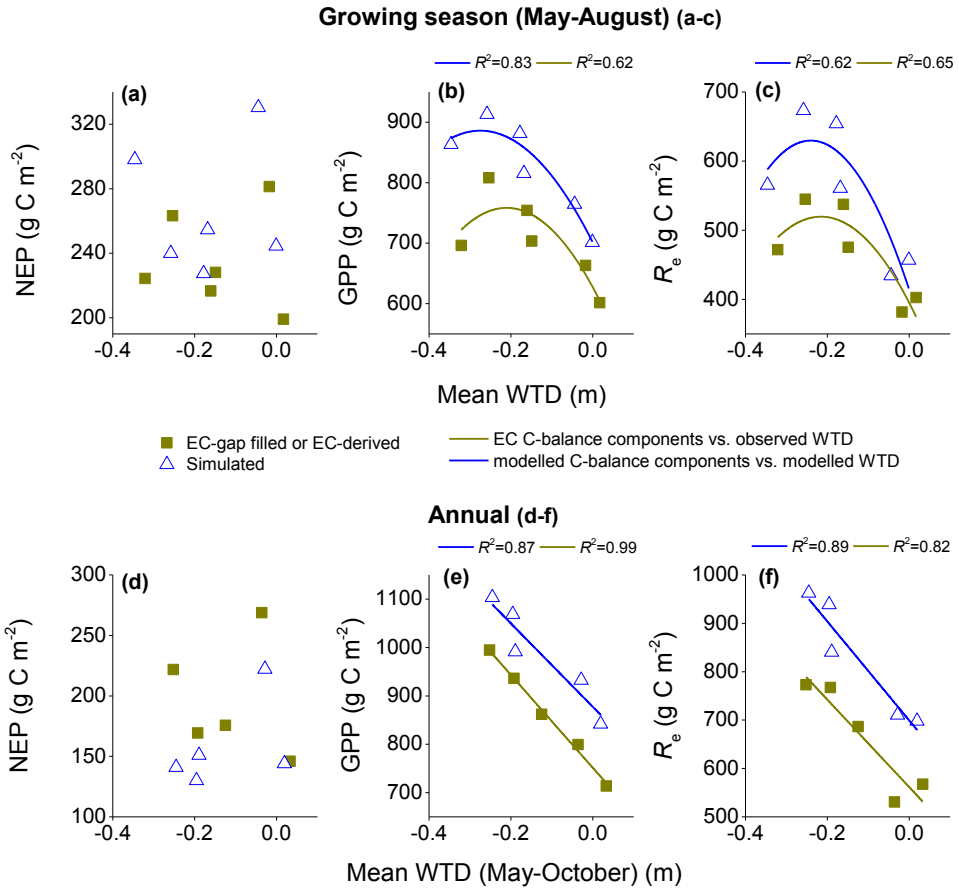

Fig. 5-7. Regressions (P<0.001) of growing season (May-August) sums of modelled and EC-derived (Flanagan and Syed 2011) (a) net ecosystem productivity (NEP), (b) gross primary productivity (GPP) and (c) ecosystem respiration (R_e) on growing season averages of modelled and observed water table depth (WTD) during 2004-2009; and regressions (P<0.001) of annual sums of modelled and EC-derived (Flanagan and Syed 2011) (d) NEP, (e) GPP and (f) R_e on average modelled and measured WTD during ice free periods (May-October) of 2004-2008 at a Western Canadian fen peatland. A negative WTD represents a depth below hollow surface and a positive WTD represents a depth above hollow surface. A positive NEP means the ecosystem is a C sink and a negative NEP means the ecosystem is a C source

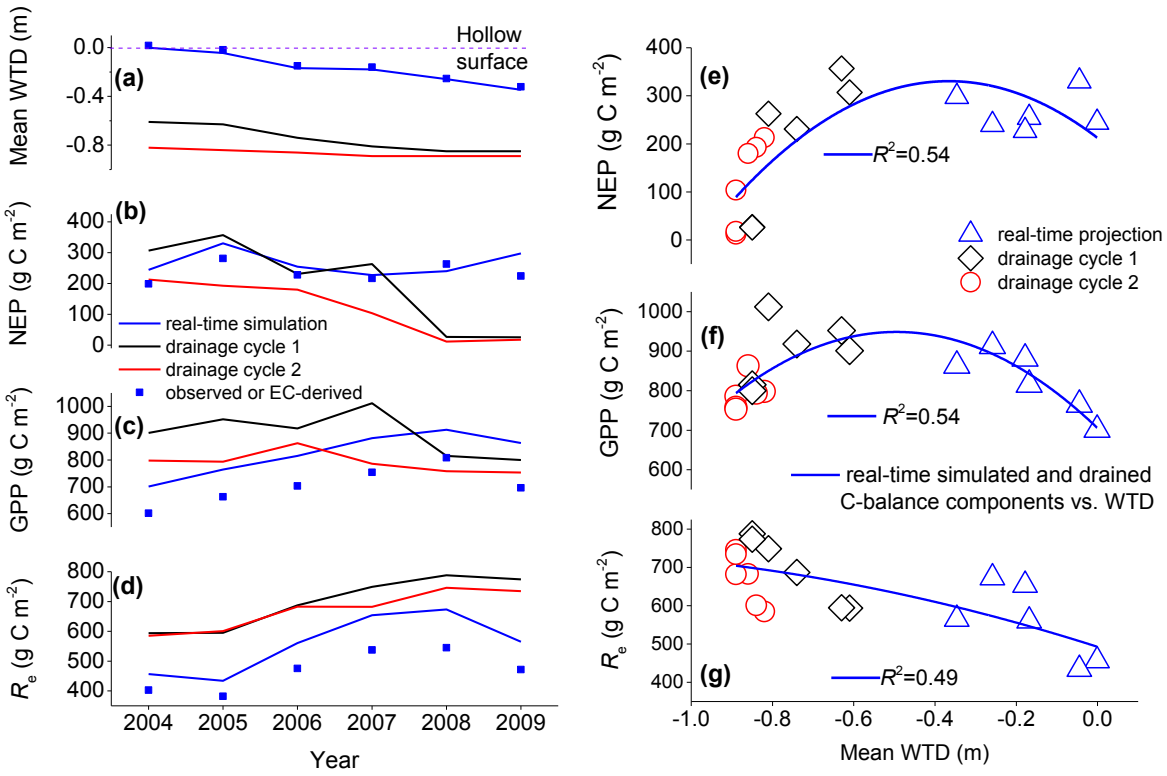

Fig. 5-8. (a) Observed, real-time simulated and projected drainage simulated (Sect. 5-2.2.6) average growing season (May-August) water table depth (WTD); EC-derived, real-time simulated and projected drainage simulated growing season sums of (b) net ecosystem productivity (NEP), (c) gross primary productivity (GPP), and (d) ecosystem respiration (R_e); and regressions (P<0.001) of real-time simulated and projected drainage simulated sums of (e) NEP, (f) GPP, and (g) R_e on real-time simulated and projected drainage simulated average growing season WTD during 2004-2009 at a Western Canadian fen peatland. A negative WTD represents a depth below hollow surface and a positive WTD represents a depth above hollow surface. A positive NEP means the ecosystem is a C sink and a negative NEP means the ecosystem is a C source

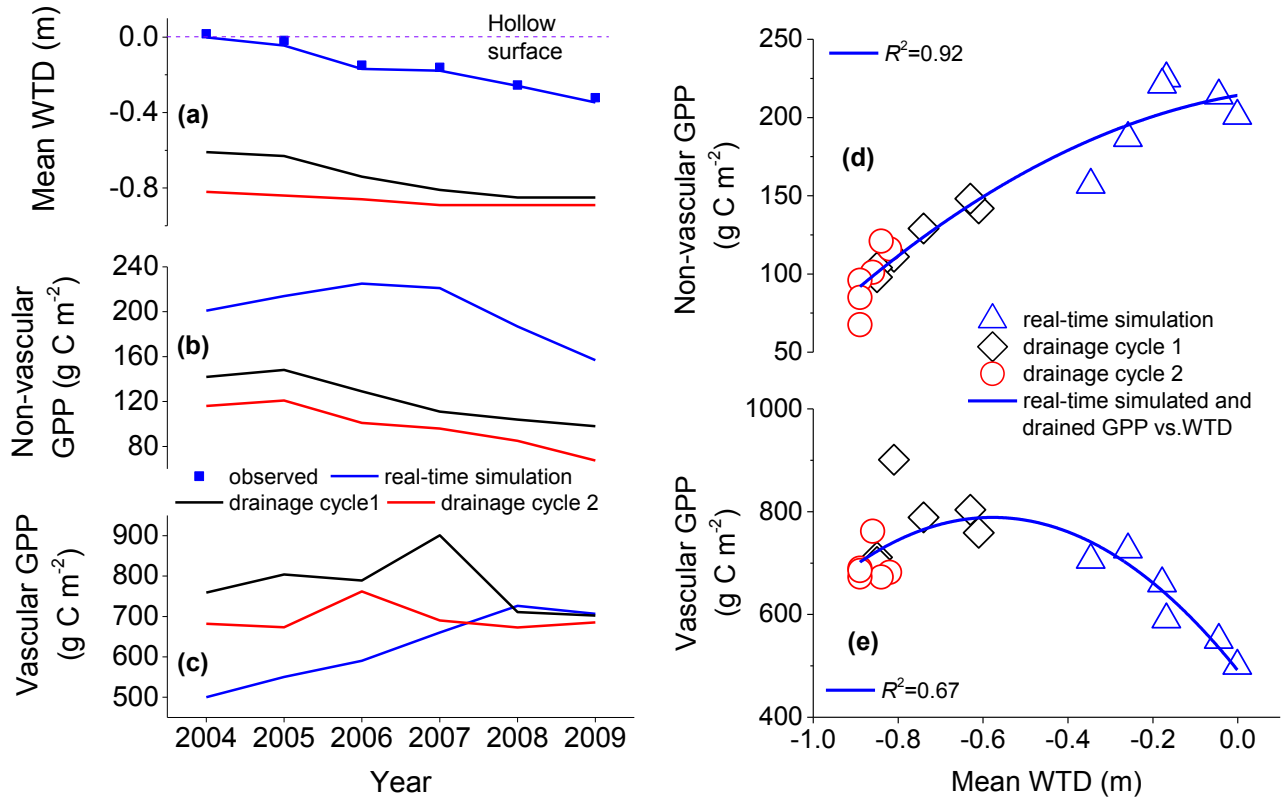

Fig. 5-9. Real-time simulated and projected drainage simulated (Sect. 5-2.2.6) (a) average growing season (May-August) water table depth (WTD), (b) growing season sums of non-vascular (moss) gross primary productivity (GPP), and (c) growing season sums of vascular GPP; and regressions (P<0.001) of real-time simulated and projected drainage simulated sums of (d) non-vascular GPP, and (e) vascular GPP on real-time simulated and projected drainage simulated average growing season WTD during 2004-2009 at a Western Canadian fen peatland. A negative WTD represents a depth below hollow surface and a positive WTD represents a depth above hollow surface

Chapter 6 : Synthesis

6-1. Modelling hydrological controls on variations in WTD and peat water contents in the two contrasting peatlands

Our modelling by using process-based ecosystem model *ecosys* successfully simulated seasonal and interannual variations of WTD and peat water contents over a wetting period from 2002 to 2005 in the tropical peatland (Fig. 2-2) (Table 2-1) and a drying period from 2004 to 2009 at the boreal peatland (Fig. 4-5) with the use of the same algorithms fed by site specific physical, hydrological and ecological inputs (Figs. 2-1 and 4-2) (Sects.2-2.2.3 and 4-2.2.3). Our results indicated that precipitation (*P*) to evapotranspiration (*ET*) ratio was the predominant control of seasonal and interannual variations in WTD and peat water contents in both of these two peatlands (Figs. 2-3, 4-6 and 4-7).

Gradually shallower WTD and consequent less peat drying from an El-Niño year 2002 to the wettest of all the study years 2005 were modelled from gradually larger *P* to *ET* ratio in the tropical peatland (Figs.2-2 and 2-3). *P* in excess of *ET* required gradually larger lateral discharge to be simulated from the driest year 2002 to the wettest year 2005 (Fig. 2-3). This was adequately simulated by the lateral boundary condition defined in *ecosys* by a specified WTD (WTD_x) representing adjacent watershed WTD with which the modelled grid cells laterally exchanged water over a specified distance (L_t) (Fig. 2-1). Shallower modelled WTD than the specified WTD_x from the driest to the wettest years yielded hydraulic gradients between modelled WTD and the WTD_x that generated higher lateral discharge using Darcy's law (Fig. 2-3).

Gradually deeper growing season (May-August) water table (WT) in the boreal peatland from 2004 to 2009 was also simulated predominantly from decreasing *P* to *ET* ratio (Figs. 4-6 and 4-7). This drying trend from 2004 to 2009 also caused deepening of regional WT that caused gradually reduced lateral water gain from the upper catchment areas (Fig. 4-7). This phenomenon was simulated by using three specified levels of WTD_x i.e. shallow (=0.19 m) for the wetter years (2003-2005), intermediate (=0.35 m) for the regular years (2006-2007) and deep (=0.72 m) for the drier years (2008-2009) to generate hydraulic gradients that yielded net lateral recharge in the wetter years and net lateral discharge in the drier years (Fig. 4-2).

Although *ecosys* successfully simulated the seasonal and interannual variations in peat water content in the tropical peatland, it substantially underestimated the peat water contents in the boreal peatland (Figs. 2-2b and 4-3a). The soil moisture retention algorithm in *ecosys* which calculates soil water matric potentials (ψ_m) as functions of soil water content (θ) uses a modified Campbell model (MCM) (Eqs. 4-1 to 4-4) (Fig. 4-1) (Campbell 1974) that was unable to simulate higher near saturation water retention before rapid drainage when ψ_m fell below a threshold i.e. air-entry potential (ψ_e) (Figs. 4-1 and 4-3). This was solved by using a van Genuchten (VGM) (Eqs.4-5 and 4-6) (Fig. 4-1) (Van Genuchten 1980) type logistic soil moisture retention curve. However, it required an additional input for ψ_m at inflection point (ψ_{in}) for each layer to calculate VGM shape parameters n and α (Eq. 4-6) (Figs. 4-1 and 4-2). To test the versatility of VGM in modelling contrasting peat water retention, we further applied this algorithm for the tropical peatland by using the additional input for ψ_{in} leaving everything else unchanged (Fig. 6-1). Peat water contents simulated by VGM vs. MCM suggested that the VGM similarly well simulated peat water contents from 0-0.2 m depth of the hummock as did the

MCM over a wetting period from 2002 to 2005 in the tropical peatland (Fig. 6-2a-d). Seasonal and interannual variations in WTD as simulated with the use of VGM moisture retention were also as good as that using MCM (Fig. 6-2e-h). Therefore, VGM algorithm in *ecosys* better simulated peat moisture retention in the boreal fen and similarly well simulated that in the tropical bog with respect to the MCM at the expense of one additional input of ψ_{in} for each peat layer. It can therefore be suggested that VGM could be a better model to simulate wide range of peat water retention in process-based modelling of peatland eco-hydrology. The advantage of VGM in simulating peat water retention was also reported in various field, laboratory and hydrological modelling studies that achieved better fits of measured soil moisture retention with the VGM in different peats (Silins and Rothwell 1998, Weiss et al. 1998, Schwärzel et al. 2006, Gnatowski et al. 2010, Dettmann et al. 2014).

6-2. Modelling effects of WTD variations on surface energy exchange of two contrasting peatlands

After successful simulation of seasonal and interannual variations in WTD and peat water contents, *ecosys* went on to reasonably well simulate the effects of these variations on surface energy exchange and vegetation water stress in the tropical and the boreal peatlands. *Ecosys* successfully modelled late dry season (August-October) water stress due to WTD drawdown from early to late dry seasons causing declines in *ET* and rises in mid-day Bowen ration β [=sensible heat (*H*)/latent heat (*LE*)] (10:00 – 14:00 local time) in the drier years 2002-2004 in the tropical bog peatland (Figs. 2-5a, d). However, *ecosys* also simulated the absence of late dry season water stress and consequent absence of decline in *ET* in the wettest dry season of 2005 (Figs. 2-5a, d). This simulation of interannual variation in late dry season plant water stress and

surface energy exchange was achieved by adequately modelling (1) vertical root water uptake profiles from vertical root distribution from differential root O_2 availability governed by root-WTD interactions and (2) equilibrium between root water uptake and plant water loss via transpiration through a series of water potentials (e.g. ψ_s=soil water potential, ψ_r=root water potential, and ψ_c=canopy water potential) and hydraulic resistances (e.g. Ω_s=soil hydraulic resistance, Ω_r=root hydraulic resistance, r_c=canopy stomatal resistance) in a soil-plant-atmosphere moisture continuum.

WTD drawdown from early (May-July) to late (August-October) dry seasons caused improved root O_2 availability and hence enhanced deeper root growth and root water uptake from wetter deeper peat layers (Fig. 2-10). However, when WTD fell below a threshold of ~1.0 m below the hollow surface, near surface peat desiccation occurred due to inadequate capillary recharge from the deep WT in the drier dry seasons of 2002-2004. This desiccation suppressed root water uptake from these near surface layers by reducing ψ_s and increasing Ω_s. These near surface peat layers were colonized by most of the tree roots due to relatively better O_2 availability in these layers that remain unsaturated even in the wet season (Fig. 2-10). Suppression of root water uptake from these near surface peat layers in dry seasons thus exceeded the increase in deeper root water uptake enabled by deeper rooting , thereby causing a net decline in root water uptake in drier dry seasons of 2002-2004 with deep WT. This decline in root water uptake caused a reduction in ψ_c (Fig. 2-9a) and canopy conductance ($g_c=1/r_c$) (Fig. 2-9b) thereby reducing transpiration and increasing β in the model corroborated by EC-gap filled site data (Figs. 2-5a, d and 2-6). However, lack of near surface peat desiccation in the wettest dry season of 2005 due to better vertical recharge of these than the other late dry seasons (2002-

2004) sustained root water uptake from these layers and prevented plant water stress (Figs. 2-5a, d and 2-9a, b).

The algorithms in *ecosys* representing balance between transpiration and root water uptake in a soil-plant-atmosphere moisture scheme also enabled us to model late growing season (mid-July to mid-August) reductions in *ET* and rises in β (2 hours before and after solar noon) when WT fell below a threshold of ~0.35 m below the hollow surface during drier years 2008 and 2009 than other years 2004-2007 in the boreal fen peatland (Figs. 4-11a, b, c). This late growing season ecosystem drying in 2008 and 2009 was modelled predominantly from the reduction in evaporation (*E*) from non-vascular (moss) canopies. Modelled mosses had shallow rhizoids due to higher intraspecific competition for light and nutrients (nitrogen and phosphorus) from larger population. These shallow rhizoids mostly colonized near surface peat layers with less saturation and higher O_2 availability throughout the year. In the drier late growing seasons of 2008 and 2009 when WT fell below the threshold of ~0.35 m below the hollow surface, inadequate capillary recharge of these near surface peat layers from deeper WT caused reductions in moss water uptake, and hence moss ψ_c and moss *E* (Figs. 4-9a and 4-10c). Unlike mosses, deeper root growth and root water uptake from deeper peat layers facilitated by improved root oxygenation during these deep WT periods enabled the vascular plants to sustain root water uptake and hence ψ_c, g_c and transpiration (Figs. 4-9a and 4-10b). However, reduction in moss *E* was greater than the sustained vascular transpiration thereby contributing to overall reduction in ecosystem *ET* and rise in β when WTD fell below the threshold of ~0.35 m below the hollow surface in the late growing seasons of 2008 and 2009 (Figs. 4-9a, b and 4-10a). Despite the successful modelling of WTD threshold effect on ecosystem drying in drier late

growing seasons, our eco-hydrology modelling could not attribute large declines in May-June *ET* and rise in May-June β from 2007 to 2008 that were apparent in EC-gap filled site data as a WTD drawdown and consequent peat drying effect (Fig. 4-11d, e, f) (Table 4-2) (Sect. 4-4.4).

6-3. Modelling WTD effects on ecosystem net CO_2 exchange of the two contrasting peatlands

After successful simulation of the effects of seasonal and interannual variations in WTD and peat moisture contents on surface energy exchange of the tropical and the boreal peatland (Sects. 6-1 and 6-2), our modelling with *ecosys* went on to further simulate how these variations affected net ecosystem CO_2 exchanges of these peatlands. In the tropical peatland, shallow WTD i.e. 0-0.3 m below the hollow surface during the rainy seasons (November-April) caused lower gross primary productivity (GPP) and hence reduced net ecosystem productivity (NEP) (Figs. 3-2 to 3-8). This GPP suppression due to shallow WTD was simulated from poor aeration under wet soils that impaired root and microbial O_2 availability, hindered root growth and nutrient mineralization and hence caused poor root nutrient availability and uptake and consequent poor foliar nutrient status (mainly Phosphorus) thereby slowing CO_2 fixation. WTD drawdown from shallow (rainy seasons) to intermediate (early dry seasons, May-July) WTD, i.e. 0.3-0.8 m below the hollow surface, raised GPP and caused no change or little decrease in ecosystem respiration (R_e), thereby causing an increase in NEP (Figs. 3-2 to 3-8). This increased GPP was modelled through the improvement of foliar nutrient status enhanced by improved root and microbial O_2 availability facilitated by the WTD drawdown. Improved microbial O_2 availability during the intermediate WTD period raised deeper peat respiration in the model which was fully or more than fully offset by the reduction in surface and near surface desiccated peat decomposition thereby causing no increase or slight decrease in R_e. Continued WTD drawdown from the early

to late dry seasons (August-October) caused WT to fall below a threshold of ~1.0 m below the hollow surface. This deep WTD caused increases in R_e and reductions in GPP thereby reducing NEP (Figs. 3-2 to 3-8). This reduction in NEP during the deep WTD period was, however, more prominent in the drier dry seasons of 2002-2004 than the wetter dry season of 2005 when WT seldom deepened below the threshold (Figs. 3-2 to 3-8). Modelled GPP in this deep WTD period in the drier years of 2002-2004 was limited by plant water stress mainly due to near surface peat drying (Sect. 6-2). However, reduction in modelled GPP was not prominent in the wetter dry season of 2005. Increases in modelled deeper peat decomposition in the deep WTD periods stimulated by enhanced aeration and microbial O_2 availability (Fig. 3-11) raised deeper peat respiration to an extent that exceeded the reduction in desiccated surface and near surface peat decomposition thereby causing a large increase in R_e (Figs. 3-2 to 3-5, 3-7 and 3-8)

Overall the tropical peatland was a large source of C throughout the study period i.e. 2002-2005 as indicated by large negative modelled and EC-gap filled NEP. Since this peatland was drained in 1997, we assumed that this would have been an artifact of unusually deep WT due to the drainage. To examine the drainage effect, we performed an undrained simulation raising the reference external WTD (WTD_x) by 0.6 m leaving everything else unchanged. Our undrained simulation predicted that the WTD in this tropical peatland would have been ~0.5 m shallower if it was not drained and this trend was also corroborated by WTD measurements from a nearby similar undrained tropical peatland (Fig. 3-9). This drained vs. undrained simulation also suggested that this tropical peatland would have been a smaller source of C if it was not drained which was also supported by EC-gap filled drained vs. undrained tropical peatland C balance study by Hirano et al. (2012) (Fig. 6-3). Hirano et al. (2012) in their study included EC-gap filled estimates of NEP and measured WTD from 2002-03 to 2008-09 in the same drained

site as in our study and NEP and WTD from 2004-05 to 2008-09 in a nearby similar undrained site (Fig. 6-3). Our drained vs. undrained simulation was consistent with the EC-gap filled study by Hirano et al. (2012), which further suggested that whether drained or not this tropical peatland was an increasingly large source of C with WTD drawdown due to increased intensity and duration of dry seasons (Fig. 6-3). The undrained model projection along with EC-gap filled estimates by Hirano et al. (2012) in a nearby undrained site also suggested that a WT very close to or above the hollow surface is required to bring this tropical peatland ecosystem at least to C neutrality (Fig. 6-3). Increased frequencies of recent climate extremes like El-Niño and consequent less precipitation and deeper WT than the long-term normal shifted this tropical peatland from a long-term C sink for last 26,000 years to a large C source in recent decades (Takahashi et al. 2004, Dommain et al. 2011).

Gradually deeper WT from 2004 to 2009 in the boreal fen peatland caused increases in both R_e and GPP (Figs. 5-6 and 5-7). Similar increases in R_e and GPP left no net WTD drawdown effect on NEP in this peatland (Fig. 5-7). The increase in R_e with WTD drawdown was modelled through improved microbial energy yields enhanced by improved microbial O_2 availability due to increased peat oxygenation caused by rapid peat pore drainage in deeper WT periods thereby facilitating rapid peat decomposition. However, when WT fell below ~0.3 m from the hollow surface, surface and near surface peat desiccation due to inadequate vertical recharge through capillary rise from the WT reduced surface and near surface peat decomposition. This reduction in surface and near surface peat decomposition more than fully offset increased deeper peat decomposition due to improved aeration thereby caused a reduction in R_e (Figs. 5-6c, 5-7c and 5-8d).

Increase in microbial decomposition due to improved aeration also enhanced rates of mineralization that increased nutrient (mainly nitrogen) availability for vascular roots. Higher root nutrient availability along with improved root O_2 availability in deeper WT periods enhanced root growth and uptake thereby raising vascular GPP with WTD drawdown (Figs. 5-6b,f and 5-7b,e). However, when modelled WT fell below ~0.10 m from the hollow surface, modelled non-vascular (moss) GPP started to decline because of inadequate rhizoid water uptake from near surface peat layers that were desiccated due to inadequate vertical recharge through capillary rise from the WT (Figs. 5-9b,d). But this decline in modelled moss GPP was more than fully offset by increased vascular GPP thereby contributing to overall increase in ecosystem GPP with WTD drawdown (Figs. 5-6b, f and 5-9c).

Our modelled drainage projection, however, showed that the resilience of current C accumulation function of this peatland might be disrupted with further drawdown of WT. When the projected WT fell below ~0.6 m from the hollow surface, modelled vascular GPP started to decline due to supressed root water uptake from peat drying and consequent plant water stress thereby contributing to overall decline in ecosystem GPP (Figs. 5-8b, c, e, f and 5-9c, e). Increased deeper R_h from peat decomposition due to improved aeration in this period was larger than the suppression of R_h from surface and near surface peat decomposition due to desiccation thereby causing overall increase in R_e (Fig. 5-8g). Decline in GPP and increase in R_e thereby caused decline in modelled NEP when the projected WT fell below ~0.45 m from the hollow surface (Fig. 5-8b, e). This short-term modelled drainage effect of declining NEP due to increasing R_e and decreasing GPP was also found in measurements and modelling of our drained tropical peatland site thereby further indicating the significance and adequacy of our modelling of WTD drawdown effects on peatland C balance (Fig. 6-3) (Table 3-4).

6-4. Concluding remarks

Our objective of simulating WTD effects on net ecosystem CO_2 exchange of the two contrasting peatlands – the tropical drained bog and the boreal pristine fen have been achieved. This simulation is achieved by adequately modelling and coupling the processes representing WTD dynamics, soil moisture retention, root and microbial redox reactions as affected by WTD and soil moisture retention, root nutrient availability and uptake, and equilibrium between root/rhizoidal water uptake and vascular/non-vascular transpiration/evaporation in a soil-microbe-plant-atmosphere carbon, water, energy and nutrient (nitrogen and phosphorus) scheme. Using the same set of algorithms in *ecosys* representing these processes, when fed with site specific inputs for peat physical, chemical, and biological properties; vegetation characteristics; and weather conditions (Figs. 2-1, 4-2, 5-1) (Table 3-1) (Sects. 2-2.2.3, 3-2.2.3,4-2.23, 5-2.2.3), enabled us to simulate WTD feedbacks to peatland NEP, GPP and R_e in these two peatlands differing vastly in climate, peat type and peat forming vegetation. This indicated that this type of modelling is reproducible across peatlands with different peat types i.e. bog vs. fen, and vegetation i.e. trees/shrubs vs. mosses developed under wide range of climates i.e. from boreal to tropical. Along with weather driven WTD drawdown, our modelling could also simulate drainage induced WTD drawdown effects on C processes in these two peatlands. This is an additional improvement in our predictive capacity of how peatland C stocks are vulnerable to artificial drainage to promote agriculture that is a common human intervention across peatlands in the world. Besides, this type of modelling can also be scaled up from site to global scale and hourly to century scale by inputting climatic, edaphic and ecological characteristics (Figs. 2-1, 4-2, 5-1) (Table 3-1) (Sects. 2-2.2.3, 3-2.2.3,4-2.23, 5-2.2.3) and not parameterizing the model algorithms. This provides a platform for launching a regional, national, continental and/or global

scale modelling for predicting how drier and warmer future climate and disturbance (e.g. drainage) driven WTD drawdown would affect the C stocks peatlands, lack of which is thus far limiting our predictive capacity on such issues. The insight gained from this modelling study is thus a significant contribution to our understanding and apprehension of how peatlands would behave with changing hydrology under future drier and warmer climates.

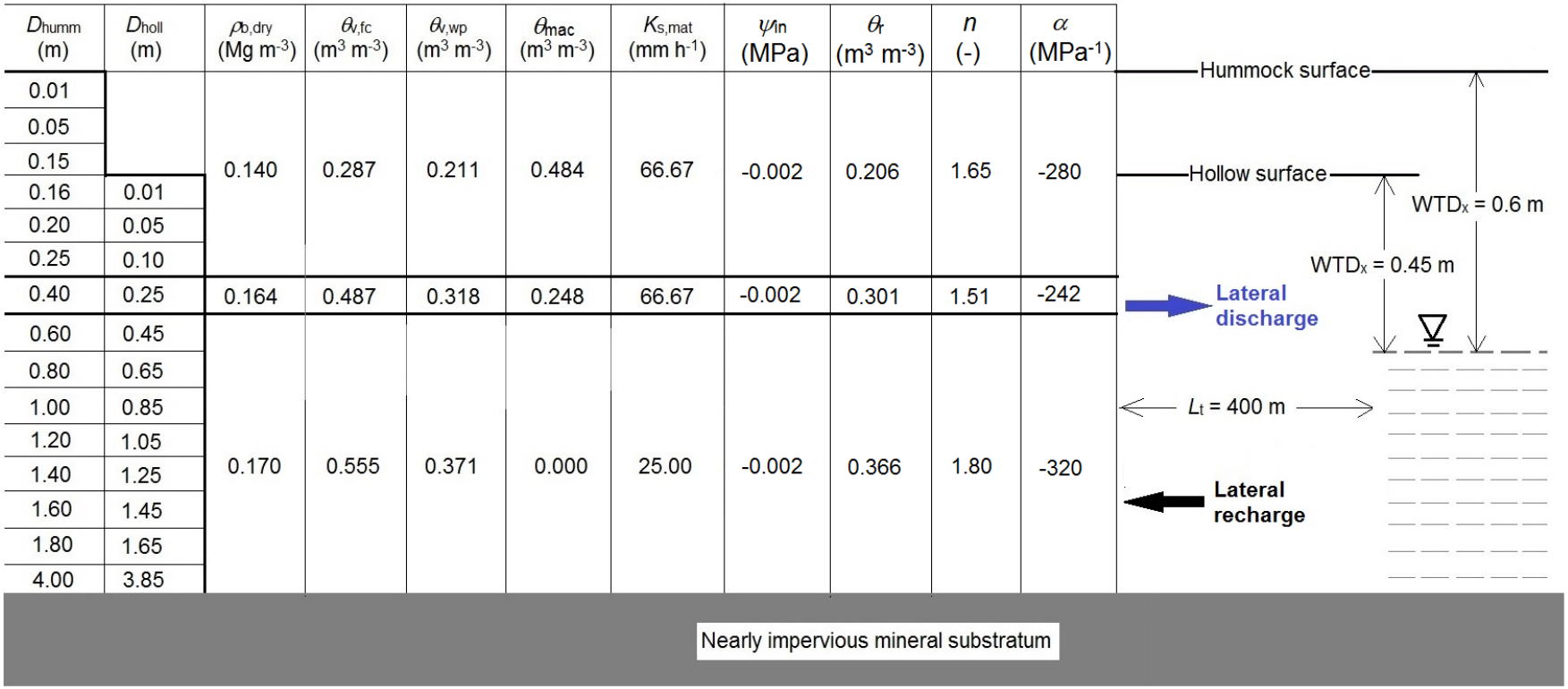

D_{humm} (m)	D_{holl} (m)	$\rho_{b,dry}$ (Mg m^{-3})	$\theta_{v,fc}$ (m^3 m^{-3})	$\theta_{v,wp}$ (m^3 m^{-3})	θ_{mac} (m^3 m^{-3})	$K_{s,mat}$ (mm h^{-1})	ψ_{in} (MPa)	θ_r (m^3 m^{-3})	n (-)	α (MPa^{-1})
0.01		0.140	0.287	0.211	0.484	66.67	-0.002	0.206	1.65	-280
0.05										
0.15										
0.16	0.01									
0.20	0.05									
0.25	0.10									
0.40	0.25	0.164	0.487	0.318	0.248	66.67	-0.002	0.301	1.51	-242
0.60	0.45	0.170	0.555	0.371	0.000	25.00	-0.002	0.366	1.80	-320
0.80	0.65									
1.00	0.85									
1.20	1.05									
1.40	1.25									
1.60	1.45									
1.80	1.65									
4.00	3.85									

Fig. 6-1. Experimental modelling layout in *ecosys* and key inputs for soil physical and hydrological properties representative of a drainage affected tropical peat swamp forest at Palangkaraya, Indonesia. Figure was not drawn to scale. D_{humm} = depth to the bottom of a layer from the hummock surface; D_{holl} = depth to the bottom of a layer from the hollow surface; $\rho_{b,dry}$ = dry bulk density (Takakai et al. 2006, Jauhiainen et al. 2012b); $\theta_{v,fc}$ = volumetric soil water content at field capacity (-0.01 MPa) and $\theta_{v,wp}$ = volumetric soil water content at wilting point (-1.5 MPa) (Kurnain et al. 2001); $K_{s,mat}$ = saturated hydraulic conductivity of soil matrix (Ong and Yogeswaran 1991); θ_{mac} = volumetric macropore fractions; WTD_x = average water table depth of the adjacent ecosystem; L_t = distance from modelled grid cells to the adjacent watershed over which lateral discharge/recharge occurs; ψ_{in}= matric water potential at the inflection point; θ_r = residual soil water content; n and α=van Genuchten model (VGM) shape parameters

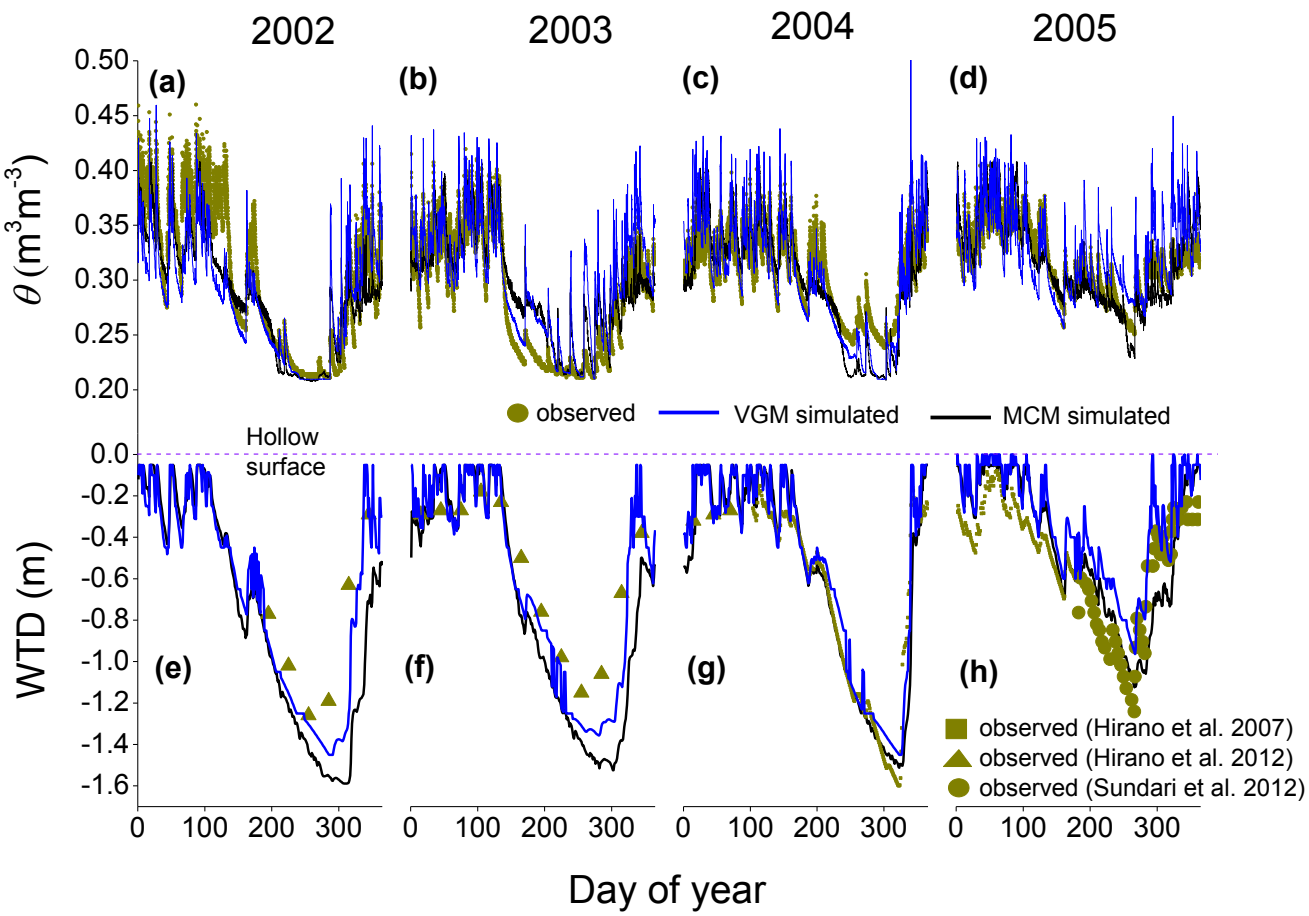

Fig. 6-2. (a-d) Hourly observed, van Genuchten model (VGM) (Van Genuchten 1980) simulated and modified Campbell model (MCM) (Campbell 1974) simulated soil water contents (θ) from 0-0.2 m depth of a hummock and (e-h) monthly and daily observed and daily VGM and MCM simulated water table depths (WTD) from 2002-2005 in a drainage affected tropical peat swamp forest at Palangkaraya, Indonesia. Negative values of WTD mean depths below the hollow surface

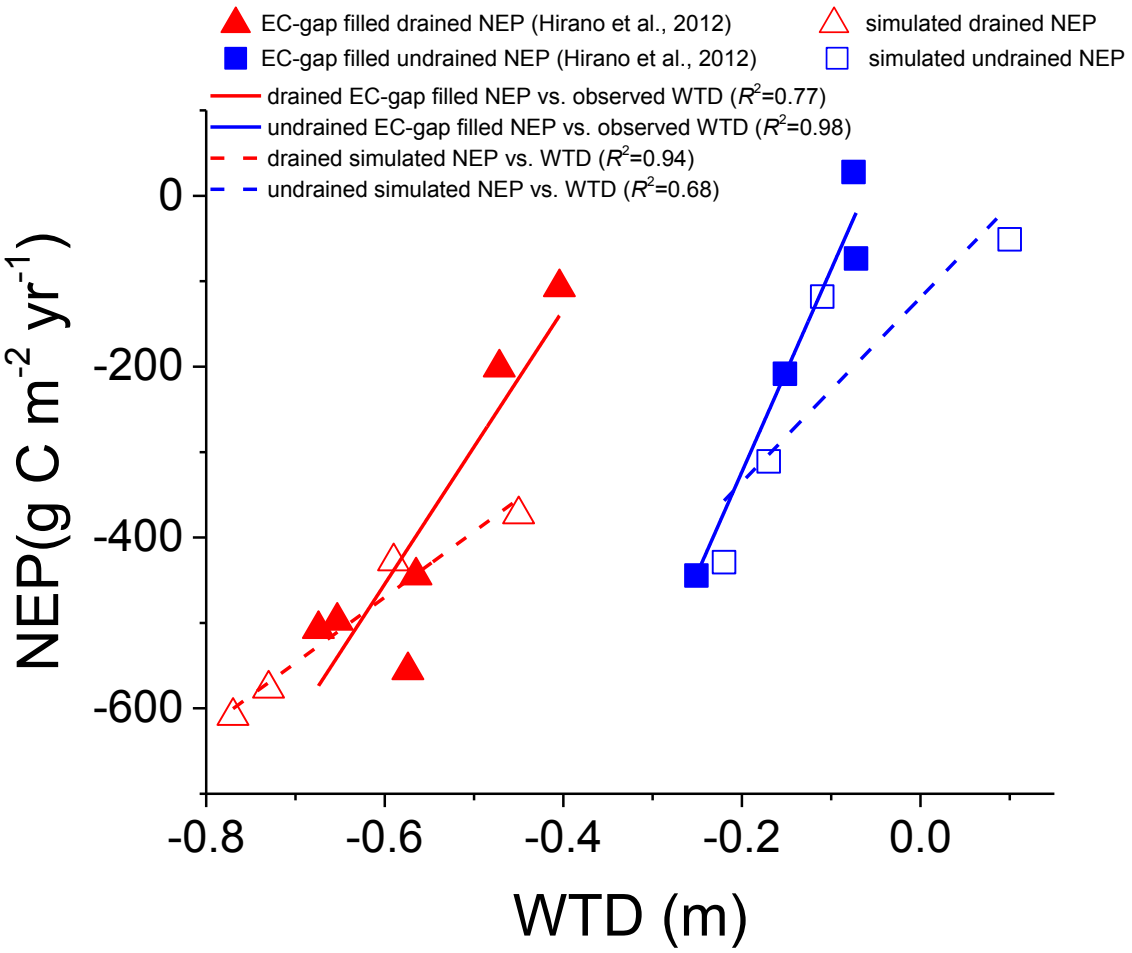

Fig. 6-3. Relationships between simulated drained/undrained (Sects. 2-2.2.5 and 3-2.2.6) net ecosystem productivity (NEP) and drained/undrained water table depths (WTD) during 2002-2005; and EC-gap filled drained NEP and observed drained WTD during 2002-03 to 2008-09 (Hirano et al. 2012) in a drainage affected tropical peat swamp forest at Palangkaraya, Indonesia; and EC-gap filled undrained NEP and observed undrained WTD during 2004-05 to 2008-09 in a undrained nearby tropical peat swamp forest (Hirano et al. 2012). Negative values of WTD mean depths below the hollow surface. Negative values of NEP mean the ecosystem is a C source and positive values of NEP mean the ecosystem is a C sink

References

Addiscott, T. 1983. Kinetics and temperature relationships of mineralization and nitrification in Rothamsted soils with differing histories. Journal of Soil Science **34**:343-353.

Aerts, R., and F. Chapin III. 2000. The mineral nutrition of wild plants revisited. Adv Ecol Res **30**:1-67.

Andriesse, J. 1988. Nature and management of tropical peat soils. Food & Agriculture Org.

Baker, I., L. Prihodko, A. Denning, M. Goulden, S. Miller, and H. Da Rocha. 2008. Seasonal drought stress in the Amazon: Reconciling models and observations. Journal of Geophysical Research: Biogeosciences (2005–2012) **113**.

Ballantyne, D. M., J. A. Hribljan, T. G. Pypker, and R. A. Chimner. 2014. Long-term water table manipulations alter peatland gaseous carbon fluxes in Northern Michigan. Wetlands ecology and management **22**:35-47.

Barber, S., and M. Silberbush. 1984. Plant root morphology and nutrient uptake. Roots, Nutrient and Water Influx and Plant Growth:65-88.

Barnes, B. V., D. R. Zak, S. R. Denton, and S. H. Spurr. 1997. Forest ecology. John Wiley and Sons.

Barr, A. G., T. Black, E. Hogg, N. Kljun, K. Morgenstern, and Z. Nesic. 2004. Inter-annual variability in the leaf area index of a boreal aspen-hazelnut forest in relation to net ecosystem production. Agricultural and Forest Meteorology **126**:237-255.

Bernacchi, C., C. Pimentel, and S. Long. 2003. In vivo temperature response functions of parameters required to model RuBP-limited photosynthesis. Plant, cell & environment **26**:1419-1430.

Bernacchi, C., E. Singsaas, C. Pimentel, A. Portis Jr, and S. Long. 2001. Improved temperature response functions for models of Rubisco-limited photosynthesis. Plant, cell & environment **24**:253-259.

Boelter, D. 1969. Physical properties of peats as related to degree of decomposition. Soil Science Society of America Journal **33**:606-609.

Boelter, D. 1970. Important physical properties of peat materials. Pages 150-154 *in* 3rd International Peat Congress Proceedings, Helsinki, Finland.

Bond-Lamberty, B., S. T. Gower, and D. E. Ahl. 2007. Improved simulation of poorly drained forests using Biome-BGC. Tree physiology **27**:703-715.

Brümmer, C., T. A. Black, R. S. Jassal, N. J. Grant, D. L. Spittlehouse, B. Chen, Z. Nesic, B. D. Amiro, M. A. Arain, and A. G. Barr. 2012. How climate and vegetation type influence evapotranspiration and water use efficiency in Canadian forest, peatland and grassland ecosystems. Agricultural and Forest Meteorology **153**:14-30.

Cai, T., L. B. Flanagan, and K. H. Syed. 2010. Warmer and drier conditions stimulate respiration more than photosynthesis in a boreal peatland ecosystem: analysis of automatic chambers and eddy covariance measurements. Plant, cell & environment **33**:394-407.

Campbell, G. 1985. Soil Physics with BASIC, 150 pp. Elsevier, New York.

Campbell, G. S. 1974. A simple method for determining unsaturated conductivity from moisture retention data. Soil science **117**:311-314.

Chambers, J. Q., E. S. Tribuzy, L. C. Toledo, B. F. Crispim, N. Higuchi, J. d. Santos, A. C. Araujo, B. Kruijt, A. D. Nobre, and S. E. Trumbore. 2004. Respiration from a tropical forest ecosystem: partitioning of sources and low carbon use efficiency. Ecological Applications **14**:72-88.

Choi, W.-J., S. X. Chang, and J. S. Bhatti. 2007. Drainage affects tree growth and C and N dynamics in a minerotrophic peatland. Ecology **88**:443-453.

Couwenberg, J., R. Dommain, and H. Joosten. 2010. Greenhouse gas fluxes from tropical peatlands in south-east Asia. Global Change Biology **16**:1715-1732.

Couwenberg, J., and A. Hooijer. 2013. Towards robust subsidence-based soil carbon emission factors for peat soils in south-east Asia, with special reference to oil palm plantations. Mires and Peat **12**:1-13.

Cronk, J. K., and M. S. Fennessy. 2001. Wetland plants: biology and ecology. CRC press.

De Vries, D. 1963. The physics of plant environments. Environmental control of plant growth:5-22.

Dettmann, U., M. Bechtold, E. Frahm, and B. Tiemeyer. 2014. On the applicability of unimodal and bimodal van Genuchten–Mualem based models to peat and other organic soils under evaporation conditions. Journal of Hydrology **515**:103-115.

Dimitrov, D. D., J. S. Bhatti, and R. F. Grant. 2014. The transition zones (ecotone) between boreal forests and peatlands: Modelling water table along a transition zone between upland black spruce forest and poor forested fen in central Saskatchewan. Ecological Modelling **274**:57-70.

Dimitrov, D. D., R. F. Grant, P. M. Lafleur, and E. R. Humphreys. 2010a. Modeling the effects of hydrology on ecosystem respiration at Mer Bleue bog. Journal of Geophysical Research: Biogeosciences (2005–2012) **115**.

Dimitrov, D. D., R. F. Grant, P. M. Lafleur, and E. R. Humphreys. 2010b. Modeling the subsurface hydrology of Mer Bleue Bog. Soil Science Society of America Journal **74**:680-694.

Dimitrov, D. D., R. F. Grant, P. M. Lafleur, and E. R. Humphreys. 2011. Modeling the effects of hydrology on gross primary productivity and net ecosystem productivity at Mer Bleue bog. Journal of Geophysical Research: Biogeosciences (2005–2012) **116**.

Dise, N. B. 2009. Peatland response to global change. Science **326**:810.

Dommain, R., J. Couwenberg, and H. Joosten. 2010. Hydrological self-regulation of domed peatlands in south-east Asia and consequences for conservation and restoration. Mires and Peat **6**:1-17.

Dommain, R., J. Couwenberg, and H. Joosten. 2011. Development and carbon sequestration of tropical peat domes in south-east Asia: links to post-glacial sea-level changes and Holocene climate variability. Quaternary Science Reviews **30**:999-1010.

Doussan, C., G. Vercambre, and L. Pagè. 1998. Modelling of the hydraulic architecture of root systems: An integrated approach to water absorption—Distribution of axial and radial conductances in maize. Annals of Botany **81**:225-232.

Farquhar, G., S. v. von Caemmerer, and J. Berry. 1980. A biochemical model of photosynthetic CO2 assimilation in leaves of C3 species. Planta **149**:78-90.

Flanagan, L. B., and K. H. Syed. 2011. Stimulation of both photosynthesis and respiration in response to warmer and drier conditions in a boreal peatland ecosystem. Global Change Biology **17**:2271-2287.

Frolking, S., N. T. Roulet, T. R. Moore, P. M. Lafleur, J. L. Bubier, and P. M. Crill. 2002. Modeling seasonal to annual carbon balance of Mer Bleue Bog, Ontario, Canada. Global Biogeochemical Cycles **16**:4-1-4-21.

Frolking, S., J. Talbot, M. C. Jones, C. C. Treat, J. B. Kauffman, E.-S. Tuittila, and N. Roulet. 2011. Peatlands in the Earth's 21st century climate system. Environmental Reviews **19**:371-396.

Gerten, D., S. Schaphoff, U. Haberlandt, W. Lucht, and S. Sitch. 2004. Terrestrial vegetation and water balance—hydrological evaluation of a dynamic global vegetation model. Journal of Hydrology **286**:249-270.

Gnatowski, T., J. Szatyłowicz, T. Brandyk, and C. Kechavarzi. 2010. Hydraulic properties of fen peat soils in Poland. Geoderma **154**:188-195.

Gorham, E. 1991. Northern peatlands: role in the carbon cycle and probable responses to climatic warming. Ecological Applications **1**:182-195.

Goulden, M. L., B. C. Daube, S. M. Fan, D. J. Sutton, A. Bazzaz, J. W. Munger, and S. C. Wofsy. 1997. Physiological responses of a black spruce forest to weather. Journal of Geophysical Research: Atmospheres (1984–2012) **102**:28987-28996.

Grant, R. 1998. Simulation in ecosys of root growth response to contrasting soil water and nitrogen. Ecological Modelling **107**:237-264.

Grant, R. 2001. A review of the Canadian ecosystem model ecosys, In 'Modelling Carbon and Nitrogen Dynamics for Soil Management'.(Ed MJ Shaffer) pp. 175-264. CRC Press: Boca Raton.

Grant, R., M. Amrani, D. Heaney, R. Wright, and M. Zhang. 2004. Mathematical modeling of phosphorus losses from land application of hog and cattle manure. Journal of environmental quality **33**:210-231.

Grant, R., D. Baldocchi, and S. Ma. 2012a. Ecological controls on net ecosystem productivity of a seasonally dry annual grassland under current and future climates: Modelling with ecosys. Agricultural and Forest Meteorology **152**:189-200.

Grant, R., A. Barr, T. Black, H. Margolis, A. Dunn, J. Metsaranta, S. Wang, J. McCaughey, and C. Bourque. 2009a. Interannual variation in net ecosystem productivity of Canadian

forests as affected by regional weather patterns–A Fluxnet-Canada synthesis. Agricultural and Forest Meteorology **149**:2022-2039.

Grant, R., A. Barr, T. Black, H. Margolis, J. McCaughey, and J. Trofymow. 2010. Net ecosystem productivity of temperate and boreal forests after clearcutting—A Fluxnet-Canada measurement and modelling synthesis. Tellus B **62**:475-496.

Grant, R., T. Black, E. Humphreys, and K. Morgenstern. 2007. Changes in net ecosystem productivity with forest age following clearcutting of a coastal Douglas-fir forest: testing a mathematical model with eddy covariance measurements along a forest chronosequence. Tree physiology **27**:115-131.

Grant, R., A. Desai, and B. Sulman. 2012b. Modelling contrasting responses of wetland productivity to changes in water table depth. Biogeosciences **9**:4215-4231.

Grant, R., and L. Flanagan. 2007. Modeling stomatal and nonstomatal effects of water deficits on CO_2 fixation in a semiarid grassland. Journal of Geophysical Research: Biogeosciences (2005–2012) **112**.

Grant, R., and J. Hesketh. 1992. Canopy structure of maize (*Zea mays L.*) at different populations: simulation and experimental verification. Biotronics **21**:11-24.

Grant, R., L. Hutyra, R. C. Oliveira, J. Munger, S. Saleska, and S. Wofsy. 2009b. Modeling the carbon balance of Amazonian rain forests: resolving ecological controls on net ecosystem productivity. Ecological monographs **79**:445-463.

Grant, R., N. Juma, and W. McGill. 1993a. Simulation of carbon and nitrogen transformations in soil: microbial biomass and metabolic products. Soil Biology and Biochemistry **25**:1331-1338.

Grant, R., N. Juma, and W. McGill. 1993b. Simulation of carbon and nitrogen transformations in soil: mineralization. Soil Biology and Biochemistry **25**:1317-1329.

Green, R., and J. Corey. 1971. Calculation of hydraulic conductivity: a further evaluation of some predictive methods. Soil Science Society of America Journal **35**:3-8.

Griffin, D. M. 1972. Ecology of soil fungi. Syracuse Univ. Press, Syracuse, NY.

Hirano, T., J. Jauhiainen, T. Inoue, and H. Takahashi. 2009. Controls on the carbon balance of tropical peatlands. Ecosystems **12**:873-887.

Hirano, T., K. Kusin, S. Limin, and M. Osaki. 2014. Carbon dioxide emissions through oxidative peat decomposition on a burnt tropical peatland. Global Change Biology **20**:555-565.

Hirano, T., K. Kusin, S. Limin, and M. Osaki. 2015. Evapotranspiration of tropical peat swamp forests. Global Change Biology **21**:1914-1927.

Hirano, T., H. Segah, T. Harada, S. Limin, T. June, R. Hirata, and M. Osaki. 2007. Carbon dioxide balance of a tropical peat swamp forest in Kalimantan, Indonesia. Global Change Biology **13**:412-425.

Hirano, T., H. Segah, K. Kusin, S. Limin, H. Takahashi, and M. Osaki. 2012. Effects of disturbances on the carbon balance of tropical peat swamp forests. Global Change Biology **18**:3410-3422.

Hirano, T., H. Segah, S. Limin, T. June, S. Tuah, K. Kusin, R. Hirata, and M. Osaki. 2005. Energy balance of a tropical peat swamp forest in Central Kalimantan, Indonesia. Phyton **45**:67-71.

Hooijer, A., S. Page, J. Canadell, M. Silvius, J. Kwadijk, H. Wösten, and J. Jauhiainen. 2010. Current and future CO_2 emissions from drained peatlands in Southeast Asia. Biogeosciences **7**:1505-1514.

Hooijer, A., S. Page, J. Jauhiainen, W. Lee, X. Lu, A. Idris, and G. Anshari. 2012. Subsidence and carbon loss in drained tropical peatlands. Biogeosciences **9**:1053-1071.

Ippisch, O., H.-J. Vogel, and P. Bastian. 2006. Validity limits for the van Genuchten–Mualem model and implications for parameter estimation and numerical simulation. Advances in Water Resources **29**:1780-1789.

Ise, T., A. L. Dunn, S. C. Wofsy, and P. R. Moorcroft. 2008. High sensitivity of peat decomposition to climate change through water-table feedback. Nature Geoscience **1**:763-766.

Jauhiainen, J., A. Hooijer, and S. Page. 2012a. Carbon dioxide emissions from an *Acacia* plantation on peatland in Sumatra, Indonesia. Biogeosciences.

Jauhiainen, J., S. Limin, H. Silvennoinen, and H. Vasander. 2008. Carbon dioxide and methane fluxes in drained tropical peat before and after hydrological restoration. Ecology **89**:3503-3514.

Jauhiainen, J., H. Silvennoinen, R. Hämäläinen, K. Kusin, S. Limin, R. Raison, and H. Vasander. 2012b. Nitrous oxide fluxes from tropical peat with different disturbance history and management. Biogeosciences **9**:1337-1350.

Jauhiainen, J., H. Takahashi, J. E. Heikkinen, P. J. Martikainen, and H. Vasander. 2005. Carbon fluxes from a tropical peat swamp forest floor. Global Change Biology **11**:1788-1797.

Jaya, A., T. Inoue, S. H. Limin, U. Darung, and I. S. Banuwa. 2010. Microclimate of developed peatland of the mega rice project in Central Kalimantan. Journal of Tropical Soils **15**:63-71.

Kellner, E. 2001. Surface energy fluxes and control of evapotranspiration from a Swedish Sphagnum mire. Agricultural and Forest Meteorology **110**:101-123.

Kimmins, J. P. 2004. Forest Ecology. 3rd edition. Pearson Prentice Hall, NJ.

Kotowska, A. 2013. The long-term effects of drainage on carbon cycling in a boreal fen. Department of Integrative Biology, University of Guelph.

Krinner, G., N. Viovy, N. de Noblet-Ducoudré, J. Ogée, J. Polcher, P. Friedlingstein, P. Ciais, S. Sitch, and I. C. Prentice. 2005. A dynamic global vegetation model for studies of the coupled atmosphere-biosphere system. Global Biogeochemical Cycles **19**.

Kuiper, J. J., W. M. Mooij, L. Bragazza, and B. J. Robroek. 2014. Plant functional types define magnitude of drought response in peatland CO_2 exchange. Ecology **95**:123-131.

Kurbatova, J., C. Li, F. Tatarinov, A. Varlagin, N. Shalukhina, and A. Olchev. 2009. Modeling of the carbon dioxide fluxes in European Russia peat bogs. Environmental Research Letters **4**:045022.

Kurnain, A., T. Notohadikusumo, B. Radjagukguk, and S. Hastuti. 2001. Peat soil properties related to degree of decomposition under different land use systems. International Peat Journal **11**:67-77.

Lafleur, P., T. Moore, N. Roulet, and S. Frolking. 2005. Ecosystem respiration in a cool temperate bog depends on peat temperature but not water table. Ecosystems **8**:619-629.

Lappalainen, E. 1996. General review on world peatland and peat resources. Global peat resources:53-56.

Larcher, W. 2003. Physiological plant ecology: ecophysiology and stress physiology of functional groups. Springer Science & Business Media.

Lawlor, D. W. 1993. Photosynthesis: molecular, physiological and environmental processes. Longman scientific & technical.

Letts, M. G., N. T. Roulet, N. T. Comer, M. R. Skarupa, and D. L. Verseghy. 2000. Parametrization of peatland hydraulic properties for the Canadian Land Surface Scheme. Atmosphere-Ocean **38**:141-160.

Li, W., R. E. Dickinson, R. Fu, G. Y. Niu, Z. L. Yang, and J. G. Canadell. 2007. Future precipitation changes and their implications for tropical peatlands. Geophysical Research Letters **34**.

Lieffers, V., and R. Rothwell. 1987. Rooting of peatland black spruce and tamarack in relation to depth of water table. Canadian Journal of Botany **65**:817-821.

Limpens, J., F. Berendse, C. Blodau, J. Canadell, C. Freeman, J. Holden, N. Roulet, H. Rydin, and G. Schaepman-Strub. 2008. Peatlands and the carbon cycle: from local processes to global implications–a synthesis. Biogeosciences **5**:1475-1491.

Lizama, H. M., and I. Suzuki. 1991. Kinetics of sulfur and pyrite oxidation by Thiobacillus thiooxidans. Competitive inhibition by increasing concentrations of cells. Canadian journal of microbiology **37**:182-187.

Long, K. D. 2008a. Methane fluxes from a northern peatland: mechanisms controlling diurnal and seasonal variation and the magnitude of aerobic methanogenesis. University of Lethbridge, Lethbridge, AB, Canada.

Long, K. D. 2008b. Methane fluxes from a northern peatland: mechanisms controlling diurnal and seasonal variation and the magnitude of aerobic methanogenesis. Lethbridge, Alta.: University of Lethbridge, Faculty of Arts and Science, 2008.

Long, K. D., L. B. Flanagan, and T. Cai. 2010. Diurnal and seasonal variation in methane emissions in a northern Canadian peatland measured by eddy covariance. Global Change Biology **16**:2420-2435.

Lovelock, C., I. C. Feller, K. McKee, B. Engelbrecht, and M. Ball. 2004. The effect of nutrient enrichment on growth, photosynthesis and hydraulic conductance of dwarf mangroves in Panama. Functional Ecology **18**:25-33.

Lovelock, C. E., M. C. Ball, B. Choat, B. M. Engelbrecht, N. M. Holbrook, and I. C. Feller. 2006a. Linking physiological processes with mangrove forest structure: phosphorus

deficiency limits canopy development, hydraulic conductivity and photosynthetic carbon gain in dwarf Rhizophora mangle. Plant, cell & environment **29**:793-802.

Lovelock, C. E., M. C. Ball, I. C. Feller, B. M. Engelbrecht, and M. Ling Ewe. 2006b. Variation in hydraulic conductivity of mangroves: influence of species, salinity, and nitrogen and phosphorus availability. Physiologia Plantarum **127**:457-464.

Lovelock, C. E., I. C. Feller, M. C. Ball, B. M. Engelbrecht, and M. L. Ewe. 2006c. Differences in plant function in phosphorus-and nitrogen-limited mangrove ecosystems. New Phytologist **172**:514-522.

Luxmoore, R., L. Stolzy, and J. Letey. 1970a. Oxygen diffusion in the soil-plant system I. A model. Agronomy Journal **62**:317-322.

Luxmoore, R., L. Stolzy, and J. Letey. 1970b. Oxygen Diffusion in the Soil-Plant System II. Respiration Rate, Permeability, and Porosity of Consecutive Excised Segments of Maize and Rice Roots. Agronomy Journal **62**:322-324.

Macdonald, S. E., and V. J. Lieffers. 1990. Photosynthesis, water relations, and foliar nitrogen of Picea mariana and Larix laricina from drained and undrained peatlands. Canadian Journal of Forest Research **20**:995-1000.

Mäkiranta, P., R. Laiho, H. Fritze, J. Hytönen, J. Laine, and K. Minkkinen. 2009. Indirect regulation of heterotrophic peat soil respiration by water level via microbial community structure and temperature sensitivity. Soil Biology and Biochemistry **41**:695-703.

Markham, J. H. 2009. Variation in moss-associated nitrogen fixation in boreal forest stands. Oecologia **161**:353-359.

Medrano, H., J. M. Escalona, J. Bota, J. Gulías, and J. Flexas. 2002. Regulation of photosynthesis of C3 plants in response to progressive drought: stomatal conductance as a reference parameter. Annals of Botany **89**:895-905.

Melling, L., K. J. Goh, C. Beauvais, and R. Hatano. 2008. Carbon flow and budget in young mature oil palm agroecosystem on deep tropical peat. Planter **84**:21.

Melling, L., R. Hatano, and K. J. Goh. 2005. Soil CO_2 flux from three ecosystems in tropical peatland of Sarawak, Malaysia. Tellus B **57**:1-11.

Miller, S. D., M. L. Goulden, M. C. Menton, H. R. da Rocha, H. C. de Freitas, A. M. e. S. Figueira, and C. A. Dias de Sousa. 2004. Biometric and micrometeorological measurements of tropical forest carbon balance. Ecological Applications **14**:114-126.

Millington, R. J., and J. M. Quirk. 1960. Transport in porous media. Pages 97-106 *in* F. A. van Beren, editor. 7th Trans. Int. Congr. Soil Sci. vol. 1. Elsevier, Amsterdam, Madison, WI.

Milner, L. E. 2009. Does soil fertility influence the vegetation diversity of a tropical peat swamp forest in Central Kalimantan, Indonesia? University of Leicester, UK.

Moore, S., C. D. Evans, S. E. Page, M. H. Garnett, T. G. Jones, C. Freeman, A. Hooijer, A. J. Wiltshire, S. H. Limin, and V. Gauci. 2013. Deep instability of deforested tropical peatlands revealed by fluvial organic carbon fluxes. Nature **493**:660-663.

Moore, T., and N. Basiliko. 2006. Decomposition in boreal peatlands. Pages 125-143 Boreal peatland ecosystems. Springer.

Mualem, Y. 1976. A new model for predicting the hydraulic conductivity of unsaturated porous media. Water Resour. Res **12**:513-522.

Munir, T., B. Xu, M. Perkins, and M. Strack. 2014. Responses of carbon dioxide flux and plant biomass to water table drawdown in a treed peatland in northern Alberta: a climate change perspective. Biogeosciences **11**:807-820.

Murdiyarso, D., K. Hergoualc'h, and L. Verchot. 2010. Opportunities for reducing greenhouse gas emissions in tropical peatlands. Proceedings of the National Academy of Sciences **107**:19655-19660.

Murphy, M., R. Laiho, and T. R. Moore. 2009. Effects of water table drawdown on root production and aboveground biomass in a boreal bog. Ecosystems **12**:1268-1282.

Murphy, M. T., and T. R. Moore. 2010. Linking root production to aboveground plant characteristics and water table in a temperate bog. Plant and soil **336**:219-231.

Nishimura, T. B., and E. Suzuki. 2001. Allometric differentiation among tropical tree seedlings in heath and peat-swamp forests. Journal of Tropical Ecology **17**:667-681.

Ong, B., and M. Yogeswaran. 1991. Peatland as a resource for water supply in Sarawak. Pages 255-268 *in* Proceedings of the International Symposium on Tropical Peatland, Kuching, Sarawak.

Ong, B. Y., and M. Yogeswaran. 1992. Peatland as a resource for water supply in Sarawak. Pages 255-268 *in* B. Y. Aminhuddin, editor. Tropical Peat, Kuching, Sarawak, Malaysia.

Page, S., A. Hosciło, H. Wösten, J. Jauhiainen, M. Silvius, J. Rieley, H. Ritzema, K. Tansey, L. Graham, and H. Vasander. 2009. Restoration ecology of lowland tropical peatlands in Southeast Asia: current knowledge and future research directions. Ecosystems **12**:888-905.

Page, S., J. Rieley, Ø. Shotyk, and D. Weiss. 1999. Interdependence of peat and vegetation in a tropical peat swamp forest. Philosophical Transactions of the Royal Society B: Biological Sciences **354**:1885-1897.

Page, S., J. Rieley, and R. Wüst. 2006. Lowland tropical peatlands of Southeast Asia. Pages 145-172 *in* I. P. Martini, A. M. Cortizas, and W. Chesworth, editors. Peatlands: Evolution and Records of Environmental and Climate Changes (Developments in Earth Surface Processes), Elsevier, Netherlands.

Page, S., R. Wűst, D. Weiss, J. Rieley, W. Shotyk, and S. H. Limin. 2004. A record of Late Pleistocene and Holocene carbon accumulation and climate change from an equatorial peat bog (Kalimantan, Indonesia): implications for past, present and future carbon dynamics. Journal of Quaternary Science **19**:625-635.

Page, S. E., J. O. Rieley, and C. J. Banks. 2011. Global and regional importance of the tropical peatland carbon pool. Global Change Biology **17**:798-818.

Päivänen, J. 1973. Hydraulic conductivity and water retention in peat soils. Acta Forestalia Fennica **129**:1-70.

Pangala, S. R., S. Moore, E. R. Hornibrook, and V. Gauci. 2013. Trees are major conduits for methane egress from tropical forested wetlands. New Phytologist **197**:524-531.

Parmentier, F., M. Van der Molen, R. de Jeu, D. Hendriks, and A. Dolman. 2009. CO_2 fluxes and evaporation on a peatland in the Netherlands appear not affected by water table fluctuations. Agricultural and Forest Meteorology **149**:1201-1208.

Peichl, M., M. Öquist, M. O. Löfvenius, U. Ilstedt, J. Sagerfors, A. Grelle, A. Lindroth, and M. B. Nilsson. 2014. A 12-year record reveals pre-growing season temperature and water table level threshold effects on the net carbon dioxide exchange in a boreal fen. Environmental Research Letters **9**:055006.

Perrier, A. 1982. Land surface processes: vegetation. Land surface processes in atmospheric general circulation models:395-448.

Pirt, S. J. 1975. Principles of microbe and cell cultivation. Blackwell Scientific Publications.

Rachmanadi, D., P. D. Susanti, Rusmana, T. W. Yuwati, P. B. Santosa, and L. L. B. Graham. 2014. Response of peat swamp forest species to drought. Pages 14-35 *in* L. L. B. Graham, editor. Tropical Peat Swamp Forest Silviculture in Central Kalimantan. Banjarbaru Forestry Research Unit, FORDA, Kalimantan Forests and Climate Partnership.

Richardson, A. D., D. Y. Hollinger, G. G. Burba, K. J. Davis, L. B. Flanagan, G. G. Katul, J. W. Munger, D. M. Ricciuto, P. C. Stoy, and A. E. Suyker. 2006. A multi-site analysis of random error in tower-based measurements of carbon and energy fluxes. Agricultural and Forest Meteorology **136**:1-18.

Rieley, J. O., and S. E. Page, editors. 2005. Wise Use of Tropical Peatlands: Focus on Southeast Asia. ALTERRA - Wageningen University and Research Centre and the EU INCO - STRAPEAT and RESTORPEAT Partnerships, Wageningen, The Netherlands.

Rippy, J. F., and P. V. Nelson. 2007. Cation exchange capacity and base saturation variation among Alberta, Canada, moss peats. HortScience **42**:349-352.

Riutta, T. 2008. Fen ecosystem carbon gas dynamics in changing hydrological conditions. Dissertationes Forestales **67**:1-46.

Riutta, T., J. Laine, and E.-S. Tuittila. 2007. Sensitivity of CO_2 exchange of fen ecosystem components to water level variation. Ecosystems **10**:718-733.

Rydin, H., and J. K. Jeglum. 2013. The Biology of Peatlands, 2e. Oxford University Press.

Saha, A. K., O. Leonel da Silveira, M. S. Ross, and F. Miralles-Wilhelm. 2010. Water source utilization and foliar nutrient status differs between upland and flooded plant communities in wetland tree islands. Wetlands ecology and management **18**:343-355.

Sayok, A. K., A. R. Nik, L. Melling, R. A. Samad, and E. Efransjah. 2007. Some characteristics of peat in Loagan Bunut National Park, Sarawak, Malaysia. Pages 27-29 *in* Carbon-climate-human interactions on tropical peatland: carbon pools, fire, mitigation, restoration and wise use, edited by: Rieley, JO, Banks, CJ, and Ragjagukguk, B.,

Proceedings of the International Symposium and Workshop on Tropical Peatland, Yogyakarta.

Schaefer, K., G. J. Collatz, P. Tans, A. S. Denning, I. Baker, J. Berry, L. Prihodko, N. Suits, and A. Philpott. 2008. Combined simple biosphere/Carnegie-Ames-Stanford approach terrestrial carbon cycle model. Journal of Geophysical Research: Biogeosciences (2005–2012) **113**.

Schulten, H.-R., and M. Schnitzer. 1997. Chemical model structures for soil organic matter and soils. Soil science **162**:115-130.

Schwärzel, K., J. Šimůnek, M. T. van Genuchten, and G. Wessolek. 2006. Measurement modeling of soil-water dynamics evapotranspiration of drained peatland soils. Journal of Plant Nutrition and Soil Science **169**:762-774.

Sharpe, P. J., and D. W. DeMichele. 1977. Reaction kinetics of poikilotherm development. Journal of Theoretical Biology **64**:649-670.

Shields, J., E. Paul, W. Lowe, and D. Parkinson. 1973. Turnover of microbial tissue in soil under field conditions. Soil Biology and Biochemistry **5**:753-764.

Shimamura, T., and K. Momose. 2005. Organic matter dynamics control plant species coexistence in a tropical peat swamp forest. Proceedings of the Royal Society of London B: Biological Sciences **272**:1503-1510.

Silins, U., and R. L. Rothwell. 1998. Forest peatland drainage and subsidence affect soil water retention and transport properties in an Alberta peatland. Soil Science Society of America Journal **62**:1048-1056.

Sitch, S., B. Smith, I. C. Prentice, A. Arneth, A. Bondeau, W. Cramer, J. Kaplan, S. Levis, W. Lucht, and M. T. Sykes. 2003. Evaluation of ecosystem dynamics, plant geography and terrestrial carbon cycling in the LPJ dynamic global vegetation model. Global Change Biology **9**:161-185.

Skopp, J. 1985. Oxygen uptake and transport in soils: Analysis of the air-water interfacial area. Soil Science Society of America Journal **49**:1327-1331.

Sonnentag, O., J. Chen, N. Roulet, W. Ju, and A. Govind. 2008. Spatially explicit simulation of peatland hydrology and carbon dioxide exchange: Influence of mesoscale topography. Journal of Geophysical Research: Biogeosciences (2005–2012) **113**.

Sonnentag, O., G. Van der Kamp, A. Barr, and J. Chen. 2010. On the relationship between water table depth and water vapor and carbon dioxide fluxes in a minerotrophic fen. Global Change Biology **16**:1762-1776.

St-Hilaire, F., J. Wu, N. Roulet, S. Frolking, P. Lafleur, E. Humphreys, and V. Arora. 2008. McGill wetland model: evaluation of a peatland carbon simulator developed for global assessments. Biogeosciences Discussions **5**:1689-1725.

St-Hilaire, F., J. Wu, N. T. Roulet, S. Frolking, P. M. Lafleur, E. R. Humphreys, and V. Arora. 2010. McGill wetland model: evaluation of a peatland carbon simulator developed for global assessments. Biogeosciences **7**:3517-3530.

Strack, M., and J. Waddington. 2007. Response of peatland carbon dioxide and methane fluxes to a water table drawdown experiment. Global Biogeochemical Cycles **21**.

Strack, M., J. Waddington, L. Rochefort, and E. S. Tuittila. 2006. Response of vegetation and net ecosystem carbon dioxide exchange at different peatland microforms following water table drawdown. Journal of Geophysical Research: Biogeosciences (2005–2012) **111**.

Sulistiyanto, Y. 2004. Nutrient dynamics in different sub-types of peat swamp forest in Central Kalimantan, Indonesia. University of Nottingham, UK.

Sulman, B., A. Desai, B. Cook, N. Saliendra, and D. Mackay. 2009. Contrasting carbon dioxide fluxes between a drying shrub wetland in Northern Wisconsin, USA, and nearby forests. Biogeosciences **6**:1115-1126.

Sulman, B. N., A. R. Desai, N. Z. Saliendra, P. M. Lafleur, L. B. Flanagan, O. Sonnentag, D. S. Mackay, A. G. Barr, and G. van der Kamp. 2010. CO_2 fluxes at northern fens and bogs have opposite responses to inter-annual fluctuations in water table. Geophysical Research Letters **37**.

Sulman, B. N., A. R. Desai, N. M. Schroeder, D. Ricciuto, A. Barr, A. D. Richardson, L. B. Flanagan, P. M. Lafleur, H. Tian, and G. Chen. 2012. Impact of hydrological variations on modeling of peatland CO_2 fluxes: Results from the North American Carbon Program site synthesis. Journal of Geophysical Research: Biogeosciences (2005–2012) **117**.

Sundari, S., T. Hirano, H. Yamada, K. Kusin, and S. Limin. 2012. Effect of groundwater level on soil respiration in tropical peat swamp forests. Journal of Agricultural Meteorology **68**:121-134.

Syed, K. H., L. B. Flanagan, P. J. Carlson, A. J. Glenn, and K. E. Van Gaalen. 2006. Environmental control of net ecosystem CO_2 exchange in a treed, moderately rich fen in northern Alberta. Agricultural and Forest Meteorology **140**:97-114.

Szymanowski, M. 1993. Basic physico-hydrological and retention properties and their relationship with bulk density of various weakly-sludged (low-ash) peat formations. Wiadomości IMUZ **17**:153-174.

Takahashi, H., M. Kayama, and S. Limin. 1999. The effects of environmental factors on diurnal changes of ground water table in a tropical peat swamp forest. Pages 321-327 *in* Proceedings of the International Symposium on Tropical Peatlands. Hokkaido University, Sapporo, Japan and Indonesian Institute of Sciences, Bogor, Indonesia, Bogor, Indonesia.

Takahashi, H., A. Usup, H. Hayasaka, M. Kamiya, and S. Limin. 2004. The importance of ground water level and soil moisture of subsurface layer on peat/forest fire in a tropical peat swamp forest. Wise Use of Peatlands **1**:760.

Takakai, F., T. Morishita, Y. Hashidoko, U. Darung, K. Kuramochi, S. Dohong, S. H. Limin, and R. Hatano. 2006. Effects of agricultural land-use change and forest fire on N_2O emission from tropical peatlands, Central Kalimantan, Indonesia. Soil Science and Plant Nutrition **52**:662-674.

Tarnocai, C. 2006. The effect of climate change on carbon in Canadian peatlands. Global and planetary Change **53**:222-232.

Tarnocai, C., V. Stolbovoy, I. Martini, A. Martínez Cortizas, and W. Chesworth. 2006. Northern peatlands: their characteristics, development and sensitivity to climate change. Peatlands: Evolution and Records of Environmental and Climate Changes, edited by: Martini, IP, Martınez Cortizas, A., and Chesworth, W., Developments in Earth Surface Processes **9**:17-51.

Thomas, D. B., T. M. Michael, M. John, and P. Jack. 1991. Biology of microorganisms. New York, USA: Prentice Hall International.

Tian, H., G. Chen, M. Liu, C. Zhang, G. Sun, C. Lu, X. Xu, W. Ren, S. Pan, and A. Chappelka. 2010. Model estimates of net primary productivity, evapotranspiration, and water use efficiency in the terrestrial ecosystems of the southern United States during 1895–2007. Forest ecology and management **259**:1311-1327.

Townsend, A. R., C. C. Cleveland, G. P. Asner, and M. M. Bustamante. 2007. Controls over foliar N: P ratios in tropical rain forests. Ecology **88**:107-118.

Tuah, S., M. Osaki, and S. Limin. 1999. Study on leaf element concentrations of some dominant tree species grown in peat swamp forest, Central Kalimantan. Pages 233-244 *in* Proceedings of the International Symposium on Tropical Peatlands, edited by: Iwakuma, T., Inoue, T., Kohyama, T., Osaki, M., Simbolon, H., Tachibana, H., Takahashi, H., Tanaka, N., and Yabe, K., Hokkaido University and Indonesian Institute of Sciences.

Turunen, J., E. Tomppo, K. Tolonen, and A. Reinikainen. 2002. Estimating carbon accumulation rates of undrained mires in Finland–application to boreal and subarctic regions. The Holocene **12**:69-80.

Updegraff, K., J. Pastor, S. D. Bridgham, and C. A. Johnston. 1995. Environmental and substrate controls over carbon and nitrogen mineralization in northern wetlands. Ecological Applications **5**:151-163.

Van Bavel, C., and D. Hillel. 1976. Calculating potential and actual evaporation from a bare soil surface by simulation of concurrent flow of water and heat. Agricultural Meteorology **17**:453-476.

Van Genuchten, M. T. 1980. A closed-form equation for predicting the hydraulic conductivity of unsaturated soils. Soil Science Society of America Journal **44**:892-898.

Van Genuchten, M. T., F. Leij, and S. Yates. 1991. The RETC code for quantifying the hydraulic functions of unsaturated soils. Robert S. Kerr Environmental Research Laboratory.

van Genuchten, R. 1978. Calculating the unsaturated hydraulic conductivity with a new closed-form analytical model. International Ground Water Modeling Center.

Van Huissteden, J., R. van den Bos, and I. M. Alvarez. 2006. Modelling the effect of water-table management on CO_2 and CH_4 fluxes from peat soils. Netherlands Journal of Geosciences **85**:3.

Veen, B. 1981. Relation between root respiration and root activity. Springer.

Visser, E., T. Colmer, C. Blom, and L. Voesenek. 2000. Changes in growth, porosity, and radial oxygen loss from adventitious roots of selected mono-and dicotyledonous wetland species with contrasting types of aerenchyma. Plant Cell and Environment **23**:1237-1245.

Waddington, J., P. Morris, N. Kettridge, G. Granath, D. Thompson, and P. Moore. 2015. Hydrological feedbacks in northern peatlands. Ecohydrology **8**:113-127.

Waring, R. H., and S. W. Running. 1998. Forest ecosystems: analysis at multiple scales. 2nd edition. Elsevier.

Weiss, R., J. Alm, R. Laiho, and J. Laine. 1998. Modeling moisture retention in peat soils. Soil Science Society of America Journal **62**:305-313.

Weng, E., and Y. Luo. 2008. Soil hydrological properties regulate grassland ecosystem responses to multifactor global change: A modeling analysis. Journal of Geophysical Research: Biogeosciences (2005–2012) **113**.

Wesely, M. L., and R. Hart. 1985. Variability of short term eddy-correlation estimates of mass exchange. Springer.

Wever, L. A., L. B. Flanagan, and P. J. Carlson. 2002. Seasonal and interannual variation in evapotranspiration, energy balance and surface conductance in a northern temperate grassland. Agricultural and Forest Meteorology **112**:31-49.

Wilhelm, E., R. Battino, and R. J. Wilcock. 1977. Low-pressure solubility of gases in liquid water. Chemical reviews **77**:219-262.

Williams, T. G., and L. B. Flanagan. 1996. Effect of changes in water content on photosynthesis, transpiration and discrimination against $^{13}CO_2$ and $C^{18}O^{16}O$ in *Pleurozium* and *Sphagnum*. Oecologia **108**:38-46.

Willmott, C. J. 1981. On the validation of models. Physical geography **2**:184-194.

Willmott, C. J. 1982. Some comments on the evaluation of model performance. Bulletin of the American Meteorological Society **63**:1309-1313.

Willmott, C. J., and D. E. Wicks. 1980. An empirical method for the spatial interpolation of monthly precipitation within California. Physical geography **1**:59-73.

Wilson, K., A. Goldstein, E. Falge, M. Aubinet, D. Baldocchi, P. Berbigier, C. Bernhofer, R. Ceulemans, H. Dolman, and C. Field. 2002. Energy balance closure at FLUXNET sites. Agricultural and Forest Meteorology **113**:223-243.

Wösten, J., E. Clymans, S. Page, J. Rieley, and S. Limin. 2008. Peat–water interrelationships in a tropical peatland ecosystem in Southeast Asia. Catena **73**:212-224.

Wu, J., L. Kutzbach, D. Jager, C. Wille, and M. Wilmking. 2010. Evapotranspiration dynamics in a boreal peatland and its impact on the water and energy balance. Journal of Geophysical Research: Biogeosciences (2005–2012) **115**.

Yu, Z. 2012. Northern peatland carbon stocks and dynamics: a review. Biogeosciences **9**:4071-4085.

Yu, Z., J. Loisel, D. P. Brosseau, D. W. Beilman, and S. J. Hunt. 2010. Global peatland dynamics since the Last Glacial Maximum. Geophysical Research Letters **37**.

Zhang, Y., C. Li, C. C. Trettin, H. Li, and G. Sun. 2002. An integrated model of soil, hydrology, and vegetation for carbon dynamics in wetland ecosystems. Global Biogeochemical Cycles **16**:9-1-9-17.

Zoltai, S. C., and D. H. Vitt. 1990. Holocene climatic change and the distribution of peatlands in western interior Canada. Quaternary Research **33**:231-240.

Supplementary Material

Appendix A: Soil C, N and P transformations

Decomposition

$$D_{Si,j,l,C} = D'_{Si,j,l,C}\, M_{i,d,l,C}\ \ f_{tgl}\,(S_{i,l,C} / G_{i,l,C})$$ decomposition of litter, POC, humus [A1a]

$$D_{Zi,j,l,C} = D'_{Zi,j,l,C}\, M_{i,d,l,C}\ f_{tgl}\,(Z_{i,l,C} / G_{i,l,C})$$ decomposition of microbial residues [A1b]

$$D_{Ai,l,C} = D'_{Ai,l,C}\, M_{i,d,l,C}\ f_{tgl}\,(A_{i,l,C} / G_{i,l,C})$$ decomposition of adsorbed SOC [A1c]

$$S_{i,l,C} = \Sigma_j\, S_{i,j,l,C}$$ total C in all kinetic components of litter, POC, humus [A2a]

$$Z_{i,l,C} = \Sigma_j\, Z_{i,j,l,C}$$ total C in all kinetic components of microbial residues [A2b]

$$G_{i,l,C} = S_{i,l,C} + Z_{i,l,C} + A_{i,l,C}$$ total C in substrate-microbe complexes [A2c]

$$M_{i,d,l,C} = M_{i,a,l,C} + \boldsymbol{q_m}\,(M_{i,a,l,C}\, G_{ix,l,C} - M_{ix,a,l,C}\, G_{i,l,C})/(G_{ix,l,C} + G_{i,l,C})$$ redistribution of active microbial biomass from each substrate-microbe complex *i* to other substrate-microbe complexes *ix* according to concentration differences (priming) [A3a]

$$M_{i,a,l,C} = \Sigma_n\, M_{i,n,a,l,C}$$ [A3b]

$$D'_{Si,j,l,C} = \{\boldsymbol{D}_{Sj,C}[S_{i,j,l,C}]\}/\{[S_{i,j,l,C}] + \boldsymbol{K_{mD}}(1.0 + [\Sigma M_{i,d,l,C}]/\boldsymbol{K_{iD}})\}$$ substrate and water constraint on *D* from colonized litter, POC and humus, microbial residues and adsorbed SOC [A4a]

$$D'_{Zi,j,l,C} = \{\boldsymbol{D}_{Zj,C}[Z_{i,j,l,C}]\}/\{[Z_{i,j,l,C}] + \boldsymbol{K_{mD}}(1.0 + [M_{i,d,l,C}]/\boldsymbol{K_{iD}})\}$$ [A4b]

$$D'_{Ai,l,C} = \{\boldsymbol{D}_{A,C}[A_{i,l,C}]\}/\{[A_{i,l,C}] + \boldsymbol{K_{mD}}(1.0 + [M_{i,d,l,C}]/\boldsymbol{K_{iD}})\}$$ [A4c]

$$\delta S_{i,j,k,l,C}/\delta t = \boldsymbol{\beta}\,\Sigma_n\,(U_{i,n,l}C - R_{hi,n,l})\,(S'_{i,j,k,l,C}/\,S'_{i,j,l,C})\ \{(S'_{i,j,l,C}/S_{i,j,l,C})/(\,S'_{i,j,l,C}/S_{i,j,l\,,C} + \boldsymbol{K_{iS}})\}$$ colonized litter determined by microbial growth into uncolonized litter [A5]

$$f_{tgl} = T_{sl}\{e^{[B - \boldsymbol{H_a}/(\boldsymbol{R}T_{sl})]}\}/\{1 + e^{[(\boldsymbol{H_{dl}} - \boldsymbol{S}T_{sl})/(\boldsymbol{R}T_{sl})]} + e^{[(\boldsymbol{S}T_{sl} - \boldsymbol{H_{dh}})/(\boldsymbol{R}T_{sl})]}\}$$

Arrhenius function for D and R_h [A6]

$$D_{Si,j,l,N,P} = D_{Si,j,l,C}(S_{i,j,l,N,P}/S_{i,j,l,C})$$

N and P coupled with C during D [A7a]

$$D_{Zi,j,l,N,P} = D_{Zi,j,l,C}(Z_{i,j,l,N,P}/Z_{i,j,l,C})$$

[A7b]

$$D_{Ai,l,N,P} = D_{Ai,l,C}(A_{i,l,N,P}/A_{i,l,C})$$

[A7c]

$$Y_{i,l,C} = \boldsymbol{k_{ts}}(G_{i,l,C}\, F_s[Q_{i,l,C}]^{\boldsymbol{b}} - X_{i,l,C})$$

Freundlich sorption of DOC [A8]

$$Y_{i,l,N,P} = Y_{i,l,C}(Q_{i,l,N,P}/Q_{i,l,C})$$

($Y_{i,l,C} > 0$) adsorption of DON, DOP [A9]

$$Y_{i,l,N,P} = Y_{i,l,C}(X_{i,l,N,P}/X_{i,l,C})$$

($Y_{i,l,C} < 0$) desorption of DON, DOP [A10]

Microbial growth

$$R_h = \Sigma_i \Sigma_n \Sigma_l R_{hi,n,l}$$

[A11]

$$\boldsymbol{R}_{hi,n,l} = \boldsymbol{R'}_{hn} \min\{C_{Ni,n,l,a}/\boldsymbol{C}_{Nj},\ C_{Pi,n,l,a}/\boldsymbol{C}_{Pj}\}$$

R_h constrained by microbial N, P [A12]

$$R_h'_{i,n,l} = M_{i,n,a,l,C}\ \{\boldsymbol{R}_{hi,n,l}\,[Q_{i,l,C}]\}/\{(\boldsymbol{K_{mQC}} + [Q_{i,l,C}])\} f_{tgl}\, f_{\psi gl}$$

R_h constrained by substrate DOC [A13]

$$R_{hi,n,l} = R_h'_{i,n,l}\,(U_{O2i,n,l}/U'_{O2i,n,l})$$

R_h constrained by O_2 [A14]

$$f_{\psi gl} = 1.0 - 6.67(1.0 - e^{(M\psi_s/(\boldsymbol{R}T_{sl}))})$$

ψ_s constraints on microbial growth [A15]

$$U'_{O2i,n,l} = 2.67 R_h'_{i,n,l}$$

O_2 demand driven by potential R_h [A16]

$$U_{O2i,n,l} = U'_{O2i,n,l}[O_{2mi,n,l}]/([O_{2mi,n,l}] + \boldsymbol{K_{O_2}})$$

active uptake coupled with radial diffusion of O_2 [A17a]

$$= 4\pi n\, M_{i,n,a,l,C}\, D_{sO2l}[\boldsymbol{r_m} r_{wl}/(r_{wl} - \boldsymbol{r_m})]([O_{2sl}] - [O_{2mi,n,l}]$$

[A17b]

$$R_{mi,n,j,l} = \boldsymbol{R}_m M_{i,n,j,l,N} f_{tml}$$

[A18]

$$f_{tml} = e^{[\boldsymbol{y}(T_{sl} - 298.16)]}$$

[A19]

$$R_{gi,n,l} = R_{hi,n,l} - \Sigma_j\, R_{mi,n,j,l}$$

[A20]

$$U_{i,n,lC} = \min(R_{hi,n,l}\,, \Sigma_j\, R_{mi,n,j,l}) + R_{gi,n,l}\,(1 + \boldsymbol{\Delta G_x}/\boldsymbol{E_m})$$

DOC uptake driven by R_g [A21]

$U_{i,n,l\mathrm{N,P}} = U_{i,n,l} Q_{i,l,\mathrm{N,P}} / Q_{i,l,\mathrm{C}}$ DON,DOP uptake driven by $U_{i,n,l\mathrm{C}}$ [A22]

$D_{Mi,n,j,l,\mathrm{C}} = \boldsymbol{D}_{Mi,j} M_{i,n,j,\mathrm{C}} f_{\mathrm{tg}}$ first-order decay of microbial C, [A23]

$D_{Mi,n,j,\mathrm{N,P}} = \boldsymbol{D}_{Mi,j} M_{i,n,j,l,\mathrm{N,P}} f_{\mathrm{tg}l} f_{\mathrm{d}i,n,l\mathrm{N,P}}$ partial release of microbial N, P [A24]

$\delta M_{i,n,j,l,\mathrm{C}}/\delta t = F_j U_{i,n,l\mathrm{C}} - F_j R_{\mathrm{h}i,n,l} - D_{Mi,n,j,l,\mathrm{C}}$ $[R_{\mathrm{h}i,n,l} > R_{\mathrm{m}i,n,j,l}]$ growth [A25a]

$\delta M_{i,n,j,l,\mathrm{C}}/\delta t = F_j U_{i,n,l\mathrm{C}} - R_{\mathrm{m}i,n,j,l} - D_{Mi,n,j,l,\mathrm{C}}$ $[R_{\mathrm{h}i,n,l} < R_{\mathrm{m}i,n,j,l}]$ senescence [A25b]

Microbial nutrient exchange

$U_{\mathrm{NH4}i,n,j,l} = (M_{i,n,j,l,C} \boldsymbol{C}_{\mathbf{N}j} - M_{i,n,j,l,N})$ $U_{\mathrm{NH_4}} < 0$ mineralization [A26a]

$U_{\mathrm{NH4}i,n,j,l} = \min\{(M_{i,n,j,l,C} \boldsymbol{C}_{\mathbf{N}j} - M_{i,n,j,l,N}),$
$\boldsymbol{U'}_{\mathbf{NH_4}} a_{i,n,j,l} ([\mathrm{NH_4^+}_{i,n,j,l}] - [\mathbf{NH_4^+{}_{mn}}])/([\mathrm{NH_4^+}_{i,n,j,l}] - [\mathbf{NH_4^+{}_{mn}}] + \boldsymbol{K}_{\mathbf{NH_4}})\}$ $U_{\mathrm{NH_4}} > 0$ immobilization [A26b]

$U_{\mathrm{NO3}i,n,j,l} = \min\{(M_{i,n,j,l,C} \boldsymbol{C}_{\mathbf{N}j} - (M_{i,n,j,l,N} + U_{\mathrm{NH4}i,n,j,l})),$
$\boldsymbol{U'}_{\mathbf{NO_3}} a_{i,n,j,l} ([\mathrm{NO_3^-}_{i,n,j,l}] - [\mathbf{NO_3^-{}_{mn}}])/([\mathrm{NO_3^-}_{i,n,j,l}] - [\mathbf{NO_3^-{}_{mn}}] + \boldsymbol{K}_{\mathbf{NO_3}})\}$ $U_{\mathrm{NO_3}} > 0$ immobilization [A26c]

$U_{\mathrm{PO4}i,n,j,l} = (M_{i,n,j,l,C} \boldsymbol{C}_{\mathbf{P}j} - M_{i,n,j,l,P})$ $U_{\mathrm{PO_4}} < 0$ mineralization [A26d]

$U_{\mathrm{PO4}i,n,j,l} = \min\{(M_{i,n,j,l,C} \boldsymbol{C}_{\mathbf{P}j} - M_{i,n,j,l,P}),$
$\boldsymbol{U'}_{\mathbf{PO_4}} A_{i,n,j,l} ([\mathrm{H_2PO_4^-}_{i,n,j,l}] - [\mathbf{H_2PO_4^-{}_{mn}}])/([\mathrm{H_2PO_4^-}_{i,n,j,l}] - [\mathbf{H_2PO_4^-{}_{mn}}] + \boldsymbol{K}_{\mathbf{PO_4}})\}$ $U_{\mathrm{PO_4}} > 0$ immobilization [A26e]

$\Phi_{i,n=fj,l} = max\{0, M_{i,n=fj,l,\mathrm{C}} \boldsymbol{C}_{\mathrm{N}j} - M_{i,n=fj,l,\mathrm{N}} - max\{0, U_{i,n=fj,l,\mathrm{N}}\}\}$ N_2 fixation driven by N deficit of diazotrophic population [A27]

$R_{\Phi i,n=fj,l} = \boldsymbol{E}_{\boldsymbol{\Phi}} \Phi_{i,n=fj,l}$ [A28]

$\delta M_{i,n,j,l,\mathrm{N}}/\delta t = F_j U_{i,n,l,\mathrm{N}} + U_{\mathrm{NH4}i,n,j,l} + U_{\mathrm{NO3}i,n,j,l} + \Phi_{i,n=fj,l} - D_{Mi,n,j,l,\mathrm{N}}$ growth *vs*. losses of microbial N, P [A29a]

$\delta M_{i,n,j,l,\mathrm{P}}/\delta t = F_j U_{i,n,l,\mathrm{P}} + U_{\mathrm{PO4}i,n,j,l} - D_{Mi,n,j,l,\mathrm{p}}$ [A29b]

$M_{i,n,a,l,\mathrm{C}} = M_{i,n,j=labile,l,\mathrm{C}} + M_{i,n,j=resistant,l,\mathrm{C}} F_{\mathrm{r}}/F_{\mathrm{l}}$ [A30a]

Humification

$H_{Si,j=\mathrm{lignin},l,\mathrm{C}} = D_{Si,j=\mathrm{lignin},l,\mathrm{C}}$ decomposition products of litter [A31]

$H_{Si,j=\text{lignin},l,\text{N,P}} = D_{Si,j=\text{lignin},l,\text{N,P}}$	added to POC depending on lignin	[A32]
$H_{Si,j\neq\text{lignin},l,\text{C}} = H_{Si,j=\text{lignin},l,\text{C}} \boldsymbol{L}_{\mathbf{h}j}$		[A33]
$H_{Si,j\neq\text{lignin},l,\text{N,P}} = H_{Si,j\neq\text{lignin},l,\text{C}} S_{i,l,\text{N,P}}/S_{i,l,\text{C}}$		[A34]
$H_{Mi,n,j,l,\text{C}} = D_{Mi,n,j,l,\text{C}} \boldsymbol{F}_{\mathbf{h}}$	decomposition products of microbes added to humus depending on clay	[A35]
$H_{Mi,n,j,l,\text{N,P}} = H_{Mi,n,j,l,\text{C}} M_{i,n,j,l,\text{N,P}}/M_{i,n,j,l,\text{C}}$		[A36]

Definition of variables in appendix A

Variable	Definition	Unit	Equation	Value	Reference
		Subscripts			
i	substrate-microbe complex: coarse woody litter, fine non-woody litter, POC, humus				
j	kinetic component: labile l, resistant r, active a				
l	soil or litter layer				
n	microbial functional type: heterotrophic (bacteria, fungi), autotrophic (nitrifiers, methanotrophs), diazotrophic, obligate aerobe, facultative anaerobes (denitrifiers), obligate anaerobes (methanogens)				
		Variables			
$A_{i,l,\text{C}}$	mass of adsorbed SOC	g C m^{-2}	[A1c,A2c]		
$[A_{i,l,\text{C}}]$	concentration of adsorbed SOC in soil	g C Mg^{-1}	[A4c]		
a	microbial surface area	m^2 m^{-2}	[A26]		
$\boldsymbol{B}$	parameter such that $f_{\text{tg}} = 1.0$ at $T_l = 298.15$ K		[A6]	26.230	

$\boldsymbol{b}$	Freundlich exponent for sorption isotherm		[A8]	0.85	(Grant et al. 1993b, a)
$\boldsymbol{\beta}$	specific colonization rate of uncolonized substrate	-	[A5]	2.5	(Grant et al. 2010)
$C_{\mathrm{N,P}i,n,a,l}$	ratio of $M_{i,n,a,\mathrm{N,P}}$ to $M_{i,n,a,\mathrm{C}}$	g N or P g C^{-1}	[A12]		
$\boldsymbol{C}_{\mathbf{N,P}j}$	maximum ratio of $M_{i,n,j,\mathrm{N,P}}$ to $M_{i,n,j,\mathrm{C}}$ maintained by $M_{i,n,j,\mathrm{C}}$	g N or P g C^{-1}	[A12,A26,A27]	0.22 and 0.13 (N), 0.022 and 0.013 (P) for j = labile and resistant, respectively	(Grant et al. 1993b, a)
$\boldsymbol{D}_{Mi,j}$	specific decomposition rate of $M_{i,n,j}$ at 30°C	g C g C^{-1} h^{-1}	[A23,A24]	0.0125 and 0.00035 for j = labile and resistant, respectively	(Grant et al. 1993b, a)
$D_{Mi,n,j,l,\mathrm{C}}$	decomposition rate of $M_{i,n,j,l,\mathrm{C}}$	g C m^{-2} h^{-1}	[A23,A25,A35]		
$D_{Mi,n,j,l,\mathrm{N,P}}$	decomposition rate of $M_{i,n,j,l,\mathrm{N,P}}$	g N or P m^{-2} h^{-1}	[A24,A29]		
$D_{\mathrm{sO2}l}$	aqueous dispersivity–diffusivity of O_2 during microbial uptake in soil	m^2 h^{-1}	[A17]		
$D_{Ai,l,\mathrm{C}}$	decomposition rate of $A_{i,l,\mathrm{C}}$ by $M_{\boldsymbol{i,d,l,}\mathrm{C}}$ producing Q in [A13]	g C m^{-2} h^{-1}	[A1c,A7c,A31c]		
$\boldsymbol{D}_{Aj,\mathrm{C}}$	specific decomposition rate of $A_{i,l,\mathrm{C}}$ by $M_{\boldsymbol{i,d,l,}\mathrm{C}}$ at 25°C and saturating[$A_{i,l,\mathrm{C}}$]	g C g C^{-1} h^{-1}	[A4c]	0.025	(Grant et al. 1993b, a)
$D_{Ai,j,\ l,\mathrm{N,P}}$	decomposition rate of $A_{i,l,\mathrm{N,P}}$ by $M_{\boldsymbol{i,d,l,}\mathrm{C}}$	g N or P m^{-2} h^{-1}	[A7c]		
$D'_{Ai,j,\ l,\mathrm{C}}$	specific decomposition rate of $S_{i,j,l,\mathrm{C}}$ by $\Sigma_n M_{i,n,a,l}$ at 25°C	g C g C^{-1} h^{-1}	[A1a,A4c]		

$D_{Si,j,l,C}$	decomposition rate of $S_{i,j,l,C}$ by $\Sigma_n M_{i,n,a,l}$ producing Q in [A13]	g C m^{-2} h^{-1}	[A1a,A7a,A31a]		
$\boldsymbol{D}_{Sj,C}$	specific decomposition rate of $S_{i,j,l,C}$ by $\Sigma_n M_{i,n,a,l}$ at 25°C and saturating[$S_{i,l,C}$]	g C g C^{-1} h^{-1}	[A4a]	1.0, 1.0, 0.15, and 0.025 for j = protein, carbohydrate, cellulose, and lignin	(Grant et al. 1993b, a)
$D_{Si,j,\,l,N,P}$	decomposition rate of $S_{i,j,l,N,P}$ by $\Sigma_n M_{i,n,a,l}$	g N or P m^{-2} h^{-1}	[A7a, A32]		
$D'_{Si,j,\,l,C}$	specific decomposition rate of $S_{i,j,l,C}$ by $\Sigma_n M_{i,n,a,l}$ at 25°C	g C g C^{-1} h^{-1}	[A1a,A4a]		
$D_{Zi,j,l,C}$	decomposition rate of $Z_{i,j,l,C}$ by $\Sigma_n M_{i,n,a,l}$ producing Q in [A13]	g C m^{-2} h^{-1}	[A1b,A7b]		
$D_{Zi,j,N,P}$	decomposition rate of $Z_{i,j,l,N,P}$ by $\Sigma_n M_{i,n,a,l}$	g N or P m^{-2} h^{-1}	[A7b]		
$\boldsymbol{D}_{Zj,C}$	specific decomposition rate of $Z_{i,j,l,C}$ by $\Sigma_n M_{i,n,a,l}$ at 25°C and saturating[$Z_{i,l,C}$]	g C g C^{-1} h^{-1}	[A4b]	0.25 and 0.05 for j = labile and resistant biomass	(Grant et al. 1993b, a)
$D'_{Zi,j,l,C}$	specific decomposition rate of $Z_{i,j,l,C}$ by $\Sigma_n M_{i,n,a,l}$ at 25°C	g C g C^{-1} h^{-1}	[A1b,A4b]		
$\boldsymbol{\Delta G_x}$	energy yield of C oxidation with different reductants x	kJ g C^{-1}	[A21]	37.5 (x = O_2); 4.43 (x = DOC)	
$\boldsymbol{E_m}$	energy requirement for growth of $M_{i,n,a,l}$	kJ g C^{-1}	[A21]	25	
$\boldsymbol{E_\Phi}$	energy requirement for non-symbiotic N_2 fixation by heterotrophic diazotrophs ($n = f$)	g C g N^{-1}	[A28]	5	(Waring and Running 1998)
$\boldsymbol{F_h}$	fraction of products from microbial decomposition that are humified (function of clay content)		[A35]	0.167 + 0.167*clay	

$\boldsymbol{F_l}$	fraction of microbial growth allocated to labile component $M_{i,n,l}$		[A25,A29,A30]	0.55	(Grant et al. 1993b, a)
$\boldsymbol{F_r}$	fraction of microbial growth allocated to resistant component $M_{i,n,r}$		[A25,A29,A30]	0.45	(Grant et al. 1993b, a)
F_s	equilibrium ratio between $Q_{i,l,C}$ and $H_{i,l,C}$		[A8]		
$f_{di,n,lN,P}$	fraction of N or P released with $D_{Mi,n,j,l,C}$ during decomposition	dimensionless	[A24]	0.33 $U_{NH4} > 0$ 1.00 $U_{NH4} < 0$ 0.33 $U_{PO4} > 0$ 1.00 $U_{PO4} < 0$	
f_{tgl}	temperature function for microbial growth respiration	dimensionless	[A1,A6,A13, A23,A24]		
f_{tml}	temperature function for maintenance respiration	dimensionless	[A18,A19]		
$f_{\psi gl}$	soil water potential function for microbial, root or mycorrhizal growth respiration	dimensionless	[A13,A15]		(Pirt 1975)
$\Phi_{i,n=f,j,l}$	non-symbiotic N_2 fixation by heterotrophic diazotrophs (n = f)	g N m^{-2} h^{-1}	[A27,A28,A29]		
$G_{i,l,C}$	total C in substrate-microbe complex	g C Mg^{-1}	[A1,A2c,A3a,A8]		
$[H_2PO_4^-]$	concentration of $H_2PO_4^-$ in soil solution	g P m^{-3}	[A26]		
$\boldsymbol{H_a}$	energy of activation	J mol^{-1}	[A6,C10]	65 x 10^3	(Addiscott 1983)
$\boldsymbol{H_{dh}}$	energy of high temperature deactivation	J mol^{-1}	[A6,C10]	225 x 10^3	

$\boldsymbol{H_{dl}}$	energy of low temperature deactivation	J mol^{-1}	[A6,C10]	198 x 10^3	
$H_{Mi,n,j,l,C}$	transfer of microbial C decomposition products to humus	g C m m^{-2} h^{-1}	[A35,A36]		
$H_{Mi,n,j,l,N,P}$	transfer of microbial N or P decomposition products to humus	g N or P m^{-2} h^{-1}	[A36]		
$H_{Si,j,l,C}$	transfer of C hydrolysis products to particulate OM	g C m^{-2} h^{-1}	[A31,A32,A33, A34]		
$H_{Si,j,l,N,P}$	transfer of N or P hydrolysis products to particulate OM	g N or P m^{-2} h^{-1}	[A32,A34]		
$\boldsymbol{K_{iS}}$	inhibition constant for microbial colonization of substrate	-	[A5]	0.5	(Grant et al. 2010)
$\boldsymbol{K_{NH_4}}$	M-M constant for NH_4^+ uptake at microbial surfaces	g N m^{-3}	[A26]	0.40	
$\boldsymbol{K_{NO_3}}$	M-M constant for NO_3^- uptake at microbial surfaces	g N m^{-3}	[A26]	0.35	
$\boldsymbol{K_{PO_4}}$	M-M constant for $H_2PO_4^-$ uptake at microbial surfaces	g P m^{-3}	[A26]	0.125	
$\boldsymbol{K_{iD}}$	inhibition constant for $[M_{i,n,a}]$ on $S_{i,C}$, $Z_{i,C}$	g C m^{-3}	[A4]	25	(Lizama and Suzuki 1991, Grant et al. 1993b, a)
$\boldsymbol{K_{mD}}$	Michaelis–Menten constant for $D_{Si,j,C}$	g C Mg^{-1}	[A4]	75	
$\boldsymbol{K_{mQ_C}}$	Michaelis–Menten constant for $R'_{hi,n}$ on $[Q_{i,C}]$	g C m^{-3}	[A13]	36	
$\boldsymbol{K_{O_2}}$	Michaelis–Menten constant for reduction of O_{2s} by microbes, roots and mycorrhizae	g O_2 m^{-3}	[A17]	0.064	(Griffin 1972)
$\boldsymbol{k_{ts}}$	equilibrium rate constant for sorption	h^{-1}	[A8]	0.01	(Grant et al. 1993b, a)

$\boldsymbol{L_{hj}}$	ratio of nonlignin to lignin components in humified hydrolysis products		[A33]	0.10, 0.05, and 0.05 for j = protein, carbohydrate, and cellulose, respectively	(Schulten and Schnitzer 1997)
$\boldsymbol{M}$	molecular mass of water	g mol^{-1}	[A15]	18	
$M_{i,d,l,C}$	heterotrophic microbial C used for decomposition	g C m^{-2}	[A1,A3a,A4]		
$M_{i,n,j,l,\mathrm{C}}$	microbial C	g C m^{-2}	[A13,A17A23,A25,A26, A30,A36]		
$M_{i,n,j,l,\mathrm{N}}$	microbial N	g N m^{-2}	[A18,A27,A29]		
$M_{i,n,j,l,\mathrm{P}}$	microbial P	g P m^{-2}	[A24,A29,A26, A36]		
$M_{i,n,a,l,\mathrm{C}}$	active microbial C from heterotrophic population n associated with $G_{i,l,\mathrm{C}}$	g C m^{-2}	[A3,A13,A17, A30]		
$[M_{i,n,a,l,\mathrm{C}}]$	concentration of $M_{i,n,a}$ in soil water = $M_{i,n,a,l,\mathrm{C}}/\theta_l$	g C m^{-3}	[A3, A5]		
$[NH_4^+{}_{i,n,j,l}]$	concentration of NH_4^+ at microbial surfaces	g N m^{-3}	[A26]		
$[\boldsymbol{NH_4^+{}_{mn}}]$	concentration of NH_4^+ at microbial surfaces below which $U_{NH_4} = 0$	g N m^{-3}	[A26]	0.0125	
$[NO_3^-{}_{i,n,j,l}]$	concentration of NH_4^+ at microbial surfaces	g N m^{-3}	[A26]		
$[\boldsymbol{NO_3^-{}_{mn}}]$	concentration of NO_3^- at microbial surfaces below which $U_{NO_3} = 0$	g N m^{-3}	[A26]	0.03	
$[H_2PO_4^-{}_{i,n,j,l}]$	concentration of $H_2PO_4^-$ at microbial surfaces	g N m^{-3}	[A26]		

$[\mathbf{H_2PO_4^-{}_{mn}}]$	concentration of $H_2PO_4^-$ at microbial surfaces below which $U_{PO_4} = 0$	g N m^{-3}	[A26]	0.002	
$[O_{2mi,n,l}]$	O_2 concentration at heterotrophic microsites	g O_2 m^{-3}	[A17]		
$[O_{2sl}]$	O_2 concentration in soil solution	g O_2 m^{-3}	[A17]		
$Q_{i,l,C}$	*DOC* from products of $D_{Si,j,l,C}$ [A3] and $D_{Zi,j,l,C}$) [A5]	g C m^{-2}	[A8,A13,A22]		
$[Q_{i,l,C}]$	solution concentration of $Q_{i,l,C}$	g C Mg^{-1}	[A8,A13]		
$Q_{i,l,N,P}$	*DON* and DOP from products of ($D_{Si,j,l,N,P} + D_{Zi,j,l,N,P}$)	g N or P m^{-2}	[A9,A22]		
$\boldsymbol{q_m}$	constant for reallocating $M_{i,a,l,C}$ to $M_{i,d,l,C}$	-	[A3a]	0.5	
$\boldsymbol{R}$	gas constant	J mol^{-1} K^{-1}	[A6,A15,C10]	8.3143	
$R_{\Phi i,n=fj,l}$	respiration for non-symbiotic N_2 fixation by heterotrophic diazotrophs ($n = f$)	g C m^{-2} h^{-1}	[A28]		
$R_{gi,n,l}$	growth respiration of $M_{i,n,a,l}$ on $Q_{i,l,C}$ under nonlimiting O_2 and nutrients	g C g C^{-1} h^{-1}	[A20]		
R_h	total heterotrophic respiration of all $M_{i,n,a,l}$ under ambient DOC, O_2, nutrients, θ and temperature	g C m^{-2} h^{-1}	[A11]		
$R_{hi,n,l}$	heterotrophic respiration of $M_{i,n,a,l}$ under ambient DOC, O_2, nutrients, θ and temperature	g C m^{-2} h^{-1}	[A5,A11,A14,A20, A21,A25]		
$\boldsymbol{R}_{hi,n,l}$	specific heterotrophic respiration of $M_{i,n,a,l}$ under nonlimiting O_2, DOC, θ and 25°C	g C g C^{-1} h^{-1}	[A12,A13]		
$\boldsymbol{R}_h{}'_n$	specific heterotrophic respiration of $M_{i,n,a,l}$ under nonlimiting DOC, O_2, nutrients, θ and 25°C	g C g C^{-1} h^{-1}	[A12]	0.125	(Shields et al. 1973)

$R_h'_{i,n,l}$	heterotrophic respiration of $M_{i,n,a,l}$ under nonlimiting O_2 and ambient DOC, nutrients, θ and temperature	g C m^{-2} h^{-1}	[A13,A14,A16]		
$\boldsymbol{R}_m$	specific maintenance respiration at 25°C	g C g N^{-1} h^{-1}	[A18]	0.0115	(Barnes et al. 1997)
$R_{mi,n,j,l}$	maintenance respiration by $M_{i,n,j,l}$	g C m^{-2} h^{-1}	[A18,A20,A21,A25]		
r_{wl}	radius of r_m + water film at current water content	m	[A17]		
$\boldsymbol{r}_m$	radius of heterotrophic microsite	m	[A17]	2.5×10^{-6}	
r_{wl}	thickness of water films	m	[A17]		
$\boldsymbol{S}$	change in entropy	J mol^{-1} K^{-1}	[A6,C10]	710	(Sharpe and DeMichele 1977)
$[S_{i,j,l,C}]$	concentration of $S_{i,j,l,C}$ in soil	g C Mg^{-1}	[A4a]		
$S_{i,j,l,C}$	mass of colonized litter, POC or humus C	g C m^{-2}	[A2a,A5,A7a,A33]		
$S'_{i,j,l,C}$	mass of uncolonized litter, POC or humus C	g C m^{-2}	[A5]		
$S_{i,j,l,N,P}$	mass of litter, POC or humus N or P	g N or P m^{-2}	[A7a,A33]		
T_{sl}	soil temperature	K	[A6,A15.A19]		
$U_{i,n,lC}$	uptake of $Q_{i,l,C}$ by $\Sigma_n M_{i,n,a,l}$ under limiting nutrient availability	g C m^{-2} h^{-1}	[A5,A21,A22,A25]		
$U_{i,n,N,P}$	uptake of $Q_{i,l,N,P}$ by $\Sigma_n M_{i,n,a,l}$ under limiting nutrient availability	g N or P m^{-2} h^{-1}	[A22,A29]		
$U_{NH4i,n,j,l}$	NH_4^+ uptake by microbes	g N m^{-2} h^{-1}	[A26, A27,A29]		

$\boldsymbol{U'_{NH_4}}$	maximum U_{NH_4} at 25 °C and non-limiting NH_4^+	g N m^{-2} h^{-1}	[A26]	5.0 x 10^{-3}
$U_{NO3i,n,j,l}$	NO_3^- uptake by microbes	g N m^{-2} h^{-1}	[A26,A27,A29]	
$\boldsymbol{U'_{NO_3}}$	maximum U_{NO_3} at 25 °C and non-limiting NO_3^-	g N m^{-2} h^{-1}	[A26]	5.0 x 10^{-3}
$U_{O2i,n}$	O_2 uptake by $M_{i,n,a,l}$ under ambient O_2	g m^{-2} h^{-1}	[A14,A17]	
$U'_{O2i,n}$	O_2 uptake by $M_{i,n,a,l}$ under nonlimiting O_2	g m^{-2} h^{-1}	[A14,A16,A17]	
$U_{PO4i,n,j,l}$	$H_2PO_4^-$ uptake by microbes	g N m^{-2} h^{-1}	[A26,A27,A29]	
$\boldsymbol{U'_{PO_4}}$	maximum U_{PO_4} at 25 °C and non-limiting $H_2PO_4^-$	g N m^{-2} h^{-1}	[A26]	5.0 x 10^{-3}
$X_{i,l,C}$	adsorbed C hydrolysis products	g C Mg^{-1}	[A8,A10]	
$X_{i,l,N,P}$	adsorbed N or P hydrolysis products	g P Mg^{-1}	[A10]	
$\boldsymbol{y}$	selected to give a Q_{10} for f_{tm} of 2.25		[A19]	0.081
ψ_s	soil or residue water potential	MPa	[A15]	
$Y_{i,l,C}$	sorption of C hydrolysis products	g C m^{-2} h^{-1}	[A8,A9,A10]	
$Y_{i,l,N,P}$	sorption of N or P hydrolysis products	g P m^{-2} h^{-1}	[A9,A10]	
$[Z_{i,j,l,C}]$	concentration of $Z_{i,j,l,C}$ in soil	g C Mg^{-1}	[A4b]	
$Z_{i,j,l,C}$	mass of microbial residue C in soil	g C m^{-2}	[A2b,A7b]	
$Z_{i,j,l,N,P}$	mass of microbial residue N or P in soil	g P m^{-2}	[A7b]	

Appendix B: Soil-plant water relations

Canopy transpiration

$Rn_{ci} + LE_{ci} + H_{ci} + G_{ci} = 0$	canopy energy balance	[B1a]
$\boldsymbol{L}E_{ci} = L\,(e_a - e_{ci(T_{ci},\psi_{ci})})/r_{ai}$	*LE* from canopy evaporation	[B1b]
$\boldsymbol{L}E_{ci} = L\,(e_a - e_{ci(T_{ci},\psi_{ci})})/(r_{ai} + r_{ci})$ - $\boldsymbol{L}E_{ci}$ from [B1b]	*LE* from canopy transpiration	[B1c]
$H_{ci} = \rho C_p (T_a - T_{ci})/r_{ai}$	*H* from canopy energy balance	[B1d]
$r_{cmini} = 0.64\,(C_b - \boldsymbol{C_i}'_i)/\,V_c'_i$	r_c driven by rates of carboxylation	[B2a]
$r_{ci} = r_{cmini} + (\boldsymbol{r_{cmaxi}} - r_{cmini})\,e^{(-\boldsymbol{\beta}\,\psi_{ti})}$	*vs*. diffusion r_c constrained by water status	[B2b]
$r_{ai} = \{(\ln((z_u - z_{di})/z_{ri})^2/(\boldsymbol{K}^2 u_a)\}/(1 - 10\,Ri)$	r_a driven by windspeed, surface	[B3a]
$Ri = \{g\,(z_u - z_{ri})/(u_a^2\,T_a)\}\,(T_a - T_c)$	r_a adjusted for stability *vs*. buoyancy	[B3b]
$\psi_{ti} = \psi_{ci}$ - $\psi_{\pi i}$		[B4]

Root and mycorrhizal water uptake

$U_{wi} = \Sigma_l \Sigma_r U_{wi,r,l}$		[B5]
$U_{wi,r,l} = (\psi_c'_i - \psi_s'_l)/(\Omega_{si,r,l} + \Omega_{ri,r,l} + \Sigma_x \Omega_{ai,r,l,x})$	U_w along hydraulic gradient	[B6]
$\psi_c'_i = \psi_{ci} + 0.01\,z_{bi}$		[B7]
$\psi_s'_l = \psi_{sl} - 0.01\,z_l$		[B8]
$\Omega_{si,r,l} = \ln\{(d_{i,r,l}/r_{i,r,l})/(2\pi L_{i,r,l}\,\kappa_{ri,r,l})\}\;\theta_{wl}/\theta_{pl}$		[B9]
$\Omega_{ri,r,l} = \boldsymbol{\Omega'_{ri,r}}/L_{i,r,l}$		[B10]
$\Omega_{ai,r,l,x=1} = \boldsymbol{\Omega'_{ai,r}}\,z_l/\{n_{i,r,l,1}\,(r_{i,r,l,1}/\boldsymbol{r'}_{i,r})^4\} + \boldsymbol{\gamma\Omega'_{ai,r}}\,z_{bi}/\{n_{i,r,l,1}\,(r_{bi}/r_b'_i)^4\}\Sigma_{i,r,l}(M_{i,r,l})/M_{i,r,l}$		[B11]
$\Omega_{ai,r,l,x=2} = \boldsymbol{\Omega_{ai,r}}\;(L_{i,r,l,2}/n_{i,r,l,2})/\{n_{i,r,l,2}\,(r_{i,r,l,2}/r'_{i,r})^4\}$		[B12]
$\delta L_{i,r,l,1}/\delta t = \delta M_{i,r,l,1}/\delta t\;\nu_r\;/\{\rho_r\;(1 - \theta_{Pi,r})\,(\pi\,r_{i,r,l,1}^2)\}$		[B13]

Canopy water potential

$(e_a - e_{i(T_{ci})})/(r_{ai} + r_{ci})$ [B1] $= \Sigma_l \Sigma_r(\psi_c'_i - \psi_s'_l)/(\Omega_{si,r,l} + \Omega_{ri,r,l} + \Sigma_x \Omega_{ai,r,l,x}) + X_{ci}\delta\psi_{ci}/\delta t$	ψ_c solved when transpiration from [B1-B4] (LHS) equals uptake from [B5-B13] + change in storage (RHS)	[B14]

Definition of variables in appendix B

Variable	Definition	Unit	Equation	Value	Reference
		Subscripts			
I	plant species or functional type: coniferous, deciduous, annual, perennial, C_3, C_4, monocot, dicot etc.				
J	branch or tiller				
K	Node				
L	soil or canopy layer				
M	leaf azimuth				
n	leaf inclination				
o	leaf exposure (sunlit *vs*. shaded)				
r	root or mycorrhizae				
		Variables			
$\boldsymbol{\beta}$	stomatal resistance shape parameter	MPa^{-1}	[B2b,C4,C9]	-5.0	(Grant and Flanagan 2007)
C_b	$[CO_2]$ in canopy air	$\mu mol\ mol^{-1}$	[B2,C2,C5]		
$\boldsymbol{C_i'}_i$	$[CO_2]$ in canopy leaves at $\psi_{c_i} = 0$ MPa	$\mu mol\ mol^{-1}$	[B2]	0.70 C_b	(Larcher 2003)
$d_{i,r,l}$	half distance between adjacent roots	m	[B9]		
E_{ci}	canopy transpiration	$m^3\ m^{-2}\ h^{-1}$	[B1,B14]		

e_a	atmospheric vapor density at T_a and ambient humidity	g m^{-3}	[B1]		
$e_{ci(T_{ci}, \psi_{ci})}$	canopy vapor density at T_{c_i} and ψ_{c_i}	g m^{-3}	[B1]		
G_{ci}	canopy storage heat flux	W m^{-2}	[B1]		
H_{ci}	canopy sensible heat flux	W m^{-2}	[B1]		
K	von Karman's constant		[B3a]	0.41	
$\kappa_{ri,r,l}$	hydraulic conductivity between soil and root surface	m^2 MPa^{-1} h^{-1}	[B9]		
γ	scaling factor for bole axial resistance from primary root axial resistance	-	[B11]	1.6 x 10^4	(Grant et al. 2007)
L	latent heat of evaporation	J g^{-1}	[B1]	2460	
LE_{ci}	latent heat flux between canopy and atmosphere	W m^{-2}	[B1]		
$L_{i,r,l}$	length of roots or mycorrhizae	m m^{-2}	[B9,B10,B12,B13]		
$M_{i,r,l}$	mass of roots or mycorrhizae	g m^{-2}	[B11,B13]		
$n_{i,r,l,x}$	number of primary (x = 1) or secondary (x = 2) axes	m^{-2}	[B11,B12]		
$\Omega'_{ai,r}$	axial resistivity to water transport along root or mycorrhizal axes	MPa h m^{-4}	[B11,B12]	4.0 x 10^9 deciduous 1.0 x 10^{10} coniferous	(Larcher 2003)
$\Omega_{ai,r,l,x}$	axial resistance to water transport along axes of primary (x = 1) or secondary (x = 2) roots or mycorrhizae	MPa h m^{-1}	[B6,B11,B12]		

$\Omega'_{ri,r}$	radial resistivity to water transport from surface to axis of roots or mycorrhizae	MPa h m^{-2}	[B10]	1.0 x 10^4	(Doussan et al. 1998)
$\Omega_{ri,r,l}$	radial resistance to water transport from surface to axis of roots or mycorrhizae	MPa h m^{-1}	[B6,B10]		
$\Omega_{si,r,l}$	radial resistance to water transport from soil to surface of roots or mycorrhizae	MPa h m^{-1}	[B6,B9]		
θ_{wl}	soil water content	m^3 m^{-3}	[B9]		
θ_{pl}	soil porosity	m^3 m^{-3}	[B9]		
$\theta_{Pi,r}$	root porosity	m^3 m^{-3}	[B13]		
Ri	Richarson number		[B3a,B3b]		(Van Bavel and Hillel 1976)
Rn_{ci}	canopy net radiation	W m^{-2}	[B1]		
r_{ai}	aerodynamic resistance to vapor flux from canopy	s m^{-1}	[B1,B3a]		
r_{bi}	radius of bole at ambient ψ_{ci}	m	[B11]		
$r_b'_i$	radius of bole at ψ_{ci} = 0 MPa	m	[B11]		
r_{ci}	canopy stomatal resistance to vapor flux	s m^{-1}	[B1,B2b]		
r_{cmaxi}	canopy cuticular resistance to vapor flux	s m^{-1}	[B2b]	5.0 x 10^3	(Larcher 2003)
r_{cmini}	minimum r_{ci} at ψ_{ci} = 0 MPa	s m^{-1}	[B2,B2b]		
$r_{i,r,l,x}$	radius of primary (x=1) or secondary (x=2) roots or mycorrhizae at ambient $\psi_{ri\ l,z}$	m	[B9,B11,B12,B13]		

$r'_{i,r}$	radius of secondary roots or mycorrhizae at $\psi_{r_i\,l,z}$ = 0 MPa	m	[B11,B12]	2.0 x 10^{-4} tree 1.0 x 10^{-4} bush 0.05 x 10^{-4} mycorrhizae	
ρ_r	root specific density	g C g FW^{-1}	[B13]	0.05	(Grant 1998)
T_a	air temperature	K	[B3b]		
T_c	canopy temperature	K	[B3b]		
U_{wi}	total water uptake from all rooted soil layers	m^3 m^{-2} h^{-1}	[B5,B14]		
$U_{wi,r,l}$	water uptake by root and mycorrhizal surfaces in each soil layer	m^3 m^{-2} h^{-1}	[B5,B6]		
u_a	wind speed measured at z_u	m s^{-1}	[B3a,B3b]		
$V_c'_i$	potential canopy CO_2 fixation rate at ψ_{c_i} = 0 MPa	μmol m^{-2} s^{-1}	[B2]		
ν_r	root specific volume	m^3 g FW^{-1}	[B13]	10^{-6}	(Grant 1998)
X_{ci}	canopy capacitance	m^3 m^{-2} MPa^{-1}	[B14]		
ψ_{ci}	canopy water potential	MPa	[B4,B7,B14]		
$\psi_c'_i$	ψ_{ci} + canopy gravitational potential	MPa	[B6,B7]		
$\psi_{\pi i}$	canopy osmotic potential	MPa	[B4]		
ψ_{sl}	soil water potential	MPa	[B8]		
$\psi_s'_l$	ψ_{sl} + soil gravitational potential	MPa	[B6,B8]		

ψ_{ti}	canopy turgor potential	MPa	[B2b,B4]	1.25 at $\psi_c = 0$
z_{bi}	length of bole from soil surface to top of canopy	m	[B7,B11]	
z_{di}	canopy zero-plane displacement height	m	[B3a]	(Perrier 1982)
z_l	depth of soil layer below surface	m	[B8,B11]	
z_r	canopy surface roughness	m	[B3a,B3b]	(Perrier 1982)
z_u	height of wind speed measurement	m	[B3a,B3b]	

Appendix C: Gross primary productivity and autotrophic respiration

C_3 gross primary productivity

$GPP = \Sigma_{i,j,k,l,m,n,o} (V_{ci,j,k,l,m,n,o} = V_{gi,j,k,l,m,n,o}) A_{i,j,k,l,m,n,o}$ solve for $C_{ii,j,k,l,m,n,o}$ at which $V_{ci,j,k,l,m,n,o} = V_{gi,j,k,l,m,n,o}$ [C1]

$V_{gi,j,k,l,m,n,o} = (C_b - C_{ii,j,k,l,m,n,o})/r_{li,j,k,l,m,n,o}$ diffusion [C2]

$V_{ci,j,k,l,m,n,o} = min\{V_{bi,j,k,l,m,n,o}, V_{ji,j,k,l,m,n,o}\}$ carboxylation [C3]

$r_{li,j,k,l,m,n,o} = r_{lmini,j,k,l,m,n,o} + (r_{lmaxi} - r_{lmini,j,k,l,m,n,o})\, e^{(-\beta\psi_{ti})}$ r_l is leaf-level equivalent of r_c [C4]

$r_{lmini,j,k,l,m,n,o} = (C_b - \boldsymbol{C_i'}_i)/ V_c'_{i,j,k,l,m,n,o}$ minimum r_l is driven by carboxylation [C5]

$V_{bi,j,k,l,m,n,o} = V_{bmaxi,j,k}(C_{ci,j,k,l,m,n,o} - \Gamma_{i,j,k})/(C_{ci,j,k,l,m,n,o}) + K_{c_i}) f_{\psi\, i,j,k,l,m,n,o}\ f_{iCi}$ CO_2, water, temperature and nutrient constraints on V_b [C6a]

$V_{bmax_{i,j,k}} = \boldsymbol{V_b'}_i \boldsymbol{F_{rubisco}}_i M_{i,j,k,prot}/A_{i,j,k}\ f_{tbi}$ [C6b]

$\Gamma_{i,j,k} = 0.5\, O_c\, V_{omax_{i,j,k}}\ \boldsymbol{K_c}_i /(V_{bmax_{i,j,k}}\ \boldsymbol{K_o}_i)$ [C6c]

$V_{omax_{i,j,k}} = \boldsymbol{V_o'}_i \boldsymbol{F_{rubisco}}_i M_{i,j,k,prot}/A_{i,j,k}\ f_{toi}$ [C6d]

$K_{c_i} = \boldsymbol{K_c}_i f_{tkci} (1 + O_c/ (\boldsymbol{K_o}_i f_{tkoi}))$ [C6e]

$V_{ji,j,k,l,m,n,o} = J_{i,j,k,l,m,n,o}\, Y_{i,j,k,l,m,n,o} f_{\psi\, i,j,k,l,m,n,o}\ f_{iCi}$ water, temperature and nutrient constraints on V_j [C7]

$$J_{i,j,k,l,m,n,o} = (\boldsymbol{\varepsilon}\, I_{i,l,m,n,o} + J_{\mathrm{max}i,j,k} - ((\boldsymbol{\varepsilon}\, I_{i,l,m,n,o} + J_{\mathrm{max}i,j,k})^2 \; - 4\boldsymbol{\alpha\varepsilon}\, I_{i,l,m,n,o} J_{\mathrm{max}i,j,k})^{0.5})/(2\boldsymbol{\alpha}) \qquad \text{[C8a]}$$

[C8b]

$$J_{\mathrm{max}i,j,k} = \boldsymbol{V_j'}_i \, \boldsymbol{F}_{\mathbf{chlorophyll}_i} M_{i,j,k,prot}/A_{i,j,k} f_{\mathrm{tj}i}$$

$$f_{\psi\, i,j,k,l,m,n,o} = (r_{\mathrm{lmin}i,j,k,l,m,n,o} \,/\, r_{\mathrm{l}i,j,k,l,m,n,o})^{0.5}$$ non-stomatal effect related to stomatal effect [C9]

$$f_{\mathrm{tb}\boldsymbol{i}} = \exp[\boldsymbol{B_v} - \boldsymbol{H_{av}}/(\boldsymbol{R}T_{ci})]/\{1 + \exp[(\boldsymbol{H_{dl}} - \boldsymbol{S}T_{ci})/(\boldsymbol{R}T_{ci})] + \exp[(\boldsymbol{S}T_{ci} - \boldsymbol{H_{dh}})/(\boldsymbol{R}T_{ci})]\}$$ Arrhenius functions for carboxylation, oxygenation and electron transport [C10a]

$$f_{\mathrm{to}\boldsymbol{i}} = \exp[\boldsymbol{B_o} - \boldsymbol{H_{ao}}/(\boldsymbol{R}T_{ci})]/\{1 + \exp[(\boldsymbol{H_{dl}} - \boldsymbol{S}T_{ci})/(\boldsymbol{R}T_{ci})] + \exp[(\boldsymbol{S}T_{ci} - \boldsymbol{H_{dh}})/(\boldsymbol{R}T_{ci})]\}$$ [C10b]

$$f_{\mathrm{tj}\boldsymbol{i}} = \exp[\boldsymbol{B_j} - \boldsymbol{H_{aj}}/(\boldsymbol{R}T_{ci})]/\{1 + \exp[(\boldsymbol{H_{dl}} - \boldsymbol{S}T_{ci})/(\boldsymbol{R}T_{ci})] + \exp[(\boldsymbol{S}T_{ci} - \boldsymbol{H_{dh}})/(\boldsymbol{R}T_{ci})]\}$$ temperature sensitivity of $\boldsymbol{K_{c}}_i$, $\boldsymbol{K_{o}}_i$ [C10c]

$$f_{\mathrm{tkc}i} = \exp[\boldsymbol{B_{kc}} - \boldsymbol{H_{akc}}/(\boldsymbol{R}T_{ci})]$$ [C10d]

$$f_{\mathrm{tko}i} = \exp[\boldsymbol{B_{ko}} - \boldsymbol{H_{ako}}/(\boldsymbol{R}T_{ci})]$$ [C10e]

$$f_{\mathrm{iC}\boldsymbol{i}} = min\{\sigma_{\mathrm{N}i,j}/(\sigma_{\mathrm{N}i,j} + \sigma_{\mathrm{C}i,j}/\boldsymbol{K_{iC_N}}),\ \sigma_{\mathrm{P}i,j}/(\sigma_{\mathrm{P}i,j} + \sigma_{\mathrm{C}i,j}/\boldsymbol{K_{iC_P}})\}$$ product inhibition of V_{b}, V_{j} from σ_{N} and σ_{P} *vs.* σ_{C} in shoots [C11]

$$\delta M_{\mathrm{L_R}i,j,k}/\delta t = \delta M_{\mathrm{L}i,j,k}/\delta t \ \min\{[\boldsymbol{N'_{leaf}} + (\boldsymbol{N_{leaf}} - \boldsymbol{N'_{leaf}})\, f_{\mathrm{iC}i}]/\mathbf{N_{prot}},\ [\boldsymbol{P'_{leaf}} + (\boldsymbol{P_{leaf}} - \boldsymbol{P'_{leaf}})\, f_{\mathrm{iC}i}]/\mathrm{P_{prot}}\}$$ leaf structural protein growth [C12]

Autotrophic respiration

$$R_{\mathrm{a}} = \Sigma_i \Sigma_j\, (R_{\mathrm{c}i,j} + R_{\mathrm{s}i,j}) + \Sigma_i \Sigma_l \Sigma_z\, (R_{\mathrm{c}i,r,l} + R_{\mathrm{s}i,r,l}) + \boldsymbol{E_{N,P}}\, (U_{\mathrm{NH4}i,r,l} + U_{\mathrm{NO3}i,r,l} + U_{\mathrm{PO4}i,r,l})$$ total autotrophic respiration [C13]

$$R_{\mathrm{c}i,j} = \boldsymbol{R}_{\mathrm{c}}'\sigma_{\mathrm{C}i,j}\, f_{\mathrm{ta}i}$$ O_2 constraint on root respiration from active uptake coupled with diffusion of O_2 from soil as for heterotrophic respiration in [A17], and from active uptake coupled with diffusion of O_2 from roots [C14a]

$$R_{\mathrm{c}i,r,l} = \boldsymbol{R}_{\mathrm{c}}'\sigma_{\mathrm{C}\,i,r,l}\, f_{\mathrm{ta}\,i,l}\ (U_{\mathrm{O2}i,r,l}/U'_{\mathrm{O2}i,r,l})$$ [C14b]

$$U_{\mathrm{O2}i,r,l} = U'_{\mathrm{O2}\,i,r,l}\ [\mathrm{O_{2r}}i,r,l]/([\mathrm{O_{2r}}i,r,l] + \boldsymbol{K_{O_2}})$$ [C14c]

$$= U_{\mathrm{w}i,r,l}[\mathrm{O_{2s}}l] + 2\pi L_{i,r,l}\, D_{\mathrm{sO2}}\, ([\mathrm{O_{2s}}l] - [\mathrm{O_{2r}}i,r,l])\, \ln\{(r_{\mathrm{s}l} + r_{\mathrm{r}i,r,l})/\, r_{\mathrm{r}i,r,l}\}$$
$$+ 2\pi L_{i,r,l}\, D_{\mathrm{rO2}}\, ([\mathrm{O_{2q}}i,r,l] - [\mathrm{O_{2}}\,\mathrm{r}i,r,l])\, \ln(r_{\mathrm{q}i,r,l})/\, r_{\mathrm{r}i,r,l})$$ [C14d]

$$U'_{\mathrm{O2}\,i,r,l} = 2.67\, R_{\mathrm{a}}'_{i,r,l}$$ [C14e]

$$R_{\mathrm{s}i,j} = -\, min\{0.0,\ R_{\mathrm{c}i,j} - R_{\mathrm{m}i,j}\}$$ remobilization when $R_{\mathrm{m}} > R_{\mathrm{c}}$ [C15]

$R_{mi,j} = \Sigma_z (N_{i,j,z} \boldsymbol{R_m'} f_{tmi})$ maintenance respiration [C16]

$R_{gi,j} = max\{0.0, min\{(R_{ci,j} - R_{mi,j}) min\{1.0, max\{0.0, \psi_{ti} - \psi_t'\}\}$ growth when $R_m < R_c$ [C17]

Growth and senescence

$l_{i,j,z,C} = R_{si,j} M_{L_N i,j} / M_{L_R i,j}$ senescence drives litterfall of non-remobilizable material [C18]

$l_{i,j,z,N} = l_{i,j,z,C} \mathbf{N_{prot}} (1.0 - \boldsymbol{X_{mx}} f_{xNi,j})$ litterfall of N and P is driven by that of C but reduced by translocation to to σ_N and σ_P according to ratios of σ_N and σ_P with σ_C [C19a]

$l_{i,j,z,P} = l_{i,j,z,C} \mathbf{P_{prot}} (1.0 - \boldsymbol{X_{mx}} f_{xPi,j})$ [C19b]

$f_{xNi,j} = \sigma_{Ci,j}/(\sigma_{Ci,j} + \sigma_{Ni,j}/\boldsymbol{K_{xN}})$ [C19c]

[C19d]

$f_{xPi,j} = \sigma_{Ci,j}/(\sigma_{Ci,j} + \sigma_{Pi,j}/\boldsymbol{K_{xP}})$

$\delta M_{Bi,j}/\delta t = \Sigma_z [R_{gi,j} (1 - \boldsymbol{Y_{gi,z}})/\boldsymbol{Y_{gi,z}}] - R_{si,j} - l_{i,j,C}$ branch growth driven by R_g [C20a]

$\delta M_{Ri,r,l}/\delta t = [R_{gi,r,l} (1 - \boldsymbol{Y_{gi,r}})/\boldsymbol{Y_{gi,r}}] - R_{si,r,l} - l_{i,r,l,C}$ root growth driven by R_g [C20b]

$\delta A_{Li,j,k,l}/\delta t = \boldsymbol{\chi} (M_{Li,j,k,l}/y_i)^{-0.33} \delta M_{Li,j,k,l}/\delta t \min\{1, \max\{0, \psi_{ti} - \psi_t'\}$ leaf expansion driven by leaf mass growth [C21a]

$\delta L_{i,r,l,1}/\delta t = (\delta M_{Ri,r,l,1}/\delta t)/y_i \nu_r / \{\boldsymbol{\rho_r} (1 - \boldsymbol{\theta_{Pi,r}}) (\pi r_{ri,r,l,1}^2)\}$ root extension of primary and secondary axes driven by root mass growth [C21b]

$\delta L_{i,r,l,2}/\delta t = (\delta M_{Ri,r,l,2}/\delta t) \nu_r / \{\boldsymbol{\rho_r} (1 - \boldsymbol{\theta_{Pi,r}}) (\pi r_{ri,r,l,2}^2)\}$ [C21c]

$f_{tai} = T_{ci}\{\exp[\boldsymbol{B_v} - \boldsymbol{H_{av}}/(\boldsymbol{R}T_{ci})]\}/\{1 + \exp[(\boldsymbol{H_{dl}} - \boldsymbol{S}T_{ci})/(\boldsymbol{R}T_{ci})] + \exp[(\boldsymbol{S}T_{ci} - \boldsymbol{H_{dh}})/(\boldsymbol{R}T_{ci})]\}$ Arrhenius function for R_a [C22a]

$f_{tmi} = e^{(0.0811*(T_{ci} - 298.15))}$ temperature function for R_m [C22b]

Root and mycorrhizal nutrient uptake

$$U_{NH4i,r,l} = \{U_{wi,r,l}[NH_4^+{}_l] + 2\pi L_{i,r,l} D_{eNH4l} ([NH_4^+{}_l] - [NH_4^+{}_{i,r,l}]) / \ln(d_{i,r,l} / r_{ri,r,l})\}$$

$$= \boldsymbol{U'_{NH_4}} (U_{O2i,r,l} / U'_{O2i,r,l}) A_{i,r,l} ([NH_4^+{}_{i,r,l}] - \mathbf{[NH_4^+{}_{mn}]}) / ([NH_4^+{}_{i,r,l}] - \mathbf{[NH_4^+{}_{mn}]} + \boldsymbol{K_{NH_4}}) f_{tijl} f_{iNi,r,l}$$

$$U_{NO3i,r,l} = \{U_{wi,r,l} [NO_3^-{}_l] + 2\pi L_{i,r,l} D_{eNO3l} ([NO_3^-{}_l] - [NO_3^-{}_{i,r,l}]) / \ln(d_{i,r,l} / r_{ri,r,l})\}$$

$$= \boldsymbol{U'_{NO_3}} (U_{O2i,r,l} / U'_{O2i,r,l}) A_{i,r,l} ([NO_3^-{}_{i,r,l}] - \mathbf{[NO_3^-{}_{mn}]}) / ([NO_3^-{}_{i,r,l}] - \mathbf{[NO_3^-{}_{mn}]} + \boldsymbol{K_{NO_3}}) f_{tijl} f_{iNi,r,l}$$

$$U_{PO4i,r,l} = \{U_{wi,r,l} [H_2PO_4^-{}_l] + 2\pi L_{i,r,l} D_{ePO4l} ([H_2PO_4^-{}_l] - [H_2PO_4^-{}_{i,r,l}]) / \ln(d_{i,r,l} / r_{ri,r,l})\}$$

$$= \boldsymbol{U'_{PO_4}} (U_{O2i,r,l} / U'_{O2i,r,l}) A_{i,r,l} ([H_2PO_4^-{}_{i,r,l}] - \mathbf{[H_2PO_4^-{}_{mn}]}) / ([H_2PO_4^-{}_{i,r,l}] - \mathbf{[H_2PO_4^-{}_{mn}]} + \boldsymbol{K_{PO_4}}) f_{tgl} f_{iPi,r,l}$$

$$f_{iNi,r,l} = \sigma_{Ci,r,l} / (\sigma_{Ci,r,l} + \sigma_{Ni,r,l} / \boldsymbol{K_{iN_C}})$$

$$f_{iPi,r,l} = \sigma_{Ci,r,l} / (\sigma_{Ci,r,l} + \sigma_{Pi,r,l} / \boldsymbol{K_{iP_C}})$$

root N and P uptake from mass flow + diffusion coupled with active uptake of NH_4^+, NO_3^- and $H_2PO_4^-$ constrained by O_2 uptake, as for microbial N and P uptake in [A26] [C23a] [C23b] [C23c] [C23d] [C23e]

product inhibition of U_{NH4}, U_{NO3} and U_{PO4} determined by σ_N and σ_P *vs.* σ_C in roots [C23f] [C23g] [C23h]

Definition of variables in appendix C

Variable	Definition	Unit	Equation	Value	Reference
	Subscripts				
i	species or functional type: evergreen, coniferous, deciduous, annual, perennial, C_3, C_4, monocot, dicot, legume etc.				
j	branch or tiller				
k	Node				
l	soil or canopy layer				
m	leaf azimuth				
n	leaf inclination				
o	leaf exposure (sunlit *vs*. shaded)				

z	organ including leaf, stem, root, mycorrhizae				
		Variables			
A	leaf, root or mycorrhizalsurface area	$m^2\ m^{-2}$	[C1,C6b,C6d,C8b, C21,C23,C32,C33 ,C47]		
$\boldsymbol{\beta}$	shape parameter for stomatal effects on CO_2 diffusion and non-stomatal effects on carboxylation	MPa^{-1}	[C4 C27,C35,]	-5.0	(Grant and Flanagan 2007)
B	parameter such that $f_t = 1.0$ at $T_c = 298.15$ K		[C36]	17.533	
$\boldsymbol{B_j}$	parameter such that $f_{tj} = 1.0$ at $T_c = 298.15$ K		[C10c]	17.363	
$\boldsymbol{B_{kc}}$	parameter such that $f_{tkc} = 1.0$ at $T_c = 298.15$ K		[C10d]	22.187	
$\boldsymbol{B_{ko}}$	parameter such that $f_{tko} = 1.0$ at $T_c = 298.15$ K		[C10e]	8.067	
$\boldsymbol{B_o}$	parameter such that $f_{to} = 1.0$ at $T_c = 298.15$ K		[C10b]	24.221	
$\boldsymbol{B_v}$	parameter such that $f_{tv} = 1.0$ at $T_c = 298.15$ K		[C10a, C22]	26.238	
C_b	$[CO_2]$ in canopy air	$\mu mol\ mol^{-1}$	[C2,C5 C25,C28]		
$C_{c(b4)}$	$[CO_2]$ in C_4 bundle sheath	μM	[C38,C39,C42,C4 4]		
$C_{c(m4)}$	$[CO_2]$ in C_4 mesophyll in equilibrium with $C_{ii,j,k,l,m,n,o}$	μM	[C29,C39]		
C_c	$[CO_2]$ in canopy chloroplasts in equilibrium with $C_{ii,j,k,l,m,n,o}$	μM	[C6]		

$C_{i(m4)}'$	[CO_2] in C_4 mesophyll air when $\psi_{ci} = 0$	µmol mol^{-1}	[C28]	0.45 x C_b	
$C_{i(m4)}$	[CO_2] in C_4 mesophyll air	µmol mol^{-1}	[C25]		
$C_{i,j,z=l}$	C content of leaf ($z = l$)	g C m^{-2}	[C18]		
$\boldsymbol{C_i'}$	[CO_2] in canopy leaves when $\psi_{ci} = 0$	µmol mol^{-1}	[C5]	0.70 x C_b	(Larcher 2003)
C_i	[CO_2] in canopy leaves	µmol mol^{-1}	[C2]		
$D_{e\ NH4l}$	effective dispersivity-diffusivity of NH_4^+ during root uptake	m^2 h^{-1}	[C23]		
$D_{e\ NO3l}$	effective dispersivity-diffusivity of NO_3^- during root uptake	m^2 h^{-1}	[C23]		
$D_{e\ PO4l}$	effective dispersivity-diffusivity of $H_2PO_4^-$ during root uptake	m^2 h^{-1}	[C23]		
D_{rO2}	aqueous diffusivity of O_2 from root aerenchyma to root or mycorrhizal surfaces	m^2 h^{-1}	[C14d]		
D_{sO2}	aqueous diffusivity of O_2 from soil to root or mycorrhizal surfaces	m^2 h^{-1}	[C14d]		
$d_{i,r,l}$	half distance between adjacent roots assumed equal to uptake path length	m	[C23]	$(\pi L_{s,z} / \Delta z)^{-1/2}$	(Grant 1998)
$\boldsymbol{E_{N,P}}$	energy cost of nutrient uptake	g C g N^{-1} or P^{-1}	[C13]	2.15	(Veen 1981)
$f_{C(c3)}$	C_3 product inhibition of RuBP carboxylation activity in C_4 bundle sheath or C_3 mesophyll	–	[C47,C48,C49]		
$f_{C(m4)}$	C_4 product inhibition of PEP carboxylation activity in C_4 mesophyll	–	[C32,C33,C34]		

$\boldsymbol{F}_{\mathbf{chl}}$	fraction of leaf protein in chlorophyll	-	[C8b]	0.025	
f_{iC}	N,P inhibition on carboxylation, leaf structural N,P growth	–	[C6a,C7,C11,C12]		
f_{iN}	N inhibition on root N uptake	–	[C23g]		
f_{iP}	P inhibition on root P uptake	–	[C23h]		
$\boldsymbol{F}_{\mathbf{rubisco}}$	fraction of leaf protein in rubisco	-	[C6b,d]	0.125	
f_{ta}	temperature effect on $R_{ai,j}$	–	[C14, C22]		
f_{tb}	temperature effect on carboxylation	–	[C6b,C10a]		
f_{tg}	temperature function for root or mycorrhizal growth respiration	dimensionless	[C23]		
f_{tj}	temperature effect on electron transport		[C8b,C10c]		
f_{tkc}	temperature effect on $\boldsymbol{K}_{\mathbf{c}_i}$		[C6e,C10d]		(Bernacchi et al. 2001, 2003)
f_{tko}	temperature effect on $\boldsymbol{K}_{\mathbf{o}_i}$		[C6e,C10e]		(Bernacchi et al. 2001, 2003)
f_{tm}	temperature effect on $R_{mi,j}$	–	[C16, C22b]	$Q_{10} = 2.25$	
f_{to}	temperature effect on oxygenation		[C6d,C10b]		
f_{tv}	temperature effect on carboxylation	–	[C32,C33,C36,C47,C48]		
f_{xN}	fraction of $\boldsymbol{X}_{\mathbf{mx}}$ N translocated out of leaf or root during senescence	–	[C19a,c]		

f_{xP}	fraction of $\boldsymbol{X_{mx}}$ P translocated out of leaf or root during senescence	–	[C19b,d]		
$f_{\psi i}$	non-stomatal water effect on carboxylation	–	[C6a,C7,C9]		(Medrano et al. 2002)
$f_{\psi i}$	non-stomatal water effect on carboxylation	–	[C32,C33,C35C47 ,C48]		
H_a	energy of activation	J mol^{-1}	[C36]	57.5 x 10^3	
$\boldsymbol{H_{aj}}$	energy of activation for electron transport	J mol^{-1}	[C10c]	43 x 10^3	(Bernacchi et al. 2001, 2003)
$\boldsymbol{H_{akc}}$	parameter for temperature sensitivity of $\boldsymbol{K_{c_i}}$	J mol^{-1}	[C10d]	55 x 10^3	(Bernacchi et al. 2001, 2003)
$\boldsymbol{H_{ako}}$	parameter for temperature sensitivity of $\boldsymbol{K_{o_i}}$	J mol^{-1}	[C10e]	20 x 10^3	(Bernacchi et al. 2001, 2003)
$\boldsymbol{H_{ao}}$	energy of activation for oxygenation	J mol^{-1}	[C10b, C22]	60 x 10^3	(Bernacchi et al. 2001, 2003)
$\boldsymbol{H_{av}}$	energy of activation for carboxylation	J mol^{-1}	[C10a, C22]	65 x 10^3	(Bernacchi et al. 2001, 2003)
$\boldsymbol{H_{dh}}$	energy of high temperature deactivation	J mol^{-1}	[C10, C22]	222.5 x 10^3	
H_{dh}	energy of high temperature deactivation	J mol^{-1}	[C36]	220 x 10^3	
$\boldsymbol{H_{dl}}$	energy of low temperature deactivation	J mol^{-1}	[C10, C22]	198.0 x 10^3	
H_{dl}	energy of low temperature deactivation	J mol^{-1}	[C36]	190 x 10^3	

I	Irradiance	μmol m^{-2} s^{-1}	[C8a,]		
$J_{(b4)}$	electron transport rate in C_4 bundle sheath	μmol m^{-2} s^{-1}	[C45,C46]		
$J_{(m4)}$	electron transport rate in C_4 mesophyll	μmol m^{-2} s^{-1}	[C30,C31]		
J	electron transport rate in C_3 mesophyll	μmol m^{-2} s^{-1}	[C7,C8a]		
J_{max}'	specific electron transport rate at non-limiting I and 25°C when $\psi_{ci} = 0$ and nutrients are nonlimiting	μmol g^{-1} s^{-1}	[C33,C48]	400	
$J_{max(b4)}$	electron transport rate in C_4 bundle sheath at non-limiting I	μmol m^{-2} s^{-1}	[C46,C48]		
$J_{max(m4)}$	electron transport rate in C_4 mesophyll at non-limiting I	μmol m^{-2} s^{-1}	[C31,C33]		
J_{max}	electron transport rate at non-limiting I, ψ_{ci}, temperature and N,P	μmol m^{-2} s^{-1}	[C8a,C8b]		
$K_{c(b4)}$	Michaelis-Menten constant for carboxylation in C_4 bundle sheath	μM	[C44]	30.0 at 25°C and zero O_2	(Lawlor 1993)
$K_{c(m4)}$	Michaelis-Menten constant for carboxylation in C_4 mesophyll	μM	[C29]	3.0 at 25°C	(Lawlor 1993)
$\boldsymbol{K_c}$	Michaelis-Menten constant for carboxylation at zero O_2	μM	[C6c,C6e]	12.5 at 25 °C	(Farquhar et al. 1980)
K_c	Michaelis-Menten constant for carboxylation at ambient O_2	μM	[C6e]		
$\boldsymbol{K_{iC_N}}$	inhibition constant for growth in shoots from σ_C *vs.* σ_N	g C g N^{-1}	[C11]	100	(Grant 1998)

$\boldsymbol{K_{iC_P}}$	inhibition constant for growth in shoots from σ_C *vs.* σ_P	g C g P^{-1}	[C11]	1000	(Grant 1998)
$K_{I\chi_{C4(b4)}}$	constant for CO_2 product inhibition of C_4 decarboxylation in C_4 bundle sheath	μM	[C38]	1000.0	
$K_{I\chi_{C4(m4)}}$	constant for C_4 product inhibition of PEP carboxylation activity in C_4 mesophyll	μM	[C34]	5 x 10^6	
$K_{I\nu_{lf}}$	constant for C_3 product inhibition of RuBP carboxylation activity in C_4 bundle sheath or C_3 mesophyll caused by $[\nu_{lfi,j}]$	g C g N^{-1}	[C49]	100	
$K_{I\pi_{lf}}$	constant for C_3 product inhibition of RuBP carboxylation activity in C_4 bundle sheath or C_3 mesophyll caused by $[\pi_{lfi,j}]$	g C g P^{-1}	[C49]	1000	
$\boldsymbol{K_{iN_C}}$	inhibition constant for N uptake in roots from $\sigma_{Ci,j}$ *vs.* σ_{Nj}	g N g C^{-1}	[C23]	0.1	(Grant 1998)
$\boldsymbol{K_{iP_C}}$	inhibition constant for P uptake in roots from $\sigma_{Ci,j}$ *vs.* $\sigma_{Pi,j}$ roots	g P g C^{-1}	[C23]	0.01	(Grant 1998)
$\boldsymbol{K_{NH_4}}$	M-M constant for NH_4^+ uptake at root or mycorrhizal surfaces	g N m^{-3}	[C23]	0.40	(Barber and Silberbush 1984)
$\boldsymbol{K_{NO_3}}$	M-M constant for NO_3^- uptake at root or mycorrhizal surfaces	g N m^{-3}	[C23]	0.35	(Barber and Silberbush 1984)
$\boldsymbol{K_{PO_4}}$	M-M constant for $H_2PO_4^-$ uptake root or mycorrhizal surfaces	g P m^{-3}	[C23]	0.125	(Barber and Silberbush 1984)

$\boldsymbol{K_{O_2}}$	Michaelis-Menten constant for root or mycorrhizal O_2 uptake	g m^{-3}	[C14c]	0.064	(Griffin 1972)
$\boldsymbol{K_o}$	inhibition constant for O_2 in carboxylation	μM	[C6c,C6e]	500 at 25 °C	(Farquhar et al. 1980)
$\boldsymbol{K_{xN}}$	inhibition constant for remobilization of leaf or root N during senescence	g N g C^{-1}	[C19c]	0.1	
$\boldsymbol{K_{xP}}$	inhibition constant for remobilization of leaf or root P during senescence	g P g C^{-1}	[C19d]	0.01	
L	root length	m m^{-2}	[C14d,C21b,C23]		
l_C	C litterfall from leaf or root	g C m^{-2} h^{-1}	[C18,C19a,b,C20]		
$l_{N,P}$	N or P litterfall from leaf or root	g C m^{-2} h^{-1}	[C19a,b]		
M_B	branch C phytomass	g C m^{-2}	[C20]		
M_L	leaf C phytomass	g C m^{-2}	[C12,C21]		
M_{L_N}, M_{L_R}	non-remobilizable, remobilizable leaf C phytomass	g C m^{-2}	[C12,C18]		
M_R	root C phytomass	g C m^{-2}	[C20,C21]		
M_{iprot}	leaf protein phytomass calculated from leaf N, P contents	g N m^{-2}	[C6b,C6d,C8b,C12]		
N,P	N or P content of organ z	g N m^{-2}	[C16, C19]		
$\mathbf{N_{prot}}$	N content of protein remobilized from leaf or root	g N C^{-1}	[C12,C19a]	0.4	
$[NH_4^+{}_{i,r,l}]$	concentration of NH_4^+ at root or mycorrizal surfaces	g N m^{-3}	[C23]		

$[\mathbf{NH_4^+}_{mn}]$	concentration of NH_4^+ at root or mycorrizal surfaces below which $U_{NH_4} = 0$	g N m^{-3}	[C23]	0.0125	(Barber and Silberbush 1984)
$[NO_3^-{}_{i,r,l}]$	concentration of NH_4^+ at root or mycorrizal surfaces	g N m^{-3}	[C23]		
$[\mathbf{NO_3^-}_{mn}]$	concentration of NO_3^- at root or mycorrizal surfaces below which $U_{NO_3} = 0$	g N m^{-3}	[C23]	0.03	(Barber and Silberbush 1984)
$[H_2PO_4^-{}_{i,r,l}]$	concentration of $H_2PO_4^-$ root or mycorrizal surfaces	g N m^{-3}	[C23]		
$[\mathbf{H_2PO_4^-}_{mn}]$	concentration of $H_2PO_4^-$ at root or mycorrizal surfaces below which $U_{PO_4} = 0$	g N m^{-3}	[C23]	0.002	(Barber and Silberbush 1984)
$\boldsymbol{N}_{leaf}$	maximum leaf structural N content	g N g C^{-1}	[C12]	0.10	
$\boldsymbol{N'}_{leaf}$	minimum leaf structural N content	g N g C^{-1}	[C12]	0.33 x $\boldsymbol{N}_{leaf}$	
N_{lf}	total leaf N	g N m^{-2} leaf	[C32,C33,C47,C48]		
$[N_{chl(b4)}]'$	ratio of chlorophyll N in C_4 bundle sheath to total leaf N	g N g N^{-1}	[C48]	0.05	
$[N_{chl(m4)}]'$	ratio of chlorophyll N in C_4 mesophyll to total leaf N	g N g N^{-1}	[C33]	0.05	
$[N_{pep(m4}]'$	ratio of PEP carboxylase N in C_4 mesophyll to total leaf N	g N g N^{-1}	[C32]	0.025	
$[N_{rub(b4)}]'$	ratio of RuBP carboxylase N in C_4 bundle sheath to total leaf N	g N g N^{-1}	[C47]	0.025	
O_{2q}	aqueous O_2 concentration in root or mycorrhizal aerenchyma	g m^{-3}	[C14c,d]		
O_{2r}	aqueous O_2 concentration at root or mycorrhizal surfaces	g m^{-3}	[C14c,d]		

O_{2s}	aqueous O_2 concentration in soil solution	g m^{-3}	[C14c,d]	
O_c	[O_2] in canopy chloroplasts in equilibrium with $O_{2\ in}$ atm.	μM	[C6c,C6e]	
$\boldsymbol{P}_{\mathbf{leaf}}$	maximum leaf structural P content	g P g C^{-1}	[C12]	0.10
$\boldsymbol{P'}_{\mathbf{leaf}}$	minimum leaf structural P content	g P g C^{-1}	[C12]	0.33 x $\boldsymbol{P}_{\mathbf{leaf}}$
$\mathbf{P}_{\mathbf{prot}}$	P content of protein remobilized from leaf or root	g P C^{-1}	[C12,C19b]	0.04
[π_{lf}]	concentration of nonstructural root P uptake product in leaf	g P g C^{-1}	[C49]	
$\theta_{\mathbf{P}}$	root or mycorrhizal porosity	m^3 m^{-3}	[C21b]	0.1 – 0.5
$\boldsymbol{R}$	gas constant	J mol^{-1} K^{-1}	[C10, C22]	8.3143
R	gas constant	J mol^{-1} K^{-1}	[C36]	8.3143
R_a	total autotrophic respiration	g C m^{-2} h^{-1}	[C13]	
R_a'	R_a under nonlimiting O_2	g C m^{-2} h^{-1}	[C14]	
$\boldsymbol{R}_c'$	specific autotrophic respiration of $\sigma_{Ci,j}$ at T_{ci} = 25 °C	g C g C^{-1} h^{-1}	[C14]	0.015
R_c	autotrophic respiration of $\sigma_{Ci,j}$ or $\sigma_{Ci,r,l}$	g C m^{-2} h^{-1}	[C13,C14,C17, C15]	
R_g	growth respiration	g C m^{-2} h^{-1}	[C17,C20]	
r_{lf}	leaf stomatal resistance	s m^{-1}	[C25,C27,C39]	
r_{lfmaxi}	leaf cuticular resistance	s m^{-1}	[C27]	

$r_{\mathrm{lfmin}i,j,k,l,m,n,o}$	leaf stomatal resistance when $\psi_{ci} = 0$	s m^{-1}	[C27,C28,C35		
$r_{\mathrm{l}i,j,k,l,m,n,o}$	leaf stomatal resistance	s m^{-1}	[C2,C4,C9]		
$r_{\mathrm{lmax}i}$	leaf cuticular resistance	s m^{-1}	[C4]		
$r_{\mathrm{lmin}i,j,k,l,m,n,o}$	leaf stomatal resistance when $\psi_{ci} = 0$	s m^{-1}	[C4,C5,C9]		
$\boldsymbol{R_{\mathrm{m}}'}$	specific maintenance respiration of $\sigma_{\mathrm{C}i,j}$ at $T_{\mathrm{c}i} = 25$ °C	g C g N^{-1} h^{-1}	[C16]	0.0115	(Barnes et al. 1997)
$R_{\mathrm{m}i,j}$	above-ground maintenance respiration	g C m^{-2} h^{-1}	[C16,C17,C15]		
$r_{\mathrm{q}i,r,l}$	radius of root aerenchyma	m	[C14d]		
$r_{\mathrm{r}i,r,l}$	root or mycorrhizal radius	m	[C14d,C21b,c,C23 a,c,e]	1.0×10^{-4} or 5.0×10^{-6}	
$R_{si,j}$	respiration from remobilization of leaf C	g C m^{-2} h^{-1}	[C13,C15,C18, C20]		
r_{sl}	thickness of soil water films	m	[C14d]		
ρ_r	dry matter content of root biomass	g g-1	[C21b]	0.125	
$\boldsymbol{S}$	change in entropy	J mol^{-1} K^{-1}	[C10, C22]	710	(Sharpe and DeMichele 1977)
S	change in entropy	J mol^{-1} K^{-1}	[C36]	710	
σ_{C}	nonstructural C product of CO_2 fixation	g C g C^{-1}	[C11, C19c,d, C23g,h]		

σ_N	nonstructural N product of root uptake	g N g C^{-1}	[C11, C19c, C23g,h]		
σ_P	nonstructural P product of root uptake	g P g C^{-1}	[C11, C19d, C23g,h]		
T_c	canopy temperature	K	[C10, C22]		
T_c	canopy temperature	^oC	[C36]		
$U_{NH4i,r,l}$	NH_4^+ uptake by roots or mycorrhizae	g N m^{-2} h^{-1}	[C23]		
$\boldsymbol{U'_{NH_4}}$	maximum U_{NH_4} at 25 ^oC and non-limiting NH_4^+	g N m^{-2} h^{-1}	[C23]	5.0 x 10^{-3}	(Barber and Silberbush 1984)
$U_{NO3i,r,l}$	NO_3^- uptake by roots or mycorrhizae	g N m^{-2} h^{-1}	[C23]		
$\boldsymbol{U'_{NO_3}}$	maximum U_{NO_3} at 25 ^oC and non-limiting NO_3^-	g N m^{-2} h^{-1}	[C23]	5.0 x 10^{-3}	(Barber and Silberbush 1984)
$U_{PO4i,r,l}$	$H_2PO_4^-$ uptake by roots or mycorrhizae	g N m^{-2} h^{-1}	[C23]		
$\boldsymbol{U'_{PO_4}}$	maximum U_{PO_4} at 25 ^oC and non-limiting $H_2PO_4^-$	g N m^{-2} h^{-1}	[C23]	5.0 x 10^{-3}	(Barber and Silberbush 1984)
$U_{O2i,r,l}$	O_2 uptake by roots and mycorrhizae under ambient O_2	g O m^{-2} h^{-1}	[C14b,c,C23b,d,f]		
$U'_{O2i,l,r}$	O_2 uptake by roots and mycorrhizae under nonlimiting O_2	g O m^{-2} h^{-1}	[C14b,c,C23b,d,f]		
$U_{w_{i,r,l}}$	root water uptake	m^3 m^{-2} h^{-1}	[C14d,C23]		
$V_{\phi(b4)i,j,k}$	CO_2 leakage from C_4 bundle sheath to C_4 mesophyll	g C m^{-2} h^{-1}	[C39,C42]		

V_b'	specific rubisco carboxylation at 25 °C	μmol g $^{-1}$ rubisco s^{-1}	[C6b]	45	(Farquhar et al. 1980)
$V_{b(b4)i,j,k}$	CO_2-limited carboxylation rate in C_4 bundle sheath	μmol m^{-2} s^{-1}	[C43,C44]		
$V_{b(m4)i,j,k,l,m,n,o}$	CO_2-limited carboxylation rate in C_4 mesophyll	μmol m^{-2} s^{-1}	[C26]		
$V_{bi,j,k,l,m,n,o}$	CO_2-limited leaf carboxylation rate	μmol m^{-2} s^{-1}	[C3,C6]		
$V_{bmax(b4)}'$	RuBP carboxylase specific activity in C_4 bundle sheath at 25°C when $\psi_{ci} = 0$ and nutrients are nonlimiting	μmol g^{-1} s^{-1}	[C47]	75	
$V_{bmax(b4)i,j,k}$	CO_2-nonlimited carboxylation rate in C_4 bundle sheath	μmol m^{-2} s^{-1}	[C44,C47]		
$V_{bmax(m4)}'$	PEP carboxylase specific activity in C_4 mesophyll at 25°C when $\psi_{ci} = 0$ and nutrients are nonlimiting	μmol g^{-1} s^{-1}	[C32]	150	
$V_{bmax(m4)i,j,k}$	CO_2-nonlimited carboxylation rate in C_4 mesophyll	μmol m^{-2} s^{-1}	[C29,C32]		
$V_{bmaxi,j,k}$	leaf carboxylation rate at non-limiting CO_2, ψ_{ci}, T_c and N,P	μmol m^{-2} s^{-1}	[C6a,C6b,C6c]		
$V_{c(b4)i,j,k,l,m,n,o}$	CO_2 fixation rate in C_4 bundle sheath	μmol m^{-2} s^{-1}	[C43]		
$V_{c(m4)i,j,k,l,m,n,o}$	CO_2 fixation rate in C_4 mesophyll	μmol m^{-2} s^{-1}	[C24,C26,C40,C41]		
$V_{c_0(m4)\ i,j,k,l,m,n,o}$	CO_2 fixation rate in C_4 mesophyll when $\psi_{ci} = 0$ MPa	μmol m^{-2} s^{-1}	[C28]		
$V_{ci,j,k,l,m,n,o}$	leaf CO_2 fixation rate	μmol m^{-2} s^{-1}	[C1,C3]		

$V_{c'i,j,k,l,m,n,o}$	leaf CO_2 fixation rate when $\psi_{ci} = 0$	μmol m^{-2} s^{-1}	[C5]		
$V_{g(m4)i,j,k,l,m,n,o}$	CO_2 diffusion rate into C_4 mesophyll	μmol m^{-2} s^{-1}	[C24,C25]		
$V_{gi,j,k,l,m,n,o}$	leaf CO_2 diffusion rate	μmol m^{-2} s^{-1}	[C1,C2]		
$\boldsymbol{V_j'}$	specific chlorophyll e^- transfer at 25 °C	μmol g^{-1} chlorophyll s^{-1}	[C8b]	450	(Farquhar et al. 1980)
$V_{j(b4)i,j,k,l,m,n,o}$	irradiance-limited carboxylation rate in C_4 bundle sheath	μmol m^{-2} s^{-1}	[C43,C45]		
$V_{j(m4)i,j,k,l,m,n,o}$	irradiance-limited carboxylation rate in C_4 mesophyll	μmol m^{-2} s^{-1}	[C26,C30]		
$V_{ji,j,k,l,m,n,o}$	irradiance-limited leaf carboxylation rate	μmol m^{-2} s^{-1}	[C3,C7]		
$\boldsymbol{V_o'}$	specific rubisco oxygenation at 25 °C	μmol g^{-1} rubisco s^{-1}	[C6d]	9.5	(Farquhar et al. 1980)
$V_{omaxi,j,k}$	leaf oxygenation rate at non-limiting O_2, ψ_{ci}, T_c and N,P	μmol m^{-2} s^{-1}	[C6c,d]		
$V_{\chi C4(b4)i,j,k}$	decarboxylation of C_4 fixation product in C_4 bundle sheath	g C m^{-2} h^{-1}	[C38,C41,C42]		
$V_{\chi C4(m4)}$	transfer of C_4 fixation product between C_4 mesophyll and bundle sheath	g C m^{-2} h^{-1}	[C37]		
$[\nu_{lf}]$	concentration of nonstructural root N uptake product in leaf	g N g C^{-1}	[C49]		
ν_r	specific volume of root biomass	m^3 g^{-1}	[C21b]		
$W_{lf(b4)}$	C_4 bundle sheath water content	g m^{-2}	[C37,C39]		

$W_{lf(m4)}$	C_4 mesophyll water content	g m^{-2}	[C37]		
X_{mx}	maximum fraction of remobilizable N or P translocated out of leaf or root during senescence	-	[C19a,b]	0.6	(Kimmins 2004)
$Y_{(b4)}$	carboxylation yield from electron transport in C_4 bundle sheath	μmol CO_2 μmol e^{-1}	[C45]		
$Y_{(m4)}$	carboxylation yield from electron transport in C_4 mesophyll	μmol CO_2 μmol e^{-1}	[C30]		
$\boldsymbol{Y_g}$	fraction of $\sigma_{Ci,j}$ used for growth expended as $R_{gi,j,z}$ by organ z	g C g C^{-1}	[C20]	0.28 (z = leaf), 0.24 (z = root and other non-foliar), 0.20 (z = wood)	(Waring and Running 1998)
y	plant population	m^{-2}	[C21]		
Y	carboxylation yield	μmol CO_2 μmol e^{-1}	[C7]		
Γ	CO_2 compensation point	μM	[C6a,C6c]		
$\Gamma_{(b4)}$	CO_2 compensation point in C_4 bundle sheath	μM	[C44]		
$\Gamma_{(m4)}$	CO_2 compensation point in C_4 mesophyll	μM	[C29]		
$\boldsymbol{\alpha}$	shape parameter for response of J to I	-	[C8a]	0.7	
α	shape parameter for response of J to I	-	[C31,C46]	0.75	

χ	area:mass ratio of leaf growth	m g^{-3}	[C21]	0.0125	(Grant and Hesketh 1992)
$\chi_{C4(b4)}$	non-structural C_4 fixation product in C_4 bundle sheath	g C m^{-2}	[C37,C38,C41]		
$\chi_{C4(m4)}$	non-structural C_4 fixation product in C_4 mesophyll	g C m^{-2}	[C37,C40]		
$[\chi_{c3(b4)}]$	concentration of non-structural C_3 fixation product in C_4 bundle sheath	g g^{-1}	[C49]		
$[\chi_{C4(m4)}]$	concentration of non-structural C_4 fixation product in C_4 mesophyll	μM	[C34]		
ε	quantum yield	μmol e^- μmol $quanta^{-1}$	[C8a]	0.45	(Farquhar et al. 1980)
ε	quantum yield	μmol e^- μmol $quanta^{-1}$	[C31,C46]	0.45	(Farquhar et al. 1980)
$\kappa_{Cc(b4)}$	conductance to CO_2 leakage from C_4 bundle sheath	h^{-1}	[C39]	20	
ψ_t	canopy turgor potential	MPa	[C4]	1.25 at $\psi_c = 0$	

Appendix D: Soil water, heat, gas and solute fluxes

Surface water flux

$$Q_{rx(x,y)} = v_{x(x,y)} d_{mx,y} L_{y(x,y)}$$

$$Q_{ry(x,y)} = v_{y(x,y)} d_{mx,y} L_{x(x,y)}$$

2D Manning equation in x (EW) and y (NS) directions [D1]

$$d_{x,y} = \max(0, d_{w(x,y)} + d_{i(x,y)} - d_{s(x,y)}) d_{w(x,y)} / (d_{w(x,y)} + d_{i(x,y)})$$

surface water depth [D2]

$v_{x(x,y)} = R^{0.67} s_{x(x,y)}{}^{0.5}/z_{r(x,y)}$	runoff velocity over E slope	[D3]
$v_{y(x,y)} = R^{0.67} s_{y(x,y)}{}^{0.5}/z_{r(x,y)}$	runoff velocity over S slope	
$v_{x(x,y)} = -R^{0.67} s_{x(x,y)}{}^{0.5}/z_{r(x,y)}$	runoff velocity over W slope	
$v_{y(x,y)} = -R^{0.67} s_{y(x,y)}{}^{0.5}/z_{r(x,y)}$	runoff velocity over N slope	
$\Delta(d_{w(x,y)} A_{x,y})/\Delta t = Q_{r,x(x,y)} - Q_{r,x+1(x,y)} + Q_{r,y(x,y)} - Q_{r,y+1(x,y)} + P - E_{x,y} - Q_{wz(x,y,1)}$	2D kinematic wave theory for overland flow	[D4]
$R = s_r d_m/[2(s_r^2 + 1)0.5]$	wetted perimeter	[D5a]
$s_{x(x,y)} = 2abs[(Z + d_s + d_m)_{x,y} - (Z + d_s + d_m)_{x+1,y}]/(L_{x(x,y)} + L_{x(x+1,y)})$	2D slope from topography and pooled surface water in x (EW) and y (NS) directions	[D5b]
$s_{y(x,y)} = 2abs[(Z + d_s + d_m)_{x,y} - (Z + d_s + d_m)_{x,y+1}]/(L_{y(x,y)} + L_{y(x,y+1)})$		
$\boldsymbol{L}E_l = L\,(e_a - e_{l(T_l, \psi_l)})/r_{al}$	evaporation from surface litter	[D6a]
$\boldsymbol{L}E_s = L\,(e_a - e_{s(T_s, \psi_s)})/r_{as}$	evaporation from soil surface	[D6b]

Subsurface water flux

$Q_{wx(x,y,z)} = K'_x(\psi_{sx,y,z} - \psi_{sx+1,y,z})$	3D Richard's or Green-Ampt equation depending on saturation of source or target cell in x (EW), y (NS) and z (vertical) directions	[D7]
$Q_{wy(x,y,z)} = K'_y(\psi_{sx,y,z} - \psi_{sx,y+1,z})$		
$Q_{wz(x,y,z)} = K'_z(\psi_{sx,y,z} - \psi_{sx,y,z+1})$		
$\Delta\theta_{w\,x,y,z}/\Delta t = (Q_{wx(x,y)} - Q_{wx+1(x,y)} + Q_{wy(x,y)} - Q_{wy+1(x,y)} + Q_{wz(x,y)} - Q_{wz+1(x,y)} + Q_{fl(x,y,z)})/L_{z(x,y,z)}$	3D water transfer plus freeze-thaw	[D8]
$K'_x = 2K_{x,y,z}K_{x+1,y,z}/(K_{x,y,z}L_{x,(x+1,y,z)} + K_{x+1,y,z}L_{x,(x,y,z)})$	in direction x if source and destination cells are unsaturated	[D9a]
$= 2K_{x,y,z}/(L_{x(x+1,y,z)} + L_{x(x,y,z)})$	in direction x if source cell is saturated	[D9b]
$= 2K_{x+1,y,z}/(L_{x(x+1,y,z)} + L_{x(x,y,z)})$	in direction x if destination cell is saturated	
$K'_y = 2K_{x,y,z}K_{x,y+1,z}/(K_{x,y,z}L_{y(x,y+1,z)} + K_{x,y+1,z}L_{y(x,y,z)})$	in direction y if source and destination cells are unsaturated	[D9a]
$= 2K_{x,y,z}/(L_{y(x,y+1,z)} + L_{y(x,y,z)})$	in direction y if source cell is saturated	[D9b]

$= 2K_{x,y+1,z}/(L_{y(x,y+1,z)} + L_{y(x,y,z)})$	in direction y if destination cell is saturated	
$K'_z = 2K_{x,y,z}K_{x,y,z+1}/(K_{x,y,z}L_{z(x,y,z+1)} + K_{x,y,z+1}L_{z(x,y,z)})$	in direction z if source and destination cells are unsaturated	[D9a]
$= 2K_{x,y,z}/(L_{z(x,y,z+1)} + L_{z(x,y,z)})$	in direction z if source cell is saturated	[D9b]
$= 2K_{x,y,z+1}/(L_{z(x,y,z+1)} + L_{z(x,y,z)})$	in direction z if destination cell is saturated	

Exchange with water table

$Qmat_{tx(x,y,z)} = Kmat_{x,y,z}\,[\psi' - \psi_{sx,y,z} + 0.01(d_{zx,y,z} - WTD_x)]/(L_{tx} + 0.5\,L_{x,(x,y,z)})$	if $d_{zx,y,z} < WTD_x$ then $\psi_{sx,y,z} > \psi' + 0.01(d_{zx,y,z} - WTD_x)$ for all depths z from $d_{zx,y,z}$ to WTD_x or if $d_{zx,y,z} > WTD_x$ then $\psi_{sx,y,z} > 0.01(WTD_x - d_{zx,y,z}) - \psi'$ for all depths z from WTD_x to $d_{zx,y,z}$	[D10]
$Qmac_{tx(x,y,z)} = Kmac_{x,y,z}\,[0.01*\min(0, d_{zx,y,z} - L_{z(x,y,z)}*(\min(1, \max(0, \theta_{mac}))-0.5) - WTD_x)]/(L_{tx} + 0.5\,L_{x,(x,y,z)})$	if $d_{zx,y,z} < WTD_x$ then $\psi_{sx,y,z} > \psi' + 0.01(d_{zx,y,z} - WTD_x)$ for all depths z from $d_{zx,y,z}$ to WTD_x or if $d_{zx,y,z} > WTD_x$ then $\psi_{sx,y,z} > 0.01(WTD_x - d_{zx,y,z}) - \psi'$ for all depths z from WTD_x to $d_{zx,y,z}$	[D10a]
$Qmac_{tx(x,y,z)} = Kmac_{x,y,z}\,[0.01*\max(0, d_{zx,y,z} - L_{z(x,y,z)}*(\min(1, \max(0, \theta_{mac}))-0.5) - WTD_x)]/(L_{tx} + 0.5\,L_{x,(x,y,z)})$		

Heat flux

$R_n + \boldsymbol{L}E + H + G = 0$	for each canopy, snow, residue and soil surface, depending on exposure	[D11]
$G_{x(x,y,z)} = 2\,\kappa_{(x,y,z),(x+1,y,z)}\,(T_{(x,y,z)} - T_{(x+1,y,z)})/(L_{x\,(x,y,z)} + L_{x\,(x+1,y,z)}) + c_w\,T_{(x,y,z)}\,Q_{wx(x,y,z)}$	3D conductive – convective heat flux among snowpack, surface residue and soil layers in x (EW), y (NS) and z (vertical) directions	[D12]
$G_{y(x,y,z)} = 2\,\kappa_{(x,y,z),(x,y+1,z)}\,(T_{(x,y,z)} - T_{(x,y+1,z)})/(L_{y\,(x,y,z)} + L_{y\,(x,y+1,z)}) + c_w\,T_{(x,y,z)}\,Q_{wy(x,y,z)}$		
$G_{z(x,y,z)} = 2\,\kappa_{(x,y,z),(x,y,z+1)}\,(T_{(x,y,z)} - T_{(x,y,z+1)})/(L_{z\,(x,y,z)} + L_{z\,(x,y,z+1)}) + c_w\,T_{(x,y,z)}\,Q_{wz(x,y,z)}$		
$G_{x(x-1,y,z)} - G_{x(x,y,z)} + G_{y(x,y-1,z)} - G_{y(x,y,z)} + G_{z(x,y,z-1)} - G_{z(x,y,z)} + \boldsymbol{L}Q_{f(x,y,z)} + c_{(x,y,z)}\,(T_{(x,y,z)} - T'_{(x,y,z)})/\Delta t = 0$	3D general heat flux equation in snowpack, surface residue and soil layers	[D13]

Gas flux

$$Q_{ds\gamma x,y,z} = a_{gsx,y,z}\, D_{d\gamma}\, (\boldsymbol{S}'_{\gamma} ft_{d_{\gamma}x,y,z}\, [\gamma_{gs}]_{x,y,z} - [\gamma_{ss}]_{x,y,z})$$

$$Q_{dr\gamma x,y,z} = a_{grx,y,z}\, D_{d\gamma}\, (\boldsymbol{S}'_{\gamma} ft_{d_{\gamma}x,y,z}\, [\gamma_{gr}]_{x,y,z} - [\gamma_{sr}]_{x,y,z})$$

volatilization – dissolution between aqueous and gaseous phases in soil and root [D14a] [D14b]

$$Q_{gs\gamma zx,y,1} = g_{ax,y}\, \{[\gamma_a] - \{2[\gamma_{gs}]_{x,y,1} D_{gs\gamma z(x,y,1)}/L_{z(x,y,1)} + g_{ax,y}\, [\gamma_a]\}/\{2\, D_{gs\gamma z(x,y,1)}/L_{z(x,y,1)} + g_{ax,y}\}\}$$

$$Q_{ds\gamma x,y,1} = a_{gsx,y,1}\, D_{d\gamma}\, (\boldsymbol{S}'_{\gamma} ft_{d_{\gamma}x,y,1}\, [\gamma_a] - [\gamma_{ss}]_{x,y,1})$$

volatilization – dissolution between gaseous and aqueous phases at the soil surface ($z = 1$) and the atmosphere [D15a] [D15b]

$$Q_{gs\gamma x(x,y,z)} = -\, Q_{wx(x,y,z)}\, [\gamma_{gs}]_{x,y,z} + 2\, D_{gs\gamma x(x,y,z)}\, ([\gamma_{gs}]_{x,y,z} - [\gamma_{gs}]_{x+1,y,z})/\, (L_{x\,(x,y,z)} + L_{x\,(x+1,y,z)})$$

$$Q_{gs\gamma y(x,y,z)} = -\, Q_{wy(x,y,z)}\, [\gamma_{gs}]_{x,y,z} + 2\, D_{gs\gamma y(x,y,z)}\, ([\gamma_{gs}]_{x,y,z} - [\gamma_{gs}]_{x,y+1,z})/\, (L_{y\,(x,y,z)} + L_{y\,(x,y+1,z)})$$

$$Q_{gs\gamma z(x,y,z)} = -\, Q_{wz(x,y,z)}\, [\gamma_{gs}]_{x,y,z} + 2\, D_{g\gamma z(x,y,z)}\, ([\gamma_{gs}]_{x,y,z} - [\gamma_{gs}]_{x,y,z+1})/\, (L_{z\,(x,y,z)} + L_{z\,(x,y,z+1)})$$

3D convective - conductive gas flux among soil layers in x (EW), y (NS) and z (vertical) directions, [D16a] [D16b]

$$Q_{gr\gamma z(x,y,z)} = D_{gr\gamma z(x,y,z)}\, ([\gamma_{gr}]_{x,y,z} - [\gamma_a])/\, \Sigma_{1,z} L_{z\,(x,y,z)}$$

convective - conductive gas flux between roots and the atmosphere [D16c]

[D16d]

$$D_{gs\gamma x(x,y,z)} = \boldsymbol{D}'_{g\gamma}\, ft_{gx,y,z}\, [0.5(\theta_{gx,y,z} + \theta_{gx+1,y,z})]^2/\theta_{psx,y,z}^{0.67}$$

$$D_{gs\gamma y(x,y,z)} = \boldsymbol{D}'_{g\gamma}\, ft_{gx,y,z}\, [0.5(\theta_{gx,y,z} + \theta_{gx,y+1,z})]^2/\theta_{psx,y,z}^{0.67}$$

$$D_{gs\gamma z(x,y,z)} = \boldsymbol{D}'_{g\gamma}\, ft_{gx,y,z}\, [0.5(\theta_{gx,y,z} + \theta_{gx,y,z+1})]^2/\theta_{psx,y,z}^{0.67}$$

gasous diffusivity as a function of air-filled porosity in soil [D17a] [D17b] [D17c]

$$D_{gr\gamma z(x,y,z)} = \boldsymbol{D}'_{g\gamma}\, ft_{gx,y,z}\, \boldsymbol{\theta}_{\mathbf{pr}x,y,z}^{\ 1.33}\, A_{r\,(x,y,z)}\, /A_{x,y}$$

[D17d]

gasous diffusivity as a function of air-filled porosity in roots

$$Q_{b\gamma z} = \min[0.0, \{(44.64\ \theta_{wx,y,z}\, 273.16/T_{(x,y,z)}) - \Sigma_\gamma ([\gamma_s]_{x,y,z}/(\boldsymbol{S}'_\gamma\, ft_{d_\gamma x,y,z} M_\gamma))\}]$$
$$([\gamma_s]_{x,y,z}/(\boldsymbol{S}'_\gamma\, ft_{d_\gamma x,y,z} M_\gamma))/\ \Sigma_\gamma ([\gamma_s]_{x,y,z}/(\boldsymbol{S}'_\gamma\, ft_{d_\gamma x,y,z} M_\gamma))\ \boldsymbol{S}'_\gamma\, ft_{d_\gamma x,y,z} M_\gamma\, V_{x,y,z}$$

bubbling (-ve flux) when total of all partial gas pressures exceeds atmospheric pressure [D18]

Solute flux

$$Q_{s\gamma x(x,y,z)} = -\, Q_{wx(x,y,z)}\, [\gamma_s]_{x,y,z} + 2\, D_{s\gamma x(x,y,z)}\, ([\gamma_s]_{x,y,z} - [\gamma_s]_{x+1,y,z})/\ (L_{x\,(x,y,z)} + L_{x\,(x+1,y,z)})$$

$$Q_{s\gamma y(x,y,z)} = -\, Q_{wy(x,y,z)}\, [\gamma_s]_{x,y,z} + 2\, D_{s\gamma y(x,y,z)}\, ([\gamma_s]_{x,y,z} - [\gamma_s]_{x,y+1,z})/\ (L_{y\,(x,y,z)} + L_{y\,(x,y+1,z)})$$

$$Q_{s\gamma z(x,y,z)} = -\, Q_{wz(x,y,z)}\, [\gamma_s]_{x,y,z} + 2\, D_{s\gamma z(x,y,z)}\, ([\gamma_s]_{x,y,z} - [\gamma_s]_{x,y,z+1})/\ (L_{z\,(x,y,z)} + L_{z\,(x,y,z+1)})$$

3D convective - dispersive solute flux among soil layers in x (EW), y (NS) and z (vertical) directions [D19]

$$D_{s\gamma x(x,y,z)} = D_{qx(x,y,z)}\ |Q_{wx(x,y,z)}| + \boldsymbol{D}'_{s\gamma}\, ft_{sx,y,z}\, [0.5(\theta_{wx,y,z} + \theta_{wx+1,y,z})]\ \tau$$

$$D_{s\gamma y(x,y,z)} = D_{qy(x,y,z)}\ |Q_{wy(x,y,z)}| + \boldsymbol{D}'_{s\gamma}\, ft_{sx,y,z}\, [0.5(\theta_{wx,y,z} + \theta_{wx+1,y,z})]\ \tau$$

$$D_{s\gamma z(x,y,z)} = D_{qz(x,y,z)}\ |Q_{wz(x,y,z)}| + \boldsymbol{D}'_{s\gamma}\, ft_{sx,y,z}\, [0.5(\theta_{wx,y,z} + \theta_{wx+1,y,z})]\ \tau$$

aqueous dispersivity as functions of water flux and water-filled porosity [D20]

$$D_{qx(x,y,z)} = 0.5\ \boldsymbol{\alpha}\, (L_{x\,(x,y,z)} + L_{x\,(x+1,y,z)})^{\boldsymbol{\beta}}$$

$$D_{qy(x,y,z)} = 0.5\ \boldsymbol{\alpha}\, (L_{y\,(x,y,z)} + L_{y\,(x,y+1,z)})^{\boldsymbol{\beta}}$$

$$D_{qz(x,y,z)} = 0.5\ \boldsymbol{\alpha}\, (L_{z\,(x,y,z)} + L_{z\,(x,y,z+1)})^{\boldsymbol{\beta}}$$

dispersivity as a function of water flow length [D21]

Definition of variables in appendix D

Variable	Definition	Unit	Equation	Value	Reference
		Subscripts			
x	grid cell position in west to east direction				
y	grid cell position in north to south direction				
z	grid cell position in vertical direction			$z = 0$: surface residue, z = 1 to n: soil layers	
		Variables			
A	area of landscape position	m^2	[D17c]		
A_r	root cross-sectional area of landscape position	m^2	[D17c]		

a_{gr}	air-water interfacial area in roots	$m^2\ m^{-2}$	[D14b]		
a_{gs}	air-water interfacial area in soil	$m^2\ m^{-2}$	[D14a,D15b]		(Skopp 1985)
$\boldsymbol{\alpha}$	dependence of D_q on L	-	[D21]		
$\boldsymbol{\beta}$	dependence of D_q on L	-	[D21]		
c	heat capacity of soil	$MJ\ m^{-2}\ {}^oC^{-1}$	[D13]		
c_w	heat capacity of water	$MJ\ m^{-3}\ {}^oC^{-1}$	[D12]	4.19	
$D_{d\gamma}$	volatilization - dissolution transfer coefficient for gas γ	$m^2\ h^{-1}$	[D14,D15a]		
$D_{gr\gamma}$	gaseous diffusivity of gas γ in roots	$m^2\ h^{-1}$	[D16d,D17d]		(Luxmoore et al. 1970a, b)
$D_{gs\gamma}$	gaseous diffusivity of gas γ in soil	$m^2\ h^{-1}$	[D15a,D16a,b,c,D17a,b,c]		(Millington and Quirk 1960)
$\boldsymbol{D'_{g\gamma}}$	diffusivity of gas γ in air at 0 ^oC	$m^2\ h^{-1}$	[D17]	6.43×10^{-2} for $\gamma = O_2$	(Campbell 1985)
D_q	dispersivity	m	[D20,D21]		
$D_{s\gamma}$	aqueous diffusivity of gas or solute γ	$m^2\ h^{-1}$	[D19,D20]		
$\boldsymbol{D'_{s\gamma}}$	diffusivity of gas γ in water at 0 ^oC	$m^2\ h^{-1}$	[D20]	8.57×10^{-6} for $\gamma = O_2$	(Campbell 1985)
d_m	depth of mobile surface water	m	[D1,D2,D5a,D6]		
d_i	depth of surface ice	m	[D2]		
d_s	maximum depth of surface water storage	m	[D2,D5b]		
WTD_x	external water table depth	m	[D10]		
d_w	depth of surface water	m	[D1,D2]		
d_z	depth to mid-point of soil layer	m	[D10]		
E	evaporation or transpiration flux	$m^3\ m^{-2}\ h^{-1}$	[D4,D11]		

e_a	atmospheric vapor density	$m^3\ m^{-3}$	[D6]	
$e_{l(T_l, \psi_l)}$	surface litter vapor density at current T_l and ψ_l	$g\ m^{-3}$	[D6a]	
$e_{s(T_s, \psi_s)}$	soil surface vapor density at current T_s and ψ_s	$g\ m^{-3}$	[D6b]	
ft_{d_γ}	temperature dependence of $\boldsymbol{S}'_\gamma$	-	[D14,D15b,D18]	(Wilhelm et al. 1977)
ft_g	temperature dependence of $\boldsymbol{D}'_{g\gamma}$	-	[D17]	(Campbell 1985)
ft_s	temperature dependence of $\boldsymbol{D}'_{s\gamma}$	-	[D20]	(Campbell 1985)
G	soil surface heat flux	$m^3\ m^{-2}\ h^{-1}$	[D11]	
G_x , G_y , G_z	soil heat flux in x, y or z directions	$MJ\ m^{-2}\ h^{-1}$	[D12,D13]	
g_a	boundary layer conductance	$m\ h^{-1}$	[D15a]	
γ	gas (H_2O, CO_2, O_2, CH_4, NH_3, N_2O, N_2, H_2) or solute (from appendix E)		[D14,D15]	
$[\gamma_a]$	atmospheric concentration of gas γ	$g\ m^{-3}$	[D15,D16d]	
$[\gamma_{gr}]$	gasous concentration of gas γ in roots	$g\ m^{-3}$	[D14b,D16d]	
$[\gamma_{gs}]$	gasous concentration of gas γ in soil	$g\ m^{-3}$	[D14a,D15a,D16a ,D16b,D16c]	
$[\gamma_{sr}]$	aqueous concentration of gas γ in roots	$g\ m^{-3}$	[D14b]	
$[\gamma_{ss}]$	aqueous concentration of gas γ in soil	$g\ m^{-3}$	[D14a,D15b,D18, D19]	
H	sensible heat flux	$MJ\ m^{-2}\ h^{-1}$	[D11]	
K	hydraulic conductivity	$m^2\ MPa^{-1}\ h^{-1}$	[D9]	(Green and Corey 1971)
$Kmat$	soil matrix hydraulic conductivity	$m^2\ MPa^{-1}\ h^{-1}$	[D10]	
$Kmac$	macropore hydraulic conductivity	$m^2\ MPa^{-1}\ h^{-1}$	[D10a]	
K'_x , K'_y , K'_z	hydraulic conductance in x, y or z directions	$m\ MPa^{-1}\ h^{-1}$	[D7,D9]	

κ	thermal conductivity	MJ m^{-1} h^{-1} $^oC^{-1}$	[D12]		(De Vries 1963)
L_t	distance from boundary to external water table in x or y directions	m	[D10]		
L_x , L_y , L_z	length of landscape element in x, y or z directions	m	[D1,D5b,D8,D9,D10,D12,D15a,D16,D19]		
$\boldsymbol{L}E_l$	latent heat flux from surface litter	[D6a]	MJ m^{-2} h^{-1}		
$\boldsymbol{L}E_s$	latent heat flux from soil surface	[D6b]	MJ m^{-2} h^{-1}		
$\boldsymbol{L}$	latent heat of evaporation	MJ m^{-3}	[D6,D11,D13]	2460	
M_γ	atomic mass of gas γ	g mol^{-1}	[D18]		
P	precipitation flux	m^3 m^{-2} h^{-1}	[D4]		
$Q_{b\gamma z}$	bubbling flux	g m^{-2} h^{-1}	[D18]		
$Q_{dr\gamma}$	volatilization – dissolution of gas γ between aqueous and gaseous phases in roots	g m^{-2} h^{-1}	[D14b]		
$Q_{ds\gamma}$	volatilization – dissolution of gas γ between aqueous and gaseous phases in soil	g m^{-2} h^{-1}	[D14a,D15b]		
Q_f	freeze-thaw flux (thaw +ve)	m^3 m^{-2} h^{-1}	[D8,D13]		
$Q_{gr\gamma}$	gaseous flux of gas γ between roots and the atmosphere	g m^{-2} h^{-1}	[D16d]		
$Q_{gs\gamma}$	gaseous flux of gas γ in soil	g m^{-2} h^{-1}	[D15a,D16a,b,c]		
Q_{rx}, Q_{ry}	surface water flow in x or y directions	m^3 m^{-2} h^{-1}	[D1,D4]		
$Q_{s\gamma}$	aqueous flux of gas or solute γ	g m^{-2} h^{-1}	[D19]		
$Qmat_t$	water flux between boundary grid cell and external water table through soil matrix in x or y directions	m^3 m^{-2} h^{-1}	[D10]		
$Qmac_t$	water flux between boundary grid cell and external water table through macropores in x or y directions	m^3 m^{-2} h^{-1}	[D10a]		

Q_{wx}, Q_{wy}, Q_{wz}	subsurface water flow in x, y or z directions	$m^3\ m^{-2}\ h^{-1}$	[D4,D7,D8,D12,D16,D19,D20]		
θ_g	air-filled porosity	$m^3\ m^{-3}$	[D17a,b,c]		
θ_{mac}	macropore water content	$m^3\ m^{-3}$	[D10a]		
$\boldsymbol{\theta_{pr}}$	root porosity	$m^3\ m^{-3}$	[D17d]	dryland spp. 0.10 wetland spp. 0.20	(Luxmoore et al. 1970a, b)
θ_{ps}	soil porosity	$m^3\ m^{-3}$	[D17a,b,c]		
θ_w	water-filled porosity	$m^3\ m^{-3}$	[D8,D18,D20]		
R	ratio of cross-sectional area to perimeter of surface flow	m	[D3,D5a]		
R_n	net radiation	$MJ\ m^{-2}\ h^{-1}$	[D11]		
r_{al}	surface litter boundary layer resistance	$m\ h^{-1}$	[D6a]		
r_{as}	Soil surface boundary layer resistance	$m\ h^{-1}$	[D6b]		
$\boldsymbol{S'_\gamma}$	Ostwald solubility coefficient of gas γ at 30 °C	-	[D14,D15b,D18]	0.0293 for $\gamma = O_2$	(Wilhelm et al. 1977)
s_r	slope of channel sides during surface flow	$m\ m^{-1}$	[D5a]		
s_x , s_y	slope in x or y directions	$m\ m^{-1}$	[D3,D5b]		
T	soil temperature	°C	[D12,D18]		
τ	Tortuosity	-	[D20]		
v_x , v_y	velocity of surface flow in x or y directions	$m\ h^{-1}$	[D1,D3]		
ψ'	soil water potential at saturation	MPa	[D10]	-2.0×10^{-2}	
ψ_s	soil water potential	MPa	[D7,D10]		
Z	surface elevation	m	[D5b]		
z_r	Manning's roughness coefficient	$m^{-1/3}\ h$	[D3]	0.01	

Appendix E: Solute transformations

Precipitation-dissolution equilibria

$Al(OH)_{3(s)} \Leftrightarrow (Al^{3+}) + 3\ (OH^{-})$	(amorphous $Al(OH)_3$)	*-33.0*	[E1] [1]
$Fe(OH)_{3(s)} \Leftrightarrow (Fe^{3+}) + 3\ (OH^{-})$	(soil Fe)	*-39.3*	[E2]
$CaCO_{3(s)} \Leftrightarrow (Ca^{2+}) + (CO_3^{2-})$	(calcite)	-9.28	[E3]
$CaSO_{4(s)} \Leftrightarrow (Ca^{2+}) + (SO_4^{2-})$	(gypsum)	*-4.64*	[E4]
$AlPO_{4(s)} \Leftrightarrow (Al^{3+}) + (PO_4^{3-})$	(variscite)	*-22.1*	[E5] [2]
$FePO_{4(s)} \Leftrightarrow (Fe^{3+}) + (PO_4^{3-})$	(strengite)	*-26.4*	[E6]
$Ca(H_2PO_4)_{2(s)} \Leftrightarrow (Ca^{2+}) + 2\ (H_2PO_4^{-})$	(monocalcium phosphate)	*-1.15*	[E7] [3]
$CaHPO_{4(s)} \Leftrightarrow (Ca^{2+}) + (HPO_4^{2-})$	(monetite)	*-6.92*	[E8]
$Ca_5(PO_4)_3OH_{(s)} \Leftrightarrow 5\ (Ca^{2+}) + 3\ (PO_4^{3-}) + (OH^{-})$	(hydroxyapatite)	*-58.2*	[E9]

Cation exchange equilibria [4]

$X\text{-}Ca + 2\ (NH_4^{+}) \Leftrightarrow 2\ X\text{-}NH_4 + (Ca^{2+})$	*1.00*	[E10]
$3\ X\text{-}Ca + 2\ (Al^{3+}) \Leftrightarrow 2\ X\text{-}Al + 3\ (Ca^{2+})$	*1.00*	[E11]

[1] Round brackets denote solute activity. Numbers in italics denote log *K* (precipitation-dissolution, ion pairs), Gapon coefficient (cation exchange) or log *c* (anion exchange).
[2] All equlilibrium reactions involving N and P are calculated for both band and non-band volumes if a banded fertilizer application has been made. These volumes are calculated dynamically from diffusive transport of soluble N and P.
[3] May only be entered as fertilizer, not considered to be naturally present in soils.
[4] X- denotes surface exchange site for cation or anion adsorption.

$X\text{-}Ca + (Mg^{2+}) \Leftrightarrow X\text{-}Mg + (Ca^{2+})$	*0.60*	[E12]
$X\text{-}Ca + 2\,(Na^{+}) \Leftrightarrow 2\,X\text{-}Na + (Ca^{2+})$	*0.16*	[E13]
$X\text{-}Ca + 2\,(K^{+}) \Leftrightarrow 2\,X\text{-}K + (Ca^{2+})$	*3.00*	[E14]
$X\text{-}Ca + 2\,(H^{+}) \Leftrightarrow 2\,X\text{-}H + (Ca^{2+})$	*1.00*	[E15]

Anion adsorption equilibria

$X\text{-}OH_2^{+} \Leftrightarrow X\text{-}OH + (H^{+})$	*-7.35*	[E16]
$X\text{-}OH \Leftrightarrow X\text{-}O^{-} + (H^{+})$	*-8.95*	[E17]
$X\text{-}H_2PO_4 + H_2O \Leftrightarrow X\text{-}OH_2^{+} + (H_2PO_4^{-})$	*-2.80*	[E18]
$X\text{-}H_2PO_4 + (OH^{-}) \Leftrightarrow X\text{-}OH + (H_2PO_4^{-})$	*4.20*	[E19]
$X\text{-}HPO_4^{-} + (OH^{-}) \Leftrightarrow X\text{-}OH + (HPO_4^{2-})$	*2.60*	[E20]

Organic acid equilibria

$X\text{-}COOH \Leftrightarrow X\text{–}COO^{-} + (H^{+})$	*-5.00*	[E21]

Ion pair equilibria

$(NH_4^{+}) \Leftrightarrow (NH_3)_{(g)} + (H^{+})$	*-9.24*	[E22]
$H_2O \Leftrightarrow (H^{+}) + (OH^{-})$	*-14.3*	[E23]
$(CO_2)_{(g)} + H_2O \Leftrightarrow (H^{+}) + (HCO_3^{-})$	*-6.42*	[E24]
$(HCO_3^{-}) \Leftrightarrow (H^{+}) + (CO_3^{2-})$	*-10.4*	[E25]

$(AlOH^{2+}) \Leftrightarrow (Al^{3+}) + (OH^{-})$	*-9.06*	[E26]
$(Al(OH)_2^{+}) \Leftrightarrow (AlOH^{2+}) + (OH^{-})$	*-10.7*	[E27]
$(Al(OH)_3^{0}) \Leftrightarrow (Al(OH)_2^{+}) + (OH^{-})$	*-5.70*	[E28]
$(Al(OH)_4^{-}) \Leftrightarrow (Al(OH)_3^{0}) + (OH^{-})$	*-5.10*	[E29]
$(AlSO_4^{+}) \Leftrightarrow (Al^{3+}) + (SO_4^{2-})$	*-3.80*	[E30]
$(FeOH^{2+}) \Leftrightarrow (Fe^{3+}) + (OH^{-})$	*-12.1*	[E31]
$(Fe(OH)_2^{+}) \Leftrightarrow (FeOH^{2+}) + (OH^{-})$	*-10.8*	[E32]
$(Fe(OH)_3^{0}) \Leftrightarrow (Fe(OH)_2^{+}) + (OH^{-})$	*-6.94*	[E33]
$(Fe(OH)_4^{-}) \Leftrightarrow (Fe(OH)_3^{0}) + (OH^{-})$	*-5.84*	[E34]
$(FeSO_4^{+}) \Leftrightarrow (Fe^{3+}) + (SO_4^{2-})$	*-4.15*	[E35]
$(CaOH^{+}) \Leftrightarrow (Ca^{2+}) + (OH^{-})$	*-1.90*	[E36]
$(CaCO_3^{0}) \Leftrightarrow (Ca^{2+}) + (CO_3^{2-})$	*-4.38*	[E37]
$(CaHCO_3^{+}) \Leftrightarrow (Ca^{2+}) + (HCO_3^{-})$	*-1.87*	[E38]
$(CaSO_4^{0}) \Leftrightarrow (Ca^{2+}) + (SO_4^{2-})$	*-2.92*	[E39]
$(MgOH^{+}) \Leftrightarrow (Mg^{2+}) + (OH^{-})$	*-3.15*	[E40]
$(MgCO_3^{0}) \Leftrightarrow (Mg^{2+}) + (CO_3^{2-})$	*-3.52*	[E41]

$(MgHCO_3^+) \Leftrightarrow (Mg^{2+}) + (HCO_3^-)$ *-1.17* [E42]

$(MgSO_4^0) \Leftrightarrow (Mg^{2+}) + (SO_4^{2-})$ *-2.68* [E43]

$(NaCO_3^-) \Leftrightarrow (Na^+) + (CO_3^{2-})$ *-3.35* [E44]

$(NaSO_4^-) \Leftrightarrow (Na^+) + (SO_4^{2-})$ *-0.48* [E45]

$(KSO_4^-) \Leftrightarrow (K^+) + (SO_4^{2-})$ *-1.30* [E46]

$(H_3PO_4) \Leftrightarrow (H^+) + (H_2PO_4^-)$ *-2.15* [E47]

$(H_2PO_4^-) \Leftrightarrow (H^+) + (HPO_4^{2-})$ *-7.20* [E48]

$(HPO_4^{2-}) \Leftrightarrow (H^+) + (PO_4^{3-})$ *-12.4* [E49]

$(FeH_2PO_4^{2+}) \Leftrightarrow (Fe^{3+}) + (H_2PO_4^-)$ *-5.43* [E50]

$(FeHPO_4^+) \Leftrightarrow (Fe^{3+}) + (HPO_4^{2-})$ *-10.9* [E51]

$(CaH_2PO_4^+) \Leftrightarrow (Ca^{2+}) + (H_2PO_4^-)$ *-1.40* [E52]

$(CaHPO_4^0) \Leftrightarrow (Ca^{2+}) + (HPO_4^{2-})$ *-2.74* [E53]

$(CaPO_4^-) \Leftrightarrow (Ca^{2+}) + (PO_4^{3-})$ *-6.46* [E54]

$(MgHPO_4^0) \Leftrightarrow (Mg^{2+}) + (HPO_4^{2-})$ *-2.91* [E55]